MECHANOTRANSDUCTION AND THERAPEUTIC TARGETING OF CELLS IN THE CIRCULATION

A Dissertation

Presented to the Faculty of the Graduate School

of Cornell University

In Partial Fulfillment of the Requirements for the Degree of

Doctor of Philosophy

by

Michael J Mitchell

August 2014

MECHANOTRANSDUCTION AND THERAPEUTIC TARGETING OF CELLS IN THE CIRCULATION

Michael J Mitchell, Ph. D.

Cornell University 2014

The application of fluid shear stress on leukocytes and tumor cells in the circulation plays a critical role in the progression of inflammation and cancer metastasis, respectively. Specifically, fluid shear forces are known to help mediate selectin-based interactions between endothelial cells and circulating cells such as tumor cells and leukocytes, which can lead to their subsequent transmigration into tissues. However, how fluid shear forces induce mechanotransduction in circulating cells remains largely unknown, and could provide insight into potentially controlling pathological conditions such as inflammation and metastasis for therapeutic purposes.

Herein, fluid forces are shown to exert control over how leukocytes respond to inflammatory agents found in the circulation. Leukocyte pre-exposure to fluid shear stress was found to suppress early leukocyte activation in the presence of the bacterial peptide fMLP, as indicated by reductions in selectin adhesion molecule shedding, integrin activation, and cell morphological changes. Conversely, leukocyte exposure can also increase leukocyte activation in the presence of platelet-activating factor, a molecule typically upregulated during vascular injury.

Utilizing the same *in vitro* system, tumor cells became sensitized to the apoptosis-inducing ligand TRAIL in the presence of fluid shear stress conditions of

the vasculature. This effect is not witnessed upon tumor cell treatment with the commonly utilized chemotherapeutic doxorubicin, which enacts its therapeutic effect via DNA intercalation. Results from this work suggest that TRAIL is well suited for systemic delivery, and that receptor-mediated apoptosis in general could be an ideal approach for circulating tumor cell therapies.

The unique apoptotic effects of TRAIL in the presence of fluid shear stress were then exploited to develop a novel nanoparticle platform for therapeutic targeting of cancer cells in the circulation *in vivo*. Specifically, E-selectin functionalized liposomes were effective at rapidly targeting and adhering to cancer cells under shear stress conditions in the circulation, while also delivering therapeutic cargo. Utilizing both E-selectin and TRAIL, a nanoparticle platform was developed to functionalize circulating leukocytes of the bloodstream in attempt to neutralize circulating cancer cells. This approach, demonstrated *in vitro* with human blood and also in the circulation of mice *in vivo*, mimics the cytotoxic activity of natural killer cells and increases the surface area available for delivery of the receptor-mediated signal. The resulting "unnatural killer cells" hold promise as an effective means to neutralize circulating tumor cells that enter blood with the potential to form new metastases.

BIOGRAPHICAL SKETCH

Michael John Mitchell was born to John and Grace Mitchell on December 20th, 1986, in Brooklyn, New York. His father, John, grew up in Brooklyn and had a successful financial career in New York City. His mother, Grace, was raised in Buenos Aires, Argentina, until leaving as a teenager with her parents for the United States. He was raised in Manalapan, New Jersey, for the majority of his youth, until beginning his undergraduate studies at the Stevens Institute of Technology in Hoboken, New Jersey. It was there that he found his passion for research, majoring in biomedical engineering and materials science, and conducting research on *in vitro* microfluidic tissue models in the laboratory of Dr. Woo Y. Lee.

Michael then began his graduate studies at Cornell University in the Department of Biomedical Engineering, in the lab of Dr. Michael R. King. His research has focused on the interface of cellular engineering, nanotechnology, and drug delivery. Specifically, he is focused on leukocyte and tumor cell mechanotransduction, nanomaterial-based approaches to isolate and kill circulating tumor cells, and the use of functionalized leukocytes to target and kill cancer cells in the bloodstream *in vivo* to interfere with metastatic progression. He has received awards from the Biomedical Engineering Research Society, American Institute of Chemical Engineers, École Nationale Supérieure des Mines de Saint Etienne, and the International Society of Biorheology for his graduate research. Michael will continue has career as a postdoctoral research fellow at the Massachusetts Institute of Technology, in the laboratory of Dr. Robert S. Langer. He looks forward to a career in biotechnology and academics, and mentoring researchers and students from diverse backgrounds.

To my parents, John and Grace, and my brother, Marc.

To my dear friend Bobby, who left us much too early.

ACKNOWLEDGMENTS

I have been quite fortunate to receive guidance, love, and support of many individuals throughout my doctoral studies, including my family, girlfriend, advisor, mentors, lab members, colleagues and friends.

I am incredibly grateful to my parents, John and Grace Mitchell, for the sacrifices they have made throughout my education. Throughout my upbringing, my parents constantly stressed education to my brother and I. However, they never pressured us into a particular field or career, but rather challenged my brother and I to search and find fields that we were passionate about. I can honestly say that I am now part of a field that I truly love; I will never be able to repay them for this gift.

Throughout my studies, I have been fortunate to receive praise from my colleagues for my ability to present to a wide range of audiences. I owe this ability to my father, John. Whether it be conversing with colleagues and co-workers, hosting a great summer party, helping a stranger, or coaching my baseball and basketball teams, my father always possessed a unique ability to bring people together. I am thankful for my mother, Grace, for providing perhaps the most important component of my studies: incredible food. My mother stressed the importance of our family having dinner together every night, and took the time to provide a delicious spread for each of those meals. I took this for granted as a child; today, I cherish those meals, and how they have kept our family so close together. I am thankful for my brother, Marc, for being kind enough to knock me off my high horse when I get excited about my research. I cannot count the number of times I have heard him say “we all know Michael got lucky and ended up with the best BME professor at Cornell.” He is right.

My loving girlfriend, Karin Wang, has had the patience to not only support, but also live with me throughout the majority of doctoral studies. I have learned much from her patience and kindness, and would not be the undergraduate mentor that I am today without her. It has been a joy to work in the same building as her, and share our research hardships and accomplishments with each other. I cannot wait to see where our future in research will take us.

I have had the privilege of conducting my doctoral studies under the supervision of Dr. Michael King, who knew long before me that I would be a great fit in his lab. Dr. King was the first person I met during my original visit to Cornell, and he was the first Professor to email me after my visit. He introduced me to the field that I love, constantly challenged me with new projects, and pushed me to achieve goals that I never thought I would be able to accomplish, such as publishing impactful journals and securing a postdoctoral position in Robert Langer's lab at MIT. He taught me how to take ownership of my research, write my first scientific paper, and present at my first conference. I will never be able to repay him for these gifts.

I would also like to acknowledge my committee members, Dr. Richard Cerione and Dr. Jeffrey Varner, for their kind support and guidance throughout my studies. I would like to thank BME Professors Dr. Cynthia Reinhart-King, Dr. David Putnam, Dr. Chris Schaffer, Dr. Ben Cosgrove, and Dr. Steven Adie for their helpful discussions and unique insights throughout my career. I would also like to thank Dr. Michael Shuler, Dr. Peter Doerschuk, and Ms. Belinda Floyd for their help with the Ph.D. admissions process, welcoming me to Cornell, and providing great support throughout my studies.

My “Fellow Kings”, also known as the members of the King lab, have been like family throughout my studies. I would like to acknowledge old members of the King lab, particularly Dr. Kuldeep Rana and Carissa Ball for ushering me into lab and being excellent role models as I began to pursue my own independent research. Andrew Hughes, Sivaprakash Agastin, Varun Ponmudi, John Lindsey, Weiwei Wang, Christina Chen, and Adelaide de Guillebon provided friendship and support, and made the King lab a special place from the very beginning. Jeff Mattison, our lab manager, has been a father-like figure to our entire lab, and a stabilizing presence from the very beginning. I have enjoyed welcoming and working with the new era of King lab, including Kevin Anderson, Anne Rocheleau, Jocelyn Marshall, Siddarth Chandrasekaran, and Thong Cao. I cannot wait to see their research come to fruition in the upcoming years. I would also like thank one honorary King lab member, Liz Wayne, and her advisor, Dr. Chris Schaffer, for partnering with us on my final research project that culminated in a new therapeutic approach to eliminate tumor cells from the bloodstream. Finally, I would like to thank the diverse group students that I had the privilege of mentoring, including Kimberly Lin, Maxine Chan, Ana Steen, Sue Yan, Dennis Zhou, Ryan Ashley, Zhexiao Wang, and Carlos Castellanos. They have reaffirmed my commitment to mentor students from diverse backgrounds as I continue my academic career.

I was able to maintain a happy and balanced life throughout my studies large due to the love and support from my friends. To my Ithaca and Cornell friends, including Mingchee, Jose, Thong, John, Joe, Kevin, Roman, Jon, Brandon, Rouge, Warden, Peter, Robby, Kuldeep, Adelaide, Christina, J.C., Ryan, Kirk, and Liz, for incredible weekends, football games outside Weill, beers at the Big Red Barn, and unforgettable conference trips across the world. To my friends from my undergraduate

days, including Scott, Henry, Sean, Steve, Dan, Amy, Kyle, Nicole, John, Dan, Brian, Dan, and Jay, I will never forget our all-nighters as we pursued engineering degrees, and our endless adventures in NYC and beyond as we all learned from each other, and grew together. To my friends from home, including Scotty Moz, Ray, Samaan, Marc, Anthony, Jay, Peter, Bucci, Sal, Jay, Cozz, Dan, Sean, Monica, Sam, Alfie, Jeff, and Alex for being there through thick and thin, all the way from our earliest school years. I am fortunate that we not only stay in touch, but still meet up with each other on a regular basis. Finally, I would acknowledge the late Robert “Bobby” Mozia, my dear friend who was taken from us much too early. We began our Ph.D. career together, and my journey would not have been possible without his larger-than-life personality, kindness, generosity, and huge heart.

TABLE OF CONTENTS

LIST OF FIGURES

LIST OF TABLES

CHAPTER 1: INTRODUCTION

1.1 EXPERIMENTAL AND COMPUTATIONAL MODELS OF CIRCULATING CELL RESPONSE TO FLUID SHEAR STRESS

*This section is adapted from the following publication: M.J. Mitchell and M.R. King. *Frontiers in Oncology.* 3(44): 1-11, 2013.

To initiate the metastatic spread of cancer through the bloodstream, tumor cells must transit through microenvironments of dramatically varying physical forces. Cancer cells a must be able to migrate through the stroma, intravasate through the endothelium into blood or lymphatic vessels, flow within the vessels and subsequently extravasate through the endothelium, and migrate and colonize in tissue at a secondary site [1-3]. In soft tissues, cancer cells are exposed to mechanical forces due to fluid shear stress, hydrostatic pressure, and tension and compression forces [4,5]. During intravasation and extravasation, cells undergo dramatic elastic deformations to transmigrate through endothelial cell-cell junctions [6,7]. Once in the circulation, tumor cells must be able to withstand immunological stress, blood cell collisions, and hemodynamic shear forces, while also utilizing flow to adhere to the endothelial wall and subsequently extravasate to form a secondary tumor [8]. Across all of these steps, a deeper understanding is needed of how biophysical forces contribute to biochemical changes in cancer cells, which can reveal novel strategies in the treatment of metastasis.

Fluid shear stress is one of the prominent forces that cells are exposed to, and its effects on blood cells, endothelial cells, smooth muscle cells, and others have been

extensively studied [9-11]. However, much less is known about fluid shear stress effects on tumor cells. Cancer cells experience two main types of fluid shear stress: stresses generated by blood flow in the vascular microenvironment, and those generated by interstitial flows in the tumor microenvironment [12,13]. Stresses generated by interstitial and blood flows could contribute to the metastatic process by enhancing tumor cell invasion and CTC adhesion to blood vessels, respectively. However, it is difficult to predict tumor cell behavior to such forces; it is difficult to experimentally measure such flows in the tumor microenvironment [14], and there is a general lack of data on force-dependent CTC receptor-ligand interactions with the endothelium [15]. Sophisticated experimental techniques coupled with computational modeling are needed to predict cell behavior upon exposure to varying complex physical forces.

Here, I provide examples of both experimental and computational methods to model and predict how cancer cells respond to fluid shear forces. I begin by describing the fluid shear forces that cancer cells are exposed to in both the tumor and vascular microenvironments, generated mainly by blood and interstitial flows. An overview is provided on computational modeling to estimate the forces exerted on cells in blood and tissues, along with simulations to predict cell behavior under such flows. I then describe recent cancer cell mechanotransduction phenomena upon exposure to fluid shear stress, such as altering cancer cell resistance to fluid shear stress, sensitivity to apoptosis-inducing ligands, and invasive and migratory potential. I conclude with current computational models that aim to integrate fluid shear forces with chemical signaling, such as the effect of the glycocalyx on transmitting physical forces and

inducing mechanotransduction in cancer cells, as well as the integration of signal transduction networks into adhesive dynamics simulations to predict cell adhesion to the microvasculature.

1.1.1 FLUID SHEAR STRESS EXPOSURE IN THE TUMOR MICROENVIRONMENT

Cancer cells in the tumor microenvironment are exposed to multiple physical forces including fluid shear stress, hydrostatic pressure, tension, and compression, which have been treated in detail previously [5,6,12]. Here, cancer cell exposure to physical forces generated by interstitial flows will be discussed briefly.

Interstitial flow is the slow movement of fluid around cells and through the pores of the extracellular matrix (ECM) that comprise the interstitium (Figure 1.1A). One of the main functions of interstitial flow is lymphatic drainage, which returns plasma from leaky capillaries back to the bloodstream. Drainage occurs due to Starling's forces, which are osmotic and hydrostatic pressure gradients between blood vessels, interstitium, and the lymphatics [16]. The composition of interstitial fluid can vary depending on the location in the body, but in soft tissues is generally similar to the blood plasma that leaks from capillaries, and contains approximately 40% of the protein concentration of plasma [17]. The velocities of interstitial flows are believed to range from 0.1-1.0 μm/s in normal tissues [18,19]. Cell surface shear stresses are believed to be on the order of 0.1 dyn/cm^2 [20,21].

Interstitial flows can be elevated significantly in the tumor microenvironment, and could play a crucial role in tumor progression. Chary *et al.* utilized fluorescence recovery after photobleaching (FRAP) to measure interstitial fluid velocities of bovine serum albumin in normal and neoplastic tissues [19]. Harrell *et al.* utilized live imaging of tumor-bearing mice to measure downstream lymph flow via injection of fluorescent nanoparticles. Measurements were performed in both normal and neoplastic tissues; all tumor-bearing mice in the study showed increases in lymph flow, compared to control mice with no tumors [22].

Elevated interstitial flows in the tumor microenvironment are likely due to increases in tumor interstitial fluid pressure (IFP). Boucher *et al.* implanted colon adenocarcinoma cells into mice, tracked the development of the tumor vasculature using intravital microscopy, and measured the IFP using micropipettes and a servo-null system [23]. IFP measurements increased significantly as the vasculature developed, demonstrating that tumor interstitial hypertension is associated with tumor angiogenesis [24]. IFP is elevated in a uniform manner throughout tumors, and drops significantly at the tumor periphery [25]. Thus, IFP gradients facilitate fluid flow outward from tumors, presenting a mass transport barrier for the delivery of chemotherapeutics [26,27].

Increased IFP also effects tumor biology, as it applies increased physical force to the ECM and alters interstitial flows that the tumor and surrounding cells are exposed to. Nearby lymphatic vessels respond to elevated interstitial flow by upregulating chemokine CCL21 expression, along with cell adhesion molecules E-selectin and ICAM-1 [28]. Secretion of CCL21 directs tumor cells toward lymphatic vessels [29],

while ICAM-1 and E-selectin upregulation enhances cell transmigration into lymphatic vessels [28,30]. Lymph nodes can also be affected, as increased interstitial flows aid in lymph node architecture remodeling to colonize tumor cells, as well as protect the tumor from an immune response [14].

Fibroblasts, which deposit, turn over, and remodel ECM to maintain connective tissue homeostasis, may aid in tumor progression due to elevated interstitial flows. Elevated interstitial flows can upregulate transforming growth factor beta-1 (TGF-β_1) expression [31-34], which can induce a tumor-associated fibroblast phenotype characterized by enhanced contractility and increased secretion of cytokines, angiogenic growth factors, and matrix metalloproteinase (MMPs) [35-38]. Recently, Shieh *et al.* demonstrated that interstitial flows can enhance tumor cell invasion when cocultured with dermal fibroblasts in a 3D collagen matrix [39]. Fibroblast invasion was enhanced due to increased expression of TGF-β_1 and MMPs, while it appeared that tumor cell invasion was enhanced due to fibroblast-dependent remodeling of the ECM [39].

1.1.2 FLUID SHEAR STRESS EXPOSURE IN THE VASCULAR MICROENVIRONMENT

To enter the vascular microenvironment, cancer cells penetrate surrounding tissue and enter nearby blood and lymphatic vessels in a process called intravasation. The underlying mechanisms that govern intravasation are not well understood; it is still in question whether intravasation is an active or passive process [40], and whether tumor

cells enter the circulation via endothelial cell-cell junctions or directly through endothelial cells themselves [41]. Regardless of their mechanism of entry, cancer cells are exposed to a new set of conditions once in the vascular microenvironment, including immunological stress, collisions with normal blood cells, and hemodynamic shear forces, all of which can affect their survival and proliferation.

Cancer cells are primarily exposed to erythrocytes, leukocytes, and platelets upon entering the bloodstream, as studies have shown that the concentration of cancer cells in the blood of patients is on the order of one in a million leukocytes [42], or one in a billion normal blood cells [43]. Exposure to such cells can lead to immunological stresses and blood cell collisions that can affect cancer cell viability [6], although there is evidence that the association of platelets with cancer cells in the bloodstream can promote tumor metastasis [44,45].

Cancer cells are also exposed to hemodynamic shear forces in the bloodstream (Figure 1.1B), which range from 1.0-4.0 dyn/cm^2 in the venous circulation and 4.0-30.0 dyn/cm^2 in arterial circulation [46]. Shear rates can range from approximately 160 s^{-1} in veins to 900 s^{-1} in arteries. Such shear stresses and rates can affect cancer cell viability and thus the chances of metastasis. For example, B16 melanoma cell exposure to fluid shear stress in a cone-and-plate viscometer at shear rates greater than 300 s^{-1} induced a significant loss of cell viability [47].

In contrast, fluid shear stress is an essential component of cancer metastasis, as it is critical for cancer cell adhesion to the endothelial cell wall and subsequent extravasation into tissues. A variety of cancer cell lines are known to express sialylated carbohydrate ligands, which adhesively interact with selectin proteins on the

inflamed microvasculature [48-50]. Thus cancer cells are believed to undergo an adhesion cascade similar to leukocytes, which consists of a sequence of steps involving tethering, rolling, and firm adhesion to the endothelium [51,52]. Multiple studies have documented that a variety of tumor cell lines bind to E-selectin proteins under physiological shear stresses of the post-capillary venules [53,54].

Much less is known about fluid shear stresses that cancer cells could be exposed to in lymphatic vessels. Lymphatic vessels have been stained with fluorescein isothiocyanate (FITC)-labeled macromolecules to measure lymphatic flow in single lymphatic capillaries of humans *in vivo* using intravital capillary microscopy [55]. The recorded median linear velocity in lymphatic capillaries was 9.7 μm/s, and shear stresses in lymph node sinuses have been estimated to be 10-fold lower than hematogenous shear stresses [56]. Despite the dramatic decrease in shear stress levels, parallel plate flow chamber studies have shown that human head and neck squamous cell cancer cells can bind to lymphocyte L-selectin at lymphatic shear stress levels of 0.07-0.08 dyn/cm^2 [56].

1.1.3 COMPUTATIONAL METHODS TO MODEL INTERSTITIAL FLOWS

Interstitial flow mechanics were initially described by French hydraulics engineer Henry Darcy, who studied the flow of water through sandbeds as a means of providing filtered drinking water to his city.

During his studies, he developed the formula known as Darcy's law:

$$\bar{u} = \frac{-K\nabla P}{\mu},$$

where K is the permeability of the medium, ∇P is the pressure gradient vector, μ is the viscosity of the fluid, and $\bar{u}$ is the averaged velocity through the bulk. Darcy's law works well when the average velocity or mass flow rate needs to be determined, but is first order with respect to velocity. To account for interstitial flows between boundaries, Brinkman developed a second order term, taking into account no-slip boundary conditions adjacent to bounding walls (Figure 1.2A) [57]. The Brinkman equation is described as:

$$\nabla P = -\frac{\mu}{K}\bar{u} + \mu\nabla^2\bar{u}.$$

Permeability measurements have been performed for a variety of tissues *in vitro*, *in vivo*, and *ex vivo*, including muscle [58], dermis [59], cartilage [60], tumors [61,62], and fibrin and collagen gels [63,64], making the Darcy and Brinkman equations useful for both experimental measurements of interstitial flows and computational models of cells exposed to such flows.

Initial models of interstitial flows exerted on cells were developed for tissues including smooth muscle, cartilage, and bone [65-67]. For example, Wang and Tarbell modeled the tunica media of an artery as a periodic array of cylindrical, impermeable

smooth muscle cells (SMCs) embedded in a matrix consisting of collagen and proteoglycans, and used Brinkman's theory to model interstitial flow across the tissue [68]. The model was able to estimate the effective hydraulic permeability of the tissue and shear stresses exerted on SMCs, which were estimated to be on the order of 1.0 dyn/cm^2 despite exposure to low interstitial flows [68]. In an early model describing the mechanics of interstitial-lymphatic transport, Swartz *et al.* developed a theoretical and experimental model demonstrating how interstitial flow is dependent on hydraulic conductivity, elasticity, and lymphatic conductance. They then utilized this model to examine fluid balance in normal and chronically swollen (edematous conditions) mouse tails, in which they found that remodeling of the matrix dampened and eventually stagnated fluid movement in the case of edema [69].

1.1.4 COMPUTATIONAL METHODS TO MODEL CELL BEHAVIOR IN THE CIRCULATION

A variety of computational methods have been developed to model cell behavior in the vascular microenvironment, including adhesive dynamics (AD), which has been utilized to simulate cell adhesion to the endothelial cell surface under flow [70,71]. The motivation of such simulations is to predict how adhesiveness quantitatively depends on factors such as shear rate and viscosity, which can reveal adhesion phenomena that might not necessarily follow intuition. Adhesive dynamics is a mechanically rigorous cell adhesion simulation that models individual molecular bonds as compliant springs. In the simulation, the cell can be modeled as a rigid

spherical particle covered with a random distribution of adhesion molecules (Figure 1.2B). The endothelial cell wall can be modeled as a surface covered with counter-receptor molecules of random distribution. Bonds randomly form between adhesion molecules of the cell and counter-receptors on the wall; these bonds can then break contingent on the appropriate kinetics, which depend on the instantaneous force loading on the spring endpoints. The rates of bond formation and rupture can be calculated using the Bell model for kinetics of single biomolecular bond failure [72,73]:

$$k_r = k_r^0 \exp(\frac{r_0 F}{k_b T})$$

where k_r is the rate of dissociation, k_r^0 is the unstressed off-rate, F is the force on the bond, r_0 is the reactive compliance, T is the temperature, and k_b is the Boltzmann constant. The rate of bond formation follows from the Boltzmann distribution of affinity, while also incorporating the effects of relative motion between the cell and surface [74]. To solve the algorithm, unbound receptors in the defined contact area are first tested for formation against the probability:

$$P_f = 1 - \exp(-k_f \Delta t)$$

where P_f is the probability of bond formation, and t is time. Next, bound receptors are tested for breakage against the probability:

$$P_r = 1 - \exp(-k_r \Delta t)$$

where P_r is the probability of bond rupture. External forces and torques on the cell are then summed, and a mobility calculation determines the motion of the cell. Cell and bond positions are updated based on the kinematics of cell motion. Torques exerted by fluid flow and hydrodynamic forces cause the adherent cell to slowly roll forward on a reactive surface. The motion of fluid is governed by the Stokes equation:

$$\mu \nabla^2 u = \nabla P, \quad \nabla \cdot u = 0,$$

where u is the velocity, μ is the viscosity of the fluid, and P is the pressure. No slip boundary conditions are applied at the cell surface and the planar wall.

While adhesive dynamics have not yet been used to model cancer cell adhesion, many simulations have been performed using leukocytes, which can be a close parallel to a circulating tumor cell that has undergone the epithelial-mesenchymal transition (EMT). Chang *et al.* utilized adhesive dynamics to develop a state diagram for leukocyte adhesion under flow [75]. In the diagram, observed adhesive behaviors (rolling, firm adhesion, or no adhesion) were plotted at given dissociation rates and bond interaction lengths, which ranged several orders of magnitude. Caputo *et al.* incorporated deformable microvilli with clustered adhesion molecules onto the surface

of the simulated leukocyte, and found that the deformability of the microvilli can affect the cell's ability to roll on a surface [76]. King *et al.* modeled the effect of cell-cell hydrodynamic interactions on the dynamics of leukocyte adhesion using Multiparticle Adhesive Dynamics (MAD), which revealed a mechanism for secondary hydrodynamic recruitment of leukocytes to the blood vessel wall, independent of leukocyte-leukocyte interactions [77,78].

Critical parameters of AD simulations are the kinetics of selectin-carbohydrate bonds, as force-dependent dissociation rates dictate the rolling adhesion of leukocytes. Numerous studies have investigated the kinetics for leukocyte selectin ligands using experimental techniques flow chamber tethering experiments, atomic force microscopy, and dynamic force spectroscopy [79], However, such kinetics for newly identified selectin ligands expressed by metastatic tumor cells, which appear distinct from those found on the surface of leukocytes [80,81], have not yet been well characterized. Future experimental studies measuring bond dissociation kinetics for selectins and CTC selectin ligands will enable the development of more predictive computational models of cancer cell adhesion to microvasculature.

1.1.5 CANCER CELL MECHANOTRANSDUCTION PHENOMENA IN EXPERIMENTS

Fluid shear stress alters cancer cell response to apoptosis-inducing ligands

The targeting and treatment of CTCs within the circulation is currently being investigated as an approach to prevent metastatic spread. For example, microfluidic devices coated with E-selectin conjugated liposomal doxorubicin have been shown to capture cancer cells from flow, deliver doxorubicin into the cell, and induce cell death [82,83]. Similarly, microfluidic devices immobilized with E-selectin and tumor necrosis factor (TNF)-related apoptosis-inducing ligand (TRAIL) have been shown to capture and kill cancer cells [84] while causing minimal effects in human leukocytes [85]. However, little is known about how fluid shear stress exposure can affect the cancer cell response to drug treatments.

Our recent study examined how colorectal adenocarcinoma COLO 205 and prostate adenocarcinoma PC-3 cancer cell exposure to physiologically relevant fluid shear stresses in a cone-and-plate viscometer altered their response to TRAIL (Figure 1.3) [86]. Experiments were devised in such a way that fluid shear stress alone had negligible effects on cancer cell death. Cancer cells were treated with both TRAIL, which can bind to death receptors DR4 and DR5 on the cancer cell surface to initiate apoptosis [87], and doxorubicin, which induces cell death via inhibition of topo-isomerase II and DNA intercalation [88,89]. Interestingly, treatment of both COLO 205 and PC-3 cancer cell lines with TRAIL followed by exposure to 2.0 dyn/cm^2 of

fluid shear stress significantly increased the number of apoptotic cells, compared to TRAIL-treated cancer cells exposed to static conditions. The sensitization effect was both fluid shear stress dose- and time-dependent, as the number of apoptotic cells increased with over a range of shear stress magnitudes (0.05-2.0 dyn/cm^2) and shear stress exposure times (1-120 min). However, such sensitization was not evident in doxorubicin treatment, as the percentage of apoptotic cells remained nearly identical in doxorubicin-treated samples exposed to either fluid shear stress or static conditions. The results indicated that such sensitization could be receptor-mediated apoptosis specific.

It is possible that death receptors on the cancer cell surface can sense and respond to fluid shear forces. The idea of circulating cells expressing mechanosensitive receptors has recently been investigated in leukocytes [90,91], where it is believed that G-protein coupled receptors can sense fluid shear stress and alter neutrophil adhesion to the microvasculature. However, little is known about the effects of fluid shear stress on CTC surface receptors. Insight into the mechanistic basis of such processes could reveal new strategies for treating cancer cells in the circulation, and reducing the likelihood of metastasis.

Cancer cell resistance to fluid shear stress

Recently, a microfluidic protocol was developed to assess cancer cell resistance to fluid shear stress [92]. In the protocol, dilute cancer cell suspensions were drawn up into a syringe, which is then loaded into an automatic syringe pump (Figure 1.4A).

Cancer cell suspensions were exposed to brief, millisecond pulses of high fluid shear stress as they were expelled from the syringe pump, and subsequently analyzed for cell viability using bioluminescent imaging. The maximum fluid shear stress that cancer cells were briefly exposed to in this experiment reached 6400 dyn/cm^2. Note that CTCs are momentarily exposed to shear stresses as high as 3000 dyn/cm^2 at vessel bifurcations, in the heart, and near the walls of large blood vessels [93,94]. While cancer cell viability decreased after repeated millisecond pulse exposures to high fluid shear stress, the study revealed that cancer cells of epithelial origin were surprisingly resistant to fluid shear stress, in comparison to non-transformed epithelial cells. Resistance to fluid shear stress was shown to be dependent on several oncogenes, as *myc*- and *ras*-transformed cell lines showed an increase in fluid shear stress resistance. The resistance response required extracellular calcium and actin polymerization, as the absence of calcium or treatment with EGTA, cytochalasin D, or ROCK inhibitor Y27632 all reduced cancer cell viability upon fluid shear stress exposure. In particular, extracellular calcium is important for cellular repair mechanisms based on an extracellular calcium-dependent membrane resealing process [95].

Fluid shear stress regulates cancer cell invasive potential

Prior work has shown that the chemokine gradients generated by interstitial flows can enhance tumor cell migration [96], however it is not well understood whether fluid shear stress can regulate intrinsic properties of cancer cells, thus altering their invasive

potential. Recent work by Qazi *et al.* detailed a Darcy flow apparatus for the application of fluid shear stress to a 3D collagen gel embedded with glioma cells, coupled with a modified Boyden chamber invasion assay [97]. In the apparatus, a double reservoir system applied hydrostatic pressure, which drove media throughout the 3D collagen gel and exerted shear stress on the glioma cell membranes (Figure 1.4B). Cancer cells were exposed to fluid shear stresses ranging from 0.1-0.6 dyn/cm^2. The media filtrate from the gel was collected in a separate reservoir, and the media collected was used to calculate flow rates, velocities, and shear stresses. Collagen gels were removed at the end of the flow period, and placed within modified Boyden chambers containing TGF-α to initiate invasion assays.

Fluid shear stress significantly reduced U87 and CNS-1 glioma cell migration by as much as 92% and 58% respectively, when compared to controls. Migration suppression was not due to flow-induced chemokine gradients, however, as cells were exposed to fluid shear stress followed by exposure to TGF-α in static Boyden chambers. Invasion was dependent on matrix metalloproteinases (MMP) MMP-1 and MMP-2, as MMP1 and MMP-2 gene expression was significantly downregulated in cancer cells upon exposure to 0.55 dyn cm^{-2} fluid shear stress. Previous studies have shown that fluid shear stress can affect MMP expression and activity in non-tumor cell types such as fibroblasts, chondrocytes, and smooth muscles cells [98-100], however this was one of first studies revealing that fluid shear stress-induced mechanotransduction is involved in interstitial flow-induced cancer cell motility.

Interstitial flow induces tumor cell focal adhesion kinase (FAK) activation

A recent study investigated two competing mechanisms which can alter tumor cell migration upon exposure to interstitial flow: an autologous chemotaxis-based mechanism which distributes autocrine chemokine via convection to create a chemokine gradient, and a mechanism whereby interstitial flow activates focal adhesion kinase (FAK) and modulates forces critical for tumor cell migration [101,102]. Polacheck *et al.* developed a microfluidic cell culture system to investigate the effects of interstitial flow on the directional bias and dynamics of tumor cell migration in a 3D matrix [103]. Utilizing two channels separated by a region in which tumor cells were suspended in a 3D collagen gel, a pressure gradient was applied across the gel to generate consistent interstitial flow velocities ranging from 0.3 to 3.0 μm/s, representative of a range of values measured *in vivo* [18,104]. Confocal reflective microscopy was used to track cell migration under flow, and it was found that interstitial flow and cell seeding density can both influence the direction of tumor cell migration.

Upon exposure to interstitial flow at low seeding densities, MDA-MB-321 metastatic breast cancer cells migrated in the downstream direction, or "with the flow". However, cancer cells exposed to interstitial flow at high seeding densities migrated upstream, or "against the flow". Treatment with CCR7 blocking antibodies, to block the binding of secreted ligand CCL21 needed to initiate autologous chemotaxis, caused cells to shift their migration directionality and migrated upstream upon exposure to flow. Cells that migrated in the opposite direction of flow displayed

increased phosphorylation at Tyr-397 in FAK, which plays a role in Src kinase activation and focal adhesion formation [105,106]. Upon blockage of Src kinase activity, upstream tumor cell migration decreased and displayed random cell migration.

1.1.6 CURRENT ADVANCES IN MODELING LEUKOCYTE AND TUMOR CELL MECHANOTRANSDUCTION PHENOMENA

Modeling glycocalyx effects on interstitial fluid shear stress transmission to cancer cells

The glycocalyx is a layer of proteoglycans and glycoproteins that covers eukaryotic cells, which can serve as a mechanosensor of fluid shear stress in endothelial and smooth muscle cells [107,108]. Tumor cells also possess a glycocalyx [109], however its effects as a mechansensor have not been previously investigated. It has been hypothesized that fluid shear stress generated by interstitial flows are too low to induce mechanotransduction.

Tarbell *et al.* recently developed a computational model to estimate the interstitial flow-generated fluid and solid stresses on the surface of a glycocalyx-covered cell embedded in ECM (Figure 1.5A). Previously estimated parameters such as the Darcy permeability of the ECM, tumor cell glycocalyx thickness, and interstitial fluid flow velocity were incorporated into the model to calculate the fluid and solid stresses on the cell surface. Brinkman equations were used to describe interstitial fluid flow

through pores of both the ECM and glycocalyx. A previously described model [110] was used to calculate mechanical equilibrium of forces in the direction of flow to calculate the solid stresses transmitted via the glycocalyx. While fluid stresses exerted on the tumor cell surface were estimated to be quite low (less than 0.1 dyn/cm^2), the solid stresses transmitted to the cell via the glycocalyx were predicted to be over 5.0 dyn/cm^2, a magnitude which is known to activate endothelial cells [93]. Future models could incorporate mechanical effects along with chemical signaling pathways to better predict cancer cell mechanotransduction in tissues.

Integrating signal transduction networks into adhesive dynamics simulations

Recently, signal transduction models were incorporated into AD simulations to couple signaling pathways with cell adhesion (Figure 1.5B,C). In the model, leukocytes were assigned a random spatial distribution of integrin lymphocyte function-associated antigen-1 (LFA-1), in addition to selectin ligands such as PSGL-1. The reactive surfaces were covered with selectin molecules and intracellular adhesion molecule-1 (ICAM-1), which binds to active LFA-1 and mediates firm arrest. Krasik *et al.* integrated the mitogen-activated protein kinase (MAPK) signal transduction pathway as a modular Hill function within the AD framework to model neutrophil arrest with deterministic activation [111]. Selectin ligation triggered the MAPK cascade in this model, which can cause inactive LFA-1 to become activated, enabling binding to ICAM-1 and subsequent neutrophil arrest. This model has since

incorporated a stochastic signal transduction model, utilizing a Monte Carlo simulation within the microvilli of model neutrophils [112].

Caputo *et al.* generated an adhesive dynamics simulation with an integrated signal transduction network that incorporates selectin, integrin, and chemokine interactions between the neutrophil and the substrate. A random distribution of the G-protein coupled receptor CXCR1 and chemokine interleukin-8 (IL-8) were displayed on the leukocyte and the reactive surfaces, respectively. CXCR1 can interact with IL-8, which initiates a signaling cascade leading to LFA-1 activation on the cell [113]. Beste *et al.* developed a model of T-lymphocyte arrest by combining AD with a kinetic model for chemokine-triggered inside-out integrin activation [114]. The model incorporated signaling data measured in experiments to simulate the time scale for T-lymphocyte arrest, and provided a predictive simulation for understanding chemokine control of T-lymphocyte recruitment. The integration of signal transduction networks into AD simulations could prove particularly useful for the study of cancer metastasis, as molecular defects could be implemented within the signaling cascade to predict its effects on CTC adhesion to the endothelium.

Computational models of integrin-ligand interactions at the ECM interface

A model based on the Adhesive Dynamics simulation was developed to both chemically and mechanically model integrin dynamics at the cell-ECM interface [115]. Paszek *et al.* developed the model to determine whether the cell glycocalyx and the chemical and physical parameters of the ECM can control the formation of integrin

clusters, which act as mechanical anchors and can regulate cell survival, motility, differentiation, and morphogenesis [116-118]. Integrin-ligand bonds were modeled as individual Hookean springs, and the Bell model was utilized to calculate kinetic rates of bond formation and rupture, which are distance-dependent [72,73]. In addition, the model included a lattice spring model (LSM) of the cell-ECM interface, consisting of a lattice of interconnecting nodes and springs to calculate the stress-strain behavior of the interface [119]. Model parameters including the glycocalyx, membrane, and bond spring constants, on- and off-rates, and receptor and ligand density were estimated based on experimental measurements.

Integrin clustering began as a fast process, as simulations showed that new integrin bond formation events were more likely to occur near existing integrin bonds where the separation distance between integrins and ligands was reduced. However, bond rearrangements due to bond breakage and reformation were found to slow down the integrin clustering process over time. Glycocalyx thickness also affected integrin clusters, with larger, denser clusters forming with increased glycocalyx thickness. The interplay between integrin-ligand affinity and cell-ECM repulsion due to the glycocalyx also affected clustering; high affinity interactions coupled with thinner glycocalyx resulted in bound integrin receptors with minimal clustering. A thicker glycocalyx relative to integrin bond length, along with an adequate receptor-ligand affinity, resulted in both integrin binding and clustering. Integrin clustering increased due to increases in the ratio of glycocalyx stiffness to membrane stiffness, as it increased the minimal matrix ligand density. Integrin clustering was shown to be sensitive to ECM stiffness; compliant substrates could not promote cooperative

binding, while integrin clustering increased with increasing substrate stiffness above 2000 Pa. While the computational model only incorporates basic biology, a combination of the mechanical model with molecular interactions revealed cell adhesion behavior observed in experiments [115,120]. Future models should focus on the incorporation of applied fluid shear forces, along with integrin-cytoskeleton interactions, to predict how adhesions on the cancer cell surface can sense and respond to the tumor microenvironment.

1.1.7 SUMMARY

Fluid shear stresses generated by blood and interstitial flows alter cancer cell behavior in the vascular and tumor microenvironments, respectively, and contribute to the progression of cancer metastasis. Interstitial flow-generated forces elevate tumor IFP, and create challenges to chemotherapeutic delivery to the tumor interior. Such forces also induce phenotypic changes of cells in the surrounding microenvironment, which enhance tumor cell migration and invasion. Shear flows in the circulation affect tumor cell viability while also playing a role in CTC adhesion to the endothelium, a crucial step for subsequent tumor cell extravasation and metastasis. Recent experimental studies have revealed that fluid shear stress can modulate intrinsic characteristics of cells, in addition to the extrinsic roles of fluid flow that have been previously documented. Cancer cell mechanotransduction observed in recent experiments, including tumor cell resistance to shear stress, regulation of migration and invasion, and sensitivity to chemotherapeutics, have potentially wide ranging

implications for metastasis. Recent computational models have incorporated mechanical fluid forces with chemical signaling networks, along with mechanotransducing components on the cancer cell surface, such as the glycocalyx. Future approaches utilizing computational models of fluid shear stress effects on intrinsic tumor cell signaling networks, coupled with *in vitro* and *in vivo* experimental validation, may better predict cell behavior in such dynamic microenvironments, and potentially provide novel approaches for the prevention of metastasis.

1.2 LEUKOCYTES AS CARRIERS FOR TARGETED CANCER DRUG DELIVERY

*This section is adapted from the following publication: M.J. Mitchell and M.R. King. *Expert Opinion on Drug Delivery.* In Press, 2014.

Cancer is one of the leading causes of death, with metastasis the cause of over 90% of cancer-related mortality [1]. Metastasis is initiated when cancer cells from a primary tumor invade the surrounding tissue, where they can then enter the bloodstream or lymphatic system to translocate to anatomically distant organs. Tumor cells may then exit the circulation, migrate into tissues, and proliferate to form secondary tumors. Surgical intervention, chemotherapy, and radiation are typically effective at treating primary tumors. However, metastases are difficult to detect, target, and treat therapeutically, and typically signal a poor patient prognosis, as only one in five patients diagnosed with metastatic cancer will survive more than five years [121].

Nanoparticles have shown promise in the treatment of cancer. Perhaps one of the most well-known nanoparticle formulations currently in the clinic is liposomal doxorubicin (Doxil ®), used to treat over 300,000 patients annually for Kaposi's sarcoma and ovarian cancer [122]. The advent of nanoparticles has reduced systemic toxicity of traditionally administered chemotherapeutics, enabled the controlled release of multiple small molecule drugs and proteins for continuous therapeutic delivery, and led to the development of targeting specific tumor cells within the body. Despite these advancements, it remains a challenge to deliver nanoparticle platforms

in patients with advanced forms of cancer. When cancer cells enter the bloodstream as circulating tumor cells (CTCs), they are difficult to target before they form metastases due to the fact that they are surrounded by billions of blood cells in vessels. Since nanoparticle platforms are typically administered systemically, disseminated tumor cells in tissues without a well-defined vascular structure can also be difficult to reach [121]. Additionally, hypoxic regions of tumors do not have a well defined vasculature, making systemic of delivery of nanoparticles inefficient [123,124]. For advanced nanoparticle platforms to fulfill their potential, new strategies must be developed to locally guide nanoparticles to poorly vascularized tumor tissue and CTCs.

Leukocytes have recently received much attention in the treatment of a cancer, particularly in the field of cancer immunotherapy, which utilizes the innate ability of leukocyte subpopulations to elicit anti-tumor immunity [125]. In a distinct avenue of therapy, leukocytes, which share similar migration patterns to tumor cells in blood and tissue, can also be utilized to carry current nanoparticle formulations to tumor sites that are difficult to reach via systemic administration of nanoparticles alone. Herein, I discuss recent advances in utilizing leukocytes as carriers of nanoparticles for targeted cancer drug delivery. I first discuss current nanoparticle platforms that are utilized in the treatment of cancer. Similarities in leukocyte and tumor cell migration in complex microenvironments such as blood and tumor tissue are then reviewed, with particular emphasis on cell margination in blood, adhesive interactions with the vessel wall, and migration along chemoattractant gradients to tumors and inflammatory sites. Methods to functionalize nanoparticles to leukocytes are also discussed, such as surface functionalization and internalization within cells. Finally, I review recent *in vitro* and

in vivo strategies that have been developed to use leukocytes to deliver cancer drugs to tumors and CTCs.

1.2.1 CURRENT NANOPARTICLE PLATFORMS FOR DELIVERY OF CANCER DRUGS

Various nanoparticle formulations have been developed for the delivery of cancer drugs, and have already been discussed in detail elsewhere [121,126,127]. Here, currently utilized nanoparticle platforms are overviewed within the following broad categories: polymeric nanoparticles, liposomes, metals, carbon and halloysite nanotubes, and molecular targeted nanoparticles.

Polymers

Polymeric materials comprise perhaps the largest category of nanoparticles for the delivery of cancer drugs, with many formulations currently in preclinical or clinical trials [127,128]. Composed mainly of biocompatible and biodegradable polymers, most polymeric nanoparticles are synthesized using a self-assembly process using block-copolymers consisting of multiple polymers of varying hydrophobicity. In an aqueous environment the copolymers will form core-shell particles, with hydrophobic polymers forming the core to minimize aqueous exposure, and hydrophilic polymers forming the shell to stabilize the core [129-131]. The core allows for a high loading capacity of hydrophobic and hydrophilic small molecules, in

addition to macromolecules such as nucleic acids and proteins [132], while the shell of the nanoparticle provides steric protection. Poly(lactic-*co*-glycolic acid) (PLGA)-based biodegradable nanoparticles are perhaps the most notable, as these materials are approved by the U.S. Food and Drug Administration and can be utilized to deliver a variety of cancer drugs [133,134]. Polymers such as poly(lactic acid) (PLA) and chitosan have also been utilized to develop polymeric nanoparticles [135,136]. The release of drugs from the nanoparticle can be controlled through surface or bulk erosion, diffusion through the polymer matrix, swelling or shrinking followed by diffusion, and by local changes in the environment, such as pH and temperature changes.

Liposomes

Lipids are amphiphilic small molecules that can self-assemble into nanoparticles referred to as liposomes, spherical nanoscale vesicles that possess an aqueous core. Perhaps one of the first nanoparticle platforms to be utilized in medicine [137], liposomes contain either single or multiple bilayers consisting of a variety of lipid types, both natural and synthetic [138]. Liposomes can be easily tailored in terms of size and carrying capacity, and can range from tens to hundreds of nanometers in diameter. Their versatility as a therapeutic carrier is a key advantage, as the aqueous core of liposomes allows for the encapsulation of hydrophilic agents, while the lamellae can be utilized for the encapsulation of hydrophobic agents. Liposomes can also be coated with polyethylene glycol (PEG) to enhance circulation time and

improve stability [138]. There are over a dozen liposomal formulations approved for clinical use, including Myocet™ and Doxil®, with many others currently undergoing preclinical and clinical trials [139,140].

Metals

Metal nanoparticles, typically composed of biocompatible, inert metals such as gold and titanium have been extensively studied as a therapeutic platform for thermoablation of tumor cells [141]. Under exposure to near-infrared (NIR) light, gold nanoparticles such as nanoshells and nanorods can release energy, which heat tumor tissue and result in tumor cell death [142]. This can also cause coagulation within the tumor vasculature, which can enhance the effects of other targeted therapeutics [143]. Conversely, metal nanoparticles have also been utilized for the controlled release of chemotherapeutics [144], and can be functionalized with therapeutic ligands [145]. The long-term effects of metal nanoparticle delivery of cancer therapeutics are still being investigated, as a fraction of the particles are retained within the body after administration, and can induce unwanted toxicity after repeated doses [146].

Carbon Nanotubes

Carbon nanotubes (CNTs) are well-ordered allotropes of carbon with a cylindrical nanostructure. CNTs have a uniquely high aspect ratio, with lengths ranging from hundreds of nanometers to several micrometers, and diameters ranging

from 0.4-2.0 nm for single-walled CNTs (SWNTs) to 2-100 nm for multi-walled CNTs (MWNTs) [147]. Similar to metal nanoparticles, SWNTs can emit heat when they absorb energy from near-infrared (NIR) light. The extensive surface area of SWNTs have been utilized for functionalization of antibodies specific to tumor cells for highly specific thermal ablation [148]. The surface area of SWCNTs has also been utilized for efficient loading of chemotherapeutics [149,150]. However, further investigation into the potential cytotoxic effects of CNTs is necessary. In terms of the immune system, CNTs have been shown to be phagocytosed by B- and T-lymphocytes, without affecting cell viability or functionality [151]. However, high concentrations of SWNTs can arrest cell division and induce apoptosis [152]. Chronic inhalation of SWNTs can also be a hazard, and have been shown to induce inflammation and the appearance of epithelial granulomas [153].

Molecularly Targeted Nanoparticles

The development of targeted cancer therapies has led to major breakthroughs in the treatment of cancer over the past two decades. Notable examples of targeted therapeutics include bevacizumab (Avastin®) which targets vascular endothelial growth factor (VEGF) to inhibit tumor angiogenesis [154,155], imatinib (Gleevec®) for inhibiting tyrosine kinases to treat chronic myelogenous leukemia [156], and trastuzumab (Herceptin®) to target human epidermal growth factor receptor type 2 (HER-2) for the treatment of breast cancer [157,158]. The success of these therapies has led to extensive studies combining targeting molecules with therapeutic-containing

nanoparticles. Ligands or antibodies conjugated to nanoparticles typically target proteins on the tumor cell surface, which can then be internalized by tumor cells to deliver therapeutics. This approach can enhance the concentration of drug achieved within tumors, and limit off-target cytotoxic effects. However, expression of the targeted protein on undesired cell populations can lead to off-target effects, and must be taken into account when choosing an appropriate molecule to create targeted nanoparticles.

Despite the recent technological advances in nanoparticle platforms for efficient loading and controlled release of therapeutics, local delivery to cancer sites remains a challenge. Due to challenges such as the lack of vasculature in hypoxic regions of tumors and the "needle in a haystack" problem of targeting and treating CTCs in the complex milieu of blood, new strategies need to be devised to guide nanoparticle therapeutics to target tumor cells.

1.2.2 TUMOR CELL/LEUKOCYTE SIMILARITIES IN FUNCTION

Leukocytes and tumor cells share common physical properties and adhesive interactions with vascular components. Similarities including their transport within blood, adhesion to the vessel wall, and migration into inflammatory sites in soft tissue, can potentially be exploited for efficient delivery of therapeutics.

Margination of CTCs and Leukocytes

Despite the fact that CTCs within the bloodstream are exposed to a variety of factors in blood that affect their viability, including immunological stresses, blood cell collisions, and fluid shear stress [6,159], a small fraction of these cells are able to survive these conditions, and proliferate to form metastases in anatomically distant organs. CTCs within the bloodstream are very difficult to target and treat within the bloodstream, as the concentration of CTCs in patient blood is on the order of one in a million leukocytes [42] or one in a billion erythrocytes [43], creating what is known as a "needle in a haystack" problem. However, what is known about rare CTCs is that they share similar migration characteristics with leukocytes within the bloodstream. Leukocytes tend to collect near the endothelial cell wall in venules, rather than in the center of the vessel, in a passive rheological mechanism termed margination (Figure 1.6A) [160,161]. During this phenomenon, highly deformable, biconcave-shaped erythrocytes experience a drift velocity away from the vessel wall and collect in the center of vessels, displacing less deformable leukocytes towards the periphery [162-164]. CTCs, which are closer to the larger volume and spherical shape of leukocytes than the deformable, biconcave disk-shaped erythrocytes, are also pushed towards the endothelial cell wall. Such margination phenomena can effectively surround CTCs within the circulating leukocyte population, thus making leukocytes a potentially attractive carrier of treatments to CTCs by exploiting their numerous adhesion receptors.

Tumor Cell/Leukocyte Adhesion to the Blood Vessel Wall

For free-flowing tumor cells and leukocytes to leave the bloodstream and migrate into soft tissues, they must first adhesively interact with endothelial cells that comprise the inner blood vessel wall (Figure 1.6B) [15]. The mechanisms behind leukocyte recruitment to the endothelial cell wall have been extensively studied over the past two decades [165,166]. Initially, free-flowing leukocytes in the post-capillary venules are captured along the endothelial cell wall, in the presence of wall shear stresses as low as 0.4-0.5 dyn/cm^2 [167-169]. After initial tethering, leukocytes exhibit rolling adhesion on the receptor-bearing endothelial cell wall. Rolling adhesion is mediated by selectins expressed on the surface of inflamed endothelial cells, which possess rapid, force-dependent binding kinetics, and selectin ligands on the surface of leukocytes included L-selectin and P-selectin glycoprotein ligand-1 (PSGL-1), [91,170-172]. Leukocytes can subsequently transition from rolling to firm adhesion to the vessel wall, mediated via intercellular adhesion molecule-1 (ICAM-1) on the endothelial cell surface binding to β_2 integrins on the leukocyte surface, such as macrophage-1 antigen (Mac-1) and lymphocyte function-associated antigen-1 (LFA-1) [173-176].

CTCs can be captured on the endothelial cell wall in a manner similar to leukocytes (Fig. 6B). Recent studies have shown that CTCs from various types of tumors possess sialylated carbohydrate ligands on their surface, which cause the tethering and rolling of CTCs on the selectin-bearing endothelial cell wall [177,178]. Under physiological flow conditions, E-selectin can induce tethering and rolling of

cancer cells originating from prostate [53,179], breast [180,181], and colon [180,182]. Initial selectin-mediated rolling adhesion of CTCs has been shown to be an important prerequisite to metastasis formation *in vivo* [183,184]. For example, the number of spontaneous colon carcinoma metastases formed *in vivo* decreased by 84% in P- and E-selectin deficient mice [49]. The remaining 16% of metastases formed within the pulmonary artery as CTCs were not able to transmigrate through the endothelium in the absence of E-selectin. It is not yet fully elucidated which receptors facilitate firm adhesion of CTCs to the endothelial cell wall, however there is some evidence that the mucin MUC1 can ligate ICAM-1 to enable firm adhesion and subsequent transmigration [185]. Taken together, CTCs and leukocytes share striking similarities in terms of their initial adhesion to the vessel wall. This makes selectin receptors a potentially important mediator between leukocytes and CTCs for drug delivery purposes.

Tumor Cell/Leukocyte Migration Toward Chemoattractant Gradients

Following firm adhesion to the blood vessel wall, leukocytes and tumor cells can transmigrate through the endothelium and migrate along gradients of extracellular matrix-bound or soluble chemoattractants to inflammatory sites and solid tumors (Figure 1.6C). Chemoattractants bind to G-protein coupled receptors (GPCRs) on the surface of leukocytes to activate downstream effectors, which initiate receptor internalization and signal transduction [186,187]. Such signaling induces the activation of β_2 integrins on the leukocyte surface, which induces cell adhesion, and

polarization of the actin cytoskeleton, which facilitates directional sensing and cell polarization [188,189]. Polarization allows small GTPases, Rac, Cdc42 and PI3K to accumulate at the leading edge of the leukocyte, PTEN tyrosine/PIP3 phosphatases at the posterior edges, and Rho GTPases and its effectors at the trailing edge [186]. These collectively initiate actomyosin contraction and tail retraction, which induces leukocyte migration [190]. The ability of leukocytes to respond and migrate in the presence of chemoattractants is essential in the response to inflammation, infection, and lymphocyte homing to tissues, to name a few [176,191,192].

Chemoattractant gradients also play a major role in tumor cell and leukocyte migration in the context of cancer progression [193,194]. In the tumor microenvironment, cancer epithelial cells produce higher levels of chemokines than their normal counterparts, in addition to increased expression of chemokine receptors [195]. This creates a highly inflammatory microenvironment that promotes the recruitment of leukocytes such as neutrophils, lymphocytes, and macrophages, which can influence the progression of cancer and its ability to metastasize [196-199]. Additionally, tumor cells can acquire chemoattractant receptors during transformation, and migrate along gradients typically utilized by leukocytes to form metastases in anatomically distant organs [187]. Leukocyte and tumor cell localization within difficult-to-reach tumor sites, along with their similarities in terms of migration to tissues, can be utilized to locally deliver agents such as therapeutics to induce cancer cell death, or anti-inflammatory agents to suppress the leukocyte's ability to support the tumor microenvironment.

1.2.3 METHODS TO ATTACH NANOPARTICLES TO LEUKOCYTES

The drug delivery vehicles described above can be attached to leukocytes using a variety of methods, ranging from cell surface functionalization to internalization by the leukocyte. Depending on the type of therapeutic delivered, the type of leukocyte targeted, and the site of delivery, one or a combination of functionalization methods may be needed for nanoparticle attachment.

Receptor-Mediated Adhesion

Receptor-ligand interactions are a potentially advantageous method to bind nanoparticles to the surface of leukocytes (Figure 1.7A), due to their reliability, reproducibility, and ability to trigger potentially desired cell receptor activation and signal transduction *in vivo*. For example, B-cells expressing CD44 have been utilized to bind cellular "backpacks" via interactions with its natural ligand, hyaluronic acid (HA) [200]. This approach has also been utilized to bind delivery vehicles to T-cells and macrophages [201-203]. Natural variations in receptor-ligand affinities must be taken into account, and could affect the binding strength of a nanoparticle to the leukocyte surface. Additionally, potential nonspecific receptor-ligand interactions with off-target cells, along with subsequent receptor activation and signaling, must be considered for *in vivo* applications. If utilized properly however, multiple receptor types may be conjugated to a single particle, to mediate the delivery of therapeutic between two cell types, such as leukocytes and cancer cells.

Covalent Binding

Covalent coupling of nanoparticles to the surface of leukocytes provides potentially stronger and more stable binding than receptor-mediated adhesion (Figure 1.7B). Traditionally utilized to bind maleimide-functionalized nanoparticles to amino (lysine-NH_2) or thiol (cysteine-SH) groups on proteins [204,205], similar covalent binding strategies have been used to stably bind nanoparticles to the surface of cells. Leukocytes in particular have many functional groups on their surface, such as thiols and amines, due to their large number of cell surface proteins [206,207]. This approach has been utilized to stably attach hundred of nanoparticles per cell, composed of materials ranging from liposomes to polymers, to the surface of T-lymphocytes without cytotoxic effects or loss of cell function [208]. In contrast to nanoparticles adsorbed to the surface, which can be removed during simple washing, covalent bonding promoted stable attachment that can withstand through several washing steps. In addition to prolonged surface retention, covalent bonding of nanoparticles to the cell surface can resist nanoparticle internalization, along with potentially undesired receptor activation that could be triggered by receptor-mediated attachment.

Selectin-Mediated Adhesion

Selectins provide a unique and effective way to rapidly attach nanoparticles to the surface of cells bearing selectin ligands (Figure 1.7C). The rapid, force-dependent

binding kinetics of selectins allow for nanoparticles to rapidly bind to the surface of selectin ligand-bearing cells under flow conditions. In particular, *in vitro* surfaces with immobilized P-selectin coated liposomes attached themselves to the surface of free flowing HL60 leukocytes. Utilizing E-selectin coated liposomes containing the chemotherapeutic doxorubicin, this strategy has also been utilized to attach drug-loaded particles to the surface of free flowing cancer cells as a form of CTC neutralization [82,83]. Most recently, selectin-coated nanoparticles have been shown to attach to the surface of leukocytes *directly* within human blood and within the circulation of mice [209]. This method is currently being employed to deliver apoptosis-inducing ligands to cancer cells in the circulation. Given that selectin ligands are expressed on the surface of most circulating leukocytes [171,191], selectin-mediated adhesion is advantageous for functionalizing a broad range of cells for therapeutic delivery within the circulation. In contrast to other forms of receptor-mediated attachment, selectins can be used for direct binding to leukocytes within the blood, eliminating the need to isolate leukocytes from blood, with subsequent incubation and culture steps needed for nanoparticle attachment.

Internalization

Nanoparticles can also be internalized by leukocytes for efficient delivery of therapeutics. One method to internalize particles is through the use of the natural phagocytic properties of certain leukocyte subpopulations to ingest particles (Figure 1.7D) [210,211]. Subpopulations of neutrophils, monocytes, and macrophages all

possess phagocytic properties, however monocytes and macrophages are particularly appropriate due to their longer lifespan and ability to be cultured *ex vivo*. Known as the "Trojan Horse" method, this approach has been used to internalize particles such as liposomal doxorubicin, gold nanoshells, fluorescent microspheres, and nanozymes within leukocytes [142,212-215]. It is important to note that this approach has been limited to certain subpopulations of leukocytes, and thus requires careful *ex vivo* isolation from blood. Additionally, biodegradable nanoparticles such as polymers and lipids can potentially release therapeutic within the cell, thus reducing the amount of drug delivered to the target site, and potentially causing unwanted side effects to the leukocyte carrier. The "Trojan Horse" approach has unique advantages, however, in that it eliminates the need to occupy the cell membrane and potentially interfere with receptor-ligand interactions. Additionally, this approach avoids undesired cell surface receptor signaling that can be encountered with receptor-mediated attachment of nanoparticles.

1.2.4 LEUKOCYTES AS CARRIERS OF NANOPARTICLES TO METASTATIC CELLS AND TUMORS: INITIAL RESULTS

Over the past several years, initial results have shown that leukocytes are effective at carrying drugs and nanoparticles to difficult-to-target sites for cancer therapy. Nanoparticles can either be stably attached to the leukocyte surface, or internalized within the cell, to efficiently deliver drugs deep within tumors, and most

recently, to deliver cell death-inducing ligands to eradicate rare tumor cells within the bloodstream.

Leukocyte "Trojan Horses" for Nanoparticle Delivery to Solid Tumors

Some of the initial studies focused on utilizing leukocytes as "Trojan Horses" for delivery of therapeutics to solid tumors. As tumors grow rapidly, the tumor core becomes distanced from the nearest capillaries, causing these cells to become necrotic and/or hypoxic [123,124]. Additionally, the lack of a vasculature hinders the delivery of nanoparticle-based therapeutics to core region of the tumor. While nanoparticles may lack the ability to reach these sites, monocytes can be recruited from the peripheral blood to sites of tumors due to chemoattractant gradients. Additionally, monocytes have an innate phagocytic ability, which can be utilized to internalize nanoparticles as a means to carry therapeutics to tumors (Figure 1.8A).

Gold nanoshells have been suggested as an ideal therapeutic to be utilized within cellular "Trojan Horses" [142], given that they can be uptaken by tumor cells and induce cell death by photoablation via near-infrared (NIR) light, which can increase tumor tissue temperature by over 30°C in the presence of nanoshells [216]. Initial work has shown that monocytes successfully phagocytose gold nanoshells over a period of 24 h. Macrophages, which are differentiated from monocytes upon migration into tumors, also successfully phagocytose gold nanoshells over similar incubation periods. Cell death was induced in nanoshell-containing macrophages via photoablation (Figure 1.8B), which induces the release of nanoshells within the tumor

to allow for tumor cell uptake, and subsequent heating and killing of tumor tissue via NIR (Figure 1.8C). In an *in vitro* model of the macrophage infiltration tumor microenvironment, macrophages and gold nanoshells were co-cultured with breast tumor spheroids. Macrophages were found to infiltrate tumor spheroids *in* vitro, and cell death of macrophages was induced by photoablation.

The "Trojan Horse" approach has also been exploited to deliver nanoparticles to experimental brain metastases. Nanoparticle uptake in the brain is hindered by physical barriers such as the blood-brain barrier (BBB) and blood-cerebrospinal fluid barrier [217,218]. However, macrophages of peripheral blood monocyte origin are able to infiltrate brain metastases despite the presence of an intact blood brain barrier[219], and are also present in clinical brain tumor specimens at contents ranging from 4 to 70% [220]. Thus, macrophages have been utilized as "Trojan Horses" to cross the BBB and deliver therapeutics to metastatic deposits in the brain. Both nanoshells and fluorescent microspheres, utilized for therapeutic and diagnostic purposes, respectively, were successfully phagocytosed and localized within vacuoles in the cytoplasm of monocytes and macrophages [213]. Utilizing brain tumor xenografts in mice, both macrophages and internalized microspheres were found within brain metastases, 24 h post-injection into mice.

The "Trojan Horse" approach can also be used to deliver chemotherapeutics to tumors *in vivo* [212]. Utilizing mouse peritoneal macrophages, which were shown to migrate into A549 subcutaneous tumors *in vivo*, liposomal doxorubicin (LP-Dox) was internalized within macrophages, which remained viable for over 12 h, even at high concentrations of LP-Dox. LP-Dox was released from macrophages and induced cell

death in A549 cancer cells *in vitro*. Upon injection *in vivo,* macrophages containing LP-Dox infiltrated the interior of A549 subcutaneous tumors, and their migration was characterized via the intrinsic fluorescence of doxorubicin. Additionally, tumor treatment with systemic injections of macrophages containing LP-Dox induced A549 subcutaneous tumor reduction over a 35-day span, compared to controls. Taken together, the ability of monocytes and macrophages to migrate along chemoattractant gradients and penetrate the BBB can be utilized in the "Trojan Horse" approach to deliver a variety of nanoparticle-based therapeutics and imaging agents to tumor tissues that are typically difficult to target via systemic injection.

Most recently, single walled carbon nanotubes (SWNTs) were found to be uptaken almost exclusively by a single subpopulation of leukocytes [221]. SWNTs were injected into the tail vein of mice, and intravital microscopy was used to observe that nanotubes were uptaken into circulating blood cells. Upon blood draw and subsequent FACS analysis of SWNT+ blood cells, only a specific monocyte subset, known as Ly-6C^{hi} lymphocytes, displayed substantial SWNT uptake. Interestingly, only <3% of neutrophils, <1% of lymphocytes, and <1% of Ly-6C^{low} lymphocytes took up SWNTs, while nearly 100% of Ly-6C^{hi} lymphocytes displayed SWNT uptake. The subpopulation of monocytes containing SWNTs were able to enter tumor interstitium, and SWNTs functionalized with an RGD peptide significantly enhanced the number of monocytes reaching the tumor site. While the mechanisms behind SWNT selectivity to specific leukocyte subpopulations and increased monocyte targeting to tumors in the presence of RGD are not yet understood, identification of specific circulating immune cell populations for the delivery of nanoparticles may

have important implications for both cancer therapeutics and diagnostics. Furthermore, the enhanced infiltration of monocytes due to presence of RGD extends the "Trojan Horse" approach, demonstrating that the delivery of nanotube-containing monocytes is not merely reliant on the innate homing abilities of monocytes.

Lymphocyte Surface Engineering for Nanoparticle Delivery to Solid Tumors

In addition to uptake and internalization, nanoparticles can also be conjugated to the extensive surface area of leukocytes for delivery into solid tumors. Exploiting the thiol-rich surface of T-lymphocytes, liposomes and lipid-coated polymer nanoparticles with thiol-reactive maleimide headgroups were stably attached to the cell surface, without affecting key cellular functions [208]. Additionally, nanoparticle conjugation to the surface of T-cells was observed to affect their ability to traffic to tumors, thus allowing nanoparticles to be effectively carried to the tumor site. Particles were loaded with cytokines interleukin-15 (IL-15) and IL-21, to amplify the therapeutic functions of T-cells to treat lung and bone metastases. While systemic injections of free cytokines and T-cells did not have a significant effect on T-cell proliferation within tumors, systemic injection of T-cells carrying cytokine-loaded nanoparticles were able to localize within tumors and robustly proliferate *in vivo*. All mice receiving nanoparticle-conjugated T-cells were able to completely eradicate lung and bone tumors.

Further investigation of maleimide-functionalized nanoparticle conjugation to thiols on the T-cell surface has shown the ability to deliver compounds into the T-cell

synapse, as a means to boost anti-tumor immunity [222]. While migrating T-cells carried surface-linked nanoparticles at the uropod, they were rapidly redistributed to the immunological synapse (IS) during target tumor cell recognition. To exploit this redistribution, nanoparticles were used to deliver an inhibitor of key phosphatases to downregulate T-cell receptor activation at the synapse, blocking suppressive signals from tumor cells that typically restrain anti-tumor activity. *In vitro*, conjugation of inhibitor-encapsulated nanoparticles to the T-cell surface significantly enhanced their proliferation, compared to controls. Conjugation of the loaded nanoparticles also promoted T-cell expansion in orthotopic prostate tumors *in vivo*, reduced tumor burden, and enhanced survival compared to controls. These results show that leukocyte-mediated delivery of therapeutics can even serve to enhance cancer immunotherapy, by locally delivering the cytokines and inhibitors necessary to enhance the T-cell response with tumors for anti-tumor immunity *in vivo*.

NK Cell Surface Engineering to Target Models of Lymph Node Micrometastasis

Approaches using functionalized leukocytes have been assessed *in vitro* for the therapeutic targeting of metastasis, which can occur via the vascular or lymphatic circulation [223]. Cancer cells traveling through the lymphatic circulation can lodge within sentinel lymph nodes (SLN), where they lie dormant for a period of time before forming micrometastases [224]. Also present within the lymphatic circulation and SLN are many immune cells that typically respond to tumor antigens, such as lymphocytes, macrophages, and antigen-presenting cells. In particular, natural killer

(NK) cells have been shown to activate apoptotic pathways in cancer cells [225], kill most tumor cells within the circulation [226], and reside within lymph nodes [227]. Despite this, cancer cells continue to evade the host immune response [228]. Evidence of morphological and functional variation in cancer patient SLNs suggests potential immune suppression, which can result in the failure to eliminate micrometastases in SLNs. Thus, the presence of micrometastases within SLNs typical signals a poor prognosis in cancer patients after surgical resection of the primary tumor [229-231].

In an attempt to functionalize NK cells to overcome immune suppression, the surface of NK cells was functionalized with TRAIL liposomes to kill cancer cells in *in vitro* models of lymph node micrometastases. TRAIL binds to death receptors DR4 and DR5 on the surface of a variety of cancer cell types, which induces apoptosis through intrinsic and extrinsic pathways [86,232,233]. Thiolated TRAIL protein and anti-CD57 were covalently bound to maleimide groups on the surface of liposomes (Figure 1.9A,B). Conjugation of liposomes to the surface of NK cells was facilitated by antibody binding to CD57 (Figure 1.9C,D), a marker found on a subpopulation of NK cells [234]. As an *in vitro* model of SLNs, functionalized NK cells were seeded into microbubbles compromised of PDMS (Figure 1.9E), which mimic both the size and elastic modulus of lymph nodes [235]. MDA-MB-231, COLO 205, and LNCaP cancer cells, which typically metastasize to lymph nodes, were then cultured within microbubbles containing functionalized NK cells. After 24 h in culture, functionalized NK cells successfully induced cancer cell apoptosis in the *in vitro* model of SLNs (Figure 1.9F). This approach provides not only an *in vitro* model to assess the sensitivity of lymph node micrometastases to therapeutics, but also a potential means

to enhance the NK cell therapeutic response to micrometastases within lymph nodes, which can become immune suppressive in cancer patients. Further studies will be required to assess successful *in vivo* functionalization and subsequent localization of NK cells to SLNs, as a means to target metastases within lymph.

Targeting Metastatic Cells in the Bloodstream

Recently, a unique approach termed "unnatural killer cells", leukocytes functionalized to target and kill cancer cells within blood, was developed as a means to neutralize circulating tumor cells (CTCs) with the potential to form new metastases [209]. To target and kill cancer cells, nanoscale liposomes were functionalized with the adhesion receptor E-selectin (ES) and the apoptosis-inducing ligand tumor necrosis factor-related apoptosis-inducing ligand (TRAIL) (Figure 1.10A). Selectins facilitate rapid, force-dependent adhesion to selectin ligands on tumor cells and leukocytes in blood (Figure 1.10A), which then allows TRAIL ligands to come within a reactive distance of death receptors on the cancer cell surface, signaling for cell apoptosis. TRAIL is an ideal therapeutic for this delivery method due to the fact that it preferentially induces apoptosis in cancer cells, while exerting minimal cytotoxic effects on most normal cells [236]. Interestingly, ES/TRAIL liposomes bound remarkably well to the surface of many types of leukocytes in blood under flow conditions (Figure 1.10B), with minimal cytotoxic effects. Upon treatment of cancer cells with ES/TRAIL liposomes in human blood under flow conditions, negligible viable cancer cells remained after only 2 h of treatment (Figure 1.10C,D). While blood

typically reduces therapeutic efficacy through cellular internalization and nonspecific binding of the therapeutic to plasma proteins, the ability of ES/TRAIL liposomes to target and kill cancer cells was enhanced in human blood, compared to conditions in buffer alone (Figure 1.10E). Alteration in hematocrit levels (Figure 1.10F), in addition to removal of all ES/TRAIL liposomes unbound to leukocytes in blood, demonstrates that blood cells are essential in the enhanced apoptotic response of cancer cells in blood. Upon addition of ES/ TRAIL liposomes to cancer cell-spiked blood, liposomes attach to the surface of leukocytes and are available for inducing apoptosis in cancer cells that they come into contact with (Figure 1.10G). Liposome tethering to the leukocyte surface can also enhance cancer cell apoptosis due to the compressive forces between cancer cells and leukocyte under flow. Compressive forces act to flatten the cancer cell glycocalyx [237], composed of biologically inert macromolecules, thus allowing TRAIL to come within a reactive distance to the cancer cell death receptors and form bonds. This approach is intended to neutralize CTCs as rare as 1-100 cells per mL in blood [42,238], and margination of leukocytes and CTCs along the vessel wall allows CTCs to essentially become surrounded by the circulating leukocyte population. Thus, upon functionalization of leukocytes in blood, CTCs can essentially be surrounded by both adhesion receptors and therapeutic ligands upon entering the bloodstream, thus increasing the probability of neutralizing rare CTCs before they are able to form new metastases.

Significant progress has been made in utilizing “unnatural killer cells” to target and kill cancer cells in the peripheral circulation of mice *in vivo*. ES/TRAIL liposomes were injected into the peripheral circulation of mice (Figure 1.10H), where they

successfully tethered to the surface of leukocytes (Figure 1.10I). Following ES/TRAIL liposome injection, tail vein injection of cancer cells was utilized to model leukocyte/CTC interactions within the mouse circulation, representing a common model of lung metastasis [239-242] since the early work of Fidler et al. [243-245]. Upon removal of the peripheral blood from the circulation after 2 h via cardiac puncture, negligible viable cancer cells were found remaining compared to controls (Figure 1.10J). Upon examination of the remaining cancer cells within the mouse vasculature using multiphoton microscopy (Figure 1.10K), it was found that there were far fewer cancer cells in the lungs of treated mice, with the majority of remaining cancer cells apoptotic in treated mice but not in the control group (Figure 1.10L). In addition to the advantages of this approach discussed above, tethering liposomes to the surface of leukocytes in blood is beneficial for increasing liposome circulation time, by avoiding renal clearance mechanisms. By focusing the therapeutic effects to within the vascular microenvironment, reduced dosages are needed to target metastatic cells, as the dosages of TRAIL used in this current study were approximately two orders of magnitude lower than the dosages used in human clinical trials [246-248]. Representing an important first step in targeting CTCs in the bloodstream, the "unnatural killer cells" approach can potentially be utilized as a preventative measure upon diagnosis of highly metastatic hematogenous cancers that originate from epithelial tissues including breast, prostate, and lung.

1.2.5 SUMMARY

Due to their shared ability to marginate in blood, adhesively interact with the blood vessel wall, and migrate along chemoattractant gradients to tumors and sites of inflammation, leukocytes have the potential to guide advanced nanoparticle platforms directed at CTCs and malignant tissues that have not previously been targeted successfully. Nanoparticles can be conjugated to the surface of leukocytes via methods such as receptor-mediated adhesion, covalent coupling, and selectin-mediated adhesion. Nanoparticles can also be internalized within phagocytic leukocytes, for efficient drug delivery while leaving the cell membrane unoccupied. Leukocyte carriers have proven effective in delivering drugs to solid tumors, models of lymph node metastasis, and cancer cells in the circulation *in vivo*. The promise of leukocytes as carriers of nanoparticle therapeutics warrants further investigation for applications including drug delivery to CTCs, metastatic tumor sites, and hypoxic regions of tumors, to name a few.

FIGURE 1.1: CANCER CELL EXPOSURE TO FLUID SHEAR STRESS IN THE TUMOR AND VASCULAR MICROENVIRONMENTS. (A) Tumor cell exposed to interstitial flow in a collagen matrix. (B) Circulating tumor cell (CTC) exposed to fluid shear forces in a blood vessel.

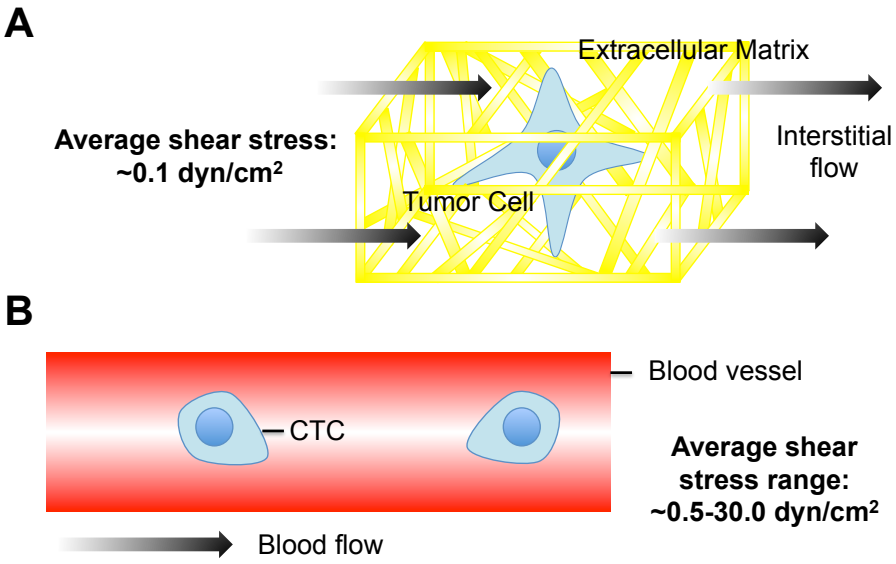

FIGURE 1.2: COMPUTATIONAL MODELS OF CELLS EXPOSED TO BLOOD AND INTERSTITIAL FLOWS. (A) Computational models utilizing the Brinkman equation to estimate interstitial flow-generated shear stresses on the cell surface [21]. u_∞: velocity far from cell surface. (B) Adhesive dynamics (AD) simulations to predict selectin-mediated adhesion to the endothelium [249]. *u*: velocity. *R*: cell radius. sLex: sialyl-Lewis-x. ICAM-1: intercellular adhesion molecule-1.

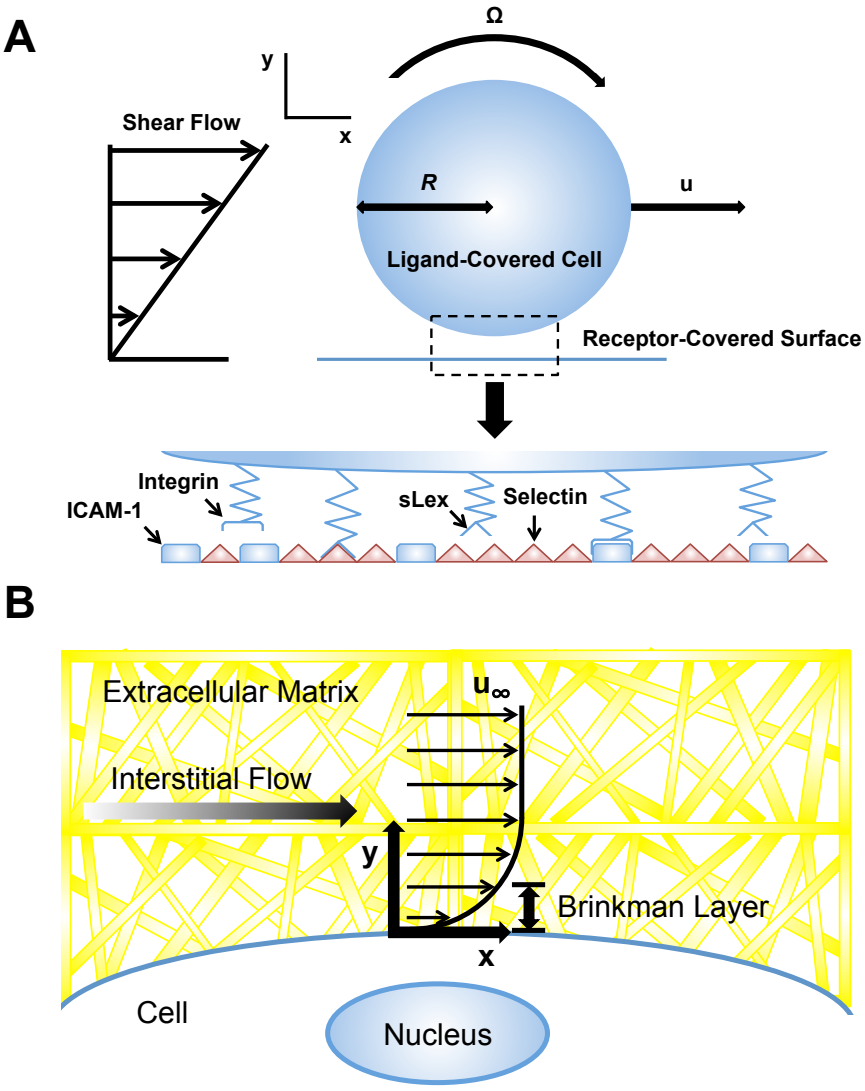

FIGURE 1.3: FLUID SHEAR STRESS SENSITIZES CANCER CELLS TO THE APOPTOSIS-INDUCING LIGAND TRAIL. Colorectal adenocarcinoma COLO 205 cells exposed to non-shear conditions (A) and fluid shear stress (B), respectively. COLO 205 cells treated with TRAIL and then exposed to non-shear conditions (C) and fluid shear stress (D). Lower left-hand and right-hand quadrants of each flow cytometry figure represent viable cells and cells in early stages of apoptosis, respectively. Upper left-hand and right-hand quadrants represent cells undergoing necrosis and late stage apoptosis, respectively. Percentage of viable (E) and apoptotic (F) COLO 205 cells after treatment with TRAIL followed by exposure to non-shear or shear conditions (n = 3). Percentage of viable (G) and apoptotic (H) PC-3 cells treated under the same conditions (n = 3). PI: propidium iodide. FITC: Fluorescein isothiocyanate. Error bars represent 95% confidence intervals. ∗P < 0.05. ∗∗P < 0.01. NS: non-significant. Figure reprinted with permission from Mitchell *et al*. [86].

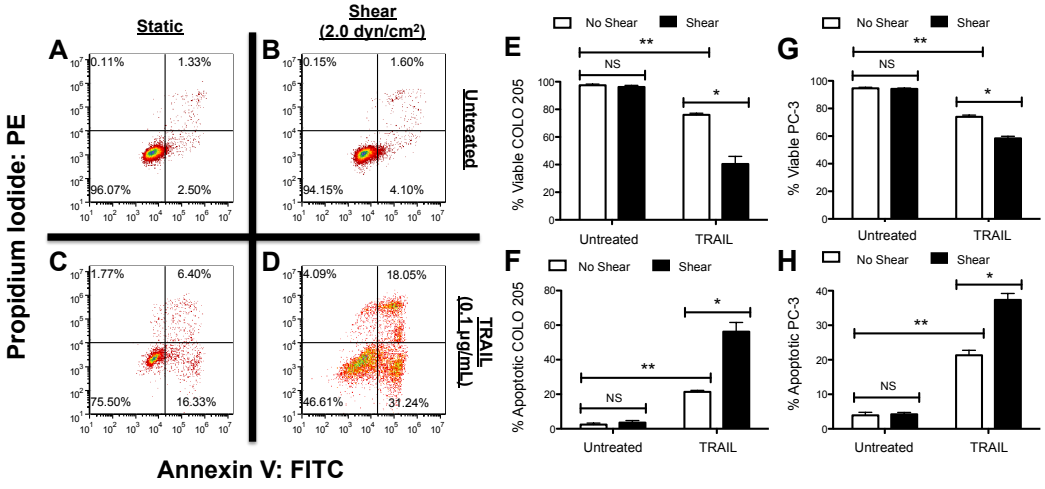

FIGURE 1.4: EXPERIMENTAL TECHNIQUES TO STUDY CANCER CELL MECHANOTRANSDUCTION. (A) Microfluidic protocol to deliver millisecond pulses of fluid shear stress to tumor cells [92]. Tumor cell resistance to fluid shear stress determined using bioluminescent imaging (BLI). (B) Darcy flow apparatus for the application of fluid shear stress in 3D to tumor cells embedded in collagen [97]. Shear stress-exposed cells are then placed in a modified Boyden chamber to measure their migratory and invasive potential in the presence of TGF-α.

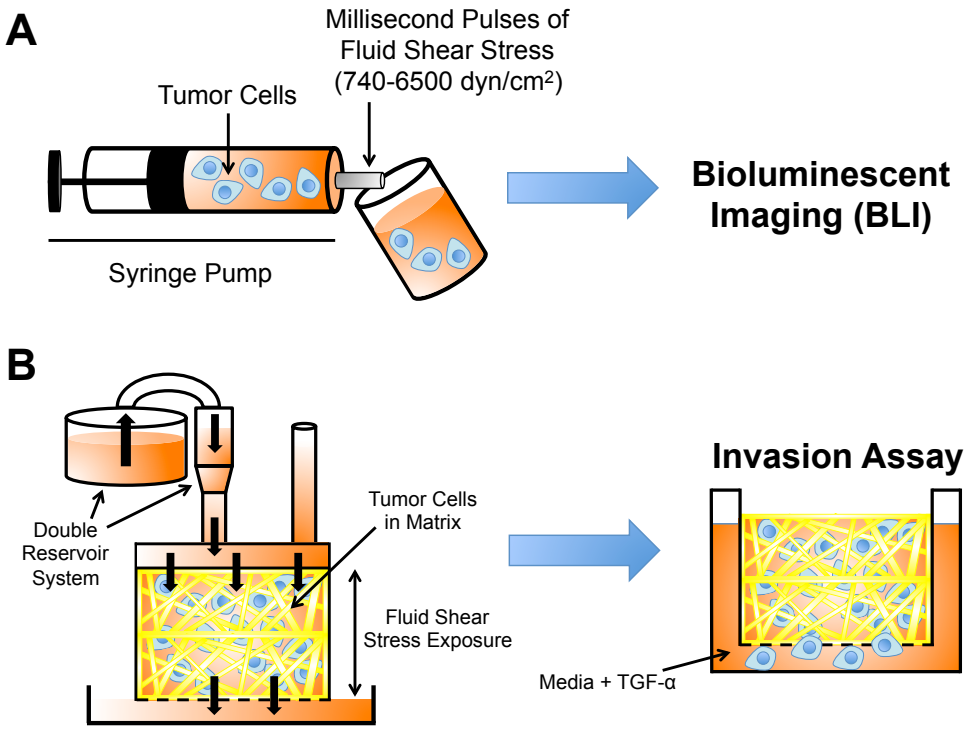

FIGURE 1.5: ADVANCES IN COMPUTATIONAL MODELING REVEAL MECHANOTRANSDUCTION PHENOMENA. (A) Interstitial flow models incorporating the force-transducing cell glycocalyx to determine interstitial flow contributions to fluid shear stress-dependent mechanotransduction [21]. u_∞: velocity far from cell surface. K_m: matrix Darcy permeability. K_g: glycocalyx Darcy permeability. H: glycocalyx layer. $u_{g\infty}$: velocity profile in glyocalyx. τ_w: surface fluid stress. τ_{wg}: surface solid stress. (B,C) Incorporation of cell signaling networks to predict flow-mediated cell adhesion in the presence of chemoattractants [113]. IL-8: interleukin-8. PSGL-1: P-selectin glycoprotein ligand-1. LFA-1: lymphocyte function-associated antigen 1.

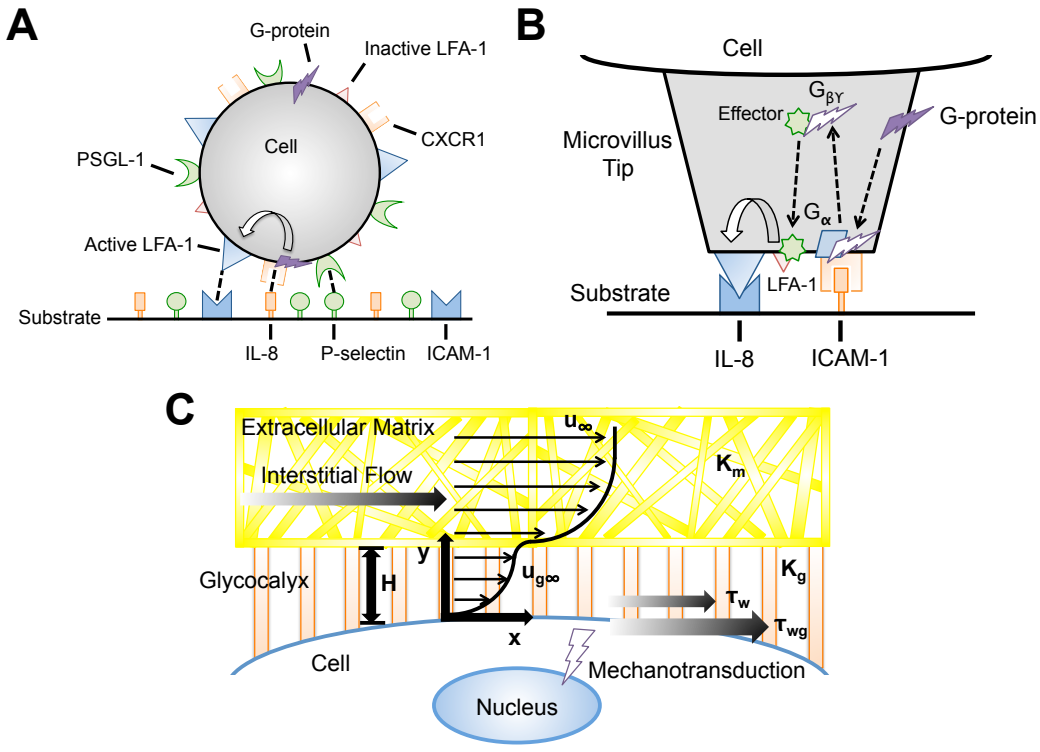

FIGURE 1.6: TUMOR CELL AND LEUKOCYTE TRAFFICKING SIMILARITIES. (**A**) Margination in the vascular system. Deformable red blood cells drive leukocytes and CTCs to a marginated position near the vessel wall, due to their higher drift velocity away from walls. (**B**) Adhesion to inflamed blood vessels. Upon the onset of inflammation, endothelial cells upregulate E-selectin expression, which can cause free flowing, selectin ligand-bearing leukocytes to adhesively interact with the endothelial cell wall. CTCs are also known to express sialylated carbohydrate ligands on their surface, which can adhere to selectins on the surface of the endothelium. (**C**) Transmigration into tissues. Upon firm adhesion to the endothelial cell wall, leukocytes are known to transmigrate into the extravascular space and migrate along chemoattractant gradients to the site of inflammation. CTCs also respond to chemoattractants and transmigrate to inflammatory sites, where they may then survive and form micrometastases.

FIGURE 1.6: TUMOR CELL AND LEUKOCYTE TRAFFICKING SIMILARITIES.

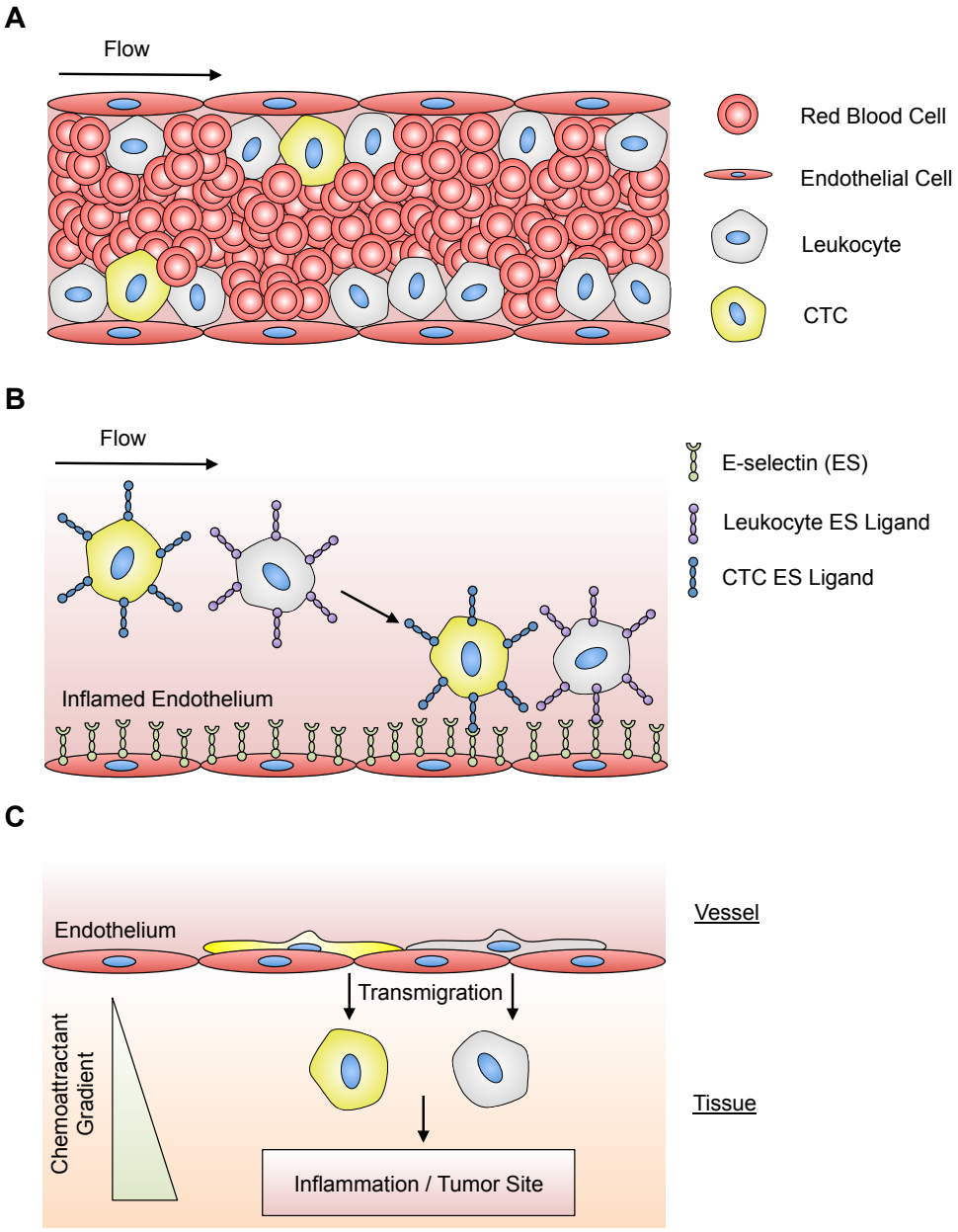

FIGURE 1.7: APPROACHES TO FUNCTIONALIZE LEUKOCYTES WITH DRUG DELIVERY VEHICLES (DDV). (**A**) Covalent bonding of maleimide-bearing DDVs to thiol groups on the protein-covered leukocyte surface. (**B**) Receptor-ligand interactions to attach DDVs to the leukocyte surface. (**C**) Selectin-coated DDVs bind to leukocytes within the circulation under flow conditions. (**D**) Internalization of DDVs by phagocytic leukocytes.

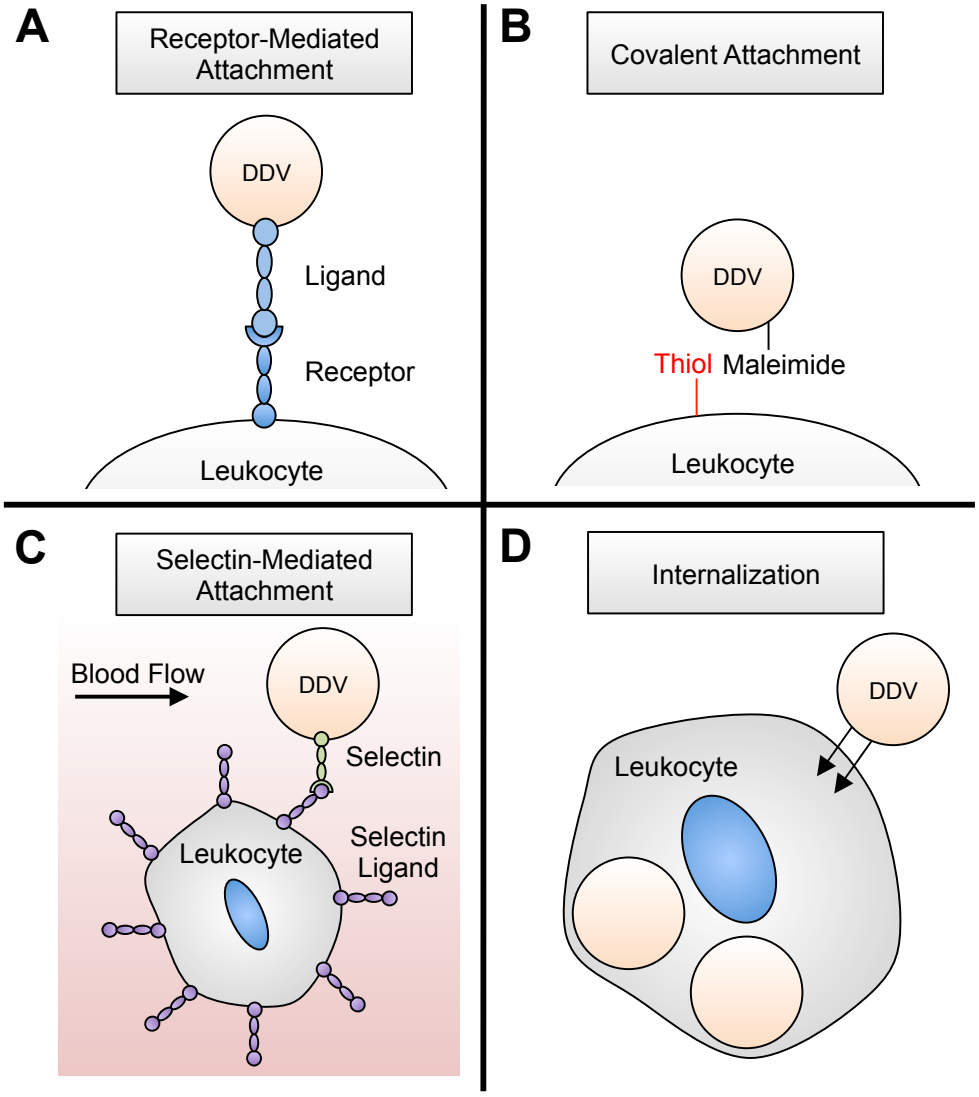

FIGURE 1.8: CELLULAR "TROJAN HORSE" MECHANISM TO DELIVER NANOPARTICLE-BASED THERAPEUTICS TO SOLID TUMORS. (**A**) Monocytes and/or macrophages that typically infiltrate solid tumors internalize therapeutic and/or diagnostic nanoparticles for delivery into tumor sites. (**B**) Monocytes/macrophages containing gold nanoshells can be photoablated by near-infrared (NIR), inducing cell death and releasing therapeutics and/or nanoshells for uptake into tumor cells. (**C**) Tumor cell death then occurs via (1) therapeutic delivery in tumor cells or (2) heating of nanoshell-containing tumor tissue by NIR.

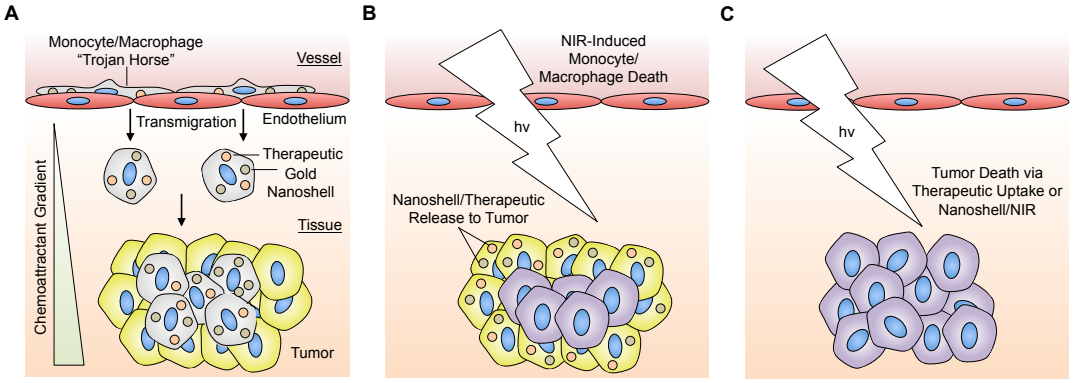

FIGURE 1.9: FUNCTIONALIZED NATURAL KILLER (NK) CELLS TO TARGET LYMPH NODE MICROMETASTASES. (**A,B**) Liposomes with maleimide groups (**A**) react with thiolated apoptosis-inducing ligand TRAIL and anti-CD57 antibodies. (**C**) Liposomes functionalized to surface of NK cells via antibody binding to CD57. (**D**) Micrographs of fluorescent liposomes functionalized to the NK cell surface. Scale bar = 100 µm. (**E**) Schematic of functionalized NK cell intervention in an *in vitro* model of lymph node micrometastasis. (**F**) Brightfield and fluorescent micrographs of functionalized NK cells inducing cancer cell apoptosis in an *in vitro* model of lymph node micrometastases comprised of MDA-MB-231, COLO 205, and LNCaP cancer cells. Cells are labeled with Annexin-V (green) and propidium iodide (red) after 12 h and 24 h to assess cell viability. Scale bar = 100 µm. Figure parts adapted from [250].

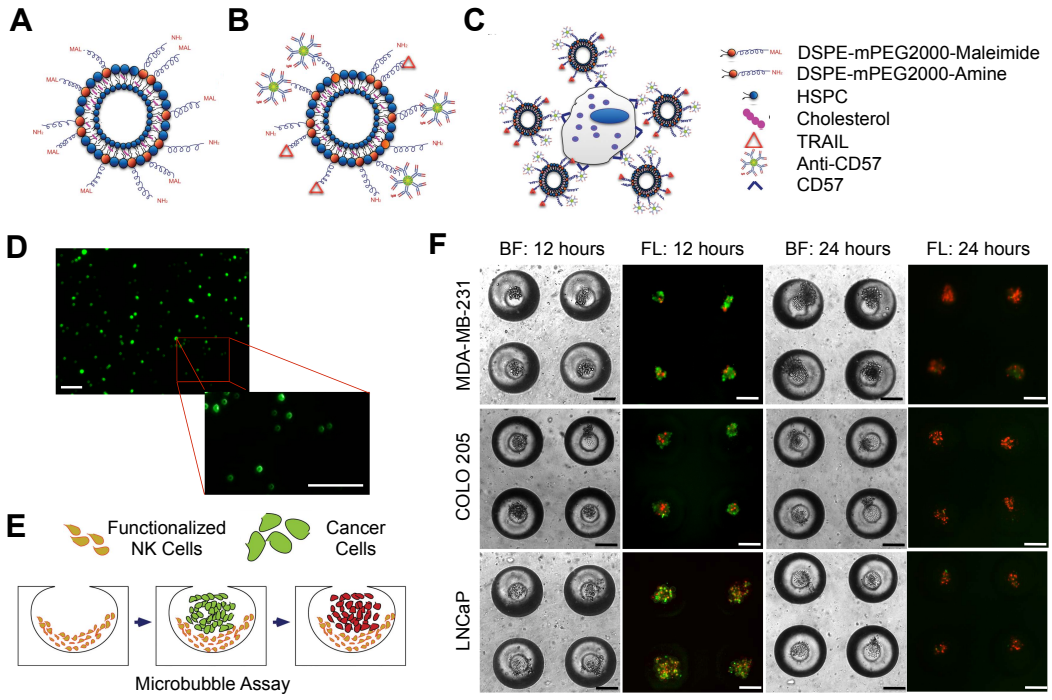

FIGURE 1.10: UNNATURAL KILLER CELLS TO TARGET AND KILL CANCER CELLS IN FLOWING HUMAN BLOOD *IN VITRO* AND IN THE PERIPHERAL CIRCULATION OF MICE *IN VIVO*. (**A**) Schematic of E-selectin(ES)/TRAIL functionalized liposome synthesis. (**B**) Confocal micrographs of fluorescent ES/TRAIL liposomes functionalized to the surface of leukocytes after exposure to blood flow. Scale bar = 5 μm. Green: ES/TRAIL liposome. Blue: leukocyte nucleus. (**C**) Micrographs of COLO 205 cells (white) after treatment with ES/TRAIL liposomes (left) or ES-conjugated liposomes in blood under shear flow for 2 h. Scale bar = 50 μm. (**D**) Flow cytometry of COLO 205 cancer cells after treatment with ES/TRAIL or ES liposomes in blood under shear flow in a cone-and-plate viscometer (shear rate: 188 s^{-1}) for 2 h. Unsheared: viable untreated cancer cell control. (**E**) Comparison of fraction of viable COLO 205 and PC-3 cancer cells after treatment with ES/TRAIL liposomes in buffer versus blood. n = 3 for all samples. Bars represent the mean ± SD in each treatment group. ***P < 0.0001 (unpaired t test). (**F**) Fraction of viable COLO 205 and PC-3 cancer cells after treatment with ES/TRAIL liposomes in blood with varying percentages of hematocrit. Hematocrit was varied whereas other blood components remained constant, based on a normal hematocrit of 45%. Plasma indicates removal of all blood cells. n = 3 for all samples. Bars represent the mean ± SD in each treatment group. *P < 0.05 (one-way ANOVA with Tukey post-test). (**G**) Schematic of two-step mechanism involving functionalization of leukocytes with liposomes (left), which then contact circulating cancer cells and activate the death receptor (right). (**H**) Schematic of *in vivo* mouse experiment to functionalize leukocytes via systemic delivery of ES/TRAIL liposomes,

followed by targeting of circulating cancer cells in the bloodstream. (**I**) Representative micrographs of COLO 205 cancer cells removed from mouse circulation after treatment with ES/TRAIL liposomes (Upper Left), sTRAIL (Upper Right), ES liposomes (Lower Left), and buffer (Lower Right) injections. Scale bar = 20 μm. (**J**) Leukocytes functionalized with fluorescent ES/TRAIL liposomes (green) upon removal from mouse circulation 2.5 h after systemic injection. Scale bar = 50 μm. (**K**) Schematic of mouse lung and example two-photon excited fluorescence (2PEF) image stack from mouse lung where Hoechst-labeled COLO 205 cells (green) are arrested in vasculature of lung (visible by autofluorescence, yellow). Scale bar = 80 μm. (**L**) 2PEF images of Hoescht-labeled COLO 205 cells (green) with Alexa Fluor 568-labeled Annexin-V apoptosis probe (red) for each experimental group. Red arrows point to apoptotic COLO 205 cells (red and green colocalized), and blue arrows indicate non-apoptotic COLO 205 cells (green only). White circles indicate regions of autofluorescence from lung tissue. Scale bar = 30 μm. Figure parts adapted from [209].

FIGURE 1.10: UNNATURAL KILLER CELLS TO TARGET AND KILL CANCER CELLS IN FLOWING HUMAN BLOOD *IN VITRO* AND IN THE PERIPHERAL CIRCULATION OF MICE *IN VIVO*.

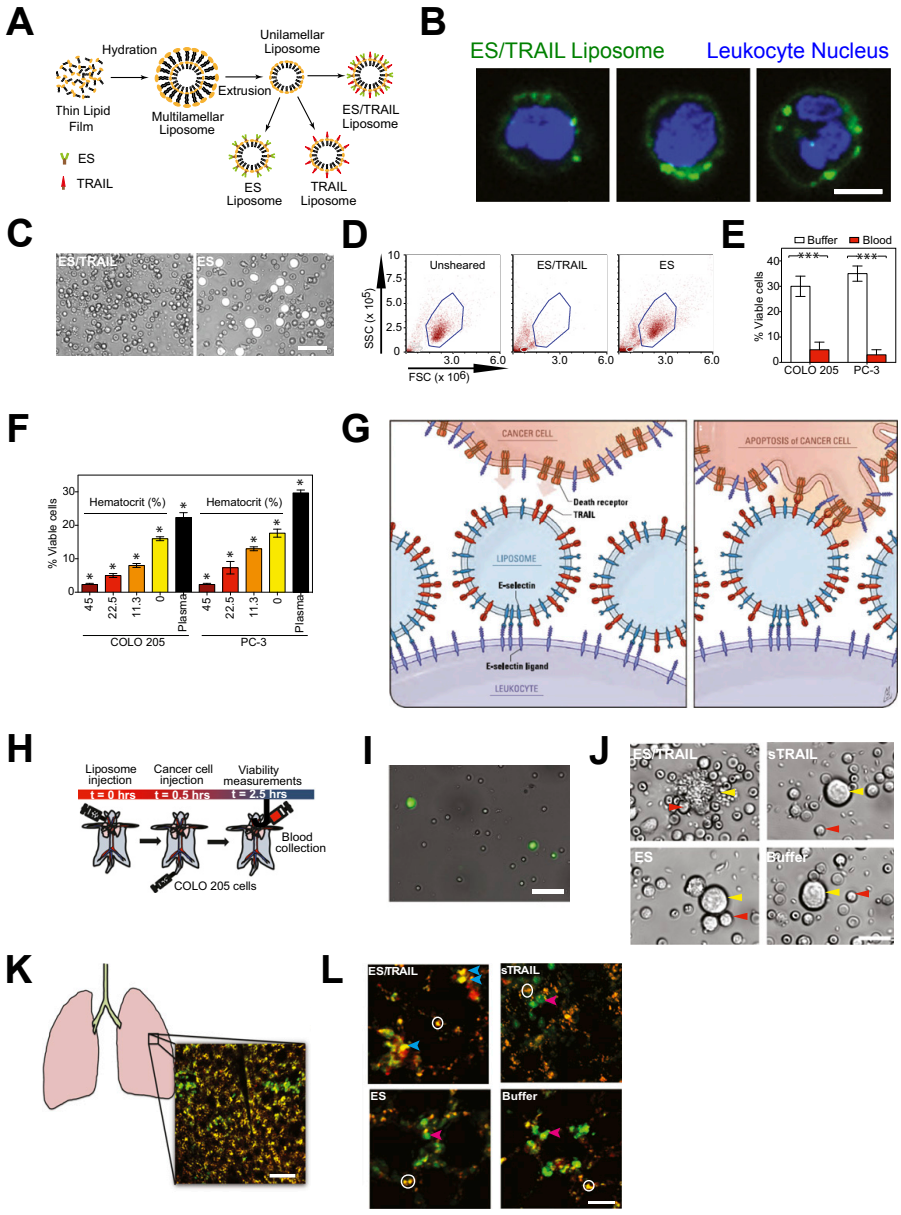

CHAPTER 2: SHEAR-INDUCED RESISTANCE TO NEUTROPHIL ACTIVATION VIA THE FORMYL PEPTIDE RECEPTOR

*This section is adapted from the following publication: M.J. Mitchell and M.R. King. *Biophysical Journal.* 102(8): 1804-1814, 2012.

2.1 INTRODUCTION

The adhesion of leukocytes to the luminal surface of the microvasculature plays an important role in the inflammatory response and lymphocyte homing to lymphatic tissues [176,192,251]. The initial step of the leukocyte adhesion cascade involves the capture and rolling of leukocytes on the receptor bearing endothelial cell layer, with L-selectin acting as an important mediator on the leukocyte surface [252]. Experiments with L-selectin knockout mice show severely impaired leukocyte migration into the inflamed endothelial wall, along with virtually no lymphocyte migration to lymphatic tissues [253,254]. While E-selectin and P-selectin are cell adhesion molecules expressed on activated endothelial cells, L-selectin is constitutively expressed on the microvilli tips of neutrophils. In contrast to E-selectin and P-selectin, L-selectin is rapidly cleaved from the neutrophil surface due to an inflammatory stimulus and cellular activation [255]. In addition, the firm adhesion of neutrophils to endothelial cells in the vasculature is mediated via intracellular adhesion molecule-1 (ICAM-1) on endothelial cells binding to β_2 integrins on neutrophils, such as CD11b/CD18 or Mac-1, and CD11a/CD18 or LFA-1 [175,176]. Together, the downregulation of L-selectin along with the active conformational change of the α_M subunit of $\alpha_M\beta_2$ integrins, leading to increased binding affinity, are key indicators of neutrophil activation [256,257]. Stimulus by fMLP, which binds to the formyl peptide receptor (FPR) on neutrophils, has shown to lead to β_2 integrin conformational changes and downregulation of L-selectin [188,189,258,259].

FPR, a chemoattractant G-protein coupled receptor (GPCR), exhibits high constitutive activity in addition to activity due to agonist binding [260,261]. Under static conditions in the absence of fluid shear stress, neutrophils spread their cytoplasm and are able to migrate on a glass substrate, in part due to constitutive GPCR activity. In the presence of fluid shear stress, neutrophils have shown to rapidly retract lamellipodia, assume a round resting state, and decrease GPCR constitutive activity [9,90,262]. Neutrophils treated with pertussis toxin, a Gi inhibitor, significantly attenuated the fluid shear stress-induced pseudopod retraction response, demonstrating the role of GPCR activity changes due to fluid shear stress [90]. Transfection of cDNA for FPR into a cell line with very low levels of FPR and low pseudopod activity led to the projection of pseudopods, which then retracted following exposure to fluid shear stress [90]. FPR depletion via siRNA delivery in differentiated HL60 cells also significantly reduced fluid shear stress-induced pseudopod retraction.

While the ability of activated leukocytes to retract pseudopods in response to fluid shear stress has been documented in several papers, a variety of different neutrophil morphological responses have been obtained. Circulating leukocytes have been shown to undergo significant shape change and morphology disruption after exposure to extended periods of fluid shear stress [263]. Leukocytes treated with dexamethasone or after centrifugation have shown to reverse their shear stress response, and can activate and project pseudopods when exposed to fluid shear stress [264,265]. Leukocytes adherent on a glass substrate without any active deformation of pseudopods have been shown to become activated and extend pseudopods upon sudden application of fluid shear stress [266]. Leukocytes activated specifically by

low concentrations of G-protein coupled receptor ligands such as platelet activating factor (PAF) and fMLP have been shown to retract pseudopods upon application of fluid shear [267].

The effect of fluid shear stress on earlier indicators of neutrophil activation, such as L-selectin shedding and $\alpha_M\beta_2$ integrin activation induced by low concentrations of fMLP, has not yet been addressed. In this study, I examined the quantitative dynamics of the shear stress-dependent response of fMLP-induced L-selectin shedding and $\alpha_M\beta_2$ integrin activation in neutrophils.

2.2. MATERIALS AND METHODS

Reagents

FITC conjugated mouse anti-human CD62L specific for human L-selectin, FITC conjugated mouse IgG1 isotype control antibody, APC conjugated mouse IgG2b isotype control antibody, APC conjugated mouse anti-human CD181 specific for CXCR1, APC conjugated mouse IgG1 isotype control antibody, and APC conjugated mouse anti-human CD182 specific for CXCR2 were purchased from BD Biosciences (San Jose, CA). PE conjugated anti-human CBRM1/5 and PE conjugated mouse IgG1 isotype control antibody were purchased from Biolegend (San Diego, CA). Primary goat anti-human FPR, which binds to the extracellular epitope of FPR, and FITC secondary donkey anti-goat IgG antibody were purchased from Santa Cruz Biotechnology (Santa Cruz, CA). Formyl-methionyl-leucyl-phenylalanine (fMLP) and

Interleukin-8 (IL-8) were purchased from R&D Systems (Minneapolis, MN). Ca^{2+} and Mg^{2+} free DPBS (Invitrogen, Carlsbad, CA), Ca^{2+} and Mg^{2+} free HBSS (Invitrogen), endotoxin-free human serum albumin (Sigma Aldrich, St. Louis, MO), calcium carbonate (Sigma Aldrich), endotoxin-free water (MO BIO Laboratories, Carlsbad, CA), and low endotoxin (1 ng/mg), essentially γ-globulin-free BSA (Sigma-Aldrich) were purchased to make buffer solutions for neutrophil isolation and viscometer assays. Tumor necrosis factor α (TNF-α) protease inhibitor-0 (TAPI-0; Peptides International, Louisville, KY), 1,10-phenanthroline (1,10-Ph; Sigma Aldrich), and GM6001 (Chemicon, Temecula, CA) were purchased for protease inhibition studies. Quantum simply cellular (QSC) anti-mouse IgG beads were purchased from Bangs Laboratories, Inc. (Fisher, IN).

Neutrophil Isolation

Human peripheral blood was obtained via venipuncture from healthy consenting blood donors and collected into sterile sodium heparin-containing tubes (BD Biosciences) after informed consent. Neutrophils were then isolated by centrifugation at 480 X *g* for 50 min at 23°C in a Marathon 8K centrifuge (Fisher Scientific, Pittsburgh, PA) using 1-Step™ Polymorphs (Accurate Chemical & Scientific Corporation, Westbury, NY). This centrifugation method creates a density gradient to separate blood into visible layers of plasma, mononuclear cells, neutrophils, and erythrocytes and platelets. The neutrophils were extracted and washed in Mg^{2+} and Ca^{2+} free HBSS to remove any remaining polymorph. Any remaining red

blood cells in the suspension were lysed hypotonically. Neutrophils were resuspended at a concentration of 0.5 x 10^6 cells/mL in HBSS containing 0.5% HSA, 2 mM Ca^{2+}, 1 mM Mg^{2+}, and 10 mM HEPES (Invitrogen), buffered to pH 7.4. For protease inhibition studies, neutrophils were incubated with 25 μM GM6001, 5 mM 1,10-Ph, or 35 μM TAPI-0 for 30 min prior to the onset of shear.

Cone-and-Plate Viscometer Assay

To study the shear stress response of neutrophils in a controlled, uniform environment, experiments were performed using a cone-and-plate device consisting of a stationary plate beneath a rotating cone (0.8° angle) maintained at 23°C or 37°C by a circulating water bath (Brookfield, Middleboro, MA). The cone and plate viscometer design allows for a uniform shear rate to be applied to the entire sample. The shear rate, G, does not depend on the distance from the cone center, and is given by:

$$G = \frac{\omega}{\tan\theta}$$

where ω is the angular velocity of the cone (rad/s) and θ is the angle of the cone (rad). A laminar flow field is expected for all experimental conditions.

Under these conditions for a Newtonian fluid, the shear stress, τ, is proportional to the shear rate being applied:

$$\tau = \mu G$$

where μ is the viscosity of the medium. Prior to the experiments, the stationary plate and rotating cone were incubated with 5% BSA at room temperature for 1 hour to block non-specific adhesion of neutrophils to the cone and plate surfaces. Neutrophil suspensions of 500 μL were placed on the plate at a concentration of 0.5 x 10^6 cells/mL, and were allowed to equilibrate for 1 min before the onset of shear. Shear stress was varied from 0.1-4.0 dyn/cm^2 for 1-120 min in duration. To maintain a constant shear rate while increasing the shear stress, the medium viscosity was increased by adding varying amounts of ultra-high molecular weight dextran polymer to the medium (2 x 10^6 MW; Sigma Aldrich) of neutrophils under both shear and static conditions. Increasing the shear rate alone caused neutrophils to collide more frequently and activate (Figure 2.1), most likely due to L-selectin binding to P-selectin glycoprotein ligand-1 (PSGL-1). After shearing, aliquots of neutrophils were immediately exposed to 0.5 nM fMLP, 5 nM IL-8, or no chemoattractant for a period of 10 min. The 10 min incubation period was chosen to observe a measurable amount of L-selectin shedding and $\alpha_M\beta_2$ integrin activation, given the low concentrations of chemoattractants that were utilized.

Flow Cytometry

After chemoattractant exposure, both sheared and non-sheared neutrophils were immediately labeled with FITC-conjugated anti-human CD62L monoclonal antibody and PE-conjugated anti-human CBRM1/5 to quantify L-selectin expression and activated CD11b subunits of β_2 integrins. Sheared and non-sheared control samples of neutrophils were labeled with FITC- and PE- conjugated mouse IgG1 isotype antibodies to distinguish non-specific from specific antibody staining. All labeled neutrophil samples were incubated for 30 min at 4°C and then washed twice with cold Ca^{2+} and Mg^{2+} free DPBS. Samples were then analyzed using an Accuri C6 flow cytometer (Accuri Cytometers Incorporated) and flow cytometry plots were created with Accuri CFlow Plus and FCS Express V3 (De Novo Software, Thornhill, Canada) software.

Brightfield Microscopy and Image Analysis

Unlabeled neutrophils were fixed with 4% paraformaldehyde (Electron Microscopy Sciences, Hatfield, PA) in Ca^{2+} and Mg^{2+} free DPBS at 4°C for 30 min and then washed twice with cold Ca^{2+} and Mg^{2+} free DPBS. Cells were then placed on coverglass and imaged by bright field and phase contrast microscopy using an Olympus IX81 inverted microscope (Olympus America Inc., Center Valley, PA). Outlines of neutrophils were created from thresholded images using edge-detection functions in Metamorph (Universal Imaging Corp., West Chester, PA). Changes in

neutrophil shape were determined using the 'shape factor' program in Metamorph, where the shape factor is given by:

$$Shape\ Factor = \frac{4\pi A}{P^2}$$

where P is the perimeter and A is the area of the object (neutrophil). Shape factor values close to 1 represent a perfect circle, while values closer to zero represent elongated or ruffled shapes. All shape factor data were imported into Microsoft Excel 2007 (Microsoft Corporation, Redmond, WA).

Surface Receptor Quantification

The average number of FPR, CXCR1, and CXCR2 receptors on the surface of neutrophils was determined using flow cytometry with QSC beads. Beads were incubated for 45 min with a FITC or APC conjugated antibody specific to the antigen on the beads. A mixture of beads with varying numbers of antigen binding capacities (ABCs) was run through a flow cytometer. Populations of beads corresponding to increasing numbers of ABCs yield increasingly fluorescent peaks in the FITC or APC fluorescence channel. The median value of each fluorescence peak was obtained using Accuri CFlow Plus software, and was used along with the ABC values reported by the manufacturer to generate a calibration curve using QuickCal v2.3 (Bangs Labs, Fisher, IN).

Immediately following the calibration step, both sheared and non-sheared neutrophils were incubated with primary anti-human FPR for 45 min at 4°C. To examine the number of IL-8 surface receptors, separate sheared and non-sheared neutrophils were labeled with anti-CD181 and anti-CD182 for 30 min at 4°C. All neutrophil samples were washed twice with cold Ca^{2+} and Mg^{2+} free DPBS, and neutrophils labeled with anti-FPR were incubated with an additional secondary IgG-FITC antibody for 30 min at 4°C. All samples were washed and then analyzed using a flow cytometer. The peak fluorescence channel was recorded from each sample, and the peak was converted into the number of receptors using the calibration curve in QuickCal.

Confocal Microscopy

Neutrophils exposed to either shear or static conditions were fixed with 4% paraformaldehyde in Ca^{2+} and Mg^{2+} free DPBS at 4°C for 30 min, and then washed twice with cold Ca^{2+} and Mg^{2+} free DPBS. Neutrophil samples were then distributed onto slides using a Shandon CytoSpin III centrifuge (Shandon, Pittsburgh, PA) at 750 RPM for 5 min. Slides were allowed to dry for 5 min, and were then rehydrated in DPBS. Samples were permeabilized in 0.2% Triton X-100 for 5 min, and then incubated in 1% BSA for 1h. Slides were incubated in primary anti-human FPR for 12 h in a humidified chamber, and then washed twice with 0.2% Tween in DPBS for 5 min each. All samples were incubated with a secondary IgG-FITC antibody for 30 min

4°C, washed twice with 0.2% Tween in DPBS, and mounted onto coverslips using Vectashield mounting medium (Vector Laboratories, Burlingame, CA).

Samples were examined with a Zeiss 710 Spectral Confocal Microscope System (Carl Zeiss MicroImaging GmbH, Jena, Germany) at 65X magnification with a FITC filter. Both individual and Z-stack images were taken and processed using Zeiss ZEN software (Carl Zeiss MicroImaging GmbH). Metamorph software was used to examine FPR internalization and fluorescence intensities within neutrophils. To measure fluorescence intensity within the cell, the cell membrane was thresholded using edge detection functions to exclude the fluorescent membrane from calculations (Fig. 8*C*). Fluorescent measurements within the cell were then recorded and averaged for 100 neutrophils from each of n=3 donors.

Statistical Analysis

Flow cytometry and shape factor data were plotted and analyzed using Prism 5.0b for Microsoft (GraphPad software, San Diego, CA). A two-tailed paired t-test was used for comparisons between two groups with $p < 0.05$ being considered significant.

2.3 RESULTS

Fluid shear stress reduces fMLP-induced L-selectin shedding and $\alpha_M\beta_2$ integrin activation in neutrophils

We initially studied the fluid shear stress response of neutrophils to L-selectin shedding and $\alpha_M\beta_2$ integrin activation after exposure to a low concentration of fMLP. Neutrophil suspensions were exposed to static conditions or 4.0 dyn/cm^2 of fluid shear stress in a cone-and-plate viscometer for 2 h at 23°C, followed by stimulation with or without 0.5 nM fMLP for 10 min. Stimulus from fMLP, an inflammatory mediator, is known to lead to a downregulation of L-selectin and conformational change in the α_M subunit of $\alpha_M\beta_2$ integrins [188,258,259]. Neutrophils exposed to static conditions (Figure 2.2A) and 4.0 dyn/cm^2 (Figure 2.2B) of fluid shear stress in the absence of fMLP did not show appreciable differences in L-selectin shedding and $\alpha_M\beta_2$ integrin activation as expected. However, neutrophils exposed to fMLP after fluid shear stress (Figure 2.2D) showed a measurable reduction in L-selectin shedding and $\alpha_M\beta_2$ integrin activation compared to neutrophils exposed to fMLP after exposure to static conditions (Figure 2.2C). No significant difference in L-selectin shedding and $\alpha_M\beta_2$ integrin activation was found between sheared and nonsheared neutrophils, while a significant reduction in fMLP-induced L-selectin shedding (Figure 2.2G) and $\alpha_M\beta_2$ integrin activation (Figure 2.2H) was found in sheared neutrophils compared to neutrophils under static conditions. Experiments were also conducted at 37°C to

compare to 23°C experiments, and similar differences were seen between neutrophils under shear and static conditions in terms of L-selectin shedding and $\alpha_M\beta_2$ integrin activation (Figure 2.3). Experiments were performed for 20 min rather than 2 h to minimize sample evaporation.

Fluid shear stress does not affect IL-8-induced L-selectin shedding and $\alpha_M\beta_2$ integrin activation

To assess whether fluid shear stress alters L-selectin shedding and $\alpha_M\beta_2$ integrin activation via other major neutrophil chemoattractant GPCRs, neutrophils were exposed to static conditions or 4.0 dyn/cm^2 of fluid shear stress in a cone-and-plate viscometer for 2 h at 23°C, followed by either stimulation with or without 5 nM of IL-8. IL-8, a chemoattractant found on the surface of endothelial cells [268-270], binds to G-protein coupled receptors CXCR1 and CXCR2, which are believed to have lower constitutive activity in comparison to FPR [260,271-273]. Neutrophils exposed to static conditions (Figure 2.2E) or 4.0 dyn/cm^2 (Figure 2.2F) of fluid shear stress followed by IL-8 treatment did not show significant differences in L-selectin shedding (Figure 2.2G) or $\alpha_M\beta_2$ integrin activation (Figure 2.2H).

fMLP-induced L-selectin shedding and $\alpha_M\beta_2$ integrin activation in neutrophils is dose-dependent in fluid shear stress magnitude

To study the effect of shear stress magnitude on fMLP-induced activation, neutrophils were exposed to varying shear stresses of 0.1-4.0 dyn/cm^2 for 2 h. These shear stress magnitudes are values typically found in the microcirculation [274]. At low shear stresses of 0.10 and 0.25 dyn/cm^2, no significant difference in L-selectin shedding (Figure 2.4A) or $\alpha_M\beta_2$ integrin activation (Figure 2.4B) was observed between cells exposed to shear followed by fMLP stimulation and cells exposed to no shear followed by fMLP stimulation. However, a shear stress of 0.75 dyn/cm^2 yielded a significant reduction in L-selectin shedding (Figure 2.4A) and $\alpha_M\beta_2$ integrin activation (Figure 2.4B) after exposure to fMLP. Shear stress exposures of 2.5 and 4.0 dyn/cm^2 showed an even greater reduction of L-selectin shedding (Figure 2.4A) and $\alpha_M\beta_2$ integrin activation (Figure 2.4B).

fMLP-induced L-selectin shedding and $\alpha_M\beta_2$ integrin activation in neutrophils is shear stress exposure time-dependent

To assess the kinetics of the FPR mechanosensing phenomenon, neutrophils were exposed to a constant shear stress of 4.0 dyn/cm^2 at 23°C while increasing the fluid shear stress exposure time from 1-120 min, followed by stimulation with 0.5 nM fMLP. The exposure time was increased to determine a threshold where the shear-induced resistance begins to develop. No significant difference in fMLP-induced L-

selectin shedding in neutrophils was found over a shear stress exposure time period of 1-10 min (Figure 2.5A). However, a significant decrease in fMLP-induced L-selectin shedding was found at a threshold shear stress exposure time of 20 min, and was found to be significantly less than neutrophils in static conditions for the range of 20-120 min. fMLP-induced $\alpha_M\beta_2$ integrin activation in neutrophils showed no significant difference in neutrophils exposed to shear and static conditions from 1-30 min (Figure 2.5B). A threshold value of 60 min was found be required to produce a significant difference in $\alpha_M\beta_2$ integrin activation in neutrophils exposed to shear and static conditions, and this response was significant over a range of 60-120 min.

Neutrophils develop a resistance to fMLP-induced L-selectin shedding and $\alpha_M\beta_2$ integrin activation with increasing shear stress magnitude and shear stress exposure time

Due to the variability in response experienced with primary neutrophils, neutrophils exposed to both shear and static conditions from each donor were directly compared over varying shear stress magnitudes and shear stress exposure durations. Neutrophil resistance responses to L-selectin shedding and $\alpha_M\beta_2$ integrin activation were directly compared using the equation:

$$\%\ Resistance = \frac{(\%\ Neutrophils\ without\ shear) - (\%\ Neutrophils\ with\ shear)}{(\%\ Neutrophils\ without\ shear)} \times 100\%$$

The resistance equation applies to neutrophils labeled for both L-selectin shedding and $\alpha_M\beta_2$ integrin activation, for varying shear stress magnitudes and shear stress durations.

By varying the shear stress magnitude, it is apparent that shear stress does not confer resistance in neutrophils to fMLP-induced L-selectin shedding (Figure 2.6A) and $\alpha_M\beta_2$ integrin activation (Figure 2.6C) at lower shear stress values of 0.10 and 0.25 dyn/cm^2. Resistance to L-selectin shedding and $\alpha_M\beta_2$ integrin activation is achieved at 0.75 dyn/cm^2 and maximum shear stress response is conferred at 2.5 dyn/cm^2. No additional increase in response is observed at a higher shear stress of 4.0 dyn/cm^2. No measurable resistance to L-selectin shedding (Figure 2.6A) or $\alpha_M\beta_2$ integrin activation (Figure 2.6C) was observed in neutrophils without fMLP stimulation. By varying the duration of shear stress exposure, it is apparent that the shear-induced resistance to fMLP-induced L-selectin shedding (Figure 2.6B) and $\alpha_M\beta_2$ integrin activation (Figure 2.6D) increases with increasing shear stress exposure time. Resistance to activation after 1-120 min of fluid shear was not observed in the absence of fMLP.

Neutrophils acquire a shear-induced resistance to fMLP-induced morphological changes

To assess how fluid shear stress alters neutrophil morphology after fMLP stimulation, neutrophils exposed to 4.0 dyn/cm^2 or static conditions for 2 h at 23°C were fixed with 4% paraformaldehyde and examined for their morphological

characteristics. Activated neutrophils project pseudopods after exposure to chemoattractants such as fMLP, platelet activating factor (PAF), C5a anaphylotoxin, leukotriene B4, and interleukin-8 [275]. To quantify this, neutrophil morphology was evaluated using Metamorph by calculating the shape factor of each cell. The shape factor approaches 1 for round, unactivated neutrophils and decreases for more extended, dendritic shapes.

No significant difference in the shape factor was found between neutrophils exposed to shear and static conditions without exposure to fMLP (Figure 2.7A). Neutrophils stimulated with 0.5 nM fMLP showed an average shape factor significantly less than 1. Interestingly, a significant difference in shape factor was found between sheared and unsheared neutrophils after exposure to 0.5 nM fMLP, as the sheared neutrophils exhibiting a shape factor close to unity. Neutrophils assumed a round morphology in the absence of fMLP (Figure 2.7B,C), while unsheared neutrophils developed a more extended morphology than sheared neutrophils in the presence of fMLP (Figure 2.7D,E).

Fluid shear stress reduces FPR surface expression

To investigate the mechanotransduction effects on FPR surface expression, neutrophils were exposed to shear stress (4.0 dyn/cm^2) and static conditions at 23°C for 2 h and immediately labeled with anti-FPR antibodies to be analyzed via flow cytometry. Sheared neutrophils displayed a reduction in FPR expression (Figure 2.8A). In comparison to nonsheared samples, QSC bead analysis indicated a

significant difference in FPR receptor count, as sheared neutrophils averaged 14,600 receptors/cell, while nonsheared samples averaged 20,100 receptors/cell (Figure 2.8D). Sheared neutrophils did not show a reduction in the expression of the two IL-8 receptors CXCR1 (Figure 2.8B) and CXCR2 (Figure 2.8C), in comparison to nonsheared neutrophils. CXCR1 and CXCR2 receptor counts using QSC beads showed no significant differences between sheared and nonsheared neutrophils.

FPR expression levels are unaltered in the presence of protease inhibitors

To assess whether FPR is enzymatically cleaved by proteases derived from the neutrophil upon exposure to fluid shear stress, neutrophils were treated with 25 μM GM6001, 5 mM 1,10-Ph, or 35 μM TAPI-0 for 30 min prior to fluid shear stress exposure. Neutrophils exposed to fluid shear stress (4.0 dyn/cm^2) and static conditions at 23°C for 2 h were then labeled with anti-FPR antibodies to be analyzed via flow cytometry, followed by surface receptor quantification. No significant differences were observed in FPR surface expression of neutrophils treated with protease inhibitors compared to untreated neutrophils exposed to shear (Figure 2.9), indicating that loss of FPR expression is not due to cleavage by neutrophil proteases under fluid shear.

Neutrophils experience FPR internalization under fluid shear

To examine potential FPR internalization as a possible cause for FPR surface expression decrease following fluid shear stress exposure, neutrophils were exposed to either fluid shear stress (4.0 dyn/cm^2) or static conditions for 2 h, permeabilized and then labeled with anti-FPR antibodies for examination via confocal microscopy. Images were thresholded (Figure 2.10C) to exclude the cell membrane from fluorescence measurements. Immunostaining revealed FPR to be clearly localized within the cell in sheared samples (Figure 2.10A), while minimal FPR was shown within neutrophils exposed to static conditions (Figure 2.10B). The average pixel intensities calculated from within neutrophils showed a significant increase in fluorescence intensity in sheared neutrophils, compared to neutrophils exposed to static conditions (Figure 2.10D).

2.4 DISCUSSION

The aim of this study was to quantify the shear stress-dependent response of fMLP-induced L-selectin shedding and $\alpha_M\beta_2$ integrin activation in neutrophils via the formyl peptide receptor. Resistance was acquired by neutrophils during exposure to physiological levels of shear stress in a force- and time-dependent manner, directly implicating fluid shear stress in this response. Interestingly, we found this resistance to be first manifest at a shear stress magnitude of 0.75 dyn/cm^2; this value is close to the 0.5 dyn/cm^2 minimum level of shear stress found to induce pseudopod retraction by

Schmid-Schonbein and colleagues, which is also believed to act through the formyl peptide receptor [9]. Additionally, a shear stress of greater than 0.4 dyn/cm^2 is required for L-selectin adhesion to CD34 on vascular tissue [169]. The kinetic studies of the shear-induced fMLP resistance showed that measurable effects began in the 5 min range for both L-selectin shedding and α_M integrin conformational change, consistent to what was observed in pseudopod retraction experiments [276].

While neutrophils acquired a resistance to both fMLP-induced L-selectin shedding and $\alpha_M\beta_2$ integrin activation, the number of cells that were resistant to both effects varied. The fact that fewer cells developed a resistance to $\alpha_M\beta_2$ integrin activation compared to L-selectin shedding could be due to the fact that the extracellular domain of CD18 can be cleaved at physiological shear stresses [277]. Cleavage of CD18 on cells due to fluid shear stress may distort the true number of cells that are positive or negative for $\alpha_M\beta_2$ integrin activation, while L-selectin has only been found to be cleaved due to fluid shear stress when rolling on carbohydrate ligand coated surfaces [278].

In addition to the variations in fMLP-induced L-selectin shedding and $\alpha_M\beta_2$ integrin activation in neutrophils, it is also apparent that a subset does not acquire any resistance due to fluid shear stress. There is evidence that fluid shear stress on the neutrophil membrane can be non-uniform; variations in the shear stress distribution on the surface of a neutrophil have been found, due to the geometric shape of the membrane [279]. While spherical in shape, neutrophils have villous membrane made up of numerous fine foldings [280] that may alter the shear stress exerted on cell surface receptors. Despite these two factors, it is notable that a measurable population

of neutrophils developed a resistance to fMLP-induced activation. The ranges of the neutrophils being examined might also explain the differences in their response to fluid shear stress. Recent studies suggest that neutrophil lifespans might be much longer than what was previously believed, with neutrophils having a circulatory lifespan of up to 5.4 days, compared to the previously, generally accepted short lifespan of less than one day [281].

Neutrophils have the ability to enzymatically cleave their surface receptors with proteases derived from within the cell upon exposure to fluid shear, including adhesion receptors such as L-selectin [278] and CD18 [277]. Cleavage of FPR by matrix metalloproteinases (MMPs) has previously been shown by others to alter the fluid shear response of neutrophils [282]. However, when neutrophils were treated with MMP inhibitors in this present study, no significant changes in FPR surface expression was observed when compared to untreated samples exposed to fluid shear. This indicates that the loss of FPR surface expression is not due to enzymatic cleavage via proteases derived from the neutrophil due to the onset of shear. Cleavage of FPR observed by other groups was due to the elevated levels of MMPs within the blood of the spontaneously hypertensive rat [282], while neutrophils used in this study were taken from normal human donors.

Our studies show that FPR surface expression downregulation could be due to the observed internalization of FPR by neutrophils upon exposure to fluid shear stress. FPR internalization is typically associated with desensitization of the receptor upon exposure to fMLP [283]. When FPR is activated due to fMLP, the receptor becomes phosphorylated by GPCR kinases, which increases FPR affinity for the cytosolic

protein arrestin [284]. Arrestin binding to GPCRs prevents the receptors from additional association with G proteins, making arrestins a major component in GPCR desensitization. FPR desensitization has also been shown to occur as a form of cross-desensitization among chemoattractant receptors. HEK293 cells coexpressing fMLP and C5a receptors have shown that activation of C5a receptors resulted in cross-desensitization of Ca^{2+} mobilization stimulated by FPR, and vice versa [285]. Neutrophils expressing combinations of chemoattractant receptors have shown that peptide chemoattractants such as fMLP, C5a, and IL-8 desensitized Ca^{2+} mobilization to one another and to PAF [286,287]. Recently, exposure to fluid shear stress has also been shown to cause FPR on leukocytes to be internalized into perinuclear compartments [279], and similar internalization responses due to shear stress have been observed in other cell types [288]. Based on the loss of FPR expression on neutrophils after the application of fluid shear stress, FPR internalization due to shear forces may also cause another form of desensitization, and thus attenuate the effects of fMLP on L-selectin shedding and α_M integrin conformational change. Since fMLP is known to induce L-selectin shedding and $\alpha_M\beta_2$ integrin conformational change [189,258,259] and FPR was internalized upon exposure to shear stress in this current study, a downregulation of FPR on the surface available for receptor-ligand binding will contribute to the neutrophil response to activation. While FPR internalization could play a major role in the downregulation of FPR on the cell surface, other causes for FPR downregulation could also be contributors. For example, it has been suggested that fluid shear may change the conformation in the seven transmembrane domain region of FPR, which can possibly also cause FPR inactivation [276].

FPR has been implicated as a sensor for fluid shear stress, however other chemoattractant GPCRs such as CXCR1 and CXCR2 did not display unique properties while exposed to shear stress in this current study. Differences in their response to fluid shear stress could involve differences in their signaling pathways, as neutrophil chemotaxis in response to either fMLP or IL-8 are known to display different properties. Chemotaxis assays have shown neutrophil migration to IL-8 to be dependent on PI3K, however FPR signaling drastically differs, as treatment with Pan-PI3K inhibitors only delays initial neutrophil migration to fMLP [289-292]. Physiologically, FPR surface expression on neutrophils might alter under shear, but not CXCR1 and CXCR2, due to the differences in the presentation of fMLP and IL-8 in tissue compared to within the bloodstream. There is extremely low fMLP concentration present within the bloodstream, as fMLP is derived from bacterial protein degradation or from mitochondrial proteins upon tissue damage. While experiencing higher shear stresses within the bloodstream, FPR might remain internalized due to low fMLP concentrations, but once under much lower shear stress conditions from interstitial flow within the tissue, FPR could present itself along the surface of the neutrophil membrane to enhance migration along the chemotactic gradient. Conversely, the differences in IL-8 concentration are not as pronounced. Significant amounts of IL-8 are known to line along venular endothelial cells in the bloodstream while also being present within the tissue during inflammatory conditions [268], necessitating CXCR1 and CXCR2 levels to remain similar both under shear and non shear conditions.

To investigate the importance of FPR internalization in the shear-induced resistance to activation, one may attempt to match the number of receptor-ligand complexes at equilibrium for sheared and nonsheared neutrophils by increasing the fMLP concentration used to stimulate sheared neutrophils. If simple monovalent receptor-ligand binding is assumed, a monovalent ligand L binds reversibly to a monovalent receptor R to form a receptor-ligand complex C (54). Neglecting ligand depletion in the neutrophil suspension and assuming the ligand concentration remains constant at its initial value, L_0, yields an estimate for the number of receptor ligand complexes at equilibrium, C_{eq} from the equation $C_{eq}=R_T L_0/K_D+L_0$, where K_D is the equilibrium dissociation constant (nM) of the receptor ligand interactions, and R_T is the number of receptors present on the cell surface (#/cell).

FPR on neutrophils displays a K_D in the range of 0.5-1.0 nM [293,294]. With the FPR receptor count for sheared neutrophils determined in the present study, one can estimate the L_0 value necessary to reach the same C_{eq} found in nonsheared neutrophils. Using K_D=1.0 nM, we predicted the fMLP concentration needed to elicit the same C_{eq} in sheared neutrophils as in nonsheared ones to be L_0=0.8 nM. Equal responses of L-selectin shedding and $\alpha_M\beta_2$ integrin activation in sheared neutrophils exposed to 0.8 nM fMLP compared to nonsheared ones exposed to 0.5 nM fMLP would suggest that FPR internalization is responsible for the shear-induced resistance. Conversely, a lower degree of L-selectin shedding and $\alpha_M\beta_2$ integrin activation in the sheared neutrophils would suggest that FPR internalization, along with other factors, combine to contribute to the resistance response. Here, sheared neutrophils stimulated with 0.8 nM fMLP showed a reduction in selectin shedding and integrin activation

compared to nonsheared neutrophils stimulated with 0.5 nM fMLP, but exhibited greater selectin shedding and integrin activation than sheared neutrophils stimulated with 0.5 nM fMLP (Figure 2.11). This analysis suggests that FPR internalization contributes along with other factors in the neutrophil shear-induced resistance to activation. However, it should be noted that we have neglected receptor dynamics that occur during the 10 min stimulation with fMLP. Taking into account the synthesis, intracellular sorting, and differential endocytosis of formyl peptide receptors [295] could help further evaluate the impact the effects of FPR downregulation in the neutrophil shear-induced resistance to activation.

2.5 CONCLUSION

The results from this study suggest that fluid shear stress has a significant effect on the activation of circulating neutrophils. Neutrophils acquired a fluid shear stress-induced resistance to activation via FPRs. The resistance was shown to be dependent on shear stress magnitude, as the resistance response increased with increasing shear stress. The mechanical response was also shown to be dependent on shear stress duration, as neutrophils increased their resistance with increased shear stress exposure time. A decrease in FPR surface expression was observed under fluid shear stress, and high-resolution confocal microscopy revealed that FPR was internalized within cells. Although other studies on mechanotransduction in neutrophils have mostly focused on morphological changes, this study focused on earlier indicators of activation, specifically fMLP-induced L-selectin shedding and

$\alpha_M\beta_2$ integrin activation. The complete signaling pathways of these receptors deserve further study, as do the molecules that mediate GPCR internalization. Other receptors that have shown high constitutive activity should be investigated to understand their contributions to the mechanosensing responses of cells within the vascular microenvironment.

FIGURE 2.1: LOSS OF NEUTROPHIL L-SELECTIN UNDER VARIOUS SHEAR RATES. Neutrophils were exposed to shear rates of 75 s^{-1}, 150 s^{-1}, 225 s^{-1}, or 450 s^{-1} in a cone and plate viscometer 2 h at 23°C and were analyzed for L-selectin shedding due to shear alone. n = 3 donors for each shear rate value. Error bars represent 95% confidence intervals.

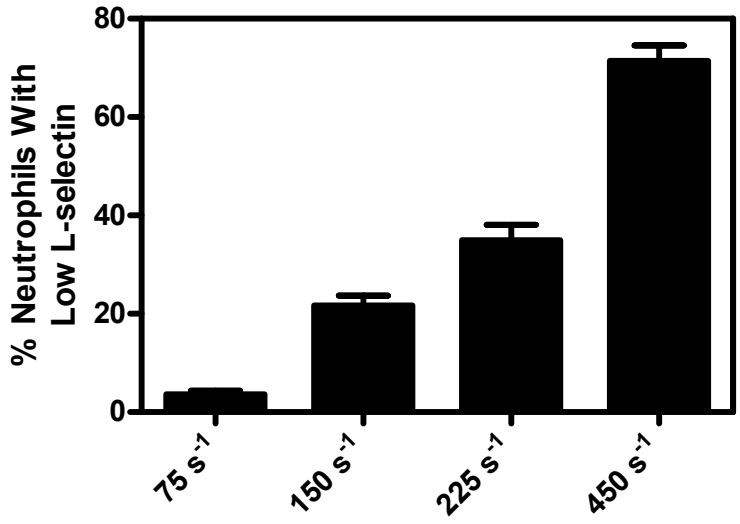

FIGURE 2.2: FLUID SHEAR STRESS INCREASES NEUTROPHIL RESISTANCE TO L-SELECTIN SHEDDING AND $\alpha_M\beta_2$ INTEGRIN ACTIVATION. Neutrophils were exposed to static conditions (*A*) and 4 dyn/cm^2 of shear (*B*) for 2 h, respectively. Neutrophils exposed to static conditions and 4 dyn/cm^2 of shear for 2 h were then immediately exposed to 0.5 nM of fMLP for 10 min (*C, D*) or 5 nM of IL-8 for 10 min (*E, F*). All conditions were repeated for significance with n = 5 donors for L-selectin shedding (*G*) and $\alpha_M\beta_2$ integrin activation (*H*). Upper two quadrants of each flow cytometry plot represent positive CBRM1/5 staining, while the lower two signify little to no CBRM1/5 staining. The two right quadrants of each plot represent positive L-selectin staining, while the two left quadrants represent the absence of L-selectin staining. Quadrants determined by labeling neutrophils with isotype antibodies corresponding to L-selectin and CBRM1/5 antibodies, which label for all nonspecific binding sites on the neutrophil surface. "Low L-selectin" represents fluorescence values no greater than isotype values. PE represents the R-Phycoerythrin fluorescence channel, while FITC represents the fluorescein isothiocyanate fluorescence channel. Error bars represent 95% confidence intervals. *$P < 0.05$ for all measurements, and NS denotes a non-significant difference.

FIGURE 2.2: FLUID SHEAR STRESS INCREASES NEUTROPHIL RESISTANCE TO L-SELECTIN SHEDDING AND $\alpha_M\beta_2$ INTEGRIN ACTIVATION.

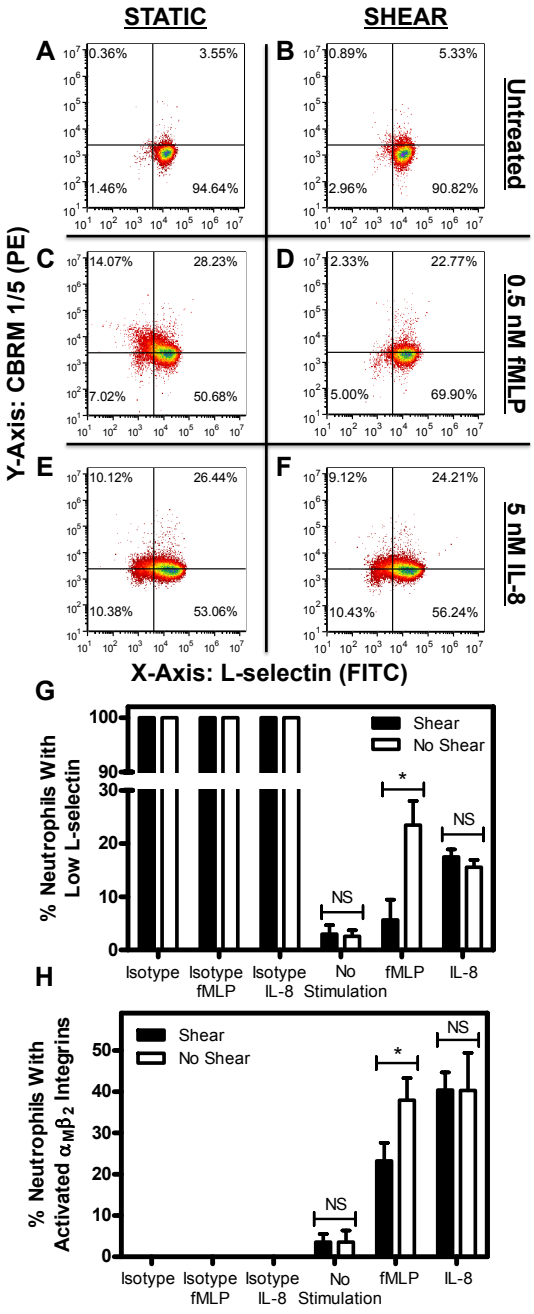

FIGURE 2.3: NEUTROPHIL SHEAR-INDUCED RESISTANCE TO ACTIVATION AT 23°C AND 37°C. Neutrophils were exposed to either shear (4.0 dyn/cm^2) or static conditions for 20 min at 23°C or 37°C, and then analyzed for L-selectin shedding (*A*) and $\alpha_M\beta_2$ integrin activation (*B*). A 20 min duration was used to minimize sample evaporation. n = 5 donors for each shear stress value. Error bars represent 95% confidence intervals. *P < 0.05 for all measurements. NS: not significant.

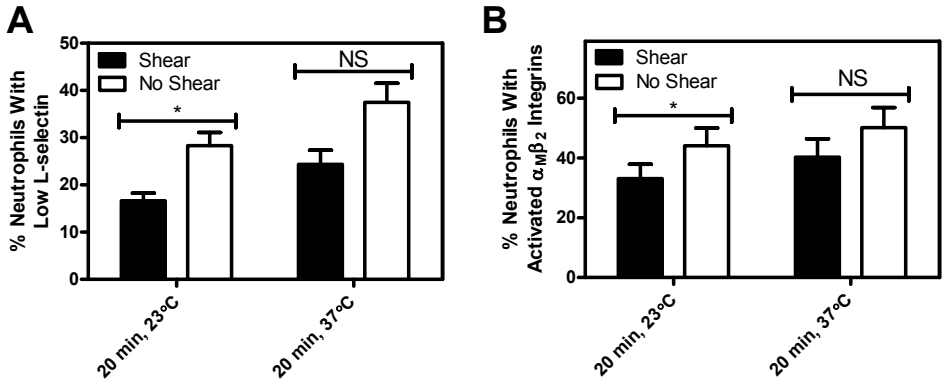

FIGURE 2.4: INCREASING FLUID SHEAR STRESS REDUCES FMLP-INDUCED L-SELECTIN SHEDDING AND $\alpha_M\beta_2$ INTEGRIN ACTIVATION OF NEUTROPHILS. Increasing fluid shear stress reduces fMLP-induced L-selectin shedding (*A*) and $\alpha_M\beta_2$ integrin activation (*B*) of neutrophils. Shear stress magnitude was varied in separate experiments from 0.1-4.0 dyn/cm^2 for 2 h at 23°C, followed by stimulation with 0.5 nM of fMLP for 10 min. n = 5 donors for each shear stress value. Error bars represent 95% confidence intervals. *P < 0.05 for all measurements.

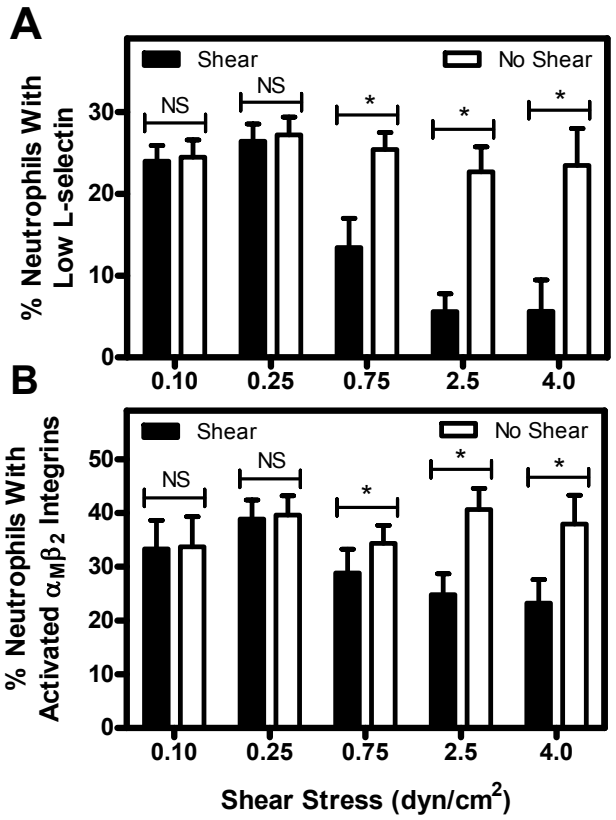

FIGURE 2.5: NEUTROPHIL RESISTANCE TO ACTIVATION INCREASES WITH INCREASING FLUID SHEAR STRESS DURATION. The time dependence of the mechanical response of neutrophils to fMLP-induced L-selectin shedding (*A*) and $\alpha_M\beta_2$ integrin activation (*B*) was determined by increasing the shear stress exposure time from 1-120 min at a uniform shear stress of 4.0 dyn/cm^2 at 23°C. n = 3 donors for each time point. Error bars represent 95% confidence intervals. *P < 0.05 for all measurements.

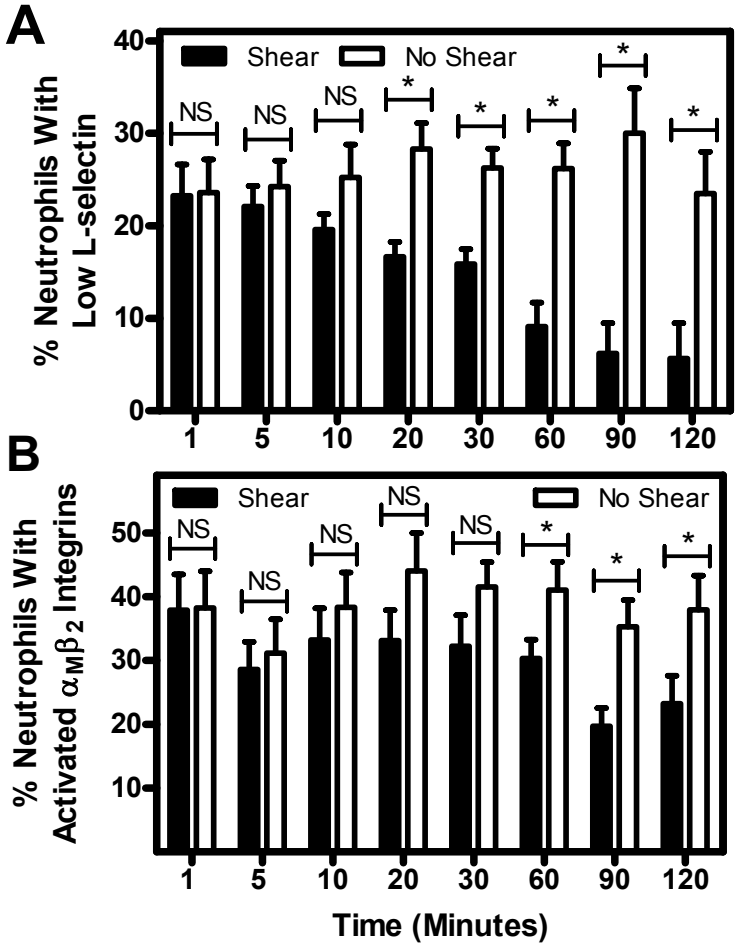

FIGURE 2.6: NEUTROPHILS DEVELOP RESISTANCE TO FMLP-INDUCED L-SELECTIN SHEDDING AND $\alpha_M\beta_2$ INTEGRIN ACTIVATION WITH INCREASING SHEAR STRESS MAGNITUDE AND SHEAR STRESS DURATION. Neutrophils develop resistance to fMLP-induced L-selectin shedding and $\alpha_M\beta_2$ integrin activation with increasing shear stress magnitude (*A, C*) and shear stress duration (*B, D*), respectively. Resistance is plotted as a function of the $\log_{10}$ of shear stress (dyn/cm^2) or time (min). n = 5 donors for each shear stress point, and n = 3 donors for each time point. Error bars represent 95% confidence intervals.

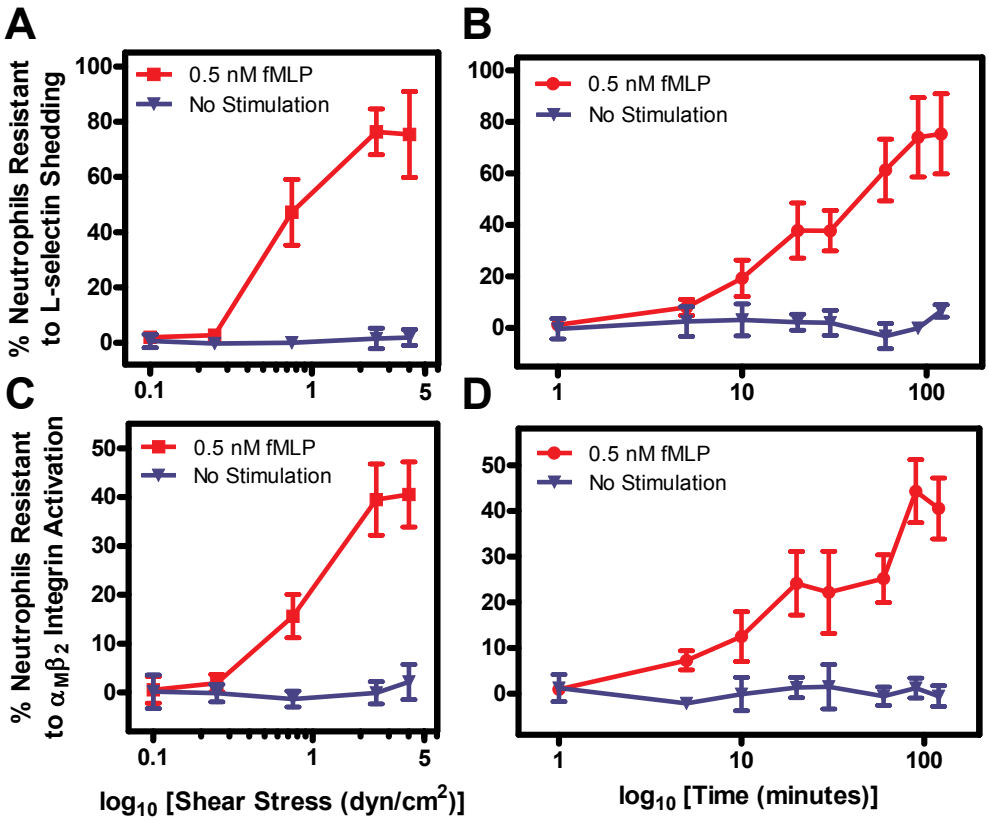

FIGURE 2.7: FLUID SHEAR STRESS ALTERS FMLP-INDUCED NEUTROPHIL MORPHOLOGY. Fluid shear stress alters fMLP-induced neutrophil morphology. Shape factor measurements of neutrophils exposed to shear stress or static conditions without and with 0.5 nM fMLP stimulation (*A*). Brightfield images of neutrophils exposed to shear stress (*B*) or static conditions (*C*) without fMLP, and neutrophils exposed to shear stress (*D*) or static conditions (*E*) with 0.5 nM fMLP. All scale bars = 50 µm. n = 3 donors, with 300 neutrophils analyzed for their shape factor for each donor condition. Error bars represent 95% confidence intervals. *P < 0.05 for all measurements.

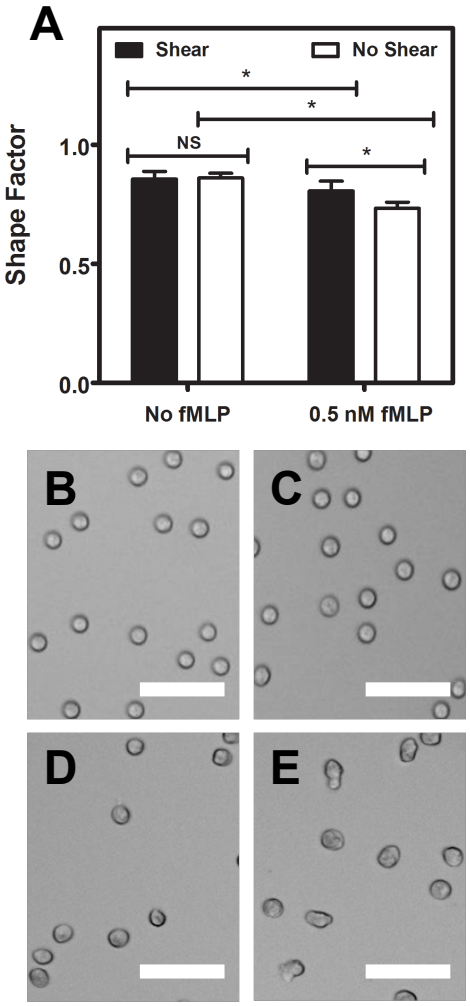

FIGURE 2.8: FLUID SHEAR STRESS INDUCES A LOSS OF FPR SURFACE EXPRESSION. Fluid shear stress induces a loss of FPR surface expression. Flow cytometry plots show FPR expression at 4.0 dyn/cm^2 for 2 h (*A*) compared to nonsheared samples, along with IL-8 receptors CXCR1 (*B*) and CXCR2 (*C*) expression of sheared and nonsheared neutrophils. Receptor quantification using QSC beads was used to determine the surface receptor count of FPR, CXCR1, and CXCR2 on neutrophils (D). n = 3 donors. Error bars represent 95% confidence intervals. *P < 0.05 for all measurements.

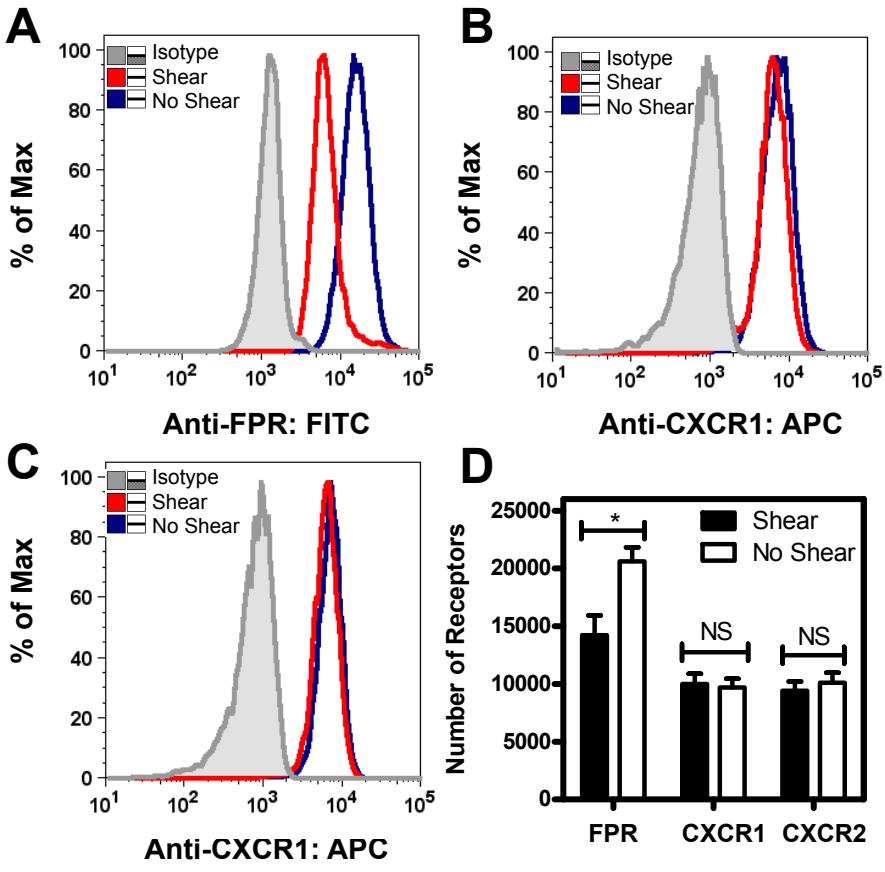

FIGURE 2.9: PROTEASE INHIBITION DOES NOT AFFECT FPR SURFACE EXPRESSION UPON EXPOSURE TO FLUID SHEAR STRESS. Untreated neutrophils and neutrophils treated GM6001, 1,10-Phenanthroline, or TAPI-0 were exposed to static conditions and 4 dyn/cm^2 of shear stress for 2 h. Samples were analyzed for FPR surface expression via flow cytometry. All conditions were repeated for significance with n = 3 donors. Error bars represent 95% confidence intervals. NS: not significant.

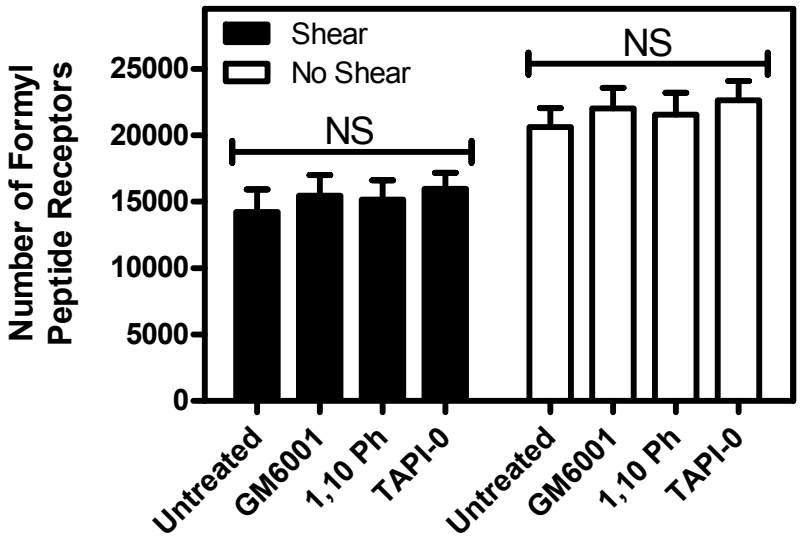

FIGURE 2.10: FLUID SHEAR STRESS INDUCES FPR INTERNALIZATION IN NEUTROPHILS. Neutrophils were exposed to 4 dyn/cm^2 of fluid shear stress (*A*) or static conditions (*B*) for 2 h. All samples were permeabilized, labeled with FPR antibodies, and examined via confocal microscopy. Images were then thresholded (*C*) to exclude the cell membrane from measurements, and the average fluorescent intensity of the inner portion of sheared and non sheared cells (*D*) was quantified. All scale bars = 5 μm. All conditions were repeated for significance with n = 3 donors. Error bars represent 95% confidence intervals. *P < 0.05 for all measurements.

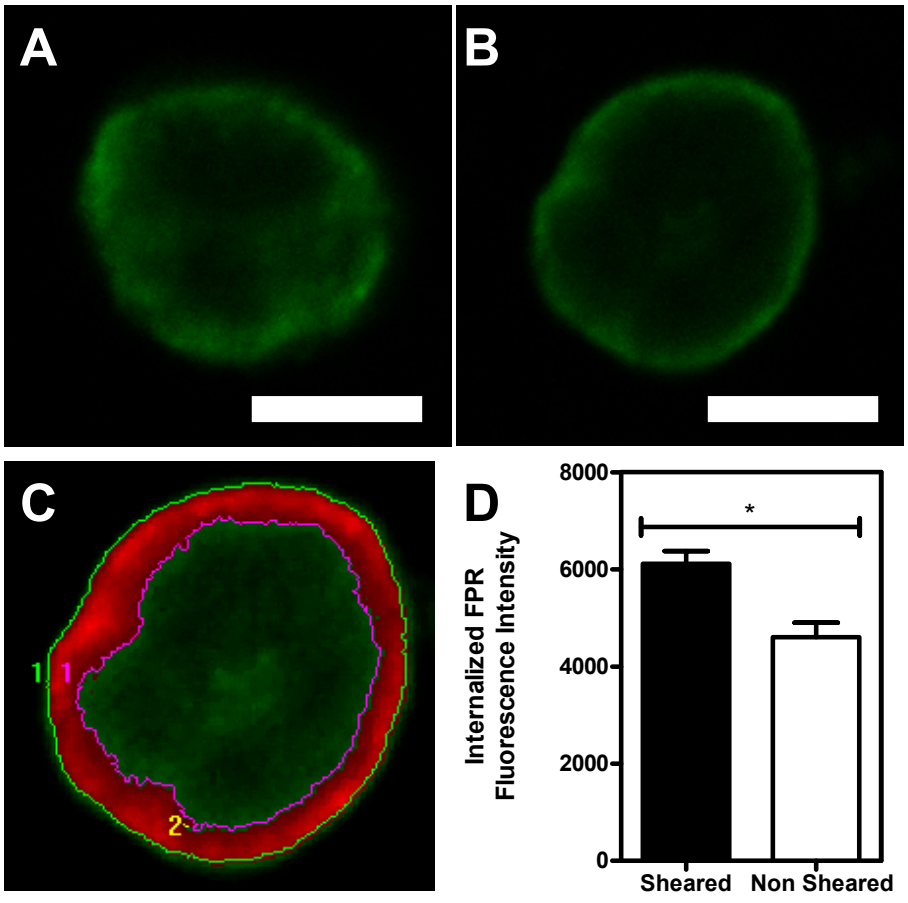

FIGURE 2.11: CHANGES IN FPR SURFACE EXPRESSION CONTRIBUTE TO THE NEUTROPHIL RESISTANCE TO ACTIVATION. Sheared neutrophils at 4.0 dyn/cm^2 for 2 h were stimulated with 0.8 nM fMLP (*A*), to approach the C_{eq} of nonsheared neutrophils stimulated with 0.5 nM, based on an assumption of simple monovalent receptor-ligand binding. Nonsheared neutrophils stimulated with 0.5 nM and 0.8 nM fMLP and sheared neutrophils exposed to both 0.5 nM and 0.8 nM fMLP (*B*) were compared for L-selectin shedding and $\alpha_M\beta_2$ integrin activation with n=3 donors. Error bars represent 95% confidence intervals. *P < 0.05 for all measurements.

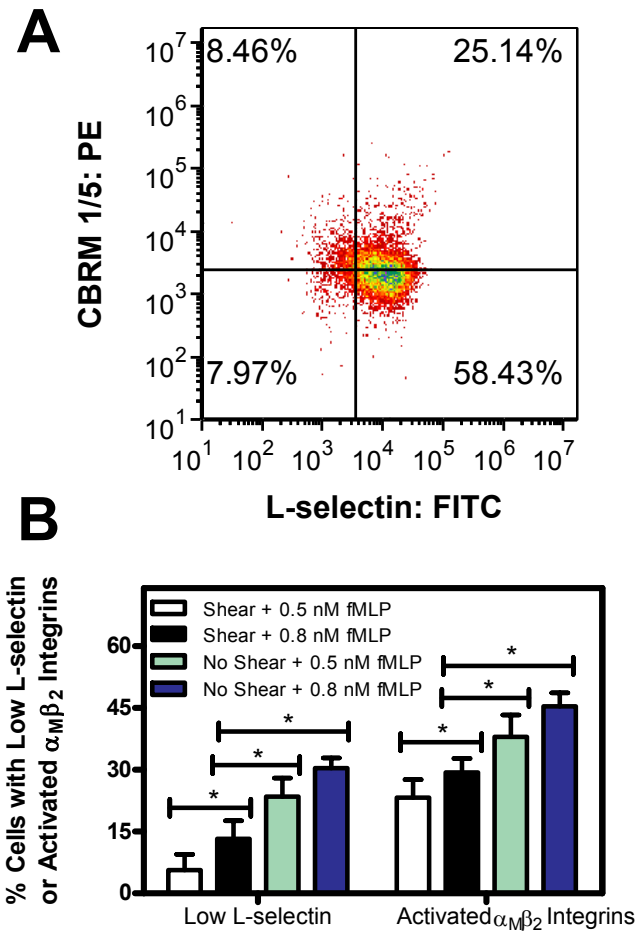

CHAPTER 3: FLUID SHEAR STRESS INCREASES NEUTROPHIL ACTIVATION VIA PLATELET ACTIVATING FACTOR

*This section is adapted from the following publication: M.J. Mitchell, K.S. Lin, and M.R. King. *Biophysical Journal.* 106(10): 2243-2253, 2014.

3.1 INTRODUCTION

The initial recruitment and adhesion of leukocytes to the endothelial cell wall is a critical event in inflammation and lymphocyte homing to lymphatic tissues [168,296]. In the initial phase of recruitment, free flowing leukocytes in postcapillary venules can be captured under the presence of hemodynamic shear forces as low as ~0.4-0.5 dyn/cm^2 [168,169], and subsequently exhibit rolling adhesion on the receptor-bearing endothelial cell wall. Rolling adhesion is mediated by rapid, force-dependent selectin-selectin ligand interactions between leukocytes and the endothelium, which can transition to firm adhesion and subsequent leukocyte transmigration into inflamed tissues [192,297]. L-selectin, an important mediator on the leukocyte surface and constitutively expressed on the tips of microvilli, can initiate capture and rolling adhesion via binding to P-selectin glycoprotein ligand-1 (PSGL-1) on the endothelium [296,298,299]. Mouse knockdown experiments using L-selectin-deficient mice show impaired neutrophil, lymphocyte, and monocyte migration into inflamed tissues [253], demonstrating the importance of L-selectin in inflammation and leukocyte homing. After initial tethering to the blood vessel wall, L-selectin can be rapidly cleaved from the cell surface by metalloprotease ADAM17, in a process known as "shedding" [300], to regulate cell rolling velocity and thus the rate of firm adhesion to the endothelium [278]. In addition to L-selectin, β_2 integrins on the surface of leukocytes bind with intercellular adhesion molecule-1 (ICAM-1) on the endothelium. Integrins such as macrophage-1 antigen (Mac-1), also known as CD11b/CD18 or integrin $\alpha_M\beta_2$, and lymphocyte function-associated antigen-1 (LFA-

1), also known as CD11a/CD18 or $\alpha_L\beta_2$, are constitutively expressed on neutrophils and initially bind to ICAM-1 in an intermediate affinity state, which can result in slow rolling adhesion under low physiological shear forces [297]. In response to increased signaling by chemotactic factors, the integrin molecules Mac-1 and LFA-1 undergo further conformational changes to achieve full activation, leading to firm adhesion. Together, the shedding of L-selectin and conformational activation of β_2 integrins are key events that characterize neutrophil activation. One such chemotactic factor that induces neutrophil activation is platelet-activating factor (PAF) [301], which has been shown to lead to a decrease in L-selectin expression and activation of $\alpha_M\beta_2$ integrins on the neutrophil surface [167,302].

Hemodynamic fluid shear stresses have the ability to regulate the neutrophil activation response observed during inflammation. Human neutrophils exposed to static conditions, either in the presence or absence of chemoattractants, spread their cytoplasm, project pseudopods, and migrate on glass substrates [9,267]. Upon the application of fluid shear stress, neutrophils have been observed to retract pseudopods, assume a round resting state, and detach from glass substrates [9,267]. Conversely, leukocytes exposed to centrifugation or treated with dexamethasone can reverse their response to shear stress, and can project pseudopods upon fluid shear stress exposure [264,265]. Additionally, extended exposure to fluid shear stress can cause leukocyte membrane disruption [263].

G-protein coupled receptors (GPCRs) have been hypothesized to serve as molecular mechanosensors on the neutrophil surface. HL60 cells differentiated into neutrophils using DMSO decreased GPCR constitutive activity in the presence of fluid

shear stress, in addition to retraction of lamellipodia, and returned to a round resting state [90,279]. Treatment with Gi inhibitor pertussis toxin or depletion of the GPCR formyl peptide receptor (FPR) via siRNA delivery significantly reduced shear-induced neutrophil pseudopod retraction [90]. cDNA FPR transfection into undifferentiated HL60 cells with low FPR expression led to the projection of pseudopods, which quickly retracted in response to fluid shear stress exposure. Recently, fluid shear stress pre-exposure was shown to suppress neutrophil activation to formyl-methionyl-leucyl-phenylalanine (fMLP), which binds to FPR on the neutrophil surface during inflammation. fMLP is a chemotactic peptide derived from bacterial protein degradation and mitochondrial proteins upon tissue damage [303,304], and is present in low concentrations in the bloodstream during inflammation. Exposure to fluid shear stress in a cone-and-plate viscometer (0.1-4.0 dyn/cm^2) prior to fMLP treatment significantly reduced fMLP-induced $\alpha_M\beta_2$ integrin activation, L-selectin shedding, and pseudopod projection [91]. Neutrophils increased their resistance to fMLP-induced activation in a fluid shear stress magnitude- and exposure time-dependent manner. Interestingly, fluid shear stress did not alter the neutrophil activation response to interleukin-8 (IL-8), which binds to GPCRs CXCR1 and CXCR2 on the neutrophil surface.

In addition to exposure to fMLP and IL-8 during inflammation, neutrophils can be exposed to platelet-activating factor (PAF), a phospholipid inflammatory mediator synthesized by monocytes, platelets, neutrophils, and endothelial cells [305]. PAF can then activate platelets, neutrophils, and other leukocytes in the bloodstream, particularly during inflammation and allergy [306]. Recognition by these cells occurs

via the PAF receptor (PAFR), a GPCR on the neutrophil surface, which leads to neutrophil migration through intercellular junctions in the endothelium to ameliorate tissue injury [307,308]. After synthesis via endothelial cells, PAF is translocated to the cell surface rather than secreted into the bloodstream, where it is available for binding to blood cells [306]. This is in contrast to fMLP, which is released from bacterial and mitochondrial proteins released from tissues. Upon recognition via interaction with PAF receptors on the surface of neutrophils, PAF induces cell adhesion and cell polarization, enhanced motility, priming of granular enzyme release, and redistribution of surface adhesion ligands in neutrophils [302]. These physiological effects occur while PAF remains associated with the endothelial membrane, showing that PAF commonly acts by juxtacrine signaling, which is necessary for tightly localized neutrophil recruitment [309]. Additionally, differences in functional response have been observed with PAF and fMLP. For example, neutrophils stimulated by fMLP can produce superoxide ions, while minimal ions are produced in neutrophils stimulated by PAF [310]. The different physiological responses to inflammation suggest that different intracellular pathways are utilized by PAFR and FPR, and that the response depends on the type of chemoattractant present (i.e., PAF or fMLP).

The effect of hemodynamic shear forces on early indicators of PAF-induced neutrophil activation remains unknown. In this study, I quantified the effects of fluid shear stress pretreatment on PAF-induced neutrophil activation.

3.2 MATERIALS AND METHODS

Reagents

APC-conjugated mouse anti-human CD62L specific for human L-selectin, APC-conjugated mouse IgG_1 isotype control antibody, and FITC-conjugated mouse IgG_1 isotype control antibody were purchased from BD Biosciences (San Jose, CA). FITC-conjugated mouse anti-human CBRM1/5, which binds to the activation epitope of CD11b, was purchased from eBioscience (San Diego, CA). Platelet-activating factor (PAF) was purchased from Millipore (Billerica, MA). Primary goat anti-human PAF-R antibody, which binds to the extracellular N-terminus of the PAF receptor, and FITC-conjugated secondary donkey anti-goat IgG antibody were purchased from Santa Cruz Biotechnology (Santa Cruz, CA). Tumor necrosis factor-α protease inhibitor-0 (TAPI-0) and p38 mitogen-activated protein (MAP) kinase inhibitor SB203580 were purchased from Peptides International (Louisville, Kentucky) and Millipore, respectively. Human TruStain FcX Fc receptor blocking solution was purchased from Biolegend (San Diego, CA). Ca^{2+} and Mg^{2+} free Hank's balanced salt solution (HBSS) and Dulbecco's phosphate buffered saline (DPBS) were purchased from Invitrogen (Carlsbad, CA). Endotoxin-free water was purchased from MO Bio (Carlsbad, CA). Endotoxin-free human serum albumin (HSA) HEPES, low-endotoxin and essentially globulin-free bovine serum albumin (BSA) were purchased from Sigma Aldrich (St. Louis, MO).

Neutrophil Isolation

Primary human neutrophils were isolated as described previously [83,209]. Whole peripheral blood was obtained via venous needle injection from healthy human donors after informed consent. Neutrophils were separated by centrifugation at 480 x g at 23°C for 50 min in a Marathon 8K centrifuge (Fischer Scientific; Pittsburgh, PA) using 1-Step Polymorphs (Accurate Chemical and Scientific Corporation; Westbury, NY) and resuspended in Mg^{2+} and Ca^{2+} free HBSS to remove excess polymorph solution. Remaining red blood cells were lysed hypotonically, and purified neutrophils were resuspended in Mg^{2+} free HBSS buffer with 0.5% HSA, 10 mM HEPES, and 2 mM Ca^{2+} at a pH of 7.4 at a concentration of 0.5 x 10^6 cells/mL. Isolation protocols were approved by the Institutional Review Board (IRB) of Cornell University.

Cone-and-Plate Viscometer Assay

Cells were exposed to uniform fluid shear stress in a cone-and-plate DV-II+ pro digital viscometer (Brookfield Engineering Laboratories; Middleboro, MA) as previously described [82,86,91]. Neutrophils were placed in a plate underneath a cone angled at 0.8°. Shear rate, G, is known to be a function of cone angle and independent of distance from the center by the following equation:

$$G = \frac{\omega}{\tan\theta}$$

where ω is the angular velocity of the cone (rad/s) and θ is the cone angle (rad) [91]. To achieve a desired shear stress, τ, assuming Newtonian fluid behavior, the shear rate was varied according to the equation:

$$\tau = \mu G$$

where μ is the viscosity of the buffer solution (Pa·s)[86]. Prior to fluid shear stress exposure, the cone and plate were incubated with 5% bovine serum albumin (BSA) for 1 hour to prevent non-specific adherence of neutrophils to the steel surfaces. Neutrophils suspensions were then placed onto the plate at a concentration of 0.5 x 10^6 cells/mL. Neutrophils were exposed to fluid shear stress (0.1 – 2.75 dyn/cm^2) for 1-120 min at 23°C. Cells were then immediately incubated with 1 μM PAF for 10 min at room temperature (RT). Cells were washed and prepared for antibody labeling, or fixed in paraformaldehyde and prepared for morphology analysis. For L-selectin inhibition studies, neutrophils were treated with 25 μM TAPI-0, an inhibitor of the L-selectin sheddase ADAM-17, or 1 μM SB203580, an inhibitor of p38 MAP kinase, for 60 min prior to fluid shear stress exposure. Neutrophil viability levels of >95%, before and after cone-and-plate assays, were confirmed using a trypan blue exclusion dye.

Flow Cytometry

Untreated and PAF-treated neutrophils were incubated with APC-conjugated mouse anti-human CD62L and FITC-conjugated mouse anti-human CBRM1/5

antibodies after PAF treatment. Control samples to measure nonspecific binding were incubated with APC-conjugated and FITC-conjugated mouse IgG_1 isotype control antibodies. All samples were incubated at 4°C for 35 minutes and washed twice with cold Ca^{2+} free and Mg^{2+} free DPBS. Data were collected and analyzed using an Accuri C6 Flow Cytometer (BD Biosciences; San Jose, CA) and FCS Express V3 (De Novo Software; Thornville, Ontario, Canada) software.

Brightfield Microscopy and Imaging Analysis

Neutrophils were prepared for morphology analysis via fixation with 4% paraformaldehyde (Electron Microscopy Sciences; Hatfield, PA) for 30 min at 4°C. Cells were washed and placed in a 24-well plate, and imaged via bright field and phase contrast microscopy using an Olympus IX81 Inverted System Microscope (Olympus America; Center Valley, PA). Metamorph Software (Molecular Devices; Sunnyvale, CA) was used to threshold outlines of neutrophils. Neutrophil circularity was quantified by calculating the shape factor, defined by the following equation:

$$Shape\ \ Factor = \frac{4\pi A}{P^2}$$

where A = area (μm^2) and P = perimeter (μm) [91]. A shape factor of 1 defines a perfect circle. All shape factor data were imported into Microsoft Excel (Microsoft Corporation, Redmond, WA) for analysis.

PAF Receptor Expression

Neutrophil surface expression of PAF receptor (PAF-R) was detected using flow cytometry. Cells were incubated in Human TruStain FcX for 10 min at RT, to block nonspecific binding between Fc regions of antibodies and Fc receptors on the cell surface. Neutrophils were then labeled with PAF-R antibody (N-17) and incubated for 1 h at 4°C. After washing twice with cold Ca^{2+} free and Mg^{2+} free DPBS, samples were incubated with FITC-conjugated secondary IgG antibody for 30 min at 4°C. Samples were washed twice and analyzed using a flow cytometer. To measure PAF receptor density of neutrophils exposed to static conditions and fluid shear stress, PAF receptor fluorescence intensity measurements were compared to the fluorescence of standard microspheres with known levels of fluorescence. Quantum FITC-5 molecules of equivalent soluble fluorochrome kits (MESF; Bangs Laboratories Inc.), consisting of four types of microspheres with increasing levels of FITC fluorochrome and one blank microsphere population, were used to create a fluorescence calibration curve according to the manufacturer's instructions. Quantum FITC-5 MESF beads were analyzed for fluorescence intensity using a flow cytometer to create a standard fluorescence curve. Neutrophils exposed to static and sheared conditions, which were labeled with PAF receptor and FITC-conjugated secondary antibodies, were then analyzed for fluorescence intensity using a flow cytometer. PAF receptor density was estimated using the standard fluorescence curve.

Statistical Analysis

Shape factor and flow cytometry data were plotted using GraphPad Prism 5 (GraphPad Software; La Jolla, CA). Statistical two-tailed paired t-tests were performed to test for significant differences between data sets, with $p<0.05$ being considered significant.

3.3 RESULTS

Fluid shear stress increases neutrophil PAF-induced L-selectin shedding and $\alpha_M\beta_2$ integrin activation

We initially examined the response of neutrophils to PAF under fluid shear stress conditions in terms of L-selectin shedding and $\alpha_M\beta_2$ integrin activation using a cone a plate viscometer, which has been previously used by our lab to examine fluid shear stress effects on neutrophils and cancer cells [86,91,159]. Neutrophils were in static conditions or exposed to a fluid shear stress of 1.0 dyn/cm^2 for 2 h and subsequently treated with 1 μM PAF for 10 min at 23°C. PAF, a phospholipid produced by endothelial cells that acts as a mediator of the inflammatory response [302], is known to increase L-selectin shedding and induce structural changes in $\alpha_M\beta_2$ integrins to an activated conformation [311]. Negligible neutrophil L-selectin shedding and $\alpha_M\beta_2$ integrin activation was observed in samples exposed to static conditions (Figure 3.1A), while fluid shear stress exposure induced a moderate

increase in both indicators of activation (Figure 3.1B). However, in response to PAF neutrophils showed a greater degree of L-selectin shedding and $\alpha_M\beta_2$ integrin activation after fluid shear stress pre-exposure (Figure 3.1D), compared to pre-exposure to static conditions (Figure 3.1C). While trends indicate that shear stress exposure alone does induce an increase in neutrophil L-selectin shedding and $\alpha_M\beta_2$ integrin activation, these changes were found to be not significant (Figure 3.1E,F). In the presence of PAF, the average percentage of neutrophils that shed L-selectin increased significantly after shear stress exposure, from approximately 35% for cells under static conditions to over 70% for cells exposed to fluid shear stress (Figure 3.1E). Similarly, the average percentage of neutrophils expressing the activated $\alpha_M\beta_2$ integrin subunit increased in PAF-treated samples, from approximately 15% for cells under static conditions to approximately 60% for cells exposed to fluid shear stress (Figure 3.1F). These results suggest that fluid shear stress pre-exposure and PAF can both act to increase neutrophil activation.

PAF activation of neutrophils increases with fluid shear stress magnitude

To assess the effect of fluid shear stress magnitude on neutrophil PAF-induced activation, cells were exposed to shear stresses ranging from 0.1—2.75 dyn/cm^2 in a cone-and-plate viscometer for 30 min, followed by treatment with 1 μM PAF for 10 min at 23°C. The range of shear stress includes that typically found in the venular microcirculation [312], which is the primary site of leukocyte interactions with the endothelium [170,274]. No differences in L-selectin shedding or $\alpha_M\beta_2$ integrin

activation were seen after exposure to low fluid shear stresses of 0.1 dyn/cm^2 (Figure 3.2A,B). However, a significant increase in neutrophil PAF-induced L-selectin shedding was observed after exposure to shear stresses of 1.0 dyn/cm^2 and 2.75 dyn/cm^2, compared to static conditions (Figure 3.2A). Fluid shear stress induced a similar increase in activation in terms of the activated $\alpha_M\beta_2$ integrin epitope, when compared to neutrophils stimulated with PAF under static conditions (Figure 3.2B).

To identify the increase in shedding of L-selectin and activated $\alpha_M\beta_2$ integrin subunit expression with respect to fluid shear stress, the neutrophil sensitization responses to L-selectin shedding and $\alpha_M\beta_2$ integrin activation were calculated using the following equation:

$$\%\ \text{PAF Activation Increase} = \frac{(\%\ \text{Cells}_{\text{Shear}})\text{-}(\%\ \text{Cells}_{\text{Static}})}{\%\ \text{Cells}_{\text{Static}}}\ \text{X}\ 100\%$$

When shear stress magnitude was varied, it was found that the PAF activation increase in neutrophils increased with increasing magnitude of fluid shear stress pre-exposure (Fig 1C).

Neutrophil PAF activation is dependent on fluid shear stress exposure time

To study the kinetics of the neutrophil PAF activation in the presence of fluid shear stress, neutrophils were sheared at 1.0 dyn/cm^2 for durations ranging from 5 to 120 min at 23°C, followed by stimulation with 1 μM PAF. While no significant differences in L-selectin shedding were observed after 10 min shear stress exposure,

L-selectin shedding significantly increased after shear stress exposure for 30 min (Figure 3.3A). A significant increase in PAF-induced $\alpha_M\beta_2$ integrin activation was also observed after 30 min of exposure to shear stress conditions (Figure 3.3B). The percent PAF increase equation used to calculate the shear stress dose response plot was also used to quantify the increase in neutrophil PAF activation over shear stress exposure time. With increasing durations of shear stress pre-exposure, neutrophils stimulated with PAF increased their level of activation (Figure 3.3C). By 30 min, the percent increase in L-selectin shedding and $\alpha_M\beta_2$ integrin activation reached ~95% and 45%, respectively.

Fluid shear stress increases PAF-induced neutrophil morphological changes

In addition to L-selectin shedding and $\alpha_M\beta_2$ integrin activation, cell polarization is among the responses exhibited in activated neutrophils after PAF stimulation [302]. During this phenomenon, neutrophils extend pseudopods to enable cell motility, allowing neutrophils to effectively extravasate through the blood vessel wall and migrate to inflamed tissue during the immune response [275]. To assess the effect of fluid shear stress on cell polarization, neutrophils were exposed to 1.0 dyn/cm^2 shear stress for 30 min, followed by stimulation with PAF. Cells were then fixed with 4% paraformaldehyde and examined for morphological changes. Qualitative evaluation of neutrophil morphology in the absence of PAF under either static conditions or 1.0 dyn/cm^2 fluid shear stress showed similar round morphologies (Figure 3.4A,B) characteristic of resting neutrophils. Upon stimulation with PAF,

neutrophils assumed a notably more elongated form with extended pseudopods (Figure 3.4C), while cells exposed to shear prior to PAF stimulation displayed more exaggerated features than those under static conditions (Figure 3.4D). To calculate neutrophil shape factor, images were thresholded to select the outline of the cells to be measured (Figure 3.4E). Neutrophils exposed to static and shear conditions in the absence of PAF stimulation both exhibited shape factors close to 1 and were not significantly different from each other (Figure 3.4F), consistent with empirical observations. While neutrophils stimulated with PAF after exposure to static and shear conditions displayed shape factor values significantly less than those in the absence of PAF, PAF-treated neutrophils exposed to shear stress showed significantly lower average shape factor than those exposed to static conditions (Figure 3.4F). These results indicate that fluid shear stress enhances changes in neutrophil morphology in response to PAF.

Neutrophil PAF surface receptor expression is unaltered in response to fluid shear stress

Previous studies showed that neutrophil response to fluid shear stress can result in changes in chemoattractant surface receptor expression [91]. To investigate whether neutrophil response to fluid shear stress alters the expression of the PAF receptor (PAFR) on the cell surface, neutrophils were exposed to fluid shear stress (1.0 dyn/cm^2) for 30 min, labeled with fluorescent anti-PAFR antibodies, and analyzed via flow cytometry. The distribution of PAFR surface expression among the neutrophil

population remained unchanged between static and shear conditions (Figure 3.5A). PAFR surface expression was quantified in terms of percent of neutrophils expressing PAF receptor, and results show no significant change in expression between neutrophils under static and shear conditions (Figure 3.5B). To measure PAF receptor densities of neutrophils exposed to shear and static conditions, quantum MESF beads were used to generate a fluorescence standard curve to estimate the number of PAF receptors per neutrophil. No significant differences in the number of PAF receptors per neutrophil were found, as neutrophils exposed to either shear or static conditions averaged ~9000 PAF receptors/cell (Figure 3.5C).

Shear stress and PAF-induced neutrophil L-selectin shedding is ADAM-17 and p38 MAP kinase-dependent

Neutrophil shedding of L-selectin is dependent on the p38 mitogen-activated protein kinase pathway [313]. This pathway subsequently leads to activation of ADAM-17, a protease involved in TNF-α activation and known to regulate L-selectin shedding [314]. To shed light upon the mechanism by which L-selectin is shed in the presence of shear stress pre-exposure followed by PAF stimulation, neutrophils were treated with 25 μM TAPI-0 (Figure 3.6C) and 1 μM SB203580 (Figure 3.6D), inhibitors of p38 MAP kinase and ADAM-17 sheddase, respectively, for 60 min prior to shear stress exposure. Untreated and PAF-treated neutrophils maintained in static conditions (Figure 3.6A,C,E,G) or fluid shear stress (Figure 3.6B,D,F,H) were then labeled with fluorescent anti-L-selectin antibodies. Expression of L-selectin on

inhibitor-treated cells was then compared to uninhibited cells with and without PAF treatment. Consistent with previous work, static neutrophils treated with TAPI-0 or SB203580 and subsequently stimulated with PAF showed minimal L-selectin shedding, relative to untreated neutrophils (Figure 3.6I). After shear stress exposure, sensitization to PAF-induced L-selectin shedding was attenuated in TAPI-0 and SB203580-treated neutrophils (Figure 3.6E-I), supporting the idea that fluid shear stress and PAF-induced L-selectin shedding is ADAM-17 and p38 MAP kinase-dependent.

3.4 DISCUSSION

The goal of this study was to characterize the effect of fluid shear stress on PAF-induced L-selectin shedding, $\alpha_M\beta_2$ integrin activation, and morphological changes in neutrophils. Our results show that neutrophil PAF activation is significantly increased after fluid shear stress pre-exposure of magnitude as low as 1.0 dyn/cm^2, consistent with previous studies. Marschel et. al., observed rapid pseudopod retraction of neutrophils adhering via β_2 integrins on a glass substrate upon fluid shear stress exposure at 1.0 dyn/cm^2 [315]. In terms of initial rolling adhesion, Finger et. al. reported that a minimal wall shear stress of 0.4 dyn/cm^2 is required for stable tethering and rolling of neutrophils via L-selectin on peripheral lymph node addressin (PNAd), with a maximal number of neutrophils rolling at 1.0 dyn/cm^2 [169]. Sundd et. al. reported that fluid shear stresses greater than 0.5 dyn/cm^2 are required for neutrophil

rolling on P-selectin. Such adhesion is a necessary precursor interaction to binding with PAF on endothelial cells during the onset of inflammation [168].

Interestingly, our previous study characterizing the effect of fluid shear stress on fMLP-induced L-selectin shedding and $\alpha_M\beta_2$ integrin activation in neutrophils showed that, in stark contrast to our current findings, neutrophils display a resistance instead of a sensitization to chemoattractant stimulation [91]. fMLP is a peptide chemoattractant released by certain bacteria and mitochondria at a site of tissue infection and/or injury, and activates neutrophils by interacting with the formyl peptide receptor on the neutrophil surface (Figure 3.7) [316]. In humans, fMLP present only at very low concentrations in the bloodstream, compared to sites of tissue infection and/or injury. Sustained activation to fMLP stimuli in the bloodstream could hinder the neutrophil response to infection by promoting pseudopod projection, increasing neutrophil transit time in blood, and enhancing neutrophil retention in the microvasculature [317,318]. Thus, if neutrophils pre-exposed to hemodynamic shear forces in the bloodstream increased fMLP-induced activation, neutrophils would be fully activated in the bloodstream and less efficient at transmigrating into localized tissues. Additionally, activation of neutrophils via fMLP also induces production of reactive oxygen species (ROS) [319], and thus shear-induced resistance to fMLP can reduce ROS-induced damage to healthy blood vessels. By developing a resistance to fMLP-induced activation when exposed to shear in the bloodstream, neutrophils avoid unnecessary activation in the bloodstream, facilitating extravasation and subsequent migration in tissues. In contrast, PAF-induced activation of neutrophils in the bloodstream is physiologically important (Figure 3.7).

PAF is a unique chemotactic factor in that it triggers both thrombotic and acute inflammatory responses after stimulation by chemical mediators found in the blood, such as thrombin and histamines, and thus links the hemostatic and innate immune responses [320]. For platelets, exposure to PAF is important for activation and aggregation at sites of vascular injury. For neutrophils, it primes the release of granular factors, which play a role in coagulation [302]. Because it is secreted by various leukocytes in the fluid phase, PAF is thought to have endocrine and paracrine signaling roles as well, which may also necessitate its presence in the vascular system for its use as a means of transport [302]. The increase in neutrophil PAF activation in the presence of fluid shear stress primes neutrophils for activation in the bloodstream, allowing them to respond to vascular injury [320]. The differences in PAF and fMLP-induced activation after shear stress pretreatment suggest that there is an underlying mechanism for neutrophils to optimize their response to their local fluid shear stress microenvironment (Figure 3.7).

While the observed sensitization response was not coupled with a shear stress-induced change in PAF receptor density on the neutrophil surface, sensitization to L-selectin shedding was shown to be p38 MAP kinase (MAPK)-dependent. The molecular mechanisms underlying $\alpha_M\beta_2$ integrin activation were not probed, as they remain poorly understood and is the subject of ongoing research [321,322]. While this study focused on mechanical force-induced increases to PAF-induced activation, increases in neutrophil PAF activation have previously been induced by chemical exposure. Human recombinant granulocyte-macrophage colony-stimulating factor (GM-CSF) was shown to prime arachidonic acid release and intracellular calcium

fluxes in neutrophils after PAF stimulation [323]. One proposed hypothesis for this phenomenon is that GM-CSF remodels the lipid profile of the neutrophil plasma membrane, causing receptors on the neutrophil surface to become more accessible to substrates [323]. This hypothesis may also explain the observed increases in PAF activation; shear forces may act on the neutrophil membrane to readily expose the PAFR for easier access by immobilized PAF, without changing receptor density. Ginkgolide B (GKB), a bioactive component of the Ginkgo biloba leaf extract 761, is another chemical found to prime neutrophils for activation. GKB primes fMLP- and zymosan-induced respiratory burst in neutrophils by acting through the PAF receptor. Although this mechanism remains unknown, it is hypothesized that this priming effect may involve phosphorylation or some conformational change of PAFR to a more activated form. It has been suggested by a number of studies in response to observations of heterogeneous low- and high-affinity binding of PAFR to PAF that PAFR may exist in various conformational states and requires activation in order to achieve high-affinity binding [324,325]. Mutations of the Ala230 and Leu231 residues on the third intracellular loop of the receptor to Glu230 and Arg231, respectively, have been shown to lead to inactive and constitutively active PAFR states [326]. This finding suggests the possibility that fluid shear stress may affect the PAF receptor directly, and future work could probe conformational changes or clustering of the receptor in response to shear.

In response to PAF stimulation, PAFR, much like other GPCRs, can internalize into cells with their respective PAF ligands to cause either desensitization or resensitization of the receptor [284,327,328]. Immediately after PAF binding,

PAFR uncouples from G-proteins, and are rapidly phosphorylated by different kinases. During densensitization, PAFR can undergo endocytosis into endosomes and be targeted for degradation via ubiquitination [328]. This can lead to an overall down regulation of PAFR, and thus desensitization in the presence of PAF ligands. Conversely, resensitization to PAF can occur, in a process where PAFR is thought to move into early endosomes and recycle to the cell membrane. Previous work by our group showed that FPR can internalize within neutrophils upon exposure to fluid shear stress, in the absence of fMLP stimulation [91]. In this study, there were no differences found in PAFR expression on the neutrophil surface after fluid shear stress exposure, thus suggesting that the fluid shear stress pre-exposure does not desensitize neutrophils to PAF stimulation. However, it is possible that fluid shear stress pre-exposure could affect PAFR internalization in the presence of the agonist, perhaps by enhancing recycling of PAFR, which would explain the increase in neutrophil PAF activation.

Neutrophil p38 MAPK signaling may also be influenced by fluid shear stress exposure. Killock et. al. showed that stimulation of resting leukocytes with calcyculin A or cantharidin led to increased levels of phosphorylated p38 MAPK, which triggers increased phosphorylation of the cytoplasmic tails of TNF-α-converting enzyme (TACE) and its subsequent expression on the cell surface, which likely caused the simultaneous increase of L-selectin shedding [329]. Fluid shear stress may increase phosphorylation of p38 MAPK in a similar manner, to induce the sensitized L-selectin shedding response observed in our study. To explore this possible mechanism, future efforts could compare the surface expression of TACE or radioactively labeled

phosphorylated p38 MAPK pre- and post-shear stress exposure. Downstream of PAFR signaling, PAF, like fMLP, is known to strongly activate MAP kinase kinase-3 (MKK3). Unlike fMLP, PAF minimally activates MAP ERK kinase kinase-1 (MEKK1), Raf, and the p42/44 (ERK) MAP kinases, all of which are pathways that are strongly activated by fMLP [310]. Fluid shear stress could act to increase activation of these pathways to enhance neutrophil PAF-induced activation.

One important difference between the experimental conditions of this study and the physiological conditions of the human body is the presentation of PAF. Physiologically, while PAF is secreted by many leukocytes in a fluid-phase form, in the inflammatory response it is most commonly synthesized by endothelial cells and is translocated onto the cell surface, where it primarily acts through a juxtacrine signaling mechanism. The main advantage to the cell-associated form of communication is to allow for spatial regulation of signaling and only permit localized activation, thus preventing activation of PMNs in free-flowing blood [330]. Because unregulated secretion of PAF has been shown to induce anaphylactic or septic shock and trauma [320], the body has adopted various mechanisms to regulate plasma PAF concentrations. One method of control is by PAF acetylhydrolase, which degrades PAF and limits its half-life to no more than a few minutes in the blood stream [302]. The half-life of PAF in a study involving patients with acute allergic reactions was found to be ~13.6 minutes in serum with the lowest PAF acetylhydrolase activity, ~6.0 minutes in serum with intermediate PAF acetylhydrolase activity, and ~3.8 minutes in serum with the highest PAF acetylhydrolase activity [331]. Our experiments were conducted in the absence of PAF acetylhydrolase, and neutrophils were treated with

PAF for a duration of 10 minutes. Thus, we expect there to be less neutrophil activation than that reported in our results in individuals with intermediate to high PAF acetylhydrolase activity. In addition to limiting the actions of PAF in the bloodstream, the body also has mechanisms to facilitate neutrophil recognition of PAF. One example of this involves granule membrane protein-140 (GMP-140), a membrane glycoprotein in the granules of platelets and endothelial cells that is translocated to the cell surface along with PAF upon stimulation by histamine or thrombin. It is found to act cooperatively with PAF in facilitating recruitment of β_2 integrins on neutrophils in an indirect manner – it initiates tethering of neutrophils to endothelial cells, bringing the otherwise inaccessible and immobilized PAF in proximity to its receptor on neutrophils [332]. In comparison, the fluid phase form of the chemoattractant in our study may make PAF more accessible to neutrophils and heighten the response. While the discrepancy between the experimental conditions of our study and those of in vivo conditions may cause differences in the degree of neutrophil activation, our reported findings still hold –fluid shear stress sensitizes PAF-induced L-selectin shedding, $\alpha_M\beta_2$ integrin activation, and morphological changes of neutrophils during the inflammatory response. Future work that explores the role of other enzymes in the p38 MAPK pathway downstream of PAFR, potential cross-talk mechanisms between integrins, and the possibility of different conformational states in the receptor itself may bring a greater understanding of the molecular details of the role of fluid shear stress in the innate immune response.

FIGURE 3.1: FLUID SHEAR STRESS EXPOSURE AND PLATELET ACTIVATING FACTOR INCREASE NEUTROPHIL ACTIVATION. Neutrophils exposed to (A) static and (B) shear conditions at 1.0 dyn/cm^2 for 2 h. PAF-treated samples were exposed to 1 μM PAF for 10 min (C, D) and analyzed for activation. Upper 2 quadrants signify activated $\alpha_M\beta_2$ integrin subunit expression. Two right-hand quadrants show L-selectin expression. Gating was determined using fluorescence intensities of isotype controls. Bar graph representation of (E) L-selectin shedding and (F) $\alpha_M\beta_2$ integrin activation. "Low L-selectin" denotes neutrophils that have shed L-selectin from their surface, and have fluorescence intensities no greater than that of isotype controls. Conditions were repeated for 3 donors (n = 3). Error bars signify 95% confidence intervals. **P* < 0.05. *NS*: not significant.

FIGURE 3.1: FLUID SHEAR STRESS EXPOSURE AND PLATELET ACTIVATING FACTOR INCREASE NEUTROPHIL ACTIVATION.

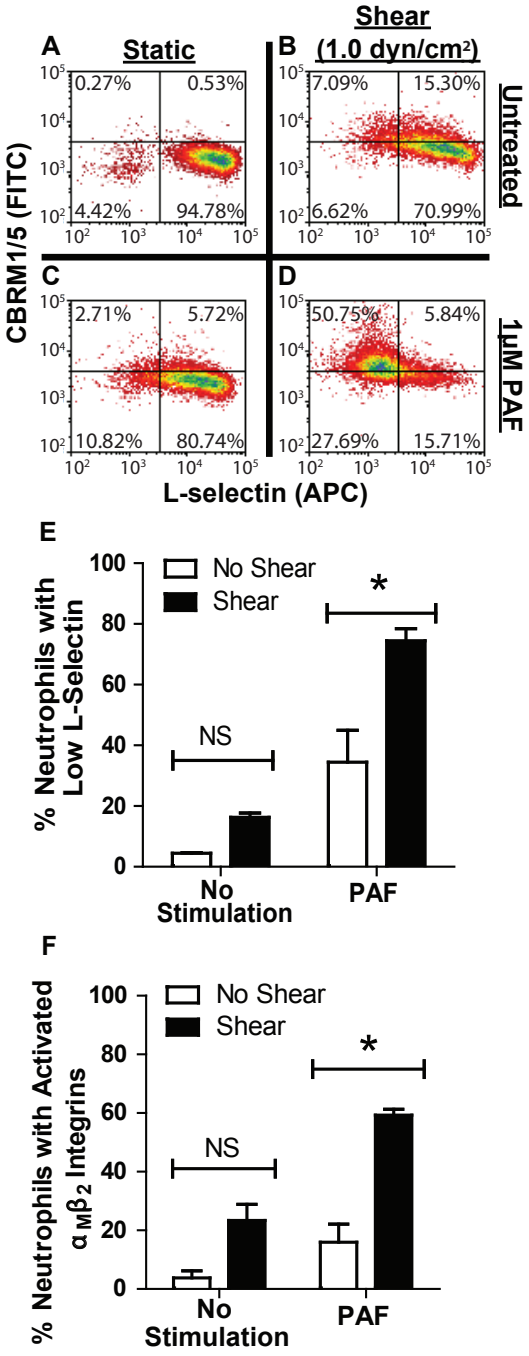

FIGURE 3.2: PAF ACTIVATION OF NEUTROPHILS IS FLUID SHEAR STRESS MAGNITUDE-DEPENDENT. Cells were exposed to a range of shear stress (0.1-2.75 dyn/cm^2) for 30 min at 23°C, followed by immediate treatment with 1 μM PAF for 10 min. Quantification of (A) L-selectin shedding and (B) activated $\alpha_M\beta_2$ integrin expression on neutrophils after exposure to increasing shear stress. (C) Percent platelet activating factor (PAF) activation increase, in terms of L-selectin shedding and $\alpha_M\beta_2$ integrin activation, plotted as a function of the $\log_{10}$ of shear stress. *$P < 0.05$, ** $P < 0.01$.

FIGURE 3.2: PAF ACTIVATION OF NEUTROPHILS IS FLUID SHEAR STRESS MAGNITUDE-DEPENDENT.

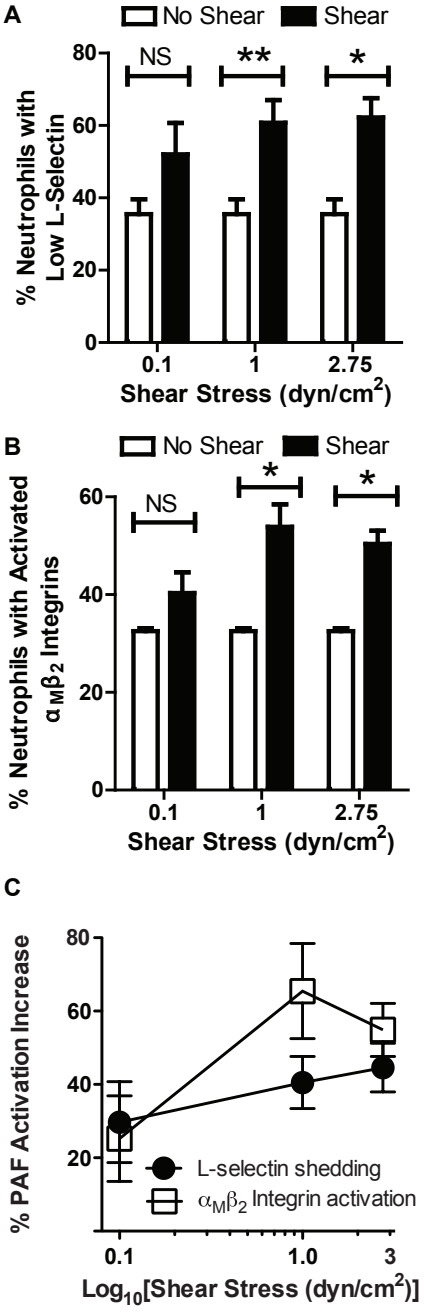

FIGURE 3.3: INCREASED NEUTROPHIL PAF ACTIVATION IS FLUID SHEAR STRESS TIME-DEPENDENT. Cells were sheared (1.0 dyn/cm^2) for a duration of 5-120 min at 23°C and immediately incubated in 1 μM PAF for 10 min. Quantification of (A) L-selectin shedding and (B) activated $\alpha_M\beta_2$ integrin expression of neutrophils over time. (C) Percent platelet activating factor (PAF) activation increase, in terms of L-selectin shedding and $\alpha_M\beta_2$ integrin activation, plotted as a function of the $\log_{10}$ of time. *$P < 0.05$, **$P < 0.01$.

FIGURE 3.3: INCREASED NEUTROPHIL PAF ACTIVATION IS FLUID SHEAR STRESS TIME-DEPENDENT.

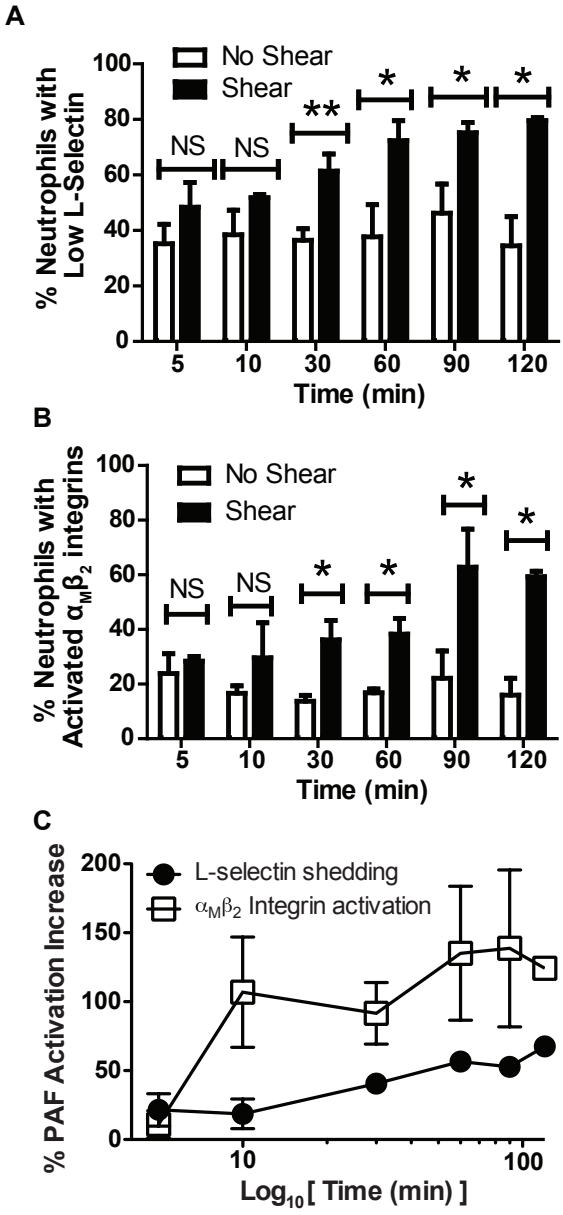

FIGURE 3.4: FLUID SHEAR STRESS INCREASES NEUTROPHIL MORPHOLOGICAL CHANGES IN THE PRESENCE OF PAF. Representative brightfield images of untreated neutrophils after exposure to (A) static and (B) shear conditions (1.0 dyn/cm^2) for 30 min, compared to cells stimulated with 1 μM PAF after exposure to (C) static and (D) shear conditions. Scale bar = 50 μm. (E) Shape factor data of neutrophils exposed to static (1.0 dyn/cm^2) or shear conditions, with and without 1 μM PAF stimulation. (E) Inset: images were thresholded to calculate shape factor of cells (scale bar = 5 μm). *n* = 3 donors, with 100 neutrophils from each donor analyzed for shape factor.

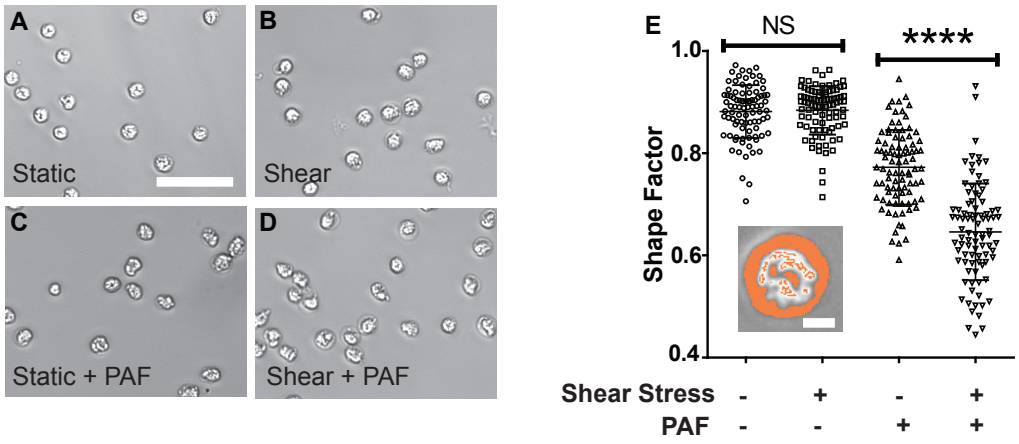

FIGURE 3.5: FLUID SHEAR STRESS DOES NOT ALTER PAF RECEPTOR EXPRESSION. Neutrophils were exposed to fluid shear stress (1.0 dyn/cm^2) for 30 min at 23°C. Flow cytometry histograms (A) and mean fluorescence intensities (B) of PAF receptor expression in sheared and nonsheared neutrophil samples. (C) PAF receptor density of neutrophils exposed to static conditions and fluid shear stress (1.0 dyn/cm^2) for 30 min at 23°C. *NS*: not significant.

FIGURE 3.5: FLUID SHEAR STRESS DOES NOT ALTER PAF RECEPTOR EXPRESSION.

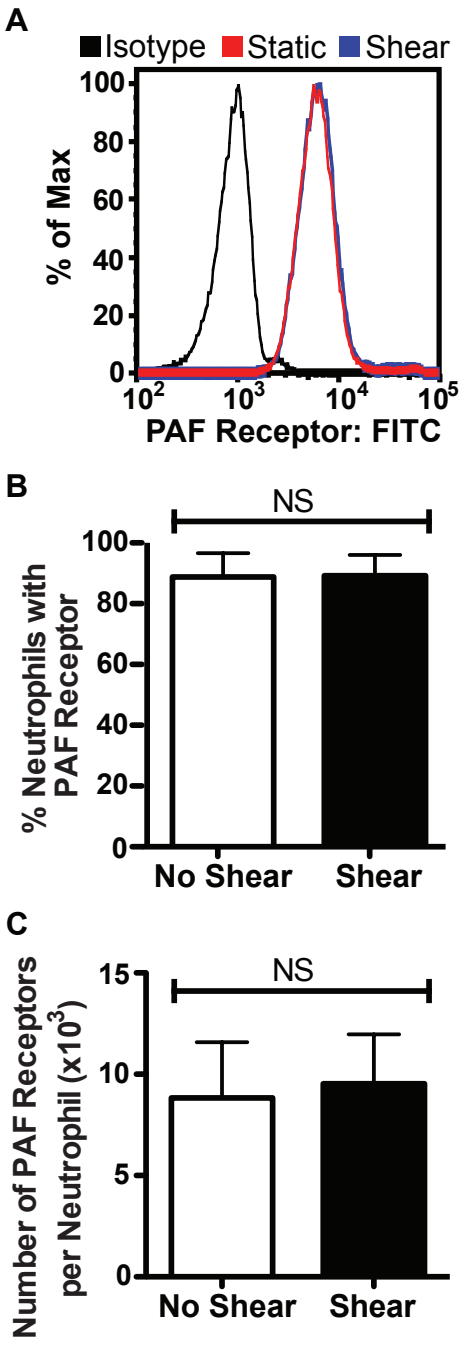

FIGURE 3.6: SHEAR AND PAF-INDUCED L-SELECTIN SHEDDING IS ADAM-17 AND P38 MAP KINASE-DEPENDENT. L-selectin expression as a function of forward scatter of nonsheared and sheared (1.0 dyn/cm^2) neutrophils in the absence of PAF (A,B) after treatment with PAF (C,D), and PAF-stimulated cells treated with TAPI-0 (E,F) and SB203580 (G,H). Gate determined using fluorescence of isotype controls. (I) Quantification of L-selectin shedding in all samples. $n = 3$ separate donors. $^*P < 0.05$. *NS*: not significant.

FIGURE 3.6: SHEAR AND PAF-INDUCED L-SELECTIN SHEDDING IS ADAM-17 AND P38 MAP KINASE-DEPENDENT.

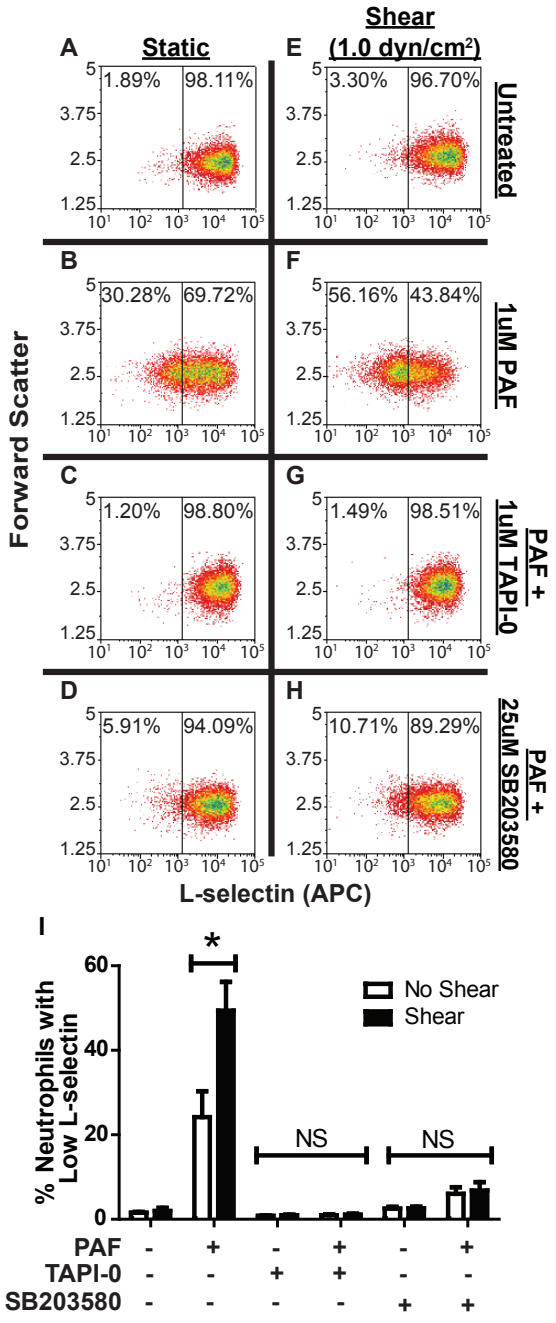

FIGURE 3.7: COMPARISON OF FLUID SHEAR STRESS EFFECTS ON NEUTROPHIL ACTIVATION VIA PAF AND FMLP. Comparison of fluid shear stress effects on neutrophil activation via PAF (A) and fMLP (B). Shear stress exposure in the microvasculature increases neutrophil activation via PAF (A), while activation is be suppressed upon exposure to fMLP (B). FSS: fluid shear stress. PAF: platelet-activating factor. PAFR: platelet-activating factor receptor. FPR: formyl peptide receptor.

FIGURE 3.7: COMPARISON OF FLUID SHEAR STRESS EFFECTS ON NEUTROPHIL ACTIVATION VIA PAF AND FMLP.

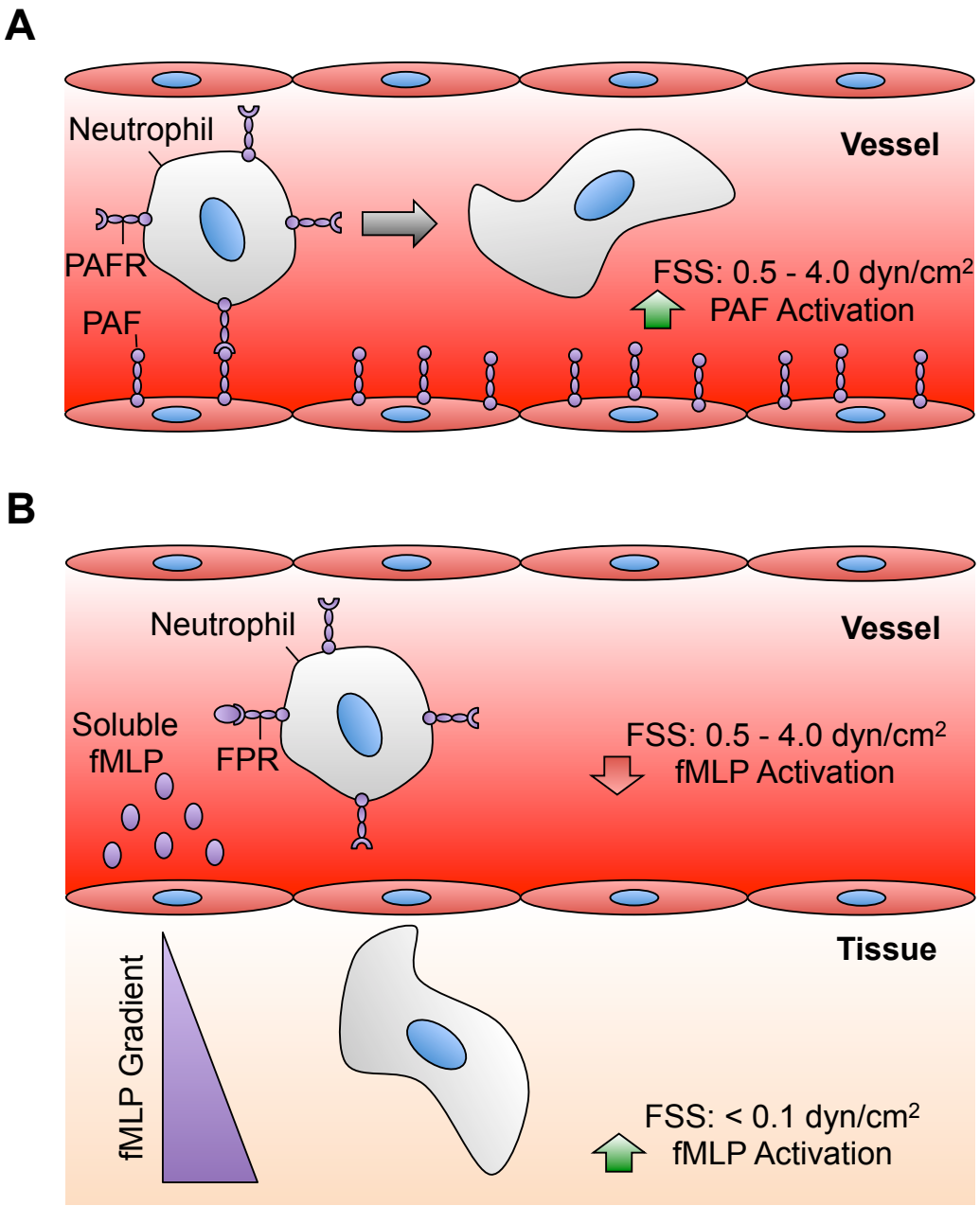

CHAPTER 4: FLUID SHEAR STRESS SENSITIZES CANCER CELLS TO RECEPTOR-MEDIATED APOPTOSIS VIA TRIMERIC DEATH RECEPTORS

*This section is adapted from the following publication: M.J. Mitchell and M.R. King. *New Journal of Physics.* 15(015008): 1-18, 2013.

4.1 INTRODUCTION

Approximately 90% of human cancer-related deaths are due to cancer metastasis [1], which consists of a series of discrete steps that allow cancer cell migration from a primary site to a distal location. For hematogenous metastasis to occur, cancer cells must detach from the primary tumor, invade surrounding tissue, and intravasate into the circulation as circulating tumor cells (CTCs) [51]. Once in the circulation, CTCs are believed to adhere to the luminal surface of the microvasculature in a manner similar to the leukocyte adhesion cascade [176]. The process consists of adhesive interactions with the receptor-bearing endothelial cell wall, including selectin-mediated cell tethering and rolling along the endothelium, followed by firm adhesion or arrest [52,176]. Once firmly adhered, CTCs may extravasate into a distal site and proliferate to form secondary tumors [333,334]. Radiation therapy, chemotherapy and surgery are generally successful in the treatment of primary tumors, however the treatment of metastases is challenging due to its systemic nature, and typically signals a poor prognosis [335]. The targeting and treatment of CTCs within the circulation are a potential solution to reduce the probability of metastasis. Several approaches have been developed to isolate patient CTCs from whole blood [336,337], along with novel strategies to target and treat CTCs with therapeutics under physiological flow [82,85].

One therapeutic that has displayed potential for the treatment of CTCs is tumor necrosis factor-related apoptosis-inducing ligand (TRAIL), a type 2 transmembrane protein of the tumor necrosis factor family [338]. TRAIL binds to death receptors (DR4 and DR5) expressed on the surface of a range of cancer cells, which can induce

cell apoptosis [84]. TRAIL also binds to three decoy receptors (DcR1, DcR2, DcR3) expressed on the surface of cells, which do not signal apoptosis and can act as competitive inhibitors to apoptosis [339]. Additionally, TRAIL does not exert apoptotic effects on most normal cells [87]. Natural killer (NK) cells, which are believed to play a physiological role in natural protection against tumor formation [340], can express TRAIL on the NK cell membrane. NK cell subpopulations in adult mouse liver constitutively expressed TRAIL in an interferon ϒ- dependent manner, and played a role in the suppression of tumor initiation and metastasis [341,342]. Interferon ϒ-dependent TRAIL expression on NK cells also plays a role in interferon ϒ-dependent tumor prevention effects of interleukin-12 (IL-12) and α-galactosylceramide (α-GalCer) [343]. In addition to its therapeutic effects as a soluble ligand, TRAIL can play a role in NK cell surveillance of CTCs and tumors [342].

The microenvironments of tumors and CTCs are remarkably different, with fluid shear forces being one factor that is dramatically altered once cancer cells enter the vascular microenvironment. In the tumor microenvironment, cancer cells are exposed to shear stresses created by interstitial flows, which range from 0.1 to 1.0 μm/s in normal tissues and higher values in the tumor microenvironment [12,18]. Such flows cause an upregulation of transforming growth factor beta (TGFβ) in fibroblasts, which can lead to myofibroblast differentiation, along with TGFβ-dependent alignment and stiffening of the extracellular matrix [34]. Interstitial flows can also upregulate matrix metalloproteinase expression to enhance glioma cell invasion [97]. Surface shear stress estimates for cancer cells exposed to interstitial flow are difficult to measure, but are estimated to be relatively low in comparison to those experienced in the

vasculature. For interstitial flow rates of 1 μm/s, one study estimated a fluid shear stress range of 0.007-0.015 dyn/cm^2 [20]. This is in contrast to shear stresses in the circulation, which range from approximately 0.5 to 4.0 dyn/cm^2 in the venous circulation and 4.0 to 30.0 dyn/cm^2 in the arterial circulation, with the maximum shear stress experienced at the vessel wall [46]. Increases in fluid shear forces could affect cancer cell survival, as only a small portion of CTCs survive the circulation to generate metastases [344]. Conversely, fluid shear forces can aid CTCs in binding to the vascular endothelium via selectin-mediated tethering and rolling, followed by firm adhesion to the endothelium [345]. While previous studies have investigated the role of fluid shear forces in CTC adhesion to the microvasculature, little is known about the effects of fluid shear forces on the viability and proliferation of CTCs [6].

The role of hemodynamic shear forces in altering receptor-mediated apoptosis of cancer cells has not yet been investigated. In this study, I investigated the role of physiological shear forces in sensitizing cancer cells to TRAIL-mediated apoptosis.

4.2 MATERIALS AND METHODS

Cell culture

Colorectal adenocarcinoma cell line COLO 205 (ATCC #CCL-222) and prostate adenocarcinoma cell line PC-3 (ATCC #CRL-1435) were purchased from American Type Culture Collection (Manassas, VA, USA). COLO 205 and PC-3 cells were cultured in RPMI 1640 and F-12K cell culture medium from Invitrogen (Grand

Island, NY, USA). Complete media was supplemented with 10% (v/v) fetal bovine serum and 1% (v/v) PenStrep, all purchased from Invitrogen. COLO 205 and PC-3 cells were incubated under humidified conditions at 37°C and 5% CO_2, and were not allowed to exceed 90% confluence.

Preparation of cell for fluid shear stress studies

COLO 205 and PC-3 cells were washed in Ca^{2+} and Mg^{2+} free Hank's balanced salt solution (HBSS) (Invitrogen, Carlsbad, CA, USA) and then treated with Accutase (Sigma Aldrich, St. Louis, MO, USA) for 5-10 min at 37°C before handling. COLO 205 and PC-3 cells were washed with Ca^{2+} and Mg^{2+} free Dulbecco's phosphate buffered saline (DPBS) (Invitrogen) at 300 X *g* for 5 min at 23°C. Cells were resuspended in media at a concentration of 0.5 x 10^6 cells/mL. Prior to performing fluid shear stress studies, 99% cell viability was confirmed using a trypan blue exclusion stain (Gibco, Grand Island, NY, USA).

For TRAIL studies, cells were treated with 0.1 μg/mL recombinant human TRAIL (R&D Systems, Minneapolis, MN, USA) prior to the application of fluid shear stress. For caspase inhibition studies, cells were treated with 50 μM of pan-caspase inhibitor Z-VAD-FMK or negative control compound Z-FA-FMK (R&D Systems) for 4 hours at 37°C prior to TRAIL treatment. For doxorubicin (DOX) studies, COLO 205 cells were treated with doxorubicin hydrochloride (Sigma Aldrich) at a concentration of 20 μM, which has previously been shown to induce COLO 205 cell death, prior to the onset of fluid shear stress [82].

Cone-and-plate viscometer assay

To study the fluid shear stress response of cancer cells in a controlled, uniform environment, studies were conducted using a cone-and-plate viscometer consisting of a stationary plate underneath a rotating cone maintained at 37°C by a circulating water bath (Brookfield, Middleboro, MA) as described previously [91]. The design of the cone-and-plate device allows a uniform shear rate to be applied to the cancer cell suspension. The shear rate (G), does not depend on distance from the center of the cone, and is given by:

$$G = \frac{\omega}{\tan\theta}$$

where ω is the cone angular velocity (rad/s) and θ is the cone angle (rad). Under all experimental conditions, a laminar flow field is expected. For a Newtonian fluid under these conditions, the shear stress, τ, is proportional to the shear rate being applied:

$$\tau = \mu G$$

where μ is the viscosity of the medium. Prior to fluid shear stress experiments, the stationary plate and rotating cone were washed thoroughly with 70% ethanol. TRAIL or doxorubicin-treated cancer cell suspensions were introduced to the plate at a concentration of 0.5 x 10^6 cells/mL, and were allowed to equilibrate for 1 min prior to

the onset of fluid shear stress. To identify a shear stress threshold required for cancer cell sensitization to TRAIL, cells were exposed to shear stresses ranging from 0.05-2.0 dyn/cm^2 for a duration of 120 min. To determine the shear stress exposure time required for TRAIL sensitization, cells were exposed to a shear stress of 2.0 dyn/cm^2 for increasing time intervals of 1-120 min. COLO 205 sensitization responses were determined by comparing samples exposed to shear and static conditions using the following equation:

$$\%\ Sensitization = \frac{(\%\ Cells, shear\ conditions) - (\%\ Cells, static\ conditions)}{(\%\ Cells, static\ conditions)} \times 100\%$$

The sensitization equation applies to COLO 205 cells labeled for apoptosis and necrosis, for both TRAIL-treated and untreated samples, at all shear stress magnitudes and exposure times.

After exposure to shear stress, cells were washed thoroughly in PBS and analyzed for cell death using an Annexin-V assay. For doxorubicin studies, cells were washed and incubated overnight prior to apoptosis analysis, as a longer incubation time was required for cells to undergo doxorubicin-induced apoptosis.

Annexin-V apoptosis assay

A FITC-conjugated Annexin-V assay (Trevigen, Gaithersburg, MD, USA) was used to assess cell apoptosis and necrosis. Due to the intrinsic fluorescence of

doxorubicin, all doxorubicin treated cells were analyzed using an APC-conjugated Annexin-V assay (BD Pharmingen, San Diego, CA, USA). The manufacturer's instructions were followed to prepare samples for flow cytometric analysis. Viable cells were identified as being negative for both Annexin-V and propidium iodide (PI), early apoptotic cells were positive for Annexin-V only, late apoptotic cells were positive for both Annexin-V and PI, and necrotic cells were positive for PI only.

Flow cytometry

Cells were incubated with Annexin-V reagents for 15 min at room temperature in the absence of light, and immediately analyzed using an Accuri C6 flow cytometer (Accuri Cytometers Incorporated, Ann Arbor, MI, USA). Flow cytometry plots were generated using Accuri CFlow Plus and FCS Express V3 software (De Novo Software, Thornhill, Canada). The following control samples were used to calibrate the instrument: unlabeled cell samples to evaluate the level of autofluorescence and adjust the instrument accordingly, and cell samples labeled individually with Annexin-V and PI to define the boundaries of each cell population.

Brightfield and phase contrast microscopy

Cell samples were placed into 6 well plates and incubated at 37°C for 60 min to allow cells to adhere to the plate surface. Cells were then imaged by brightfield and phase contrast microscopy using an Olympus IX81 inverted microscope (Olympus

America Inc., Center Valley, PA) to observe the presence of viable cells and membrane blebbing, which is characteristic of cells undergoing apoptosis. All images were processed using ImageJ software (U.S. National Institutes of Health, Bethesda, MD, USA).

Death receptor quantification

The average number of death receptors on the surface of cancer cells was determined using flow cytometry calibration with Quantum simply cellular (QSC) anti-mouse IgG beads (Bangs Laboratories, Inc., Fisher, IN, USA). QSC beads were incubated for 45 min at 4°C with a phycoerythrin (PE)-conjugated antibody specific to the antigen on the beads. A mixture of antibody-conjugated beads with a range of antigen binding capacities (ABCs) was run through a flow cytometer. Bead populations corresponding to increasing numbers of ABCs yield increasingly fluorescent peaks in the PE fluorescence channel. Median values of each fluorescence peak were obtained using Accuri CFlow Plus software. Fluorescence data and ABC values reported by the manufacturer were used to generate a calibration curve using QuickCal v2.3 (Bangs Labs, Fisher, IN).

Following the calibration step, surface expression of death receptors DR4 and DR5 on cancer cells was determined using flow cytometry. COLO 205 cells were exposed to static conditions or fluid shear stress (2.0 dyn/cm^2) in a cone-and-plate viscometer for 120 min, followed by immediate incubation with either a PE-conjugated isotype or PE-conjugated DR4 and DR5 antibodies (Biolegend, San Diego, CA, USA) for 45

min at 4°C. Cells were then washed and analyzed for death receptor expression using flow cytometry. Median values of each fluorescence peak were recorded from each sample, and the fluorescence data was converted into the number of receptors using the calibration curve in QuickCal.

Statistical analysis

Data sets were plotted and analyzed using Prism 5.0b for Mac OS X (GraphPad software, San Diego, CA, USA). A two-tailed paired t-test was used for comparisons between two groups with $p < 0.05$ considered significant.

4.3 RESULTS

Fluid shear stress increases TRAIL-induced cancer cell apoptosis

We first characterized the effect of fluid shear stress on TRAIL-treated cancer cells in terms of cell viability. COLO 205 cells were treated with TRAIL (0.1 μg/mL) and then exposed to either static conditions or 2.0 dyn/cm^2 of fluid shear stress in a cone-and-plate viscometer for 120 min at 37°C. TRAIL binds to death receptors DR4 (TRAIL-R1) and DR5 (TRAIL-R2) on the cell surface, which signal apoptosis [339]. Both death receptors are expressed on the surface of COLO 205 cells [346]. COLO 205 cells exposed to static conditions (Figure 4.1A) or 2.0 dyn/cm^2 of fluid shear stress (Figure 4.1B) for 120 min maintained high cell viability (>94%), with minimal

apoptosis observed in the absence of TRAIL (<6%). As expected, COLO 205 cells treated with TRAIL exposed to static conditions for 120 min reduced cell viability by ~25%, with >22% of the cell population becoming apoptotic (Figure 4.1C). However, cells exposed to the same dosage of TRAIL followed by exposure to fluid shear stress (Figure 4.1D) induced a greater decrease in cell viability (>53%) and more than doubled the amount of apoptotic cells (>47%), compared to TRAIL-treated samples exposed to static conditions. Experiments performed in triplicate revealed that fluid shear stress alone did not affect cell viability (Figure 4.1E) or apoptosis (Figure 4.1F), yet induced a significant decrease in cell viability and increase in apoptosis in the presence of TRAIL. Similar effects on cell viability (Figure 4.1G) and apoptosis (Figure 4.1H) were also found in experiments performed with prostate adenocarcinoma cell line PC-3. Brightfield microscopy images revealed that COLO 205 cells remained viable and retained their characteristic morphology when exposed to static conditions (Figure 4.2A) or 2.0 dyn/cm^2 of fluid shear stress (Figure 4.2B). A greater number of viable cells was observed in TRAIL-treated COLO 205 samples exposed to static conditions (Figure 4.2C) compared to TRAIL-treated samples exposed to 2.0 dyn/cm^2 of fluid shear stress (Figure 4.2D), with fewer viable cells and a greater degree of membrane blebbing, characteristic of cell apoptosis. PC-3 cells also remained healthy under static (Figure 4.2E) and shear (Figure 4.2F) conditions, while a greater number of apoptotic cells was observed in TRAIL-treated samples exposed to shear (Figure 4.2H) compared to TRAIL-treated samples exposed to static conditions (Figure 4.2G).

Fluid shear stress does not alter TRAIL-induced cancer cell necrosis

To assess whether fluid shear stress sensitizes cancer cells to TRAIL-induced necrosis, another form of cell death, cells treated with 0.1 μg/mL TRAIL followed by shear stress exposure were stained with propidium iodide (PI) dye and characterized using flow cytometry. Cells positive for PI labeling but negative for Annexin-V were determined to be necrotic, as the cytoplasmic membrane is compromised but lacks the membrane flipping of phosphatidylserine (PS), which is characteristic of apoptosis. Untreated COLO 205 (Figure 4.3A) and PC-3 (Figure 4.3B) cells exposed to static conditions or fluid shear stress did not show significant differences in necrotic cell death. Treatment with 0.1 μg/mL TRAIL increased COLO 205 and PC-3 necrotic cell death, compared to untreated samples. However, fluid shear stress did not induce significant differences in TRAIL-mediated COLO 205 and PC-3 necrotic cell death, compared to samples exposed to static conditions. These results indicate that the shear stress sensitization response is TRAIL-mediated apoptosis-specific.

Cancer cell sensitization to TRAIL-induced apoptosis is fluid shear stress dose-dependent

The effect of increasing shear force on cancer cell sensitization to TRAIL-mediated apoptosis was evaluated by exposing TRAIL-treated COLO 205 cells to a range of shear stress from 0.05 to 2.0 dyn/cm^2, for an exposure period of 120 min. The shear stress range is representative of shear stress values experienced in the

microcirculation [274], and was used to identify a shear stress threshold that induces sensitization to apoptosis. At shear stresses of 0.05 and 0.1 dyn/cm^2, no significant differences in cell viability or apoptosis were found in TRAIL-treated COLO 205 cells, compared to samples exposed to static conditions. Interestingly, a shear stress of 0.4 dyn/cm^2 significantly decreased cell viability (Figure 4.4A) and increased apoptosis (Figure 4.4B), compared to TRAIL-treated cells exposed to static conditions. A shear stress range of 1.0-2.0 dyn/cm^2 induced a more pronounced decrease in cell viability and increase in cell apoptosis, indicating that the sensitization to apoptosis is fluid shear stress dose-dependent.

Cancer cell sensitization to TRAIL-induced apoptosis is fluid shear stress time-dependent

To assess the kinetics of the sensitization response, TRAIL-treated COLO 205 cells were exposed to a shear stress of 2.0 dyn/cm^2, while the fluid shear stress exposure time was increased in parallel experiments from 10 to 120 min. The exposure time was increased to determine a threshold exposure time needed to induce cancer cell sensitization to TRAIL. No significant differences in cell viability (Figure 4.5A) and apoptosis (Figure 4.5B) were observed in TRAIL-treated COLO 205 cells exposed to fluid shear stress for 10-30 min, compared to samples exposed to static conditions for the same duration. Exposure to fluid shear stress for 60 min significantly decreased COLO 205 cell viability (Figure 4.5A) and increased apoptosis (Figure 4.5B), compared to TRAIL-treated cells exposed to static conditions. Shear

stress exposure times of 90-120 min caused a further decrease in cell viability and increase in COLO 205 apoptosis, providing evidence that the sensitization to TRAIL-induced apoptosis is fluid shear stress time-dependent.

Cancer cells develop an increased sensitization to TRAIL-induced apoptosis with increasing shear stress magnitude and shear stress exposure time

Sensitization to TRAIL was quantified by determining the relative difference in COLO 205 cell death for sheared and nonsheared samples, over a range of shear stress magnitudes and exposure times. By varying the magnitude of fluid shear stress, it is apparent that shear stress values of 0.05-0.10 dyn/cm^2 induce minimal sensitization of COLO 205 cells to TRAIL (Figure 4.6A) as measured by apoptosis, necrosis, and overall cell death. COLO 205 sensitization to TRAIL is readily apparent at a shear stress value of 0.4 dyn/cm^2, as cells are sensitized to overall cell death and apoptosis, but not necrosis. Interestingly, sensitization plots also showed that the average percent sensitization to TRAIL-mediated cell death and apoptosis increased with each increasing shear stress, from 0.4-2.0 dyn/cm^2 (Figure 4.6A). Untreated control samples do not show sensitization to apoptosis, necrosis, and overall cell death across the range of shear stresses.

By varying the exposure time of cells to a fluid shear stress of 2.0 dyn/cm^2, a similar trend is observed where short shear stress exposure times of 10 and 30 min do not induce cancer cell sensitization to TRAIL (Figure 4.6B). After 60 min of shear stress exposure, COLO 205 cells develop a sensitization to cell death and apoptosis,

but not necrosis. From there, sensitization increased linearly with increasing exposure time (Figure 4.6B). As expected, untreated control samples do not show sensitization to apoptosis, necrosis, or overall cell death due to fluid shear stress exposure over the time intervals studied.

Fluid shear stress does not sensitize cancer cells to doxorubicin-mediated apoptosis

To assess the effect of fluid shear stress on the cancer cell response to other therapeutics that induce apoptosis, cancer cells were also treated with doxorubicin prior to the onset of fluid shear stress. While TRAIL binds to death receptors on the surface of the cancer cell membrane to signal cell death, doxorubicin induces cell death via inhibition of topo-isomerase II and DNA intercalation [88,89]. COLO 205 cells analyzed using an APC-conjugated Annexin-V assay showed that untreated COLO 205 cells exposed to static conditions (Figure 4.7A) or fluid shear stress (Figure 4.7B) do not show measurable differences in apoptotic cell death. Doxorubicin-treated COLO 205 cells experienced an increase in cell apoptosis (22-23%), however minimal differences were found between doxorubicin treated COLO 205 cells exposed to static conditions (Figure 4.7C) and fluid shear stress (Figure 4.7D). Experiments performed in triplicate revealed no significant differences in untreated cells exposed to static and shear conditions (Figure 4.7E), and doxorubicin-treated cells showed no significant differences in apoptosis. Sensitization plots over varying shear stress magnitudes (Figure 4.7F) and exposure times (Figure 4.7G) show

that while a shear-induced sensitization to TRAIL is apparent, COLO 205 cells are not sensitized to doxorubicin treatment upon exposure to fluid shear stress.

Cancer cell shear-induced sensitization to TRAIL occurs via caspase-dependent apoptosis

To assess whether shear-induced sensitization to apoptosis is caspase-dependent, COLO 205 cells were incubated with the pan caspase inhibitor Z-VAD-FMK before treatment with TRAIL, followed by exposure to fluid shear stress. The binding of TRAIL to death receptors on the cancer cell surface can activate caspases that initiate the caspase cascade, which triggers cell apoptosis. Z-VAD-FMK is a general caspase inhibitor that irreversibly binds to the catalytic site of caspase proteases, which inhibit apoptosis [347]. FITC-conjugated Annexin-V analysis revealed that untreated COLO 205 cells exposed to static conditions (Figure 4.8A) or fluid shear stress undergo minimal cell death, while cells treated with TRAIL showed characteristic sensitization to apoptosis when exposed to fluid shear stress (Figure 4.8D), compared to exposure to static conditions (Figure 4.8C). While the negative control inhibitor Z-FA-FMK did not affect the sensitization response to TRAIL (Figure 4.8E,F), treatment with general caspase inhibitor Z-VAD-FMK abolished the sensitization response (Figure 4.8G,H), as the differences in apoptosis between TRAIL treated samples exposed to shear and static conditions were not significant (Figure 4.8I). These results indicate the shear-induced sensitization to TRAIL is caspase-dependent.

Fluid shear stress does not alter death receptor expression on the cancer cell surface

To investigate fluid shear stress effects on DR4 and DR5 surface expression, COLO 205 cells were exposed to shear stress (2.0 dyn/cm^2) and static conditions at 37°C for 120 min and immediately labeled with anti-DR4 and anti-DR5 antibodies for flow cytometric analysis. COLO 205 cells exposed to either static conditions or fluid shear stress did not show measurable differences in DR4 (Figure 4.9*A*) or DR5 surface expression (Figure 4.9*B*). QSC bead analysis did not show significant differences in COLO 205 DR4 surface expression, with sheared and nonsheared samples averaging approximately 30,000 receptors/cell (Figure 4.9*C*). COLO 205 cells also did not show significant differences in DR5 surface expression, with sheared and nonsheared samples averaging approximately 150,000 receptors/cell.

4.4 DISCUSSION

The aim of this study was to quantify the role of fluid shear stress in altering the cancer cell response to receptor-mediated apoptosis. TRAIL-treated colon and prostate cancer cells were sensitized to receptor-mediated apoptosis under the presence of physiological fluid shear stresses (Figures 4.1,4.2). Previous studies have shown that cancer cells can become chemically sensitized to TRAIL therapy. TRAIL resistant LNCaP cells treated with aspirin have been sensitized to TRAIL treatment via downregulation of NF-κB, a regulator of antiapoptotic proteins [348]. Combined treatment of the demethylating agent 5-Aza-20-deoxycytidine (5-dAzaC) and

interferon-ϒ (IFN-ϒ) sensitize neuroblastoma and medulloblastoma cells to TRAIL-induced apoptosis via upregulation of caspase-8 expression [349]. Second mitochondria-derived activator of caspase (SMAC) synthetic peptides sensitized multiple tumor cell types to TRAIL *in vitro* and enhanced the antitumor effect of TRAIL *in vivo* in a human glioma xenograft model [350]. Our results show that rather than by chemical sensitization, fluid shear forces alone sensitize cancer cells to TRAIL-induced apoptosis.

While fluid shear stress sensitized cancer cells to apoptosis via TRAIL, fluid shear forces did not alter TRAIL-induced cell necrosis (Figure 4.3). TRAIL can induce apoptosis, necrosis, or a combination of both in a variety of cancer cell lines. TRAIL has been shown to induce cell death in prostate adenocarcinoma TRAMP-C2 and Jurkat cell lines via necrosis [351,352]. In particular, TRAMP-C2 cell death was via necrosis only, as cells lacked apoptotic characteristics such as an annexin V^+/PI^- population, SAPK/JNK phosphorylation, caspase activation, or cytochrome *c* release [351]. Recently, acidic extracellular pH has been shown to alter the form of TRAIL-induced cell death, from apoptosis to receptor interacting protein kinase 1 (RIPK1)-dependent regulated necrosis in colon adenocarcinoma HT29 and hepatocarcinoma HepG2 cell lines [353,354]. Shear-induced sensitization to TRAIL did not show a shift from TRAIL-induced apoptosis to TRAIL-induced necrosis, indicating that the sensitization response is apoptosis-specific.

Cancer cells developed a shear-induced sensitization to TRAIL-induced apoptosis in a fluid shear stress force- and time-dependent manner, directly implicating fluid shear stress in this response (Figures 4.4,4.5,4.6). While low shear

forces representative of those generated by interstitial flows did not sensitize cancer cells to TRAIL, a minimum shear stress of 0.4 dyn/cm^2 induced a significant increase in TRAIL-induced apoptosis. In the tumor microenvironment, cancer cells are exposed to slow interstitial flows in and around the tumor tissue [355]. The mechanisms behind how cancer cells sense interstitial flow are not well understood, however shear stress values have been estimated in 3D *in vitro* matrices [20]. For flow rates of 1 μm/s, cell surface shear stress estimates are extremely low, ranging from 0.007-0.015 dyn/cm^2 [20]. Cancer cells are exposed to greater fluid shear forces upon entering the circulation, and such conditions may play a role in sensitization to TRAIL-induced apoptosis. It is interesting to note that the cone-and-plate viscometer shear experiments were designed so that fluid shear forces alone would not induce significant cancer cell death, compared to cancer cells exposed to static conditions. Thus, we were able to isolate fluid shear stress effects on receptor-mediated apoptosis, implicating shear-induced sensitization to TRAIL as a synergistic response.

While fluid shear stress sensitized cancer cells to TRAIL-induced apoptosis, cancer cells did not show an increase in doxorubicin-induced apoptosis under the presence of fluid shear forces (Figure 4.7). Much like TRAIL, chemical sensitization to doxorubicin has been investigated previously. Gliotoxin, MG132, and Sulfasalazine sensitized typically resistant pancreatic carcinoma Capan-1 and A818-4 cell lines to doxorubicin-induced apoptosis via inhibition of NF-κB [356]. Selenium treatment combined with doxorubicin was successful in enhancing apoptosis in MCF-7 breast cancer cells, a doxorubicin-resistant cell line, via depression of Akt phosphorylation [357]. Small molecule inhibitors of the Hdm2:p53 complex, allowing for activation of

tumor suppressor p53, exerted synergistic effects with doxorubicin in an A375 melanoma cell line xenograft model to decrease tumor growth [358]. Due to the fact that shear stress-induced sensitization to apoptosis was not observed with doxorubicin treatment, it is possible that the fluid shear stress effects originate at the cell surface receptor level, where TRAIL ligand binds to death receptors DR4 and DR5 while exposed to fluid shear stress. This is in direct contrast to doxorubicin, which interacts with DNA within the cell to exert its apoptotic effects.

Treatment with Z-VAD-FMK revealed that shear-induced sensitization to TRAIL-induced apoptosis is caspase-dependent (Figure 4.8). Caspase activation is a critical step in the apoptotic pathway, induced by TRAIL binding to death receptors [359]. In contrast to extrinsic apoptosis pathways such as TRAIL-mediated apoptosis, intrinsic pathways are initiated by DNA and cellular damage, along with the permeabilization of mitochondria [360]. During this process, mitochondrial factors including cytochrome *c*, AIF (apoptosis-inducing factor), and SMAC are released, with AIF-induced apoptosis occurring via a caspase-independent process [361]. DNA-damaging agents have previously shown to sensitize hepatic carcinoma cell lines to TRAIL, due to ATM kinase activation [362]. ATM kinase activity in turn leads to a downregulation of antiapoptotic protein cFLIP, and subsequent sensitization to TRAIL. Since our sensitization process is caspase-dependent, it is likely that the shear-induced sensitization is not due to DNA-damaging events, providing further support that the sensitization phenomena may occur at the cell surface. Inhibition of WEE1, a cell cycle checkpoint regulator, has been shown to sensitize a variety of basal breast cancer cell lines to TRAIL-induced apoptosis due to increased surface

expression of death receptors and increased caspase activation [363]. Our results show that COLO 205 surface expression of death receptors DR4 and DR5 is not altered after exposure to fluid shear stress (Figure 4.9), and thus sensitization to TRAIL-induced apoptosis is not likely due to shear-induced changes in receptor expression. It is likely that a combination of fluid shear stress effects along with TRAIL stimulation, rather than fluid shear stress alone, cause changes in death receptor trimerization and signaling. Death receptors, upon binding to TRAIL, are known to trimerize and recruit adaptor proteins to form a signaling complex required for TRAIL-induced apoptosis [364]. It is possible that mechanical shear forces could enhance death receptor trimerization in the presence of TRAIL, and assist in the formation of signaling complexes for TRAIL-induced apoptosis. The effects of fluid shear stress on death receptor trimerization upon binding to TRAIL could lead to further insight into the mechanistic basis of shear stress-induced TRAIL sensitization.

4.5 CONCLUSION

Results from this study indicate that hemodynamic shear forces have a significant effect on receptor-mediated apoptosis of cancer cells in the presence of TRAIL. Fluid shear stress was found to sensitize both colon and prostate cancer cell lines to TRAIL-mediated apoptosis. Cancer cells were not sensitized to TRAIL-mediated necrosis upon exposure to fluid shear stress. TRAIL sensitization was shown to be shear stress dose-dependent, as sensitization was found to increase with increasing fluid shear stress. TRAIL sensitization was also fluid shear stress time-

dependent, as sensitization to apoptosis was enhanced with increasing fluid shear stress exposure time. The response was TRAIL-specific, as shear stress did not sensitize cancer cells to doxorubicin treatment over varying shear stress magnitudes and exposure times. Caspase inhibition assays revealed the sensitization response to be caspase-dependent. These results shed new light on the cancer cell response to soluble apoptotic agents within the circulation. The effects of fluid shear stress on mechanosensing death receptors on the cancer cell surface, along with their signaling pathways, can reveal new strategies for treating circulating cancer cells and reducing the likelihood of metastasis.

FIGURE 4.1: FLUID SHEAR STRESS SENSITIZES CANCER CELLS TO TRAIL. COLO 205 cancer cells exposed to static conditions (*A*) and 2.0 dyn/cm^2 of fluid shear stress (*B*) for 120 min at 37°C, respectively. COLO 205 cells treated with 0.1 µg/mL TRAIL and then exposed to static conditions (*C*) and 2.0 dyn/cm^2 of fluid shear stress (*D*) for 120 min at 37°C. Percent viable (*E*) and apoptotic (*F*) COLO 205 cells after treatment with 0.1 µg/mL TRAIL followed by exposure to static conditions and 2.0 dyn/cm^2 of fluid shear stress (n = 3). Percent viable (*G*) and apoptotic (*H*) PC-3 cells after treatment with 0.1 µg/mL TRAIL followed by exposure to static conditions and 2.0 dyn/cm^2 of fluid shear stress (n = 3). Lower lefthand and righthand quadrants of each flow cytometry plot represent viable and early apoptotic cells, respectively. Upper lefthand and righthand quadrants of each flow cytometry plot represent necrotic and late apoptotic cells, respectively. PI: propidium iodide. FITC: Fluorescein isothiocyanate. Error bars represent 95% confidence intervals. *P < 0.05. **P < 0.01. NS: non-significant.

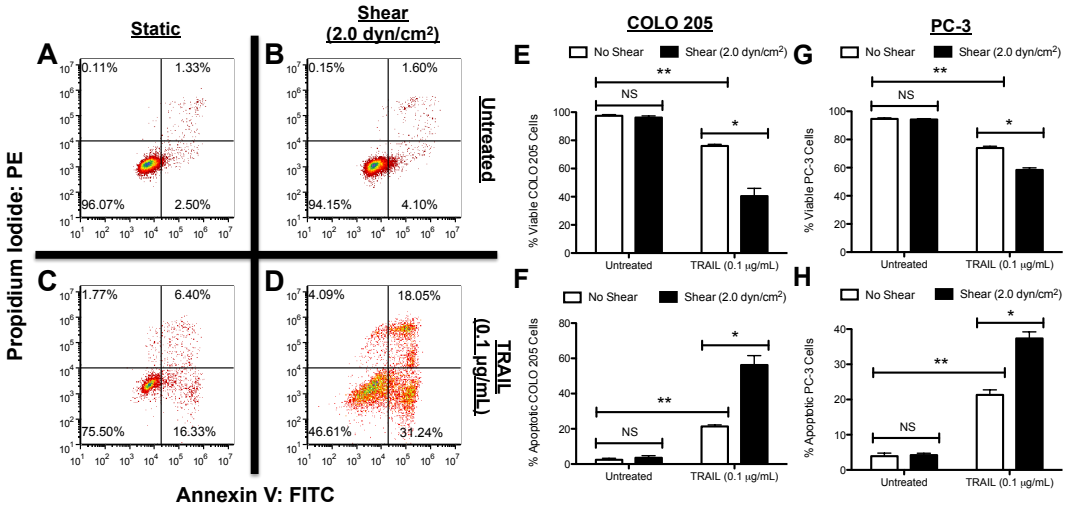

FIGURE 4.2: BRIGHTFIELD MICROSCOPY IMAGES OF COLO 205 CELLS EXPOSED TO STATIC CONDITIONS AND 2.0 DYN/CM^2 OF FLUID SHEAR STRESS BOTH IN THE ABSENCE AND PRESENCE OF TRAIL. Brightfield microscopy images of untreated COLO 205 cells exposed to static conditions (*A*) and 2.0 dyn/cm^2 of fluid shear stress (*B*) for 120 min at 37°C. COLO 205 cells treated with 0.1 μg/mL TRAIL and then exposed to static conditions (*C*) and 2.0 dyn/cm^2 of fluid shear stress (*D*) for 120 min at 37°C. Untreated PC-3 cells exposed to static conditions (*E*) and 2.0 dyn/cm^2 of fluid shear stress (*F*) for 120 min at 37°C. PC-3 cells treated with 0.1 μg/mL TRAIL and then exposed to static conditions (*G*) and 2.0 dyn/cm^2 of fluid shear stress (*H*) for 120 min at 37°C. Scale bars = 30 μm.

FIGURE 4.2: BRIGHTFIELD MICROSCOPY IMAGES OF COLO 205 CELLS EXPOSED TO STATIC CONDITIONS AND 2.0 DYN/CM^2 OF FLUID SHEAR STRESS BOTH IN THE ABSENCE AND PRESENCE OF TRAIL.

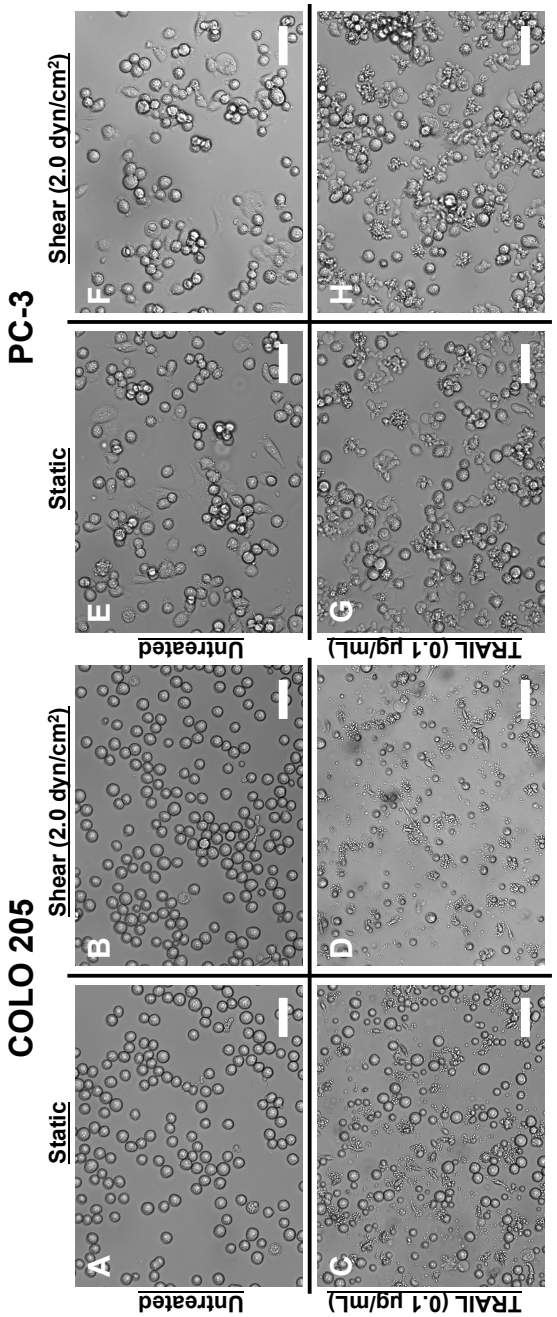

FIGURE 4.3: PERCENT NECROTIC COLO 205 AND PC-3 CELLS AFTER TREATMENT WITH TRAIL UNDER STATIC AND SHEAR STRESS CONDITIONS. Percent necrotic COLO 205 cells (*A*) after treatment with 0.1 μg/mL TRAIL followed by exposure to static conditions and 2.0 dyn/cm^2 of fluid shear stress (n = 3) 120 min at 37°C. Percent necrotic PC-3 cells (*B*) after treatment with 0.1 μg/mL TRAIL followed by exposure to static conditions and 2.0 dyn/cm^2 of fluid shear stress (n = 3) 120 min at 37°C. Error bars represent 95% confidence intervals. NS: non-significant.

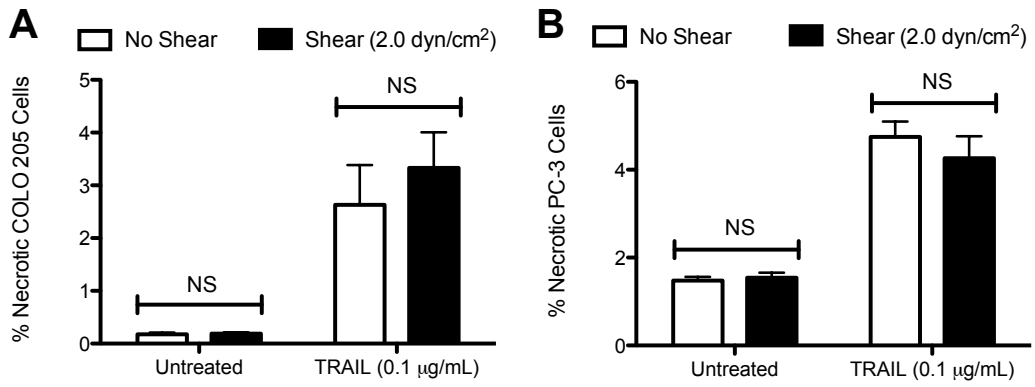

FIGURE 4.4: INCREASED FLUID SHEAR STRESS SENSITIZES CANCER CELLS TO TRAIL. Percent viable (*A*) and apoptotic (*B*) COLO 205 cells (n = 3). Shear stress magnitude was varied in separate experiments from 0.05 - 2.0 dyn/cm^2 for 120 min at 37°C. COLO 205 cells were treated with 0.1 μg/mL TRAIL prior to the onset of fluid shear stress. Error bars represent 95% confidence intervals. *P < 0.05 for all measurements.

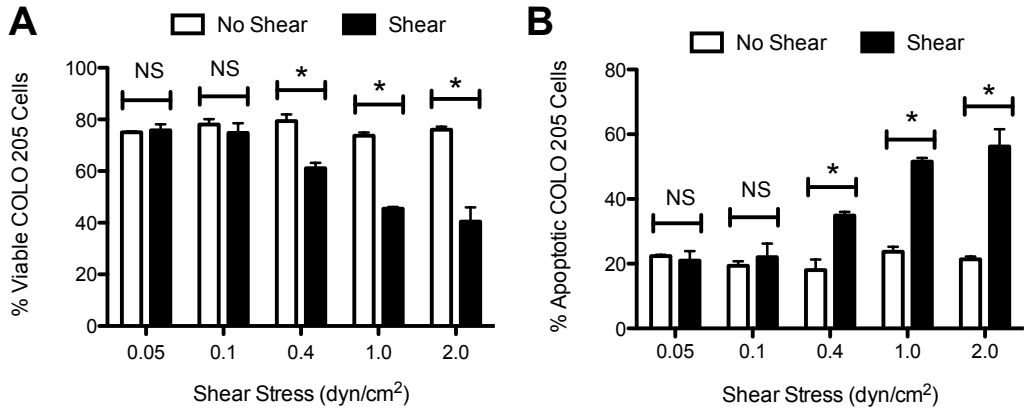

FIGURE 4.5: SHEAR-INDUCED SENSITIZATION TO TRAIL INCREASES WITH INCREASING FLUID SHEAR STRESS EXPOSURE TIME. Percent viable (*A*) and apoptotic (*B*) COLO 205 cells (n = 3). Time dependence of shear-induced sensitization was determined by increasing the fluid shear stress exposure time from 10 - 120 min at a uniform shear stress of 2.0 dyn/cm^2 at 37°C. COLO 205 cells were treated with 0.1 μg/mL TRAIL prior to the onset of fluid shear stress. Error bars represent 95% confidence intervals. *P < 0.05 for all measurements.

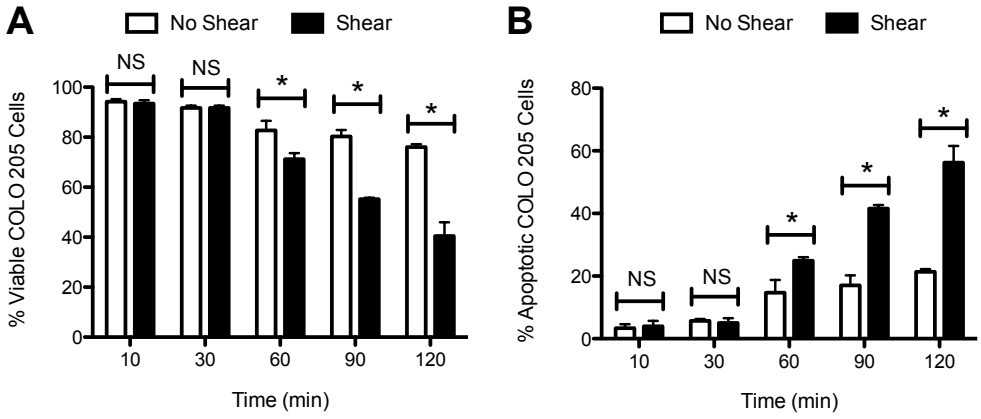

FIGURE 4.6: CANCER CELLS DEVELOP SENSITIZATION TO TRAIL-MEDIATED APOPTOSIS WITH INCREASING SHEAR STRESS MAGNITUDE AND EXPOSURE TIME. Cancer cells develop sensitization to TRAIL-mediated apoptosis with increasing shear stress magnitude (*A*) and exposure time (*B*) (n = 3). Resistance is plotted as a function of the $\log_{10}$ of shear stress (dyn/cm^2) or $\log_{10}$ of time (min). Error bars represent 95% confidence intervals.

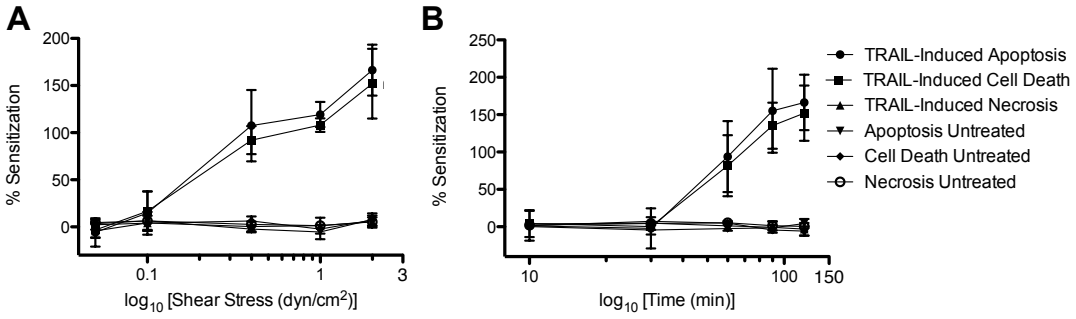

FIGURE 4.7: FLUID SHEAR STRESS DOES NOT SENSITIZE CANCER CELLS TO DOXORUBICIN. COLO 205 cells exposed to static conditions (*A*) and 2.0 dyn/cm^2 of fluid shear stress (*B*) for 120 min at 37°C. COLO 205 cells treated with 20 μM doxorubicin and then exposed to static conditions (*C*) and 2.0 dyn/cm^2 of fluid shear stress (*D*) for 120 min at 37°C. Percent apoptotic (*E*) COLO 205 cells after treatment with 20 μM doxorubicin followed by exposure to static conditions and 2.0 dyn/cm^2 of fluid shear stress (n = 3). Comparison of cancer cell shear-induced sensitization to TRAIL and doxorubicin with increasing shear stress magnitude (*F*) and exposure time (*G*) (n = 3). Resistance is plotted as a function of the $\log_{10}$ of shear stress (dyn/cm^2) or $\log_{10}$ of time (min). Error bars represent 95% confidence intervals. Gated region of flow cytometry histograms represent apoptotic COLO 205 cells. Gates determined by labeling viable COLO 205 control samples with Annexin-V APC staining. APC: allophycocyanin. NS: non-significant.

FIGURE 4.7: FLUID SHEAR STRESS DOES NOT SENSITIZE CANCER CELLS TO DOXORUBICIN.

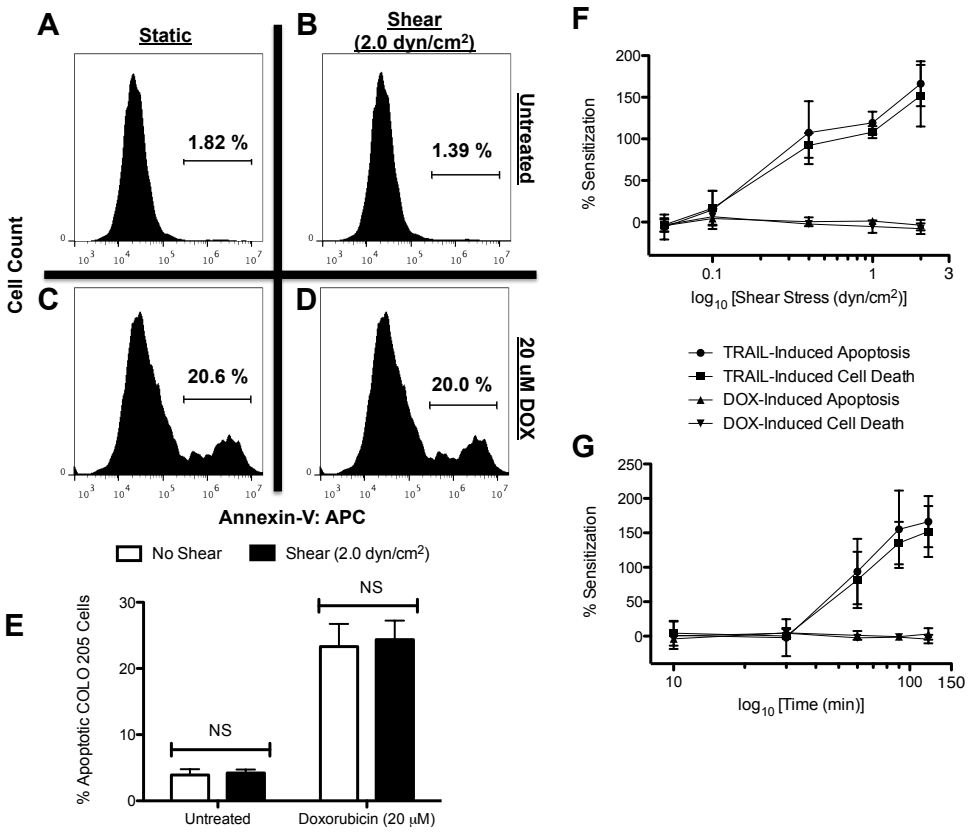

FIGURE 4.8: FLUID SHEAR STRESS SENSITIZATION TO TRAIL-MEDIATED APOPTOSIS IS CASPASE-DEPENDENT. COLO 205 cells (*A,B*) treated with 0.1 μg/mL TRAIL (*C,D*), negative control inhibitor Z-FA-FMK followed by 0.1 μg/mL TRAIL (*E,F*), and pan caspase inhibitor Z-VAD-FMK followed by 0.1 μg/mL TRAIL (*G,H*), exposed to static conditions and 2.0 dyn/cm^2 of fluid shear stress for 120 min at 37°C, respectively. Percent apoptotic COLO 205 cells (n = 3) after exposure to various treatments (I). Gated region of flow cytometry histograms represent apoptotic COLO 205 cells. Gates determined by labeling viable COLO 205 control samples with Annexin-V FITC staining. FITC: fluorescein isothiocyanate. NS: non-significant.

FIGURE 4.8: FLUID SHEAR STRESS SENSITIZATION TO TRAIL-MEDIATED APOPTOSIS IS CASPASE-DEPENDENT.

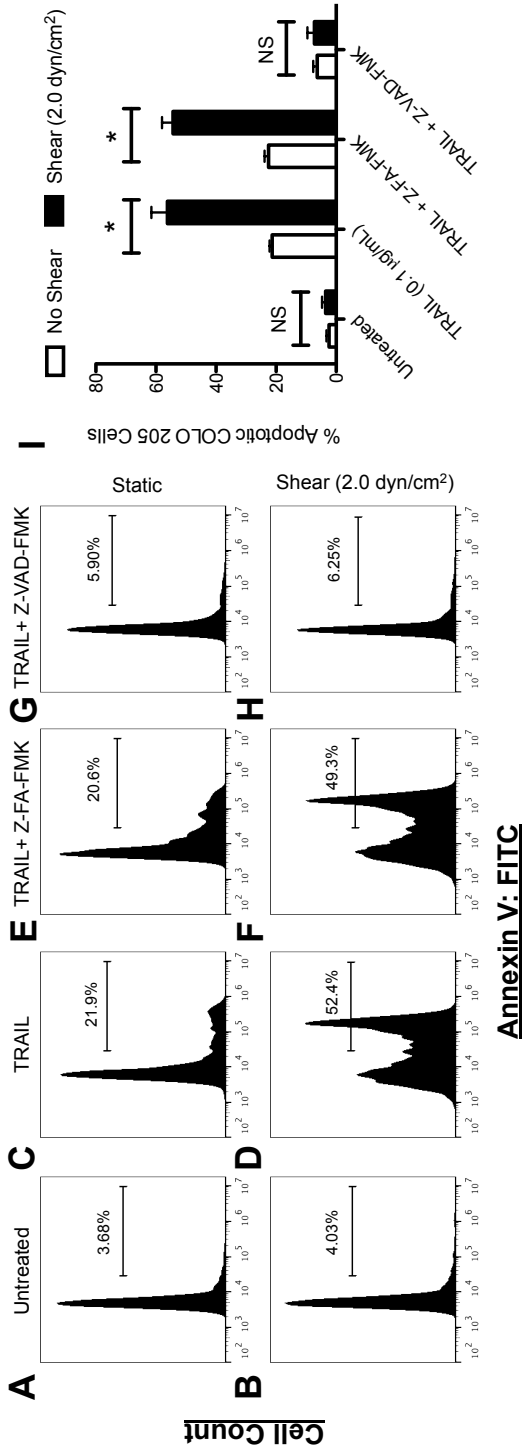

FIGURE 4.9: FLUID SHEAR STRESS DOES NOT ALTER DEATH RECEPTOR SURFACE EXPRESSION. COLO 205 cells exposed to static conditions and 2.0 dyn/cm^2 of fluid shear stress for 120 min at 37°C were labeled with anti-DR4 (A) and anti-DR5 (B) antibodies, respectively. (C) QSC receptor quantification of DR4 and DR5 on the surface of COLO 205 cells exposed to static conditions and fluid shear stress (n = 3). NS: non-significant.

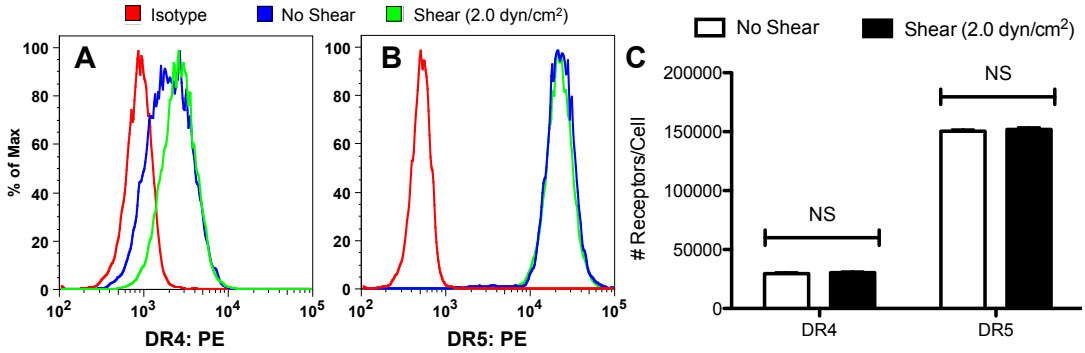

CHAPTER 5: E-SELECTIN LIPOSOMAL AND NANOTUBE-TARGETED DELIVERY OF DOXORUBICIN TO CIRCULATING TUMOR CELLS

*This section is adapted from the following publication: M.J. Mitchell, C.S. Chen, V. Ponmudi, A.D. Hughes, and M.R. King. *Journal of Controlled Release.* 160(3): 609-617, 2012.

5.1 INTRODUCTION

Cancer is one of the leading causes of death, as approximately 90% of human cancer deaths are attributed to cancer metastasis [1,333]. The process of metastasis can involve the presence of circulating tumor cells (CTCs), which are believed to undergo an adhesion cascade similar to leukocytes. This process consists of a discrete sequence of steps involving tethering, rolling, and firm adhesion between cells and the inflamed endothelial lining of the vasculature [51,52]. Cells from the primary tumor detach, invade the surrounding tissue, and intravasate into the blood or lymphatic circulation as CTCs [1,51,365,366]. Following intravasation, CTCs interact with the vasculature by selectin-mediated rolling and cell arrest, where a fraction of cells are presumed to extravasate into the tissue of a distant organ and proliferate to form a secondary tumor [1,51,52]. Although metastasis is an inefficient process with only about 0.01% of CTCs surviving the pathway [334,367], the development of metastases remains as the primary cause of cancer-related mortality.

Doxorubicin (DXR), an adriamyacin anthracycline antibiotic, is a common chemotherapy agent that has been used in treating a variety of cancers, including metastatic breast cancer, Kaposi's sarcoma, acute leukemia, Hodgkin's Disease and other lymphomas and sarcomas [88]. The drug's potent antineoplastic ability stems from its function in DNA-intercalation, inhibition of topo-isomerase II, and formation of free radicals [88,89,368]. However, the non-specific activity of DXR can lead to systemic toxicity, tissue necrosis, neutropenia, and side effects including

cardiomyopathy, myelosuppression, alopecia, mucositis, nausea and vomiting [88,369,370].

To increase delivery efficiency and reduce toxicity of doxorubicin, a number of delivery systems such as polymers, dendrimers, liposomes, and nanoparticles have been developed [369,371]. In particular, liposomal doxorubicin (L-DXR) has been shown to improve the drug's efficacy by altering its pharmacokinetics, greatly increasing its circulation time in blood, reducing drug accumulation in organs, and dampening toxic side effects [372-376]. Furthermore, the addition of polyethylene glycol (PEG) coupled to the liposomal surface provides steric stabilization, reducing drug clearance, protein interactions, and opsonization by the reticulo-endothelial system [377-379]. Known as "stealth" liposomes, PEG-conjugated nanoparticles further extend the circulation time of the drug, which due to enhanced permeability and retention effects, aids in tumor uptake [380,381]. The success of liposomal doxorubicin has been shown in pre-clinical and clinical studies as evidenced by Doxil®, a commercially available L-DXR formulation that has been approved by the FDA for use in treating Kaposi's sarcoma, and Myocet®, a non-PEGylated L-DXR for the treatment of metastatic breast cancer [382].

While PEGylated L-DXR is effective in treating tumors, the drug vehicle remains limited in its ability to target specific cells. Many CTCs express sialylated carbohydrate ligands on their surface, which adhere to selectin proteins along the inflamed endothelium during metastasis [48-50,383,384]. Targeting of CTCs in the bloodstream via selectin bonds could reduce the probability of metastasis. In this study, targeted L-DXR particles were developed by functionalizing the liposome

surface with a combination of PEG and recombinant human E-selectin. I then investigated the targeting, capture, and killing of model CTCs using targeted L-DXR (1) immobilized within a microtube device while exposed to physiologically relevant shear stresses, and (2) in a dilute suspension under shear flow in a cone-and-plate viscometer. Naturally-occurring halloysite nanotubes (HNT), which have recently been shown to enhance cell capture under shear flow, were used as a nanostructured surface coating within microtubes to enhance targeted DXR delivery [385].

5.2 MATERIALS AND METHODS

Cell lines and cell culture

Colorectal adenocarcinoma cell line COLO 205 (ATCC # CCL-222) and acute promyelocytic leukemic cell line KG-1a (ATCC # CCL-246.1) were purchased from American Type Culture Collection (Manassas, VA, USA). Cells were cultured in RPMI 1640 cell culture medium with 10% (v/v) fetal bovine serum and 1% (v/v) PenStrep, all purchased from Invitrogen (Grand Island, NY, USA), and incubated under humidified conditions at 37°C and 5% CO_2 (complete media). COLO 205 cells were not allowed to exceed 90% confluence, and KG-1a cells were maintained at less than $1x10^6$ cells/mL.

Liposomal doxorubicin preparation

Multilamellar liposomes (Figure 5.1) were prepared using a thin lipid film hydration method [386,387] with 125 mM ammonium sulfate (Sigma-Aldrich, St. Louis, MO, USA) followed by 10 freeze-thaw cycles and then extrusion as previously described [388] to prepare empty liposomes (EL). To prepare L-DXR, DXR HCL (Sigma-Aldrich) was encapsulated within ELs using the ammonium sulfate remote loading method as described previously [387] at a doxorubicin-to-lipid ratio of 0.2:1 (w/w). Non-encapsulated DXR was removed using gel-exclusion chromatography with Sephadex G-50 (Sigma-Aldrich). The liposomal doxorubicin concentration was determined by spectrophotometry (λ=490 nm), and the loading efficiency of doxorubicin was determined to be >95%.

Preparation of targeted liposomes

Recombinant human E-selectin/Fc chimera (rhE/Fc) (R&D Systems, Minneapolis, MN) was conjugated to 1,2-Distearoyl-sn-Glycero-3-Phosphoethanolamine-N-Maleimide 2000 (DSPE-PEG_{2000} maleimide) (Avanti Polar Lipids, Alabaster, AL, USA) via thiolation, and conjuguates were covalently attached to diluted EL or L-DXR as previously described [388] to make two forms of targeted liposomes, E-selectin-PEG-conjugated liposomal doxorubicin (ES-PEG L-DXR) and E-selectin-PEG-conjugated empty liposomes (ES-PEG EL). The volume ratio of EL or L-DXR in phosphate-buffered saline (PBS) and rhE/Fc-DSPE-PEG_{2000} maleimide to

the diluted liposomes was 1:1 and 1:12, respectively. All liposomes were stored at 4°C for no more than one week until usage.

Liposomes were freshly prepared and diluted with phosphate-buffered saline (PBS), and the mean particle diameter and zeta potential were measured by dynamic light scattering using a Malvern Zetasizer nano ZS (Malvern Instruments Ltd., Worcestershire, UK), according to the manufacturer's protocols. To confirm that E-selectin was successfully conjugated to the liposome surface, 10 μL of fluorescently tagged liposomes were mixed with 490 μL COLO 205 or KG-1a cells (10^6 cells/mL) and sheared in a cone and plate viscometer at 2.0 dyn/cm^2 for 10 min. All cells were analyzed for fluorescent liposomes conjugated to the surface using an Accuri C6 flow cytometer (Accuri Cytometers, Inc., Ann Arbor, MI, USA). Adhesion of fluorescent liposomes to the cell surface was confirmed via confocal microscopy.

Doxorubicin encapsulation and leakage studies

A 5 μL sample of L-DXR was treated with or without 20 μL of 10% Triton X-100. Samples of EL, L-DXR, PEG L-DXR, and ES-PEG L-DXR (30 μL) were used for the leakage study. PBS was added to all solutions to achieve a total volume of 200 μL. Fluorescence intensity of DXR in 200 μL solutions was measured in fluorescence units (fu) using a spectrophotometer (SmartSpec Plus; Bio-Rad Laboratories, Philadelphia, PA, USA). To assess DXR leakage, fluorescence readings were recorded over a span of 39 days.

Static experiments

COLO 205 and KG-1a cells were cultured in complete media at a concentration of $1x10^5$ cells/mL and $3x10^6$ cells/mL, respectively, on 24-well plates (Becton Dickinson, Franklin Lakes, NJ, USA). Cells were treated with ES-PEG L-DXR, naked L-DXR, soluble DXR (20 μM), or naked EL at volumes of 0, 0.001, 0.01, 0.1, 0.5, 1, 2, and 5 μL for 18 hours. Adherent COLO 205 cells were then treated with Accutase (Sigma-Aldrich) for 5 min at 37°C to remove cells from the surface. Both COLO 205 and KG-1a cells were then washed with 1x PBS at 1000 rpm in a refrigerated centrifuge (Allegra XX-22R Centrifuge; Beckman Coulter, Brea, CA, USA) and resuspended in fresh media. After 4 days, cell viability was evaluated on a hemocytometer (Hausser Scientific, Horcham, PA, USA) using trypan blue exclusion dye (Lonza, Wilkersville, MD, USA). The percentage of dead cells was determined by comparing the number of viable cells for treated and untreated cells. For treatment of 0.5 μL liposomes on COLO 205 cells, cell viability was assessed each day for 4 days. Brightfield images were taken of COLO 205 cells at day 4 using an inverted microscope (IX-81; Olympus America Inc., Melville, NY, USA) coupled to a CCD camera (Hitachi) and processed using ImageJ software (U.S. National Institutes of Health, Bethesda, MD, USA).

Preparation of cells for capture experiments

COLO 205 cells were treated with Accutase for 5 min at 37°C before handling. KG-1a and COLO 205 cells were washed with 1x PBS at 1000 rpm and resuspended in flow buffer at a concentration of $1x10^6$ cells/mL. The assay buffer consisted of PBS saturated with Ca^{2+} and Mg^{2+}, which activated recombinant human E-selectin receptors to facilitate cell capture. Prior to performing capture experiments, 95% cell viability was confirmed by using trypan blue.

To prepare blood cells for capture experiments, Human peripheral blood was obtained via venipuncture from healthy consenting blood donors and collected into sterile sodium heparin-containing tubes (BD Biosciences) after informed consent. Mononuclear cells (MNCs) and red blood cells (RBCs) were isolated by centrifugation at 480 X g for 50 min at 23°C in a Marathon 8K centrifuge (Fisher Scientific, Pittsburgh, PA) using 1-Step™ Polymorphs (Accurate Chemical & Scientific Corporation, Westbury, NY). This centrifugation method creates a density gradient to separate blood into visible layers of plasma, mononuclear cells, neutrophils, and erythrocytes and platelets. MNCs and RBCs were extracted separately and washed in Mg^{2+} and Ca^{2+} free HBSS to remove any remaining Polymorphs. The MNC sample was further purified from remaining red blood cells in the suspension by hypotonic lysis. RBC and MNC samples were resuspended at a concentration of 1.0×10^6 cells/mL in HBSS containing 0.5% HSA, 2 mM Ca^{2+}, 1 mM Mg^{2+}, and 10 mM HEPES (Invitrogen), buffered to pH 7.4.

Preparation of microtube surfaces

Microrenathane tubing (Braintree Scientific, Braintree, MA, USA) of 300 μm inner diameter was cut to 55 cm in length and washed with 75% ethanol. HNT-coated surfaces were prepared as previously described [385]. Briefly, HNT solution (6.6% by weight) (NaturalNano Rochester, NY, USA) was treated via sonication and then filtration. Microtubes were then washed with distilled water followed by a 5-minute incubation with 2:8 poly-L-lysine (0.1% w/v in water) (Sigma-Aldrich) and a 3-minute incubation with treated HNTs. Excess HNTs were removed with distilled water and microtubes were incubated overnight at RT. Immobilization of E-selectin targeted liposomes (ES-PEG L-DXR or ES-PEG EL) onto the surface of both HNT-coated and smooth tubes was achieved by incubation with liposomes for 2.5 hours. Surfaces were then blocked for 1 hour with 5% bovine serum albumin (BSA) (Sigma-Aldrich), in PBS (v/v) for smooth tubes and 5% milk protein in PBS for HNT-coated tubes. Blotting grade blocker nonfat dry milk was obtained from Bio-Rad Laboratories (Hercules, CA, USA). All incubations were preceded and followed by PBS washes. Control tubes were incubated with 5% BSA or 5% milk protein for 3.5 hours. To activate immobilized E-selectin proteins, microtubes were incubated with calcium-enriched flow buffer prior to beginning cell capture experiments. All steps were performed at RT or 4°C.

Cell capture experiments

Microtubes were fastened onto the stage of an Olympus IX81 motorized inverted microscope following surface functionalization. Perfusion of cells suspended in flow buffer through microtubes was controlled via a motorized syringe pump (KDS 230; IITC Life Science, Woodland Hills, CA, USA). Cells were initially perfused through microtubes at a rate of 0.008 mL/min (wall shear stress of 0.5 dynes/cm^2) for 15 minutes, and then 0.04 mL/min (wall shear stress of 2.5 dynes/cm^2) for 2 hours. Captured cells were collected by perfusion of flow buffer and air embolism at 0.1 mL/min (wall shear stress $\geq$ 10 dynes/cm^2). Cells were cultured in 24-well plates in complete media and analyzed for cell viability at day 4 via trypan blue exclusion.

Cone-and-plate shear assay

COLO 205 and KG-1a cells were washed and resuspended in 490 μL of Hank's buffered salt solution (HBSS) (Invitrogen) saturated with Ca^{2+} (HBSS+) at a concentration of 1x10^6 cells/mL. Samples of ES-PEG L-DXR, naked L-DXR, or ES-PEG EL (10 μL) were then added to the cell suspension to produce a total volume of 500 μL. Dilute suspensions of both cancer cells and liposomes were then sheared in a LVDV-II+ Pro cone-and-plate viscometer (Brookfield Engineering Laboratories, Inc., Middleboro, MA, USA) for 2 hours at 2 dynes/cm^2. Collected cells were placed in culture and analyzed for cell viability at day 4 via trypan blue exclusion.

Fluorescence microscopy

To assess cellular internalization of L-DXR and ES-PEG L-DXR in static experiments, KG-1a and COLO 205 cells were incubated with 0.5 μL of L-DXR for 2 hours at 37°C and then washed twice with PBS to remove free liposomes from the cell suspension. To determine successful immobilization of ES-PEG L-DXR onto the inner surface of the microtube, surfaces were prepared as previously described and visualized prior to performing capture experiments. Images of intrinsic DXR fluorescence were taken using an Olympus IX81 microscope.

To determine cellular adhesion and uptake of liposomes following shearing and capture experiments, cells were treated with fluorescent ES-PEG EL for both experiments. Fluorescent liposomes were constructed by replacing ovine wool cholesterol with BODIPY-cholesterol (Avanti Polar Lipids). Cell nuclei were visualized by staining with 2 μL of 10 mg/mL trihydrochloride trihydrate (Hoechst 33342) (Invitrogen, Carlsbad, CA, USA) for 15 minutes. Cells were washed twice with PBS and then placed on a glass slide and visualized with either a Zeiss 710 Spectral Confocal Microscope System (Carl Zeiss MicroImaging GmbH, Jena, Germany), or a Leica TCS SP2 system (Leica Microsystems Heidelberg GmbH, Mannheim, Germany) at 65X magnification with FITC and DAPI filters. Both individual and Z-stack images were taken and processed using Zen 2009 light edition software (Carl Zeiss MicroImaging GmbH) or LCS software (Leica Microsystems Heidelberg GmbH).

Statistical Analysis

Results were reported as mean ± standard error of the mean and statistical significance was calculated using GraphPad Prism Software (San Diego, CA, USA). Paired two-tailed *P*-value *t*-tests were performed for static and cell capture experiments, and unpaired *t*-tests were performed for cone-and-plate experiments. *P*-values less than 0.05 were considered significant.

5.3 RESULTS

Characterization of targeted liposomes

The physical characteristics of the liposomes are summarized in Table 5.1. The diameters of L-DXR and PEG L-DXR were similar, while ES-PEG L-DXR was 35–40 nm larger in diameter than non-targeting liposomes. The zeta potential of L-DXR was reduced by PEG surface modification from -24.56 mV to -8.49 mV, compared to the zeta potential of naked liposomes. Attachment of ES-PEG showed a slight increase in the zeta potential compared to PEG modified liposomes, but remained lower than the naked liposome zeta potential.

To assess whether functional E-selectin was successfully conjugated to the surface, fluorescently tagged liposomes were sheared with COLO 205 and KG-1a cells in a cone-and-plate viscometer for 10 min at a shear stress of 2.0 dyn/cm^2. Liposomes lacking E-selectin showed negligible adhesion to the cells, due to the lack

of E-selectin interactions with E-selectin ligands on the cell surface. Cells sheared with ES-PEG L-DXR showed nearly 99.9% adherence to fluorescent liposomes (Figure 5.2A). A nearly identical percentage of cells adhered to ES-PEG EL, suggesting that the fluorescence was due to E-selectin adhesion, rather than fluorescence due to DXR drug release. The 10 min shear duration was sufficient for complete adhesion to all cell surfaces with negligible time for significant liposome internalization to occur (Figure 5.2B).

Encapsulation with minimal leakage of DXR from liposomes

To evaluate encapsulation efficacy of DXR, the fluorescence intensity of intrinsically fluorescent DXR in the presence or absence of Triton X-100 was measured, and showed that DXR was successfully encapsulated into liposomes (Figure 5.3A). The fluorescence intensity of both samples was compared to 1 μM soluble DXR in PBS, which revealed 3-fold greater fluorescence intensity compared to the sample without Triton X-100. The leakage profile of DXR from L-DXR demonstrates minimal release of the drug over time, regardless of E-selectin and/or PEG conjugation to the liposome surface (Figure 5.3B).

Cellular uptake and toxicity of L-DXR

COLO 205 and KG-1a cancer cell lines were treated with 0.001 – 5 μL of L-DXR, EL, soluble DXR, or ES-PEG L-DXR for 18 h and assessed for cell viability at

day 4. The dose response curves for both KG-1a (Figure 5.4A) and COLO 205 (Figure 5.4B) cells showed a significant decrease in cell viability with all treatment doses of L-DXR and ES-PEG L-DXR when compared to untreated cells. Fluorescence from DXR was visible within the cell, indicating liposome internalization (Figure 5.5). Conjugation of ES-PEG to the liposome surface did not decrease the effectiveness of the liposome formulation, as treatment of cancer cells with L-DXR and ES-PEG showed no significant difference in static conditions, and maximum efficacy was observed at 0.5 μL. Neither KG-1a (Figure 5.4A) nor COLO 205 (Figure 5.4B) cells were affected by treatment with EL. The growth curve of COLO 205 cells treated with 0.5 μL of EL over 4 days was not significantly different from that of untreated cells (Figure 5.6), further implying that liposomes themselves do not negatively affect cell viability. The difference in treatment responses is readily seen in brightfield images taken at day 4 (Figure 5.7).

Microtubes coated with ES-PEG L-DXR capture and kill cancer cells under flow

Previously, we demonstrated that E-selectin could be absorbed onto the inner surface of microrenathane tubes and cause rolling adhesion of cells expressing E-selectin ligand [84,385]. Microrenathane tubes, which were previously demonstrated as a vascular shunt prototype in rats to successfully capture CD34+ hematopoietic stem and progenitor cells from the circulation [389], as well as for use in multiple *in vitro* studies examining leukocyte adhesion [278,390] and cancer cell adhesion [84,391] along the inflamed endothelium, were used as a model of human vasculature

in our experiments. To ensure that ES-PEG L-DXR was successfully immobilized onto the inner surface of microtubes, fluorescence microscopy was used to detect the intrinsic fluorescence of DXR from liposomes in the coated tubes. Tubes coated with ES-PEG L-DXR displayed a uniform amount of fluorescence throughout the tube (Figure 5.8B), while control tubes showed minimal auto-fluorescence (Figure 5.8A). Untreated control tubes were coated with BSA to prevent non-specific binding. After targeted liposomes were immobilized onto the surface of the microtube, KG-1a or COLO 205 cells were perfused through coated microtubes at physiological shear stresses to mimic the behavior of CTCs in the vasculature. COLO 205 and KG-1a were chosen as model CTCs for these experiments because they are cancer cell lines that express sialylated carbohydrate ligands and have been shown to exhibit rolling adhesion along immobilized selectin proteins [84,385], characteristics that leukocytes use for the initial steps in diapedesis [178,392,393]. Both KG-1a cells and COLO 205 cells were captured by ES-PEG liposomes (Figure 5.8C). No rolling, tethering, or adhesion was observed in control tubes, indicating that cells were specifically captured by ES-PEG liposomes in microtubes (Figure 5.8D).

After perfusion, captured cells were collected and placed in culture. Of captured KG-1a cells, there was a significant reduction in cell viability of approximately 20% for cells captured with ES-PEG L-DXR compared to untreated cells and those captured with ES-PEG EL (Figure 5.9A). Viability of COLO 205 cells was also reduced by ~30% when captured and treated with ES-PEG L-DXR (Figure 5.9A). For both cell lines, cell viability was not significantly affected when captured with ES-PEG EL.

The cytotoxic effects of the targeting mechanism on healthy blood cells was assessed using red blood cells and mononuclear white blood cells from healthy human donors. RBCs are not targeted by this mechanism, as they did not display significant adhesion to ES-PEG liposome coated surfaces compared to BSA coated surfaces (Figure 5.9B). MNCs only experienced ~16% decrease in cell viability after perfusion through the device (Figure 5.9C).

ES-PEG L-DXR enhances cancer cell death in a dilute suspension under flow

To assess the effectiveness of targeted liposomes in suspension under flow, KG-1a and COLO 205 cells were exposed to liposomes in a dilute suspension and sheared in a cone-and-plate viscometer for 2 hours. The cone-and-plate assay mimics targeted liposomes freely circulating in the bloodstream to target CTCs, as an injectable, alternative method to liposomes immobilized along a microtube platform. Confocal microscopy images taken of KG-1a (Figure 5.10A) and COLO 205 (Figure 5.10B) cells illustrate the adhesion and internalization of targeted liposomes to cells following shearing experiments. Green and blue fluorescence represents liposomes and the cell nuclei, respectively.

KG-1a cells treated with ES-PEG L-DXR experienced a nearly 75% decrease in cell viability compared to EL and untreated controls (Figure 5.11). When compared to naked L-DXR, ES-PEG L-DXR also significantly reduced cell viability by nearly 65%, indicating targeted liposomes are more effective than naked liposomes in adhering to and killing cancer cells expressing E-selectin ligands. Similarly, viability

of COLO 205 cells treated with ES-PEG L-DXR experienced a 90% decrease in cell viability compared to untreated cells. Taken together, these results suggest that increased interaction between cells and liposomes are necessary for improved targeted delivery of liposomal doxorubicin.

HNTs promote the delivery and cytotoxic potential of immobilized ES-PEG L-DXR to cancer cells under flow

A nanostructured surface coating of HNTs was applied to the microtube surfaces to enhance the adhesion of cancer cells to E-selectin liposomes, and thus improve their uptake into cancer cells (Figure 5.12). For COLO 205 and KG-1a cells treated with ES-PEG L-DXR coated on HNT-coated microtubes, cell viability decreased by over 87% and nearly 35% respectively, when compared to that on smooth tubes and decreased by approximately 96% and 45% respectively, when compared to control HNT-coated microtubes (Figure 5.13A,B). For both cell lines, cell viability was not negatively affected by control HNT-coated microtubes and either smooth or HNT-coated tube treated with ES-PEG EL. Confocal microscopy images taken of COLO 205 cells following perfusion over targeted liposomes coated on smooth (Figure 5.14A) and HNT-coated (Figure 5.14B) tubes illustrate the location of liposomes on the cell surface.

5.4 DISCUSSION

The capture and killing of cancer cells was successfully achieved using a combination of E-selectin functionalized L-DXR immobilized along the inner surface of a blood-compatible microfluidic device. Preliminary results on the use of L-DXR in our study suggest that liposomes were satisfactory for cytotoxic evaluation and effective in killing cancer cells. Over the course of several weeks, L-DXR maintained its retention of the drug, even without the addition of PEG (Figure 5.3). This was consistent with previous results [387,394] and can be attributed to two factors: the lipid composition and method of DXR loading. The cholesterol formulation for L-DXR exhibits resistance to strong shear forces, which aid in withstanding forces applied during the extrusion process [387]; thus, providing liposomal stability when encapsulating DXR. Remote loading of DXR was facilitated using an ammonium sulfate gradient, which lies between the basic outer phase and the acidic inner phase of the liposome, and drives DXR inside and ammonium ions out of the vesicle [395]. DXR precipitates as it is driven into liposomes, enhancing drug retention.

In treating model CTCs, L-DXR nanoparticles demonstrated great potential in their cytotoxicity to cancer cells. With over 95% of cells killed, a treatment dosage 0.5 μL of liposomal doxorubicin was shown to have a maximum therapeutic efficacy in both KG-1a and COLO 205 cancer cell lines (Figure 5.4A,B), despite physiological differences between the cell lineages. This high cell death rate can be attributed to DXR alone. For both cell lines, empty liposomes tended to have either little or no effect following internalization of the liposomes, which occurs within 2 hours of

treatment for KG-1a and COLO 205 cells (Figure 5.5). Moreover, free DXR and liposomes were removed from the media with multiple washes, suggesting that DXR released from L-DXR inside the cells was responsible for triggering cell death.

Cytotoxic potential to CTCs was shown to be equally or more effective with the functionalization of L-DXR using E-selectin. E-selectin, an adhesion molecule that mediates tumor cell dissemination [50,396], was chosen to decorate the surface of liposomes for target-specificity and DXR delivery to cancer cells expressing E-selectin ligands. The addition of PEG was used to provide stability and charge neutralization of liposomes. To incorporate both E-selectin and PEG to the surface of the liposomes, E-selectin was attached to PEG via a maleimide group [397]. Using COLO 205 and KG-1a cells as model CTCs, static experiments confirmed that ES-PEG L-DXR was no less effective than L-DXR, making them a good candidate for targeting under flow conditions. Cell capture experiments demonstrated that CTCs could be captured and killed under flow conditions, while leukocytes only experienced a minimal decrease in cell viability. While both CTCs and leukocytes express ligands for E-selectin on their surface, metastatic cancer cells typically have very high expression of E-selectin ligands [179,398-400]. Thus, more liposomes are likely to be adhering to cancer cells than leukocytes, which could explain the differences in cell death. Red blood cells do not possess E-selectin ligands, and thus experienced negligible adhesion and cell death using this novel targeting mechanism.

Under shear flow in a cone-and-plate viscometer, improved cytotoxicity of targeted liposomes was evident from a substantial increase in cell death compared to delivery using liposome-coated microtubes. The dynamic environment of the

viscometer mimics sustained flow through a closed system, and in contrast to static conditions, allows for an increased number of collisions between the cells and nanoparticles, thus delivering more L-DXR to the cells. Although naked L-DXR contributes considerably to cell death, the bond between E-selectin and its ligands expressed by cells is strong and remains so even after several washes, as evidenced by a light red pellet following centrifugation of the sample. This further supports the conclusion that the target-specificity of ES-PEG L-DXR is a strong improvement over naked L-DXR and in general, confirms the demonstrated improvement of ligand-targeted liposomes described in previous studies [396,401]. However in the bloodstream, suspension liposomes could have less opportunity to adhere to CTCs in the complex milieu of blood, which would necessitate high concentrations of chemotherapeutics that could cause undesired side effects. An immobilized platform along a microtube would adhesively interact only with cells that circulate along the near-wall region of blood vessel. Here, margination elevates the local concentration of leukocytes and CTC above those in the systemic circulation by several-fold, allowing more opportunities for an immobilized platform to interact with CTCs. The nanostructured coating of HNTs along the microtube surface enhanced the CTC capture and killing of the microtube platform to similar levels as the cone and plate assay, providing potential that an immobilized platform of targeted chemotherapeutic can be used to capture and kill CTCs, and possibly decrease the probability of metastasis.

5.5 CONCLUSION

In this study, we demonstrated the efficacy of targeting, capturing, and killing model CTCs using a novel combination of E-selectin functionalized L-DXR and a biomimetic microtube device. Targeted ES- PEG L-DXR was shown to increase cancer cell killing in both static and dynamic environments. The cone-and-plate shear experiments demonstrated the effectiveness of target-specific nanoparticles in solution, which can aid in the development of drugs intended for systemic delivery. Furthermore, by immobilizing liposomes onto HNT- coated microtubes, capture and kill rates of cells in flow were significantly increased. One advantage of this device for capturing and killing of CTCs is that by immobilizing liposomes onto the microtube surface, the potential distribution of targeted L-DXR into circulation is reduced and a lower dose of the drug is necessary. The proposed device demonstrates potential application of HNT-coated microtubes for reducing the probability of metastasis, and suggests new strategies for enhancing targeted delivery of chemotherapeutics to CTCs.

FIGURE 5.1: **SCHEMATIC OF E-SELECTIN-TARGETED PEGYLATED LIPOSOME SYNTHESIS.** DXR: doxorubicin, ES: E-selectin, PEG: polyethylene glycol.

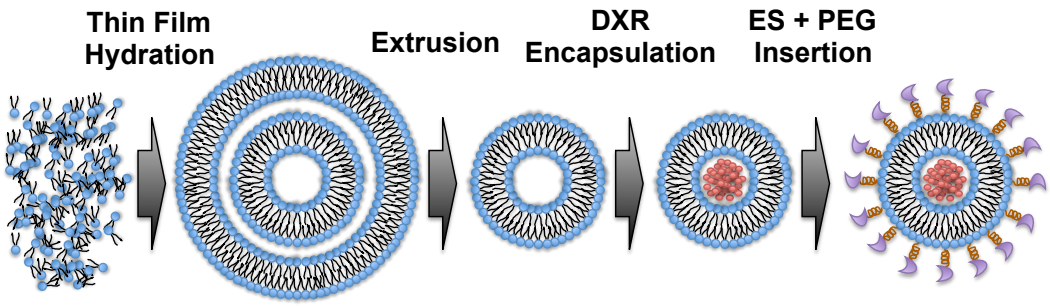

TABLE 5.1: HYDRODYNAMIC RADIUS AND ZETA POTENTIAL OF LIPOSOME FORMULATIONS. DXR: doxorubicin, ES: E-selectin, PEG: polyethylene glycol, nm: nanometers, mV: millivolts.

	L-DXR	PEG L-DXR	ES-PEG L-DXR
Particle size (nm)	106.3 +/− 5.9	111.5 +/− 6.4	143.7 +/− 11.2
Zeta potential (mV)	−24.56 +/− 6.34	−8.49 +/− 5.85	−13.12 +/− 6.28

FIGURE 5.2: E-SELECTIN CONJUGATED LIPOSOME ADHESION TO THE CANCER CELL SURFACE. (A) Percent of COLO 205 and KG-1a cells with liposomes adhered to the surface. Data presented as mean ± SEM (n=3). (B) Representative COLO 205 cell (blue = cell nuclei) with fluorescent ES-PEG liposomes (green) adhered to the surface. Scale bar = 10 μm.

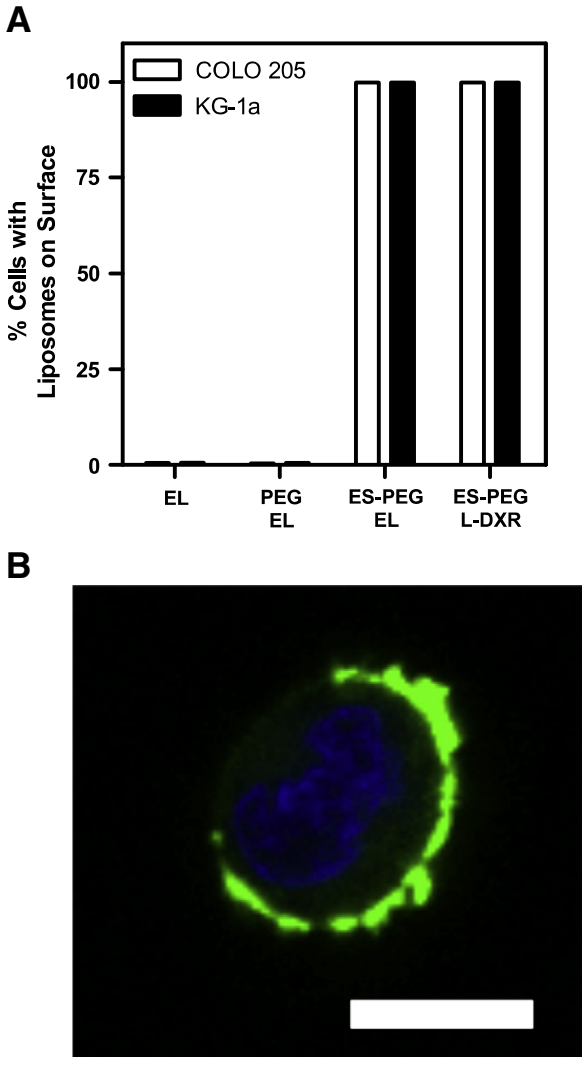

FIGURE 5.3: DOXORUBICIN ENCAPSULATION AND LEAKAGE FROM LIPOSOMES. (A) Fluorescence intensity of soluble DXR (1 μM) and 5 μL L-DXR in the presence or absence of 10% Triton X-100. Results expressed in fluorescence units (fu). (B) Leakage profile of 30 μL liposomes over time as measured by fluorescence intensity. Data presented as mean ± SEM (n=3).

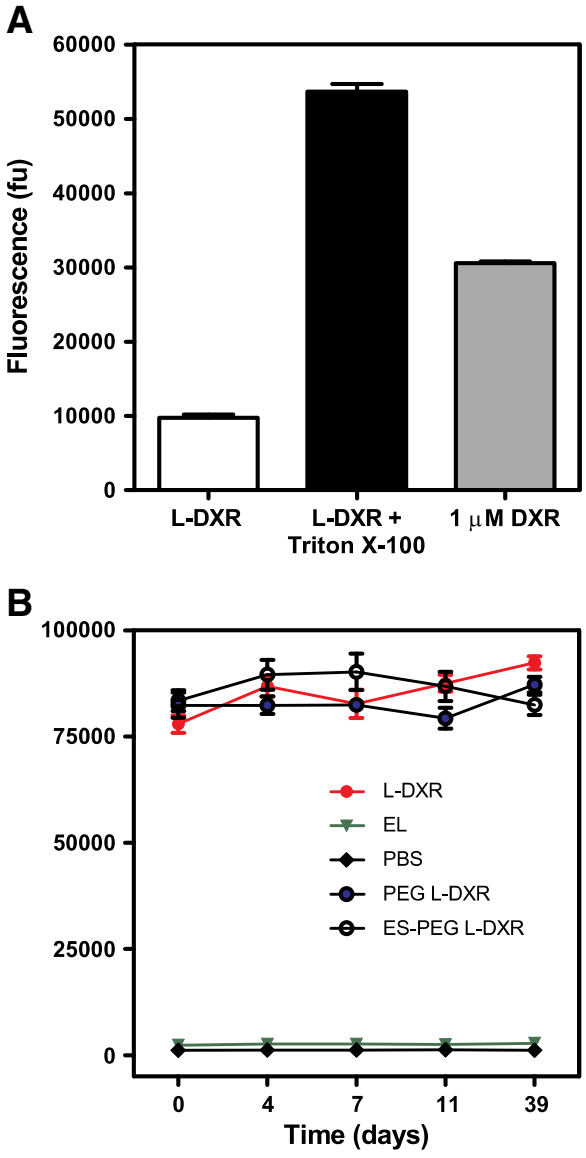

FIGURE 5.4: LIPOSOME UPTAKE AND CYTOTOXIC POTENTIAL ON CANCER CELLS UNDER STATIC CONDITIONS. KG-1a cells (A) and COLO 205 cells (B) were placed in static conditions for 4 days and evaluated for viability using trypan-blue. (A,B) Dose response curves relating the volume of L-DXR, EL, ES-PEG L-DXR or soluble DXR treatment and viability of cells. All data presented as mean ± SEM (n=3). *** denotes $P < 0.001$.

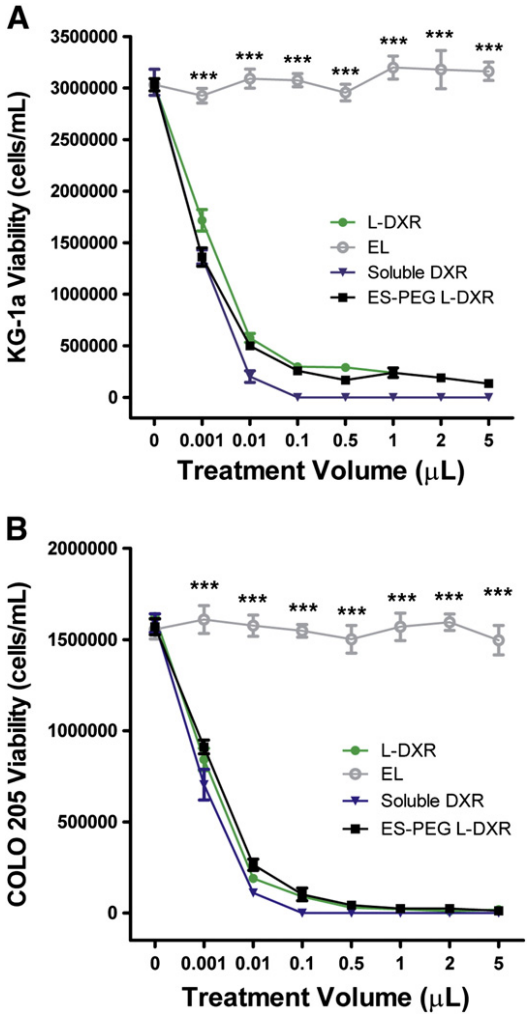

FIGURE 5.5: E-SELECTIN CONJUGATED LIPOSOMAL DOXORUBICIN INTERNALIZATION WITHIN CANCER CELLS. Fluorescent images of L-DXR internalization by KG-1a cells (A,B) and COLO 205 cells (C, D) after treatment with L-DXR (A,C) and ES-PEG L-DXR (B,D). Scale bar = 30 μm.

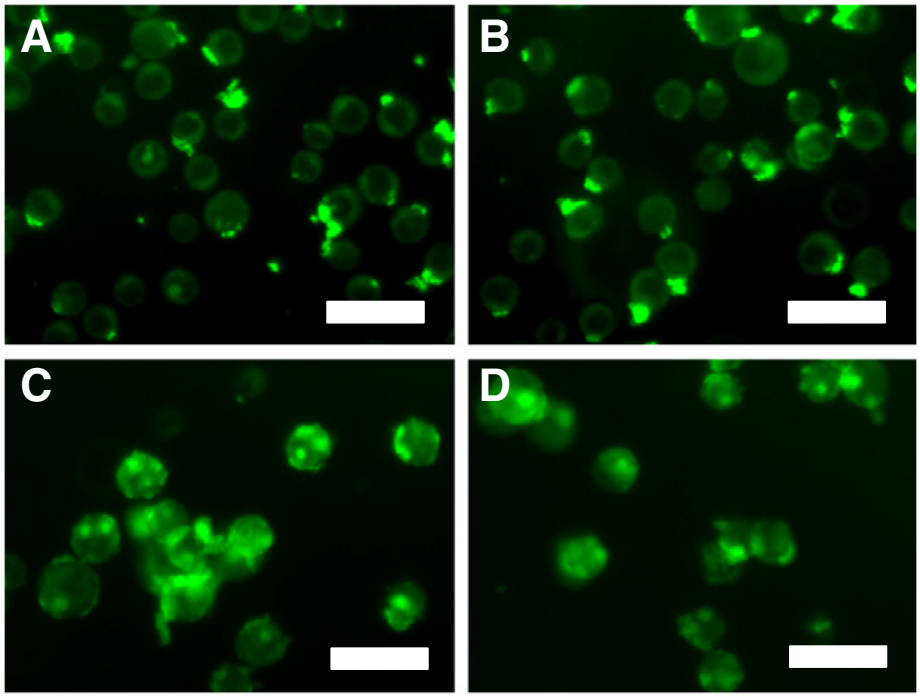

FIGURE 5.6: GROWTH CURVES OF CANCER CELLS AFTER TREATMENT WITH E-SELECTIN CONJUGATED LIPOSOMAL DOXORUBICIN. Viability of COLO 205 cells over 4 days after treatment with 0.5 µL of ES-PEG L-DXR, naked L-DXR, or naked EL. All data presented as mean ± SEM (n=3). * denotes $P < 0.05$, and ** denotes $P < 0.01$.

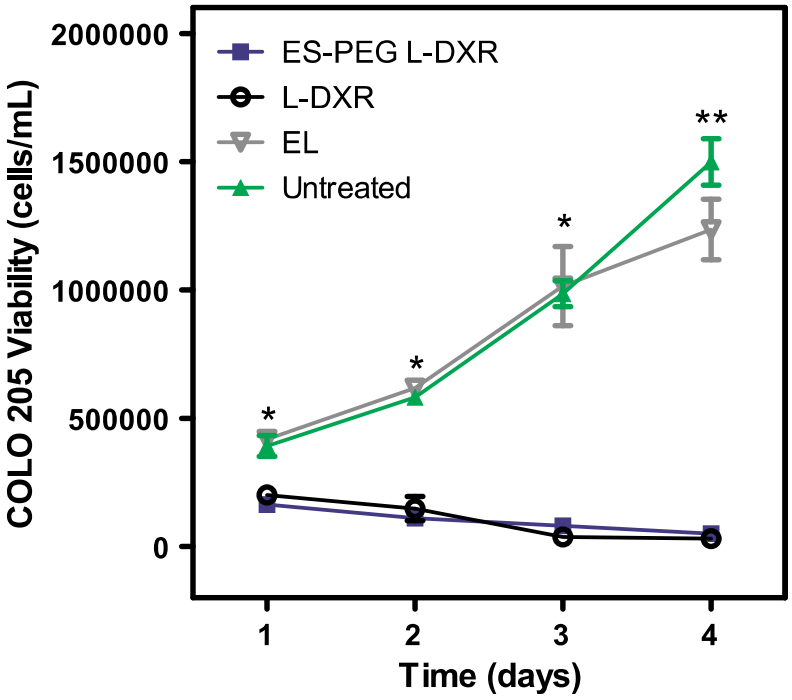

FIGURE 5.7: CANCER CELL MORPHOLOGY AFTER TREATMENT WITH E-SELECTIN CONJUGATED LIPOSOMAL DOXORUBICIN. Brightfield images of COLO 205 cells (A) untreated or treated with 0.5 uL of (B) EL, (C) naked L-DXR, or (D) ES-PEG L-DXR taken 4 days after treatment. Scale bar = 50 μm.

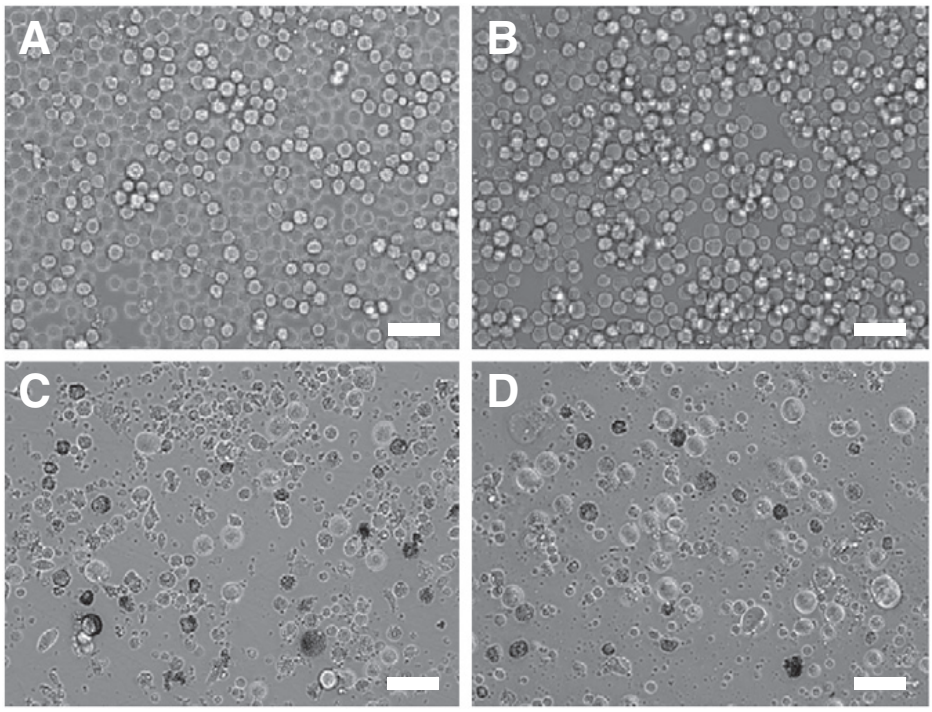

FIGURE 5.8: E-SELECTIN CONJUGATED LIPOSOMAL DOXORUBICIN IMMOBILIZATION TO MICROTUBE SURFACE. Fluorescent images of a (A) control tube and (B) tube coated with ES-PEG L-DXR. Video frames of COLO 205 cells perfusing through a (C) ES-PEG L-DXR coated tube and (D) BSA-coated control tube. Scale bar = 100 μm.

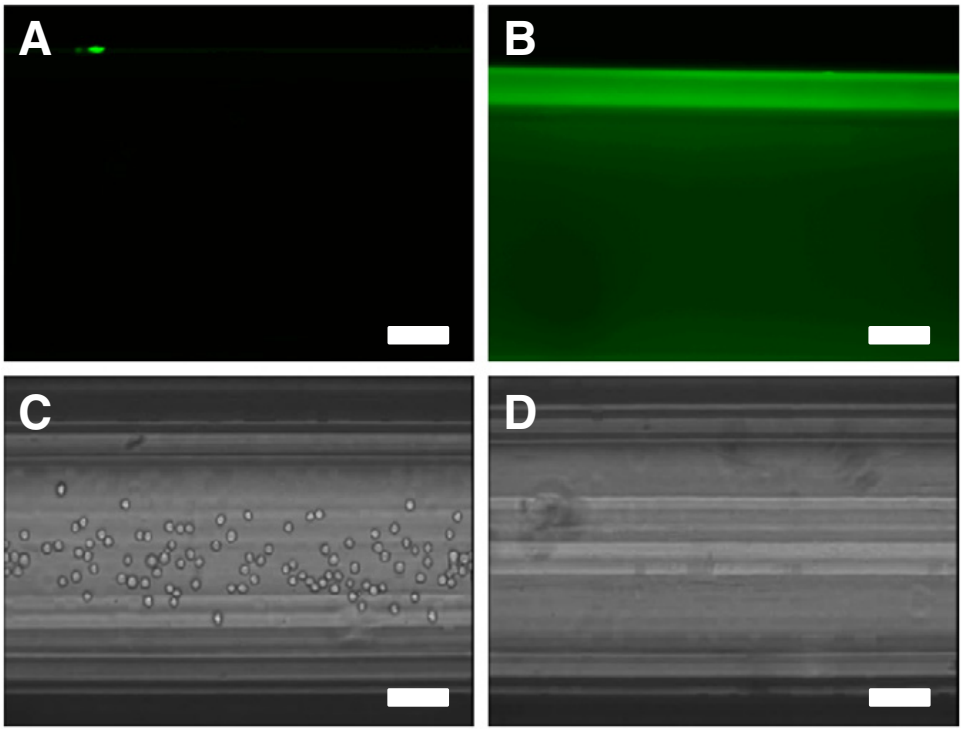

FIGURE 5.9: VIABILITY AND RECOVERY OF FLOWING CANCER CELLS, ERYTHROCYTES, AND LEUKOCYTES AFTER EXPOSED TO IMMOBILIZED E-SELECTIN FUNCTIONALIZED LIPOSOMAL DOXORUBICIN. (A) Comparison of viability of COLO 205 and KG-1a cells following perfusion through control tubes (BSA-coated or 20 μM DXR) or tubes coated with ES-PEG L-DXR or ES-PEG EL. Viability of KG-1a and COLO 205 cells were taken at day 4 (n=3). (B) Percent of nonadhered, flowing RBCs recovered following perfusion through device. (C) Viability of MNCs following perfusion through control tubes or tubes coated with liposomes. Data presented as mean ± SEM.* denotes $P < 0.05$. NS denotes not significant.

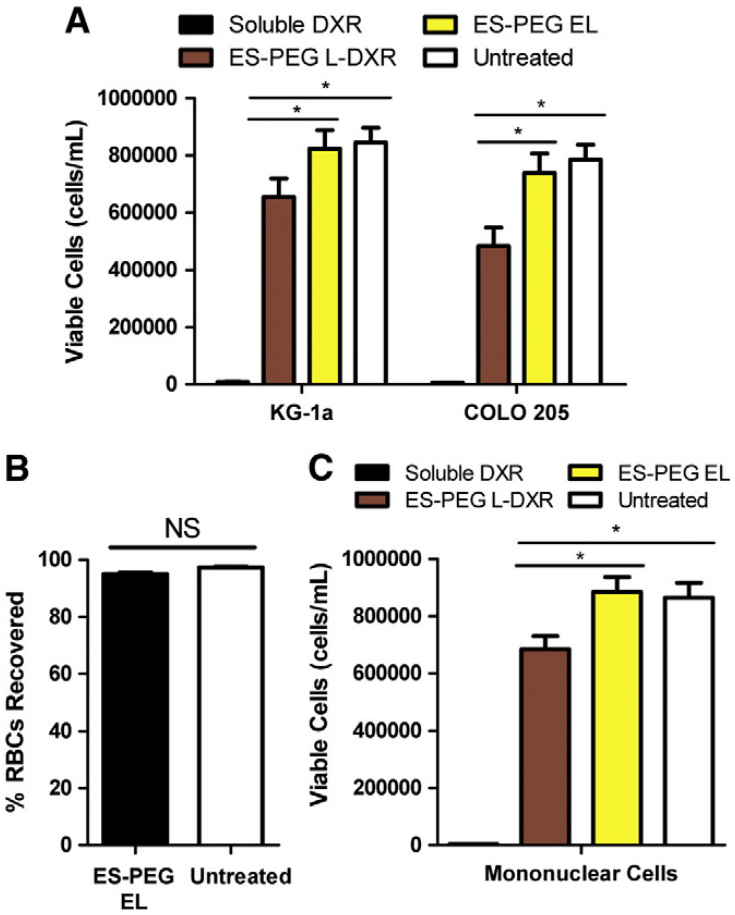

FIGURE 5.10: CONFOCAL MICROGRAPHS OF E-SELECTIN FUNCTIONALIZED LIPOSOMAL DOXORUBICIN ADHERED TO THE SURFACE OF KG-1A AND COLO 205 CELLS AFTER EXPOSURE TO SHEAR FLOW. Overlay of brightfield and fluorescence microscopy images taken of KG-1a (A) and COLO 205 (B) cells after 2 hrs of shearing in a dilute suspension. Scale bars = 10 μm. Green fluorescence labels liposomes and the blue fluorescence labels DNA.

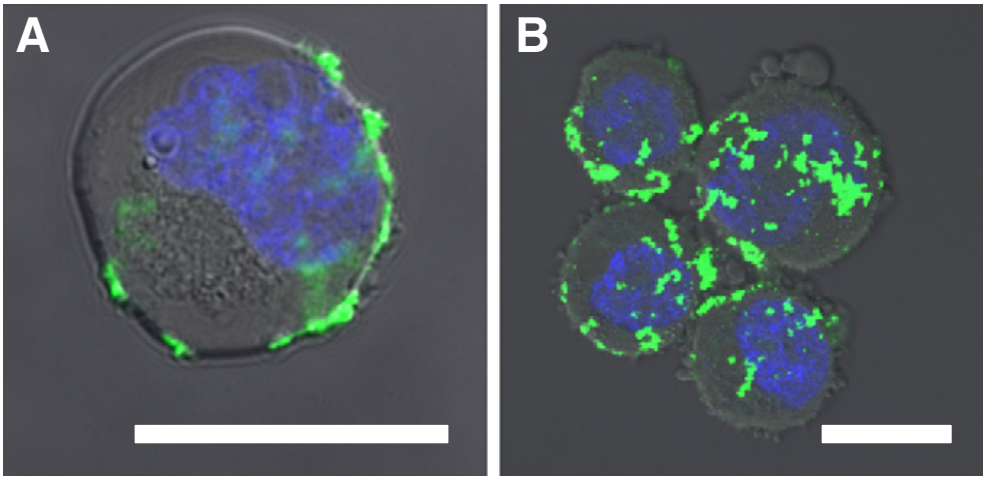

FIGURE 5.11: VIABILITY OF KG-1A AND COLO 205 CELLS AT DAY 4 FOLLOWING TREATMENT WITH TARGETED L-DXR UNDER SHEAR IN A DILUTE SUSPENSION. Data presented as mean ± SEM (n=3). *** denotes $P < 0.001$.

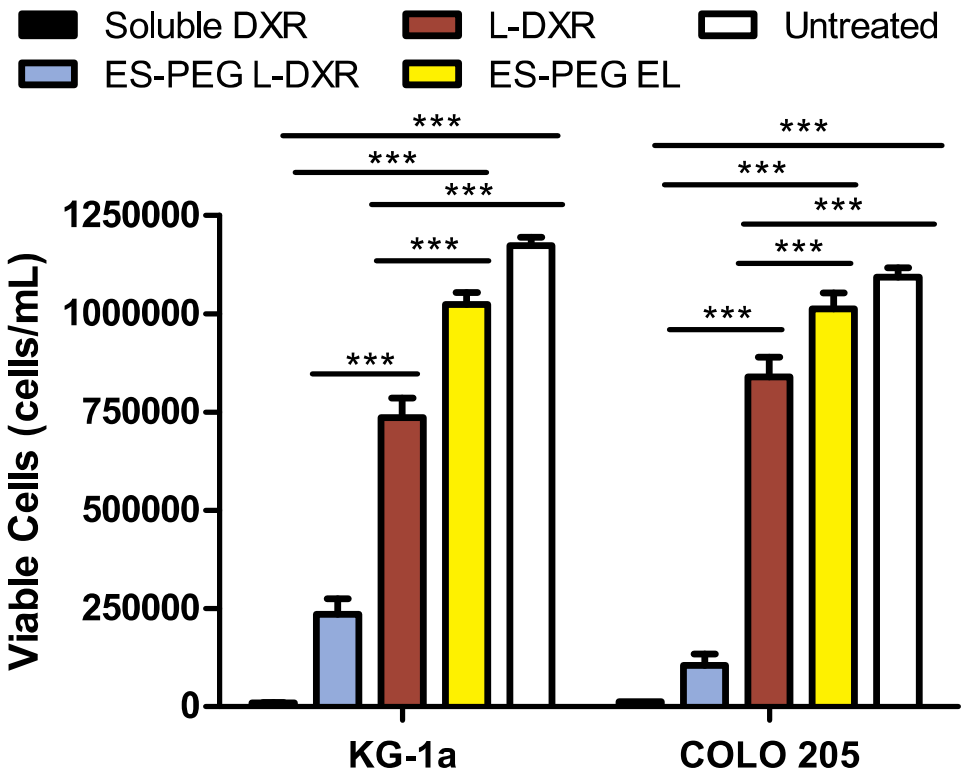

FIGURE 5.12: SCHEMATIC OF HALLOYSITE NANOTUBE (HNT)-COATED MICROTUBE DEVICE WITH IMMOBILIZED TARGETED L-DXR TO ENHANCE CAPTURE AND KILLING OF TUMOR CELLS UNDER FLOW. ES-PEG L-DXR: E-selectin functionalized liposomal doxorubicin.

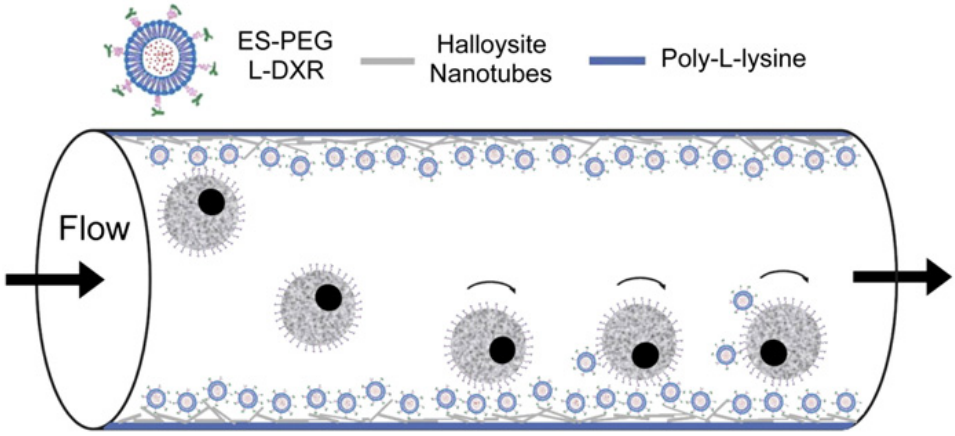

FIGURE 5.13: COMPARISON OF SMOOTH AND HNT-COATED TUBE WITH IMMOBILIZED E-SELECTIN CONJUGATED LIPOSOMAL DOXORUBICIN ON CANCER CELL VIABILITY AFTER PERFUSION THROUGH MICROTUBES. Comparison of smooth and HNT-coated tube with immobilized E-selectin conjugated liposomal doxorubicin on cell viability of (A) KG-1a and (B) COLO 205 after perfusion through microtubes. Cell viability of KG-1a and COLO 205 cells were taken at day 4 (n=3), respectively. Data presented as mean ± SEM. * denotes $P < 0.05$, ** denotes $P < 0.01$.

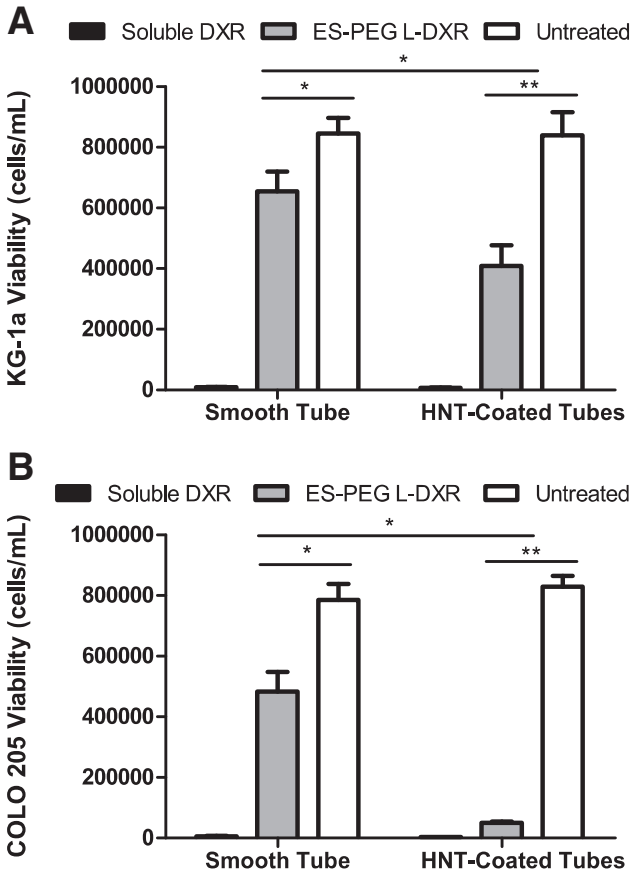

FIGURE 5.14: E-SELECTIN FUNCTIONALIZED LIPOSOMAL DOXORUBICIN ADHESION TO CANCER CELLS AFTER EXPOSURE TO HNT-COATED MICROTUBES. Overlay of brightfield and fluorescence microscopy images of COLO 205 cells following perfusion through a (A) smooth tube and (B) HNT-coated tube incubated with fluorescently-tagged ES-PEG EL. Scale bar = 30 μm.

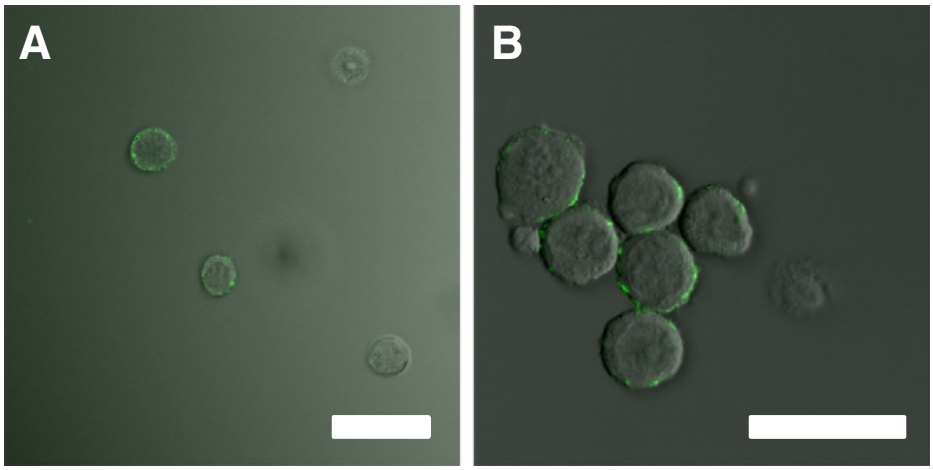

CHAPTER 6: NANOSTRUCTURED SURFACES TO TARGET AND KILL CIRCULATING TUMOR CELLS WHILE REPELLING LEUKOCYTES

*This section is adapted from the following publication: M.J. Mitchell, C.A. Castellanos, and M.R. King. *Journal of Nanomaterials.* 2012(5): 1-10, 2012.

6.1 INTRODUCTION

Hematogenous metastasis typically signals a poor patient prognosis, with over 90% of cancer deaths attributed to the metastatic spread [1]. For metastasis to occur, cancer cells detach from the primary tumor, invade through the basement membrane, and intravasate into the peripheral circulation as circulating tumor cells (CTCs) [8]. CTCs that express sialylated carbohydrate ligands on their surface can adhesively interact with selectin proteins on the inflamed endothelial cell wall, leading to selectin-mediated CTC tethering and rolling on the endothelium, followed by firm adhesion and arrest [1,52]. CTCs can then extravasate to the tissue of a distal organ to form secondary metastases, and while the percentage of CTCs that survive this pathway is small (<0.01%), the formation of such metastases remains the primary cause of cancer-related deaths [8,334,367].

Several chemotherapeutics are currently in use for the treatment of cancers, including doxorubicin, which is in use for the treatment of Kaposi's sarcoma, acute leukemia, metastatic breast cancer and other lymphomas and sarcomas [88]. Doxorubicin is an adriamyacin anthracycline antibiotic that can induce cancer cell death via DNA intercalation, inhibition of topo-isomerase II, and formation of free radicals [89,368]. However, the non-specific effects of doxorubicin are numerous, and include systemic toxicity, tissue necrosis, neutropenia, and cardiomyopathy [369,370]. Nanobiotechnology has contributed to the development of novel drug delivery vehicles to both enhance the efficiency of doxorubicin while reducing its toxic effects, such as polymers, dendrimers, and liposomes [371]. Liposomal doxorubicin (L-DXR)

in particular has been shown to enhance overall drug efficacy by altering pharmacokinetics, increasing circulation time, and reducing non-specific toxic effects [372,373,379]. Polyethylene glycol (PEG) conjugation to the liposome surface provides steric stabilization and increased circulation time of the drug, and can also aid in tumor uptake due to enhanced permeability and retention effects [379,381]. The efficacy of L-DXR has been shown clinically as evidenced by Doxil®, which has been approved by the FDA for use in treating Kaposi's sarcoma [382]. However, current L-DXR formulations lack the targeting mechanisms to treat individual CTCs in bloodstream, due to the rarity of CTCs amongst healthy circulating blood cells. The concentration of CTCs in the bloodstream of patients is approximately one in a million leukocytes [238], or one in a billion of all healthy blood cells [42].

Cell adhesion molecules known as selectins hold promise in targeting drug delivery vehicles to CTCs under physiological shear flow, due to their rapid, force-dependent binding kinetics [171,335]. Sialylated carbohydrate ligands are expressed on the surface of many CTCs, which have the ability to bind to selectin proteins on the inflamed endothelium during metastasis [48,50,384]. Targeting of CTCs in the bloodstream via selectin-mediated adhesion could reduce the probability of metastasis. However, healthy circulating leukocytes are also known to express sialylated carbohydrate ligands on their surface [176]. Thus, strategies to reduce healthy blood cell adhesion are required for selectin-mediated targeting of therapies to CTCs.

The development of nanostructured surfaces to enhance the capture of CTCs for chemotherapeutic delivery while preventing healthy cell adhesion has not yet been investigated. Here, I assessed the application of a nanostructured surface consisting of

halloysite nanotubes and nanoscale L-DXR to increase cancer cell recruitment while preventing leukocyte adhesion.

6.2 MATERIALS AND METHODS

Cell culture

Colorectal adenocarcinoma cell line COLO 205 (ATCC #CCL-222) and breast adenocarcinoma cell line MCF7 (ATCC #HTB-22) were purchased from American Type Culture Collection (Manassas, VA, USA). COLO 205 cells were cultured in RPMI 1640 medium supplemented with 10% (v/v) fetal bovine serum and 1% (v/v) PenStrep, all purchased from Invitrogen (Grand Island, NY, USA). MCF7 cells were cultured in Eagle's Minimum Essential Medium (EMEM) supplemented with 0.01 mg/ml bovine insulin, 10% (v/v) fetal bovine serum, and 1% (v/v) PenStrep, all purchased from Invitrogen. All cancer cell lines were incubated under humidified conditions at 37°C and 5% CO_2, and were not allowed to exceed 90% confluence.

Neutrophil isolation

Neutrophils were isolated as previously described [91]. Briefly, human peripheral blood was obtained from healthy blood donors after informed consent via venipuncture, and collected using sterile sodium heparin-containing tubes (BD Biosciences, San Jose, CA). Neutrophils were isolated from blood by centrifugation at

480 X *g* for 50 min at 23°C, in a Marathon 8K centrifuge (Fisher Scientific, Pittsburgh, PA) using 1-Step™ Polymorphs (Accurate Chemical & Scientific Corporation, Westbury, NY). Neutrophils were extracted and washed in Mg^{2+} and Ca^{2+} free Hank's balanced salt solution (HBSS), and all remaining red blood cells in the suspension were lysed hypotonically. Neutrophils were resuspended at a concentration of 1.0 x 10^6 cells/mL in HBSS containing 0.5% HSA, 2 mM Ca^{2+}, and 10 mM HEPES (Invitrogen), buffered to pH 7.4.

Liposomal doxorubicin synthesis

Nanoscale liposomes were synthesized as described previously [82]. Briefly, lipids were dried overnight, and rehydrated using a thin lipid film hydration method [386,387] with 125 mM ammonium sulfate (Sigma-Aldrich, St. Louis, MO, USA). Lipids were then subjected to 10 freeze-thaw cycles and extruded to prepare empty liposomes (EL). Doxorubicin hydrochloride (Sigma-Aldrich) was encapsulated within ELs using an ammonium sulfate remote loading method, at a doxorubicin-to-lipid ratio of 0.2:1 (w/w). Excess DXR was removed using gel-exclusion chromatography with Sephadex G-50 (Sigma-Aldrich). Liposomal doxorubicin concentration was determined by spectrophotometry (λ=490 nm). The loading efficiency of doxorubicin was determined to be >95%.

Targeted liposome preparation

E-selectin functionalized L-DXR (ES-PEG L-DXR) and E-selectin functionalized empty liposomes (ES-PEG EL) were prepared using a post-insertion technique [402]. Recombinant human E-selectin/Fc chimera (rhE/Fc) (R&D Systems, Minneapolis, MN) was thiolated and conjugated to 1,2-Distearoyl-sn-Glycero-3-Phosphoethanolamine-N-Maleimide 2000 (DSPE-PEG_{2000} maleimide) (Avanti Polar Lipids, Alabaster, AL, USA). To incorporate ES-polyethylene glycol (ES-PEG) conjuguates into the lipid bilayer, ES-PEG was incubated with liposomes at 50°C for 30 min. Liposomes were stored at 4°C for <1 week until usage.

The mean particle diameter and zeta potential of the liposome formulations were measured by dynamic light scattering, using a Malvern Zetasizer nano ZS (Malvern Instruments Ltd., Worcestershire, UK) according to the manufacturer's protocols. Mean particle diameter and zeta potential measurements of the liposome formulations were similar to values previously reported [82]. To determine successful E-selectin conjugation to liposome surface, 10 μL of fluorescently tagged liposomes were mixed with 490 μL of MCF7 cells (10^6 cells/mL) and exposed to a shear flow in a cone and plate viscometer at 2.0 dyn/cm^2 for 10 min. Fluorescent liposomes adhered to the cell surface were measured using an Accuri C6 flow cytometer (Accuri Cytometers, Inc., Ann Arbor, MI, USA). To assess fluorescent liposome adhesion and internalization to MCF7 cells, sheared samples were incubated for 60 min at 37°C and then imaged using confocal microscopy.

Confocal microscopy

Fluorescent ES-conjugated liposomes were used to verify selectin-mediated adhesion to cancer cells. Fluorescent lipids were synthesized using fluorescent BODIPY-cholesterol (Avanti Polar Lipids). Cells were incubated with 2 μL of 10 mg/mL trihydrochloride trihydrate (Hoechst 33342) (Invitrogen, Carlsbad, CA, USA) for 15 minutes to image cell nuclei. Cells were then placed on glass coverslips and visualized with a Zeiss 710 Spectral Confocal Microscope System (Carl Zeiss MicroImaging GmbH, Jena, Germany) at 65X magnification with FITC and DAPI filters. Images were processed using Zen 2009 light edition software (Carl Zeiss MicroImaging GmbH).

MCF7 breast cancer cell static assays

MCF7 cells were cultured in complete media at a concentration of $1x10^5$ cells/mL on 12-well plates (Becton Dickinson, Franklin Lakes, NJ, USA). Cells were treated with ES-PEG L-DXR, L-DXR, or EL at volumes of 0 to 5 μL for 18 hours. MCF7 cells were treated with Accutase (Sigma-Aldrich) for 5 min at 37°C, to remove adherent cells from the surface. Cells were then washed with phosphate buffered saline (PBS) at 1000 rpm in a refrigerated centrifuge (Allegra XX-22R Centrifuge; Beckman Coulter, Brea, CA, USA) and resuspended in fresh media. After 4 days, cell viability was evaluated on a hemocytometer (Hausser Scientific, Horcham, PA, USA) using a trypan blue exclusion assay (Lonza, Wilkersville, MD, USA). Cells were also

treated with 0.5 μL of liposome solution and assessed for viability over a period of 1-4 days. Cell morphology and uptake of doxorubicin were imaged using brightfield and fluorescence microscopy, respectively.

Cancer cell and neutrophil preparation for capture experiments

MCF7 and COLO 205 cells were treated with Accutase (Sigma, St. Louis, MO) for 5-10 min before handling. MCF7 and COLO 205 cells were washed in PBS and resuspended at a concentration of 1.0 x 10^6 cells/mL, in a flow buffer of HBSS containing 0.5% HSA, 2 mM Ca^{2+}, and 10 mM HEPES (Invitrogen), buffered to pH 7.4. For neutrophil capture experiments, freshly isolated neutrophils were resuspended in flow buffer at a concentration of 1.0 X 10^6 cells/mL. For combined cell capture assays, MCF7 or COLO 205 cells were resuspended in flow buffer with neutrophils at a 1:1 cancer cell to neutrophil ratio, at a concentration of 1.0 X 10^6 cells/mL.

Halloysite nanotube-liposome immobilization to microtube surface

Microrenathane microtubing (Braintree Scientific, Braintree, MA, USA) of inner diameter 300 μm was cut to 55 cm in length and washed with 75% ethanol. To prepare HNT-coated microtube surfaces, a 6.6% by weight HNT solution (NaturalNano Rochester, NY, USA) was treated via sonication, followed by filtration [82]. Microtubes were washed using distilled water, followed by incubation with 2:8 poly-L-lysine (0.1% w/v, Sigma) for 5 min and then incubation with treated HNT

solution for 3 min. Microtubes were washed thoroughly with distilled water to remove excess HNTs in solution, and incubated overnight at RT. Surface immobilization of liposomes was achieved by incubating E-selectin functionalized liposome solution (ES-PEG L-DXR or ES-PEG EL) for 2.5 hours within HNT-coated microtubes. Smooth microtubes were prepared by immobilizing liposomes on the surface in the absence of HNTs. All surfaces were blocked for non-specific adhesion for 1 h with 5% bovine serum albumin (BSA) (Sigma-Aldrich) in PBS (w/v). All incubation steps were preceded and followed by thorough washes with PBS. Immobilized E-selectin proteins were activated prior to cell capture experiments via perfusion of calcium-enriched flow buffer.

Cell capture experiments

To visualize cell adhesion and capture, functionalized microtubes were secured onto the stage of an Olympus IX81 motorized inverted microscope (Olympus, Center Valley, PA, USA). A motorized syringe pump (KDS 230; IITC Life Science, Woodland Hills, CA, USA) was used to perfuse cell suspensions through microtubes at physiologically relevant flow rates. Cancer cells and combined cell solutions were initially perfused through microtubes at a rate of 0.008 mL/min (wall shear stress of 0.5 dynes/cm^2) for 30 min, and then 0.04 mL/min (wall shear stress of 2.5 dynes/cm^2) for another 30 min. Isolated neutrophils were perfused at 0.04 mL/min for 60 min. Microtubes were washed with calcium-enriched PBS at 1.0 dyn/cm^2 to remove all non-adherent cells. Accutase was gently perfused into the microtube and allowed to

incubate for 10 min to detach adherent cells, followed by perfusion of medium for cell collection. For combined cell assays, neutrophils were separated from cancer cells by centrifugation using 1-Step Polymorphs after cell collection. Cells were cultured in 6-well plates in complete media, and analyzed for cell viability at day 4 via trypan blue exclusion.

Data acquisition

Videos of cell capture experiments were recorded using a microscope-linked Hitachi CCD camera KP-M1AN (Hitachi, Japan) and a Sony DVD Recorder DVO-1000MD (Sony Electronics Inc., San Diego, California, USA). Video frames were utilized to determine the number of captured cells per 100,000 μm^2. For combined cell experiments, cancer cell and neutrophil capture measurements were determined based on differences in cell diameter.

Shape factor analysis

Brightfield images of neutrophils captured in smooth and HNT-coated tubes were analyzed for morphological changes using a shape factor analysis. Outlines of neutrophils were created from thresholded brightfield images using edge-detection functions in Metamorph software (Universal Imaging Corp., West Chester, PA). Neutrophil morphological changes were determined using a shape factor program in Metamorph, where shape factor is determined by:

$$Shape\ Factor = \frac{4\pi A}{P^2}$$

where P is the perimeter and A is the area of the object (neutrophil). Shape factor values close to 1 correspond to a circle, while values approaching 0 represent spindly or dendritic shapes.

Statistical analysis

Data sets were plotted and analyzed using Prism 5.0b for Mac OS X (GraphPad software, San Diego, CA, USA). All results were reported as the mean +/- standard error of the mean. A two-tailed paired t-test was used for comparisons between two groups. *P*-values less than 0.05 were considered significant.

6.3 RESULTS AND DISCUSSION

ES-PEG L-DXR targets and induces breast cancer cell death

To assess the functionality of E-selectin conjugated to the liposome surface, fluorescently tagged ES-PEG L-DXR was incubated with human breast cancer MCF7 cells and sheared in a cone-and-plate viscometer for 10 min at 2.0 dyn/cm^2. MCF7 cells have previously been shown to roll on ES-coated surfaces, a process that is mediated by CD24 expressed on the MCF7 cell surface [181]. MCF7 cells sheared with fluorescent ES-PEG L-DXR increased in fluorescence by >99.9%, compared to

MCF7 cells sheared with fluorescent liposomes lacking E-selectin (Figure 6.1A). Confocal microscopy revealed that ES-PEG L-DXR not only binds to the cancer cell surface but also internalizes within the cell over time (Figure 6.1B), making this targeting mechanism well suited for the internalization of ES-PEG L-DXR within cancer cells. Static assays verified cellular uptake and cytotoxicity of ES-PEG L-DXR at levels comparable to L-DXR (Figure 6.1C,D). MCF7 cells treated with either L-DXR (Figure 6.1G) or ES-PEG L-DXR (Figure 6.1H) had observable membrane blebbing and were non-adherent, characteristic of MCF7 cell death. MCF7 cells treated with EL (Figure 6.1F) were adherent, and displayed a morphology similar to healthy, untreated MCF7 cells (Figure 6.1E). Fluorescence microscopy confirmed comparable doxorubicin uptake in MCF7 cells treated with L-DXR (Figure 6.1K) and ES-PEG L-DXR (Figure 6.1L), compared to control samples in the absence of doxorubicin (Figure 6.1I,J). It is apparent from these images that E-selectin adhesion to the cell surface does not hinder internalization and cytotoxic effects of L-DXR on MCF7 cells, making this targeting mechanism suitable for MCF7 treatment under physiological flow.

Nanostructured surfaces enhance breast and colon cancer cell adhesion to immobilized ES-PEG L-DXR

Our lab has previously demonstrated that selectin proteins and selectin-coated nanoparticles can be immobilized on the inner surfaces of microtubes for the capture of circulating cells [388], as well as for use as *in vitro* models of the microvasculature

to examine the rolling adhesion of leukocytes [278] and cancer cells [391]. In this study, smooth microtubes were coated with only ES-PEG L-DXR. HNT-liposome coated microtubes were coated with HNTs, followed by ES-PEG L-DXR immobilization. MCF7 or COLO 205 cells were perfused through microtubes at shear stresses (0.5-2.5 dyn/cm^2) observed in the microvasculature *in vivo* [274]. Both cell lines were chosen as model CTCs because they express sialylated carbohydrate ligands and exhibit rolling adhesion properties on immobilized E-selectin surfaces [85,181]. MCF7 cells were captured from flow in both smooth (Figure 6.2A) and HNT-liposome coated microtubes (Figure 6.2B). However, an increase in the number of MCF7 cells captured was observed on HNT-liposome surfaces, compared to smooth surfaces. A significant three-fold increase in MCF7 (Figure 6.2C) and two-fold increase in COLO 205 cell capture (Figure 6.2D) per 100,000 μm^2 were observed on HNT-liposome coated surfaces, compared to smooth surfaces coated with ES-PEG L-DXR. HNT-coated microtubes have been previously shown to increase the adsorption of selectin proteins [385], compared to the adsorption of selectins within microtubes in the absence of HNTs. It is likely that HNT coatings can also enhance the deposition of ES-PEG L-DXR, which could increase the recruitment of flowing cancer cells.

Nanostructured surfaces reduce neutrophil adhesion to ES-PEG L-DXR

While HNT-coated surfaces can enhance the delivery of chemotherapeutics to CTCs via selectin-mediated adhesion, it is also important to examine the effects of

such surface interactions with healthy blood cells. Leukocytes, which express sialylated carbohydrate ligands, outnumber CTCs by roughly one million to one in patients, on average [337]. Thus, leukocytes could potentially uptake the majority, if not all of the encapsulated chemotherapeutic being delivered. However, capture assays revealed that the number of neutrophils adhered to HNT-liposome coated surfaces (Figure 6.3B) was largely diminished compared to smooth surfaces (Figure 6.3A), the opposite of the trend observed in cancer cell capture studies. Similar trends were also observed in the isolation of CTCs from a suspension of mononuclear cells [336]. A significant >94% reduction of neutrophils captured per 100,000 μm^2 was confirmed in HNT-liposome coated microtubes, compared to smooth microtubes coated with ES-PEG L-DXR (Figure 6.3C).

Cytoskeletal projections known as pseudopods were observed consistently on neutrophils adhered to smooth surfaces, characteristic of firmly adhered and activated neutrophils (Figure 6.3A) [176]. Neutrophils on HNT-liposome coated surfaces displayed a rounder morphology, characteristic of weaker adhesion of resting neutrophils (Figure 6.3B). Shape factor analysis has previously been utilized to assess neutrophil morphological changes [82], and was performed in this study to determine the effect of adhesion to HNT-liposome coated surfaces on morphological changes. On a scale of 0 (elongated shapes) to 1 (circularity), shape factor analysis verified a significantly higher shape factor in neutrophils adhered to HNT-liposome coated surfaces (Figure 6.3D) compared to those adhered to smooth surfaces, adding further support that neutrophils display weaker adhesion on HNT-liposome coated surfaces.

To examine if the reduction in neutrophil adhesion and capture is due to prevention of ES-PEG L-DXR adsorption, ES-PEG L-DXR was fluorescently tagged and immobilized on smooth and HNT-coated microtubes. However, fluorescence microscopy confirmed that ES-PEG L-DXR immobilized within both smooth (Figure 6.4B) and HNT-coated microtubes (Figure 6.4C), compared to control microtubes in the absence of fluorescent ES-PEG L-DXR (Figure 6.4A). Thus, the reduction in neutrophil adhesion could not be caused by prevention of ES-PEG L-DXR adsorption.

Halloysite nanotube-liposome surfaces capture cancer cells and repel neutrophils under flow from a mixture containing both cell types

The use of HNT-liposome coated surfaces for CTC capture from a combined cell suspension was assessed via perfusion of a 1:1 mixture of cancer cells and neutrophils over liposome-coated surfaces. Neutrophils and MCF7 cells were identified based on size; cells 15 μm in diameter or less were identified as neutrophils, while cells greater than 15 μm were identified as MCF7 or COLO 205 cells. Upon perfusion of neutrophils and MCF7 cells, the number of neutrophils captured decreased on HNT-liposome coated surfaces (Figure 6.5B) compared to smooth surfaces (Figure 6.5A). Simultaneously, an increase in MCF7 cell capture was observed on HNT-liposome coated surfaces (Figure 6.5B) compared to smooth surfaces (Figure 6.5A). The number of both MCF7 (Figure 6.5C) and COLO 205 (Figure 6.5D) cells captured was significantly increased on HNT-liposome coated surfaces, with significant reductions in neutrophil capture (Figure 6.5E).

Halloysite nanotube-liposome surfaces specifically induce cancer cell death under flow from a mixture containing both neutrophils and cancer cells

The ability to successfully deliver doxorubicin to cancer cells within a combined cell suspension was assessed by the removal and collection of captured cells from surfaces, separation of cancer cells from neutrophils, and placement into culture for viability tests. Neutrophils, which have a short lifespan *in vivo* and typically undergo cell death *in vitro* within 18-28 hours post-isolation [403], showed negligible differences in viability whether captured within microtubes or placed directly into culture upon isolation. After a 4-day incubation, brightfield microscopy confirmed that MCF7 cells captured on smooth surfaces were adherent and displayed healthy morphology (Figure 6.6A). However, MCF7 cells captured on HNT-liposome coated surfaces were non-adherent and displayed significant membrane blebbing, characteristic of apoptosis (Figure 6.6B). MCF7 cells captured on smooth surfaces exhibited minimal doxorubicin uptake based on fluorescence images (Figure 6.6C), while MCF7 cells captured on HNT-liposome coated surfaces displayed increased doxorubicin uptake (Figure 6.6D). Cell viability assays confirmed doxorubicin-induced cell death, with a significant decrease in MCF7 (Figure 6.6E) and COLO 205 cell viability (Figure 6.6F) when captured on smooth tubes coated with ES-PEG L-DXR, compared to control smooth surfaces coated with ES-PEG EL. However, the number of viable MCF7 and COLO 205 cells captured on HNT-liposome coated surfaces was significantly reduced, compared to the number of viable cells captured on

smooth surfaces. Similar trends were observed previously in KG-1a and COLO 205 cells captured from a solution consisting only of cancer cells [82]. These results demonstrate that a combined surface of HNTs and ES-PEG L-DXR can serve a dual role in: (1) delivering chemotherapeutics to CTCs, and (2) reducing leukocyte adhesion and interaction with chemotherapeutics, and thus reducing toxic side effects on healthy blood cells.

6.4 CONCLUSION

Here, we have demonstrated a technique utilizing cell adhesion molecules to deliver therapeutics to CTCs while actively preventing blood cell adhesion. ES-PEG L-DXR was shown to adhesively interact with MCF7 breast cancer cells and induce cell death. Under physiological flow rates, HNT-liposome coated surfaces significantly increased the number of captured MCF7 and COLO 205 cancer cells, compared to smooth surfaces coated with ES-PEG L-DXR. The opposite trend occurred with healthy blood cells, as perfusion of neutrophils over HNT-liposome coated surfaces significantly reduced the number of captured cells. In a combined solution of cancer cells and neutrophils, HNT-liposome coated surfaces simultaneously increased the number of MCF7 and COLO 205 cells captured, while significantly reducing neutrophil capture to minimal levels. Liposomal doxorubicin was successfully delivered to MCF7 and COLO 205 cells in flow assays with a combined solution of cancer cells and neutrophils. The application of HNT-liposome surfaces can enhance chemotherapeutic delivery to CTCs and reduce the probability of

metastasis. Additionally, the unique ability of such surfaces to prevent normal blood cell interactions can reduce toxic non-specific effects and dramatically reduce chemotherapeutic dosages required for CTC treatment.

FIGURE 6.1: E-SELECTIN TARGETED LIPOSOMES ADHESIVELY BIND AND DELIVER DOXORUBICIN TO MCF7 BREAST CANCER CELLS. (A) Flow cytometry fluorescence histograms of MCF7 cells adhered to fluorescently-tagged (FL) liposomes and fluorescent E-selectin targeted liposomes (FL ES-PEG) after exposure to fluid shear stress in a cone-and-plate viscometer. FITC: Fluorescein isothiocyanate. (B) Confocal microscopy image of FL ES-PEG (green) bound to MCF7 cells after fluid shear stress exposure. Cell nucleus = blue. Scale bar = 10 μm. (C) Number of viable MCF7 cells after treatment with empty liposomes (EL), liposomal doxorubicin (L-DXR) or E-selectin targeted L-DXR (ES-PEG L-DXR) under static conditions for a period of 1-4 days. (D) Dose response of MCF7 cells after treatment with liposomes over a 4 day period. (E-H) Brightfield microscopy images of untreated MCF7 cells (E) and those treated with EL (F), L-DXR (G), and ES-PEG L-DXR (H) after a 4 day period. Scale bars = 100 μm. (I-L) Fluorescence microscopy images of doxorubicin uptake (red) of untreated MCF7 cells (I) and those treated with EL (J), L-DXR (K), and ES-PEG L-DXR (L) after a 4 day period.

FIGURE 6.1: E-SELECTIN TARGETED LIPOSOMES ADHESIVELY BIND AND DELIVER DOXORUBICIN TO MCF7 BREAST CANCER CELLS.

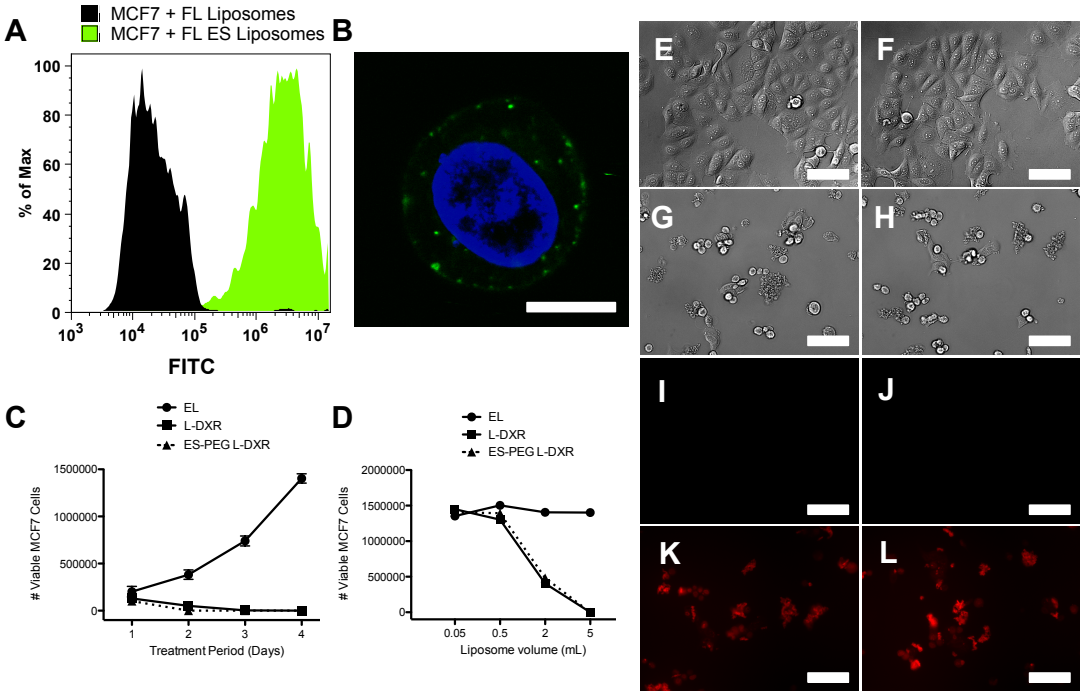

FIGURE 6.2: HNT-LIPOSOME COATED SURFACES ENHANCE MCF7 AND COLO 205 CELL CAPTURE. (A) MCF7 breast cancer cells adhered to a smooth microtube coated with ES-PEG L-DXR. Scale bar = 100 μm. (B) MCF7 cells adhered to an HNT-coated microtube with ES-PEG L-DXR. Scale bar = 100 μm. (C) Number of MCF7 cells adhered to smooth and HNT-coated microtubes per 100,000 μm^2. (D) Number of COLO 205 cells adhered to smooth and HNT-coated microtubes per 100,000 μm^2. * $P < 0.01$. ** $P < 0.001$.

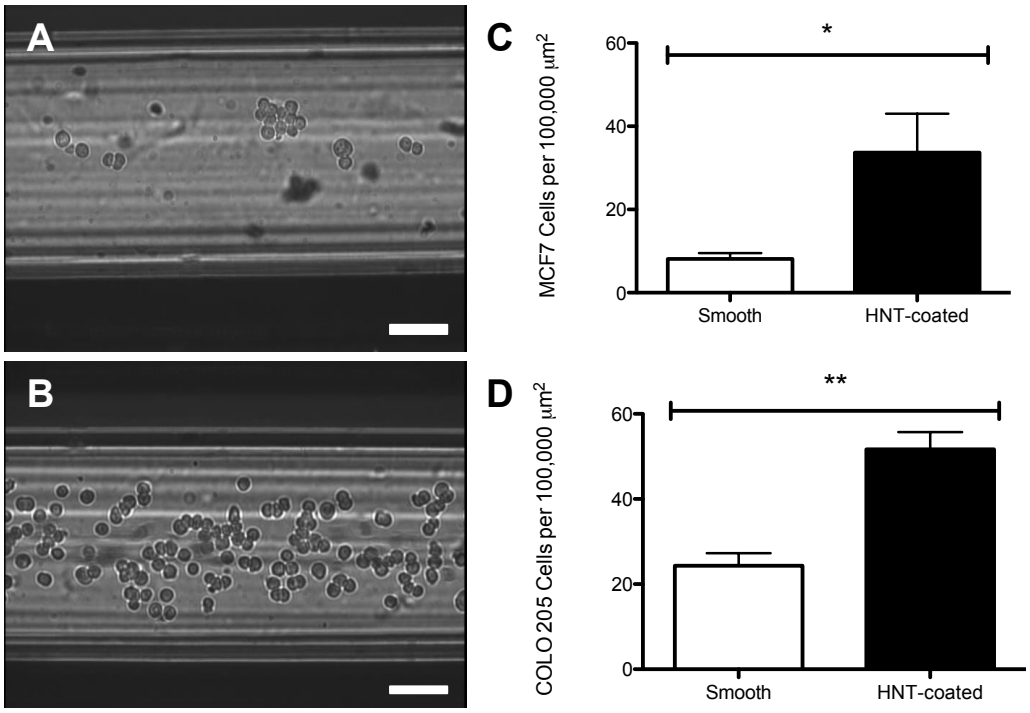

FIGURE 6.3: HNT-LIPOSOME COATED SURFACES REDUCE AND WEAKEN NEUTROPHIL ADHESION. (A) Neutrophils adhered to a smooth microtube coated with ES-PEG L-DXR. Scale bar = 100 μm. (B) Neutrophils adhered to an HNT-coated microtube with ES-PEG L-DXR. Scale bar = 100 μm. Insets show representative cell shapes at higher magnification (approximately 20x20 um). (C) Number of neutrophils adhered to smooth and HNT-coated microtubes per 100,000 μm^2. (D) Shape factor analysis of neutrophils adhered to smooth and HNT-coated microtubes. ** $P < 0.001$.

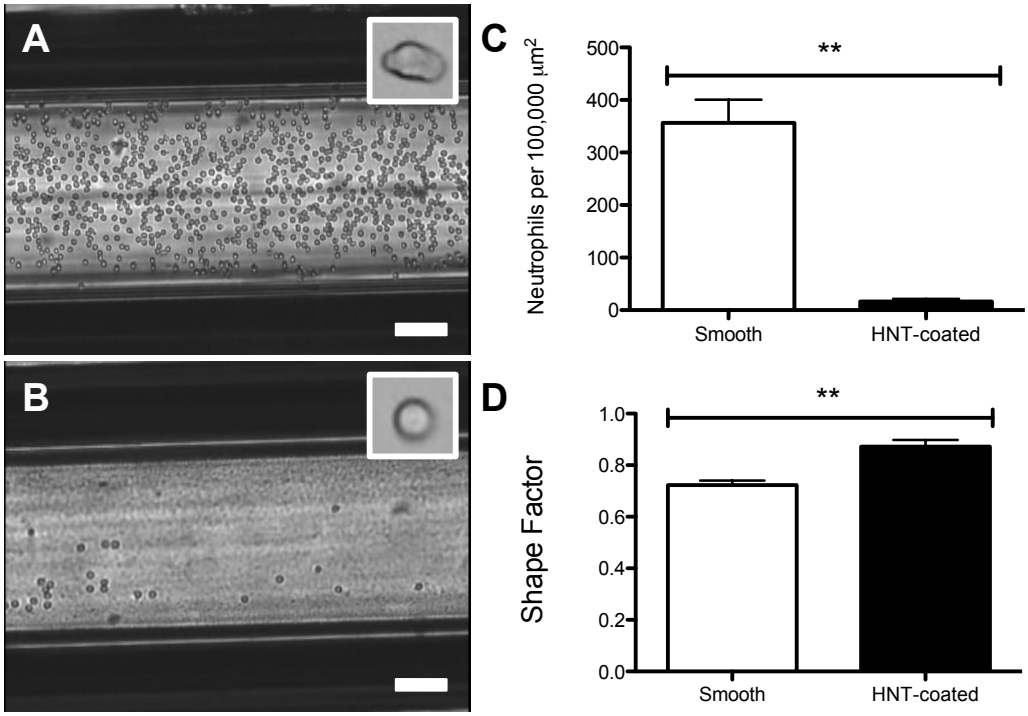

FIGURE 6.4: E-SELECTIN TARGETED LIPOSOMES IMMOBILIZE ON BOTH SMOOTH AND HNT-COATED MICROTUBE SURFACES. (A-C) Fluorescence microscopy images of microtubes coated with BSA (A), smooth microtubes coated with fluorescent ES-PEG L-DXR (B), and HNT-coated microtubes with immobilized fluorescent ES-PEG L-DXR (C). Scale bar = 100 μm.

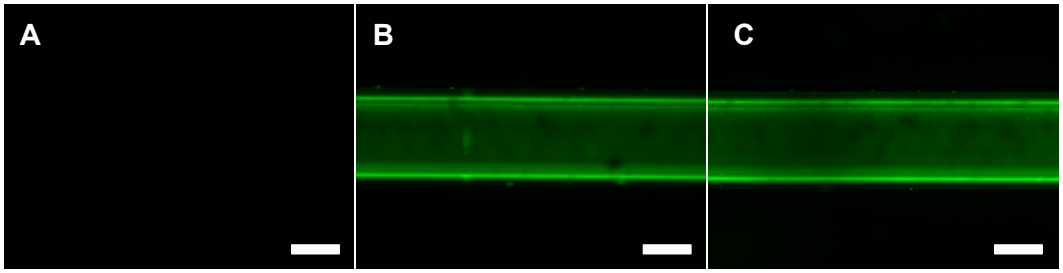

FIGURE 6.5: HNT-LIPOSOME SURFACES SIMULTANEOUSLY ENHANCE MCF7 AND COLO 205 CELL ADHESION AND REDUCE NEUTROPHIL ADHESION FROM A COMBINED SUSPENSION OF CANCER CELLS AND NEUTROPHILS. (A) MCF7 (red arrow) and neutrophils (yellow arrow) adhered to a smooth microtube coated with ES-PEG L-DXR. Scale bar = 100 μm. (B) MCF7 (red arrow) and neutrophils (yellow arrow) adhered to an HNT-coated microtube with immobilized ES-PEG L-DXR. Scale bar = 100 μm. (C) Number of MCF7 cells adhered to smooth and HNT-coated microtubes per 100,000 μm^2. (D) Number of COLO 205 cells adhered to smooth and HNT-coated microtubes per 100,000 μm^2. (E) Number of neutrophils adhered to smooth and HNT-coated microtubes per 100,000 μm^2. * $P < 0.01$.

FIGURE 6.5: HNT-LIPOSOME SURFACES SIMULTANEOUSLY ENHANCE MCF7 AND COLO 205 CELL ADHESION AND REDUCE NEUTROPHIL ADHESION FROM A COMBINED SUSPENSION OF CANCER CELLS AND NEUTROPHILS.

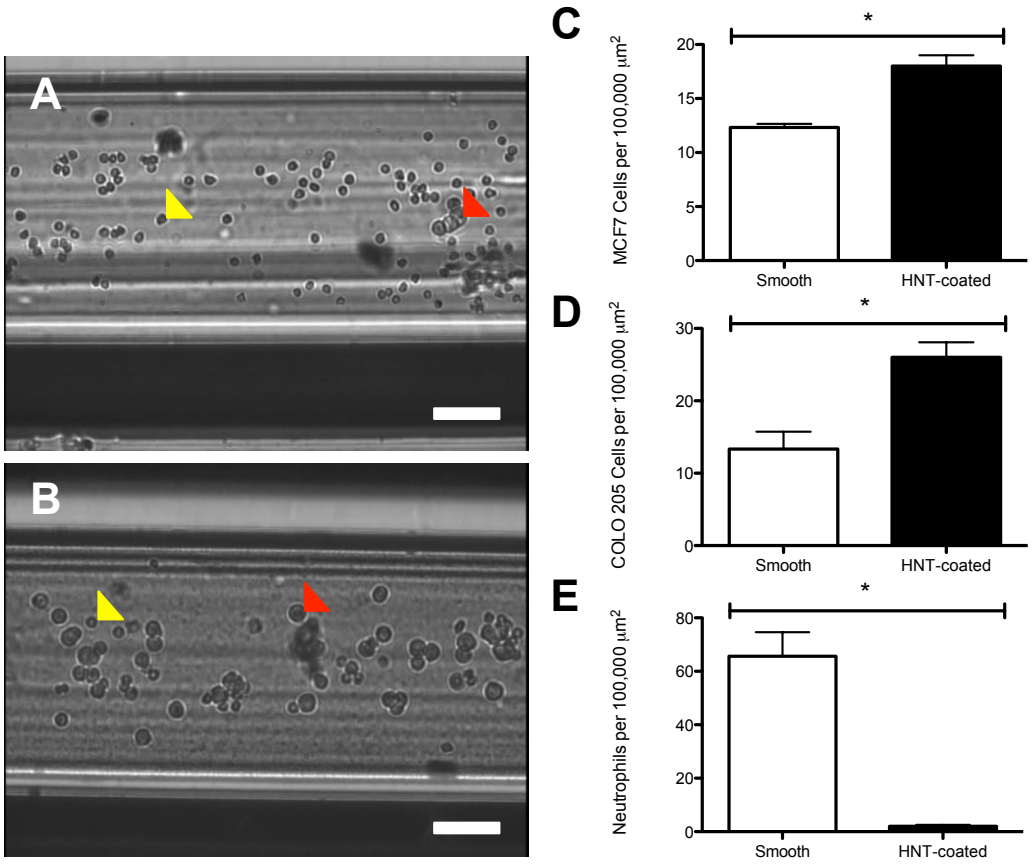

FIGURE 6.6: HNT-LIPOSOME COATED SURFACES SUCCESSFULLY DELIVER DOXORUBICIN TO CANCER CELLS FROM A COMBINED SOLUTION OF CANCER CELLS AND NEUTROPHILS. Brightfield images of MCF7 cells captured on a smooth surface (A) and an HNT-liposome coated surface (B), from a combined solution of cancer cells and neutrophils. Internalization of doxorubicin (red) in MCF7 cells captured on a smooth surface (C) and an HNT-liposome coated surface (D), from a combined solution of cancer cells and neutrophils. All images were taken after a 4-day incubation at 37°C. Scale bar = 100 μm. Number of viable MCF7 (E) and COLO 205 (F) cells after capture on smooth and HNT-liposome coated surfaces. Control samples represent viable cells captured by ES-PEG EL. * $P < 0.01$. ** $P < 0.001$.

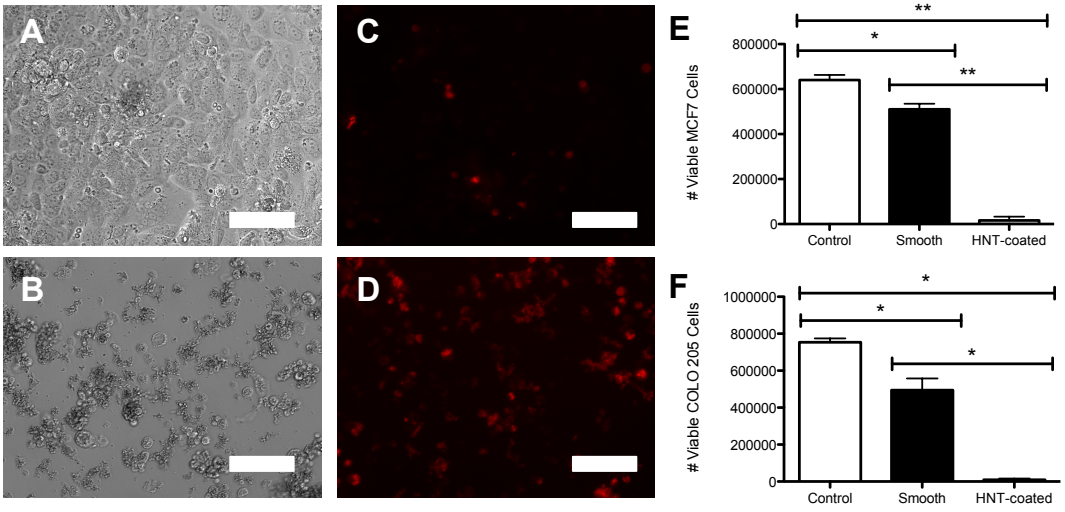

CHAPTER 7: UNNATURAL KILLER CELLS. TRAIL-COATED LEUKOCYTES THAT KILL CANCER CELLS IN THE CIRCULATION

*This section is adapted from the following publication: M.J. Mitchell, E. Wayne, K. Rana, C.B. Schaffer, and M.R. King. *Proceedings of the National Academy of Sciences.* 111(3): 930-935, 2014.

7.1 INTRODUCTION

Over 90% of cancer-related deaths are due to cancer metastasis, the spread of cancer cells from a primary tumor to anatomically distant organs [1]. In many types of cancer, cancer cells from the primary tumor can intravasate into the peripheral circulation as circulating tumor cells (CTCs) [42,404]. These CTCs can then interact with the receptor-bearing endothelial cell wall under flow in other organs, in a manner similar to leukocyte extravasation during inflammation and lymphocyte homing to lymphatic tissues [52]. Recent studies have shown that CTCs from many types of primary tumors express sialylated carbohydrate ligands similar to leukocytes, which mediate interactions with selectins on the endothelium [177,178]. Selectins possess rapid, force-dependent binding kinetics, which can trigger the rolling adhesion of CTCs along the blood vessel wall [49,405]. CTCs can subsequently transition from rolling to firm adhesion, allowing for transendothelial migration into tissues and eventual formation of micrometastases [185]. Surgery and radiation has proven effective at treating primary tumors that do not invade the basement membrane, however the difficulty of detecting distant micrometastases has made the majority of metastatic cancer treatments unsuccessful.

The development of technologies to directly target CTCs *in vivo* holds promise in reducing both the metastatic load and the formation of new tumors. While studies have reported that as many as 1×10^6 cancer cells detach from the primary tumor (per gram) of patients per day [406,407], CTCs are difficult to detect due to their sparse concentrations in the bloodstream, as low as 1-100 cells/mL [42,238]. Additionally,

there are approximately 1 x 10^6 leukocytes or 1 x 10^9 erythrocytes per single CTC in blood [43]. Despite the difference in numbers, both leukocytes and CTCs share similar characteristics in terms of their migration within the bloodstream. Highly deformable erythrocytes experience a drift velocity away from the vessel wall and collect in the center region, displacing less deformable leukocytes and CTCs to the near-wall region in a mechanism termed margination [163]. Such margination phenomena can effectively surround CTCs within the circulating leukocyte population, thus making leukocytes a potentially attractive carrier of treatments to CTCs by exploiting their numerous adhesion receptors.

The utilization of leukocytes to treat CTCs directly within the bloodstream has not previously been explored. Here, I describe a therapeutic approach to target and kill circulating cancer cells in the bloodstream by functionalizing leukocytes with the apoptosis-inducing ligand TRAIL, and the adhesion receptor E-selectin directly within blood under shear flow. The functionalization of leukocytes under flow, effectively creating a form of "unnatural killer cells" within the bloodstream, is shown to be highly effective at treating circulating cancer cells in flowing human blood *in vitro*, and in the peripheral circulation of mice *in vivo*.

7.2 MATERIALS AND METHODS

Reagents and antibodies

Human serum albumin (HSA), bovine serum albumin (BSA), Accutase™, HEPES, DMSO, NaCl, $MgCl_2$, $CaCO_3$ and chloroform (ACS grade with 0.5 – 1% ethanol added as stabilizer) were all obtained from Sigma-Aldrich (St Louis, MO). RPMI 1640 cell culture media, fetal bovine serum (FBS), Hank's balanced salt solution (HBSS), penicillin-streptomycin (PenStrep) and Dulbecco's phosphate buffered saline (DPBS) were all obtained from Invitrogen (Grand Island, NY). His-tagged recombinant human tumor necrosis factor-related apoptosis-inducing ligand (TRAIL), his-tagged recombinant human E-selectin-IgG chimera (ES) and Annexin-V FITC Apoptosis Detection Kit were purchased from R&D Systems (Minneapolis, MN). BCECF AM solution and trypsin-EDTA solution were obtained from Invitrogen (Carlsbad, CA). PBS-based enzyme-free cell dissociation media was purchased from Millipore (Billerica, MA). L-α-lysophosphatidylcholine from egg (Egg PC), sphingomyelin from egg (Egg SM), ovine wool cholesterol (Chol), 1,2-dioleoyl-sn-glycero-3-[(N-(5-amino-1-carboxypentyl) iminodiacetic acid) succinyl] (nickel salt) (DOGS NTA-Ni) and 23-(dipyrromethene boron difluoride)-24-norcholesterol (Bdp-Chol, Ex/Em 490 nm/504 nm) either dissolved in chloroform (Egg PC, Egg SM, Chol, DOGS NTA-Ni) or in powder form (Bdp-Chol) were purchased from Avanti Polar Lipids (Alabaster, AL). Rat anti-human CD62E (E-selectin) antibody was purchased from Abcam (Cambridge, MA). Anti human CD3, CD14, CD16, CD19 and CD56

conjugated with Pacific Blue™, APC Cy7™, PERCP-Cy5.5, APC, and PE respectively along with corresponding isotypes were all purchased from BD Biosciences (San Jose, CA).

Cell lines and cell culture

Colon cancer cell line COLO 205 (ATCC number CCL-222) was obtained from ATCC (Manassas, VA) and cultured in RPMI 1640 supplemented with 2 mM L-Glutamine, 25 mM HEPES, 10% v/v FBS and 100 U/mL PenStrep (complete media) under humidified conditions at 37˚C and 5% CO_2. Prostate cancer cell line PC-3 (ATCC number CRL-1435) was obtained from ATCC and cultured in F-12K medium supplemented with 10% v/v FBS and 100U/mL PenStrep. Human umbilical vein endothelial cells (HUVEC) were purchased from Cascade Biologics (Portland, OR) and maintained in Medium 200 (Cascade Biologics) supplemented with low-serum growth supplement (Cascade Biologics) and 5% fetal bovine serum (Invitrogen). HUVECs were utilized from passages 2-5 for experiments. For all experiments, >95% viability was assessed by trypan blue exclusion dye.

Preparation of liposomes

Multilamellar liposomes, composed of egg L-α-lysophosphatidylcholine (Egg PC), egg sphingomyelin (Egg SM), ovine wool cholesterol (Chol), 1,2-dioleoyl-sn-glycero-3-[(N-(5-amino-1-carboxypentyl) iminodiacetic acid) succinyl] (nickel salt)

(DOGS NTA-Ni) at weight ratios 60-50%:30%:10%:0-10% (Egg PC/Egg SM/Chol/DOGS NTA-Ni), were prepared by thin lipid film method [388]. DOGS-NTA-Ni is a lipid conjugated to nickel-nitrilotriacetic acid (Ni-NTA) that allows for attachment to his-tagged proteins. Briefly, stock solutions of all lipids were prepared by dissolving powdered lipids in chloroform to produce a final concentration of 5 mg/mL Egg PC, 20 mg/mL Egg SM, 5 mg/mL Chol and 20 mg/mL DOGS-NTA-Ni in glass containers and stored at -20°C. Appropriate volumes of the lipids were taken from the stock solution to make lipids with varying concentrations of DOGS NTA-Ni in a glass tube and gently dried under nitrogen. To ensure complete removal of chloroform, the lipids were left under vacuum for an additional 12 h. With increasing amounts of DOGS NTA-Ni, the corresponding amount of Egg PC was decreased (Table 7.1). The lipid film was hydrated with a liposome buffer composed of 150 mM NaCl, 10 mM HEPES and 1 mM $MgCl_2$ dissolved in nuclease-free water to create multilamellar liposomes. The resulting multilamellar liposomes were sized by repeated thawing and freezing, and then subjected to 15 extrusion cycles at 60ºC through two different pore size (200 and 100 nm) polycarbonate membranes (Nucleopore, Whatman, NJ, USA) to produce unilamellar nanoscale liposomes. Recombinant human ES and TRAIL were dissolved in nuclease-free sterile water to a final concentration of 1 mg/mL and 100 µg/mL. Aliquots of stock solutions were stored at –20 ºC and used as needed within 60 days. Freshly prepared nanoscale liposomes were then incubated with ES (final concentration 71.43 nM) and TRAIL (250 nM final concentration) for 30 min at 37ºC and then overnight at 4ºC, to ensure maximum protein binding via the interaction between his-tag and Ni-NTA. Based on

approximations for ligand density on liposomes suggested in previous work by Huang and Mason [408], there were approximately 65 TRAIL and 19 E-selectin proteins present on the surface of each liposome, assuming a unilamellar liposome diameter of 100 nm. To remove unbound TRAIL and ES, liposomes were diluted 1:6 with liposome buffer and subjected to ultracentrifugation at 100000g for 3 h at 4ºC. The supernatant with unbound TRAIL and ES was carefully removed and collected for further evaluation, and the remaining liposomes were gently resuspended in buffer. A similar procedure was used to create fluorescent conjugated liposomes by replacing ovine wool cholesterol with 23-(dipyrromethene boron difluoride)-24-norcholesterol. Freshly prepared nanoscale liposomes were diluted in buffer, and the mean particle diameter and surface charge (zeta potential) were measured by dynamic light scattering using a Malvern Zetasizer nano ZS (Malvern Instruments Ltd., Worcestershire, UK), according to the manufacturer's protocols. Conjugated liposomes were measured to be 117.8 ± 10.3 nm in diameter, with a zeta potential of -5.7 ± 4.6 mV.

Static experiments

COLO 205 cells were seeded in multiwell plates at a seeding density of 300,000 cells/mL, 1 day prior to experimentation to ensure that the cells were in the linear phase of the growth cycle. Media was changed prior to experimentation. Cells were incubated with either the supernatant from ultracentrifugation or 10 µL of conjugated and purified liposomes. The cells were maintained in culture conditions

with the supernatant or nanoscale lipids for 24 h and later analyzed by an Annexin-V assay to quantify the proportion of viable cells.

Uniform shear flow experiments

To simulate the shear stress conditions of blood flow, cancer cells were subjected to uniform shear in a cone-and-plate viscometer [86,91]. Cancer cells seeded one day prior to the experiment were gently detached from the surface using PBS-based enzyme-free cell detachment solution or accutase. Cells were then washed twice in 1X DPBS and resuspended in buffer at a concentration of 1 x 10^6 cells/mL. 10 μL of lipids was added to 490 μL of cell suspension (at 10^6 cells/mL) and immediately added to the cone-and-plate viscometer. Shear rate was set to 188 s^{-1} for 2 h. All samples were exposed to shear flow at RT, to prevent potential sample evaporation and/or drying in the cone-and-plate viscometer over prolonged periods of shear. After 2 h, the cells were removed and washed twice in resuspension buffer at 200g for 5 min. Cells were resuspended in complete media and cultured for 24 h. In the case of fluorescent lipids, an aliquot was taken for visual inspection on an inverted microscope (Olympus America Inc, Melville, NY) equipped with fluorescence and an intensified CCD digital camera (Cooke Corporation, Romulus, MI) to record images. For spiking experiments, peripheral blood was collected into Vacutainer tubes containing heparin and allowed to equilibrate to RT before use. 1 x 10^6 COLO 205 or PC-3 cells were tagged fluorescently with 3 μM BCECF AM solution for 15 min at 37°C, washed twice and collected via centrifugation at 200g for 5 min. The

supernatant was discarded, and the collected cells were resuspended in 1 mL of whole blood. 10 μL of lipid was then added to 490 μL of spiked blood and immediately added to a cone-and-plate viscometer previously coated with 5% BSA. Spiked blood was subjected to a uniform shear rate of 188 s^{-1} for 2 h. As an additional comparison for spiking experiments, identical experiments were performed in buffer instead of whole blood. In leukocyte functionalization experiments, 10 μL of lipid was added to 490 μL human blood, sheared in a cone-and-plate viscometer at a uniform shear rate of 188 s^{-1} for 2 h, and subsequently centrifuged to remove the plasma containing unbound liposomes. The removed plasma was replaced with freshly isolated plasma, and the blood samples were used for identical spiking experiments mentioned above. After shearing, the blood sample was collected from the device and carefully layered over 1.5 mL of Ficoll and centrifuged at 480g for 50 min at RT. The buffy coat containing MNCs and cancer cells was recovered and washed twice in resuspension buffer, collected, cultured for 24 h, and analyzed for viable fluorescent cancer cells using flow cytometry. To evaluate the effect of hematocrit, the number of RBCs was varied by removal via centrifugation. Volumes of RBCs were replaced with excess plasma from the same blood donor. Cancer cells were spiked into blood samples as mentioned earlier, at a concentration of 1 x 10^6 cells/mL. 10 μL of liposome solution was added to 490 μL of blood and sheared for 2 h at 188 s^{-1}. Samples were collected, incubated, and analyzed for viability on a flow cytometer as described above. In some experiments, 490 μL of whole blood was sheared with 10 μL of liposome solution, and the plasma and any remaining unbound liposomes and/or liposome fragments were separated by centrifugation. To determine the effects of remaining unbound liposomes

and/or liposome fragments on cancer cell viability, the recovered plasma was incubated with 500,000 COLO 205 cells for 24 h at 37°C and analyzed for cell viability using flow cytometry.

Polymorphonuclear (PMN) and mononuclear cell (MNC) isolation

All human subject protocols were approved by the Institutional Review Board for Human Participants of Cornell University. Peripheral blood was collected from healthy, willing donors after informed consent into Vacutainer tubes containing heparin and allowed to equilibrate at room temperature (RT) before use [91,390]. 3 mL of blood diluted with resuspension buffer was carefully layered over 3 mL of 1-Step™ Polymorphs (Accurate Chemical & Scientific Corporation, Westbury, NY) and centrifuged at 480g for 50 min at RT. Two separate layers of MNCs and PMNs were collected and washed twice with resuspension buffer.

Leukocyte functionalization with ES/TRAIL liposomes in whole blood

To assess the adhesion of ES/TRAIL liposomes to leukocytes in whole blood under flow, 490 μL of whole blood was sheared with 10 μL of fluorescent ES/TRAIL liposome solution for 30 min in a cone-and-plate viscometer at a shear rate of 188 s^{-1}. Leukocytes were then separated using 1-Step™ Polymorphs and assessed for adherent ES/TRAIL liposomes using confocal microscopy. To assess the fraction of leukocyte subpopulations that adhere to ES/TRAIL liposomes, leukocytes were labeled with

anti-human CD3, CD14, CD16, CD19 and CD56, along with corresponding isotype controls, and analyzed for adherent ES/TRAIL liposomes using flow cytometry. To assess the specificity of the ES interaction with leukocytes, liposomes were incubated with a functional blocking anti-human E-selectin antibody prior to shearing in whole blood. To assess the fraction of leukocytes in blood adhered to ES/TRAIL liposomes before shear, fluorescent ES/TRAIL liposomes were added to whole blood and then separated using 1-Step™ Polymorphs.

Endothelial cell viability assay

40 mm diameter circular glass coverslips (Thermo Scientific, Waltham, MA) were plasma treated (Harrick Plasma Cleaner, Ossining, NY) for 2 min and subsequently incubated in 1% polyethylenemine (PEI) at room temperature for 10 min. Coverslips were then washed in water 3 times and treated with 0.1% glutaraldehyde (Sigma-Aldrich, St. Louis, MO) in PBS at room temperature for 30 min. Coverslips were washed in water 3 times, dried, and treated with 0.1 mg/mL of type I rat-tail collagen (Becton Dickinson, Franklin Lakes, NJ) in HEPES (pH 8.0, Sigma-Aldrich, St. Louis, MO) for 2 h at 4°C. Coverslips were placed in petri dishes (60 mm x 15 mm; Sigma-Aldrich), washed 3 times in PBS, and briefly sterilized via UV exposure for 15 min. HUVECs were plated on coverslips, at a density of 500,000 cells per coverslip, in Medium 200 supplemented with low-serum growth supplement (Cascade Biologics), 5% fetal bovine serum (Invitrogen), and 100U/mL PenStrep. HUVECs were cultured for 4 days on coverslips prior to experiments, and then

adhered to the plate of a cone-and-plate viscometer using vacuum grease. HUVECs were then treated with 2.94 mL of human blood and 60 μL of PBS, ES/TRAIL (TRAIL final concentration: 0.3 μg/mL), or soluble TRAIL in PBS (TRAIL final concentration: 0.3 μg/mL) for 4 h at 37°C in a humidified cone-and-plate viscometer at a shear rate of 188 s^{-1}. As a positive control, HUVECs were treated with a high concentration of soluble TRAIL (15 μg/mL). Coverslips were removed from the viscometer, gently washed in PBS, and placed in Medium 200 supplemented with low-serum growth supplement, 5% fetal bovine serum (Invitrogen), and 100U/mL PenStrep. HUVEC morphology was assessed using brightfield and phase contrast microscopy. HUVECs were immediately placed into culture for 8 h, maintained at 37°C and 5% CO_2. HUVECs were then treated with 0.25% Trypsin-EDTA solution (Gibco) for 2 min at 37°C, followed by treatment with an equal volume of trypsin neutralizer solution (Gibco). HUVECs were collected from coverslips, washed twice in PBS, and assessed for viability using an Annexin-V assay.

Liposome and COLO 205 cell injection in mice

C57BL/6J mice aged 16-20 weeks (both sexes), weighing 25-32 g, were obtained from The Jackson Laboratory. Mice were anesthetized using isoflurane (5%) for all procedures. Either 120 μL of saline, sTRAIL (15 μg/mL; TRAIL plasma concentration ~ 1.0 μg/mL), ES/TRAIL (TRAIL injection concentration: 15 μg/mL; TRAIL plasma concentration ~ 1.0 μg/mL) liposomes or ES liposomes suspended in saline were injected retro-orbitally using a 30-G needle and animals were removed

from anesthesia. Three mice were used in each group. Thirty minutes later, animals were re-anesthetized and ~$2x10^6$ COLO 205 cells, labeled by 2 μg/mL Hoescht (#H1399, Invitrogen) or 3 μM BCECF AM suspended in saline were injected into the tail vein. Animals were removed from anesthesia and the cancer cells were allowed to circulate for 2 h. All animal procedures were approved by the Cornell University Institutional Animal Care and Use Committee.

Analysis of circulating COLO 205 cancer cells

Animals were euthanized with a lethal dose of pentobarbital. Blood was removed from the heart via cardiac puncture and collected into sodium heparin-coated tubes. Leukocytes and circulating COLO 205 cells were separated using Ficoll-Paque PLUS™. After centrifugation, the MNC buffy coat was collected, washed in buffer containing Ca^{2+} and cultured for 2-3 h in multiwell plates. Cell viability was assessed using flow cytometry.

Two-photon imaging of lung tissue

Animals were anesthetized and received injections of saline, sTRAIL, ES/TRAIL liposomes or ES liposomes, followed by an injection of Hoescht-labeled cancer cells, as described above. After two hours of cancer cell circulation, an Alexa Fluor 568 labeled Annexin-V probe (#A13202, Invitrogen) was injected retro-orbitally and allowed to circulate for 2 h to ensure maximum detection of apoptotic cells.

Animals were then given a lethal dose of pentobarbital. After euthanasia, intact lungs were resected and immediately imaged via two-photon excited fluorescence microscopy. Two-photon imaging was conducted on a locally-designed microscope using a train of 800-nm, 87-MHz, 100-fs pulses from a Ti:sapphire laser oscillator (MIRA HP, pumped by a Verdi-V18, Coherent) for excitation. Laser scanning and data acquisition were controlled by ScanImage software. For high-resolution imaging of COLO 205 Hoechst-labeled nuclei and Annexin V labeling a 20X (numerical aperture: 0.95) water-immersion objective (Olympus) was used. Fluorescence was detected using emission filters with 460-nm and 645-nm center wavelength with 65-nm bandwidth to image Hoescht and Alexa Fluor 568 (Invitrogen), respectively. Spectrally-broad autofluorescence from the lung tissue was visible in both channels.

Counting and viability scoring of COLO 205 cells in lung

Hoechst-labeled COLO 205 cells were manually counted from ~10 representative two-photon image stacks taken from the lung in each mouse using Image J (NIH) cell counting software. The Hoechst signal was of similar magnitude to the background lung autofluorescence in the 460-nm channel. To aid in identifying nuclei, the Hoechst channel was compared with the 645-nm channel, where autofluorescence was also visible, but Hoescht was not and Alexa Fluor 568 signal was significantly brighter than autofluorescence. In addition, attributes such as size and shape to distinguish the labeled COLO 205 cells were used. Each imaged volume was about 0.022 mm^3. The total number of cells in the lung was estimated by scaling

the imaged volumes to the total lung volume, which was measured via a volume displacement method. Counts were recorded by two different observers, each blinded to the treatment received, and averaged. To determine which COLO 205 cells were apoptotic, we determined whether Alexa Fluor 568 Annexin V labeling was present at each of the COLO 205 cell nuclei we identified.

Flow cytometry

Mode of cell death was analyzed using an Annexin-V apoptosis assay on an Accuri C6 flow cytometer. Samples were prepared for as per the manufacturer's instructions. Briefly, cells were classified into four categories based on dye uptake: viable cells (negative for Annexin-V and propidium iodide (PI)), early apoptotic cells (positive for Annexin-V only), late apoptotic cells (positive for Annexin-V and PI) and necrotic cells (positive for PI only). For blood spiking experiments, fluorescent untreated cancer cells and liposome treated samples were assessed for viability using a flow cytometer. A gate was set based on a viable, untreated cancer cell control. Equal volumes from all samples were used for analysis. Cell viability was determined by measuring the amount of cells positive for fluorescent BCECF staining. For *in vivo* animal experiments, 100 μL of each sample was processed. A gate denoting viable, BCECF AM-labeled cancer cells was established by processing a viable, fluorescent sample of COLO 205 cells in buffer. COLO 205 cells recovered from mouse blood were differentiated based on size and fluorescence using flow cytometry. The number

of cancer cells per milliliter of mouse blood was determined based on the amount of mouse blood recovered from each animal.

Statistical analysis

Where appropriate, student's t-test and one-way ANOVA with Tukey post test comparing all means were employed at a significance level of $\alpha = 0.05$. All statistical analyses were performed using GraphPad Prism 5.0c for Mac OS X GraphPad software (San Diego, CA USA) and Kaleidagraph (Synergy) software.

7.3 RESULTS

ES/TRAIL liposomes adhesively interact and induce apoptotic cancer cell death under shear flow

Many types of circulating tumor cells (CTC), and cancer cell lines derived from colon, breast, prostate, and pancreas are known to display glycosylated ligands that allow them to adhesively interact with E-selectin (ES) under physiological shear flow [50]. This has been proposed to explain why some cancers home to tissue specific capillary beds such as the bone marrow and liver [48,53]. In an attempt to target and kill cancer cells of this form, nanoscale liposomes conjugated with a mixture of recombinant human E-selectin (ES) protein and tumor necrosis factor (TNF)-related apoptosis inducing ligand were developed (TRAIL; Figures 7.1A, 7.2

and Table 7.1). TRAIL binds to death receptors 4 and 5 on the surface of cancer cells to induce apoptosis through the intrinsic and extrinsic pathways [232,233]. ES/TRAIL liposomes consisting of a 10% weight ratio of DOGS-Ni-NTA, utilized to conjugate ES and TRAIL to the liposome surface, were found to be most effective at inducing apoptotic cell death in a colorectal adenocarcinoma (COLO 205) cell line under static conditions (Figure 7.3), as determined using an Annexin-V apoptosis assay.

In the post-capillary venules where selectin-mediated adhesion and cell extravasation into tissues typically occur, moderate shear rates can initiate flowing cell interactions with the endothelial cell wall [159,274]. To recreate these physical forces *in vitro*, a cone-and-plate shear assay was developed to probe the interactions of cancer cells and ES/TRAIL liposomes under venular shear rates. After exposure to shear flow (shear rate: 188 s^{-1}) for 2 h, COLO 205 cells exposed to ES liposomes displayed their normal morphology, while substantial membrane blebbing was observed in those exposed to ES/TRAIL liposomes, characteristic of cells undergoing apoptosis (Figure 7.1B). Annexin-V assay revealed that exposure to shear flow for 2 h induced minimal COLO 205 cell apoptosis in untreated controls (Figure 7.1C), in addition to treatment with liposomes in the absence of conjugated protein (Figure 7.1D) or conjugated solely with ES (Figure 7.1E) or TRAIL (Figure 7.1F). However, a combination of ES/TRAIL conjugated to the liposome surface induced a significant decrease in COLO 205 viability following exposure to shear flow (Figure 7.1G, H).

To investigate the adhesive characteristics of ES/TRAIL liposomes to cancer cells under flow, COLO 205 cells were exposed to ES/TRAIL liposomes consisting of fluorescent cholesterol and exposed to shear flow as in previous *in vitro* shear assays.

Flow cytometry revealed that >99.9% of the COLO 205 cell population was adhered to ES/TRAIL liposomes after exposure to shear flow (Figure 7.4A,B). Fluorescent micrographs and brightfield overlay images clearly displayed ES/TRAIL liposomes adhered to the surface of COLO 205 cells (Figure 7.4C,D). These data suggest that the presence of the ES adhesion receptor enhances the effect of TRAIL by promoting tighter contacts with the cancer cell membrane.

ES/TRAIL liposomes functionalize leukocytes in whole blood under shear flow in vitro

In addition to CTCs, circulating leukocytes also possess ligands for E-selectin, which are necessary in the inflammatory response and lymphocyte homing to lymphatic tissues [1,176]. To assess the potential to functionalize leukocytes with ES/TRAIL to target and kill CTC, we treated whole human blood with fluorescent ES/TRAIL liposomes under shear flow in a cone-and-plate viscometer. Upon exposure to shear (shear rate: 188 s^{-1}), ES/TRAIL liposomes readily bind to leukocytes via selectin ligands on the leukocyte surface (Figure 7.5A).

To quantify leukocyte subpopulations that adhere to ES/TRAIL liposomes under flow, leukocytes were separated from whole blood and analyzed for both leukocyte marker expression and adherent ES/TRAIL liposomes using flow cytometry. Functionalized leukocytes were labeled with CD3, CD14, CD16, CD19, and CD56 antibodies, as such markers are commonly expressed on most T-lymphocytes, monocytes, neutrophils, B-lymphocytes, and natural killer (NK) cells, respectively [409]. Minimal adhesion of ES/TRAIL liposomes to leukocytes in blood

was observed in the presence of a functional blocking ES antibody (Figure 7.5B-G). Minimal ES/TRAIL liposome adhesion was also observed immediately after treatment with whole blood. However, after exposure to shear flow, flow cytometry analysis revealed that leukocyte subpopulations positive for CD3 (Figure 7.5B), CD14 (Figure 7.5C), CD16 (Figure 7.5D), CD19 (Figure 7.5E), and CD56 (Figure 7.5F) adhered to ES/TRAIL liposomes to varying degrees (Figure 7.5G). Adhesion was also observed on populations of lymphocytes, which suggests that some cytotoxic patrolling of the lymphatic system may also occur *in vivo*. Leukocyte subpopulations can vary in their E-selectin ligand expression [410] and thus could explain the variations in the number of bound ES/TRAIL liposomes.

ES/TRAIL functionalization does not induce significant leukocyte or endothelial cell death

To assess the effects of ES/TRAIL functionalization on leukocyte viability, mononuclear leukocytes isolated from human blood were treated with ES/TRAIL liposomes under both static and shear flow conditions. Annexin-V assays revealed no significant differences in leukocyte viability when leukocytes were incubated with ES (Figure 7.6B) or ES/TRAIL (Figure 7.6C) liposomes under static conditions for 24 h, compared to untreated leukocyte controls (Figure 7.6A,D). Upon functionalization with liposomes under shear flow for 2 h (shear rate: 188 s^{-1}), no significant decreases were found in ES (Figure 7.6F) or ES/TRAIL (Figure 7.6G) functionalized leukocytes, compared to untreated leukocyte controls (Figure 7.6E,H). Our data suggest that

ES/TRAIL liposomes can functionalize leukocytes under flow to target and kill cancer cells, while exerting negligible cytotoxic effects on leukocytes. It is important to note that individual subpopulations of leukocytes have shown apoptotic effects in the presence of TRAIL [411], however this study focused on the overall effects of ES/TRAIL liposomes on bloodborne leukocytes.

To assess the effects of ES/TRAIL functionalization on endothelial cell viability, human umbilical vein endothelial cells (HUVEC) were treated with ES/TRAIL liposomes in human blood under shear flow conditions *in vitro*. Treatment with ES/TRAIL liposomes or an equivalent concentration of soluble TRAIL in human blood under shear flow for 4 h induced no significant differences in HUVEC viability, compared to untreated HUVEC exposed to shear in human blood (Figure 7.7). Our data suggest that ES/TRAIL-functionalized leukocytes exert negligible toxic effects on human endothelial cells under blood flow conditions.

Apoptotic effects of ES/TRAIL therapy are enhanced in human blood under flow

Clinically, CTCs are sparsely distributed in the complex milieu of whole blood, at concentrations as low as 1-100 cells/mL [42,238]. To examine whether ES/TRAIL liposomes would effectively target cancer cells in the presence of blood cells and serum under flow conditions, we fluorescently labeled colorectal COLO 205 and prostate PC-3 cancer cell lines and spiked them into human peripheral blood. Surprisingly, under identical shear flow conditions ES/TRAIL therapy was even *more* effective at killing cancer cells in the presence of human blood (Figure 7.8A–D),

compared to shearing COLO 205 or PC-3 cells alone in buffer (Figure 7.8E), with <5% of the fluorescent, viable cancer cell populations remaining after ES/TRAIL treatment (Figure 7.8E). These results suggest that ES/TRAIL therapy is effective at targeting circulating cancer cells derived from multiple organs in human blood.

To evaluate the impact of blood cells on the efficacy of ES/TRAIL treatment, fluorescent COLO 205 and PC-3 cells were spiked in human blood of varying hematocrit percentages. All additional blood cell components were maintained, while the volume of removed erythrocytes was replaced with plasma from the same blood donor. Interestingly, the apoptotic effects were hematocrit-dependent, as higher hematocrit significantly decreased the number of viable COLO 205 and PC-3 cells after ES/TRAIL treatment (Figure 7.8F). The enhanced apoptotic effect suggests that blood cell collisions under flow can promote the apoptotic effects of ES/TRAIL liposomes and agrees with our intuitive understanding of blood rheology, as the presence of erythrocytes is known to create erratic cell paths with frequent cross-streamline displacements [412] and increase the lifetime of colliding doublets to promote aggregate formation [413].

To assess the mechanism by which leukocytes act as a pervading carrier surface for functional TRAIL, blood was pretreated with ES/TRAIL liposomes under shear flow, with blood cells subsequently separated from unbound ES/TRAIL via centrifugation and replaced with fresh blood plasma. ES/TRAIL therapeutic effects under shear flow remained nearly identical, as COLO 205 and PC-3 cells spiked into a suspension of blood with washed, pretreated blood cells were killed at roughly the same rate as unwashed blood (Figure 7.9A-C). Thus, upon addition of the ES/TRAIL

liposomes to cancer cell-spiked blood, liposomes attach to the surface of leukocytes, and are available for inducing apoptosis in cancer cells that they come into contact with (Figure 7.9D,E). As an indicator of unbound ES/TRAIL liposomes and/or liposome fragments remaining in human blood after shearing pretreatment, the toxicity of supernatant collected from pretreated blood was tested in COLO 205 culture. An Annexin-V assay showed minimal COLO 205 cell death after treatment with a supernatant of human plasma and unbound ES/TRAIL, compared to cells treated with plasma supernatant alone (Figure 7.10). These data suggest that ES/TRAIL liposomes readily bind to the surface of leukocytes, with minimal unbound liposomes remaining, to target and kill cancer cells under flow.

ES/TRAIL functionalized leukocytes reduce number of viable cancer cells in mouse circulation in vivo

To assess and compare the cytotoxic effects *in vivo* to our previous results *in vitro*, ES/TRAIL liposomes were also tested for their ability to kill cancer cells flowing in the peripheral circulation of mice. Two million fluorescently labeled COLO 205 cells were injected into the tail vein of immunocompetent C57BL/6J mice, 30 min after injection of 120 μL of either ES/TRAIL liposomes, ES liposomes, or soluble TRAIL (Figure 7.11A). Tail vein injection was utilized to model leukocyte/CTC interactions in mouse circulation, as this technique has been an accepted and widely used model of lung metastasis [239-242] since the pioneering work of Fidler et al. [243-245]. For these studies, the use of recombinant human E-selectin was continued

because of its ability to bind both human COLO 205 cancer cells and mouse neutrophils, which were previously shown to have cross reactivity and roll on E-selectin [414]. Mice were sacrificed 2.5 h after the initial injection, and cancer cells were recovered from the circulation via cardiac puncture. Cancer cells were placed back into culture for 2-3 h before the number of viable cells were quantified.

Using flow cytometry, we measured ~130,000 cancer cells/mL blood for mice injected with control ES liposomes, compared to <2,000 cancer cells/mL blood surviving from ES/TRAIL treated mice (Figure 7.11B,C). Mice injected with buffer or soluble TRAIL had intermediate numbers of cells (Figure 7.11C) compared to ES and ES/TRAIL-treated samples, likely indicating that ES functionalized liposomes help to retain cancer cells in the circulation by blocking selectin-mediated interaction of the COLO 205 cells with the endothelium. Brightfield micrographs of COLO 205 cells exposed to buffer and soluble TRAIL showed characteristic cancer cell morphology (Figure 7.11D). Micrographs of COLO 205 cells exposed to ES revealed adherent leukocytes on the COLO 205 cell surface without significant morphological change, while, whereas the cancer cells from ES/TRAIL-treated mice showed notable membrane blebbing of COLO 205 cells in the proximity of leukocytes (Figure 7.11D). To assess the adhesion of ES/TRAIL liposomes to leukocytes in mouse circulation, mice were injected with ES/TRAIL liposomes tagged with fluorescent cholesterol, and were allowed to circulate for 2.5 h. Brightfield overlay micrographs showed that leukocytes recovered from the mouse circulation were functionalized with ES/TRAIL liposomes (Figure 7.11E), suggesting that ES/TRAIL remains functionalized to leukocytes, which can exert cytotoxic effects onto cancer cells in mouse circulation.

ES/TRAIL treatment reduces number and increases apoptosis of remaining circulating COLO 205 cells lodged in vivo in mouse lung

Previous studies have shown that more than 90% of tumor cells that enter the vasculature via tail vein injection lodge into lung vasculature within the first two hours [415]. To assess the viability of the remaining circulating cancer cells lodged within mice, fluorescent COLO 205 cells lodged within the lungs of mice were identified using two-photon excited fluorescence microscopy (Figure 7.12A,B). Immediately following euthanasia, the lungs were resected, and two-photon images were acquired in three regions of the lung that were identical for each animal, to obtain an accurate estimate of cell counts (Figure 7.12A). Roughly twice as many cells were found in the ES, sTRAIL, and buffer treated animals as the ES/TRAIL treated animals (Figure 7.12C), suggesting many COLO 205 cells had already died and degenerated. The cancer cell density found in lung suggests about 1.4 million cancer cells were lodged in the lung for buffer treated animals (assuming a lung volume of ~0.4 mL), representing the bulk of the two million COLO 205 cells injected.

We then evaluated the apoptotic effects of ES/TRAIL liposomes on cancer cells that have already lodged into the lungs of mice. After the injections of liposomes and COLO 205 at previously used time points (Figure 7.12A), we injected a solution of Annexin-V tagged with a fluorescent Alexa 594 dye to assess for phosphatidylserine flipping on the COLO 205 cell membrane, characteristic of apoptosis. Mouse lungs were imaged using two-photon microscopy to determine

whether Hoescht-labeled COLO 205 cells were also positive for Annexin-V labeling. In addition to the decreased density of cancer cells lodged in mouse lung (Figure 7.12C), we also found a dramatic increase in apoptosis of the cancer cells (Figure 7.12B,D) in the ES/TRAIL liposome treated mice as compared with other groups. Soluble TRAIL protein injected into mice following the same protocol displayed minimal cytotoxic activity comparable to control, as expected due to its short circulation half-life [416]. Mice injected with ES/TRAIL liposomes survived for over two weeks with no loss in body weight (n = 3). These data suggests that ES/TRAIL treatment serves to decrease the number of remaining circulating COLO 205 cells lodged in mouse lung, while increasing the fraction of them that are apoptotic.

7.4 DISCUSSION

Natural killer cells, activated by interleukin-2 or other factors, are induced to present TRAIL protein on their surface. These cells participate in immunosurveillance against micrometastases in the body, and comprise 10-20% of peripheral blood mononuclear cells [417,418]. While the liposome-coated leukocytes described here are not specifically programmed to actively invade tissues and seek out solid tumors, they do have frequent opportunities for incidental contact with CTCs in the bloodstream. Interestingly, infiltration of neutrophils and macrophages throughout the interior of solid tumor masses has been found in dynamic, self-seeding tumors, suggesting that some degree of homing of normally-functioning leukocytes to solid tumors could be expected [419,420]. I find that TRAIL is most potent when in its natural state –

tethered to the surface of leukocytes in shear flow – rather than freely soluble or on untethered liposomes in the absence of blood. Tethering nanoscale liposomes to the surface of peripheral blood leukocytes is also beneficial for increasing liposome circulation time, by avoiding renal clearance mechanisms.

So why do leukocytes coated with ES/TRAIL liposomes have much higher cytotoxic activity in shear flow, compared to isolated ES/TRAIL liposomes or soluble TRAIL protein? The answer may lie in the compressive force between surfaces. Two spherical particles colliding in linear shear flow will experience a compressive force between them which scales as $F_c \sim \mu*G*a*b$, where μ is the fluid viscosity, G is the shear rate, and a and b are the radii of the smaller and larger sphere, respectively [421]. Thus, a 10 μm diameter leukocyte colliding with a cancer cell will experience 100 times the compressive force of a 100 nm liposome colliding with a cancer cell. Compressive forces act to flatten down any cell surface glycocalyx composed of biologically inert macromolecules, thus allowing TRAIL to come within a reactive distance to the cancer cell death receptors and form bonds. The physics of force-induced flattening and penetration of cell glycocalyx to facilitate surface receptor binding to ligands on an opposing cell surface has been analyzed in the context of leukocyte adhesion to the vascular endothelium [422,423].

Recombinant human TRAIL/Apo2L, also known as PRO1762 developed by Amgen/Genentech, has been the subject of numerous Phase 1, 1a, 2, and 3 clinical trials over the past decade, with minimal adverse effects reported [247,248]. There are many intracellular proteins, such the inhibitors of apoptosis protein (IAPs) family members that also confer TRAIL resistance to normal cells [236]. Additionally, the

dosages of TRAIL used in this current study ranged from 0.06 – 0.08 mg/kg, two orders of magnitude lower than the clinical dosages of 1 – 30 mg/kg used in human clinical trials. While different types of cancer cells show different levels of sensitivity to TRAIL-induced apoptosis, it has been well documented that there is a wide range of agents known to sensitize cancer cells to TRAIL-mediated apoptosis, including conventional chemotherapeutics (camptothecin, cisplatin, doxorubicin, 5-fluorouracil, irinotecan, paclitaxel, gemcitabine), proteasome inhibitors, Bcl-2 inhibitors, IAP antagonists, HDAC inhibitors, CD20 antibodies, irradiation, synthetic triterpenolds, Sorafenib, aspirin, and natural products such as curcumin and piperlongumine [232].

What remains to be seen is whether ES/TRAIL liposomes can successfully prevent the formation of metastatic tumors; future work should focus on addressing this question. Additionally, human hepatocytes have shown sensitivity to TRAIL [424], though ES/TRAIL liposome adhesion to the leukocyte surface could reduce TRAIL uptake by the reticulo-endothelial system in the liver. The present study, however, represents an important first step towards the targeting of CTCs in the bloodstream as a means to prevent cancer metastasis. Clinically, for instance, one could envision using these liposomes as a preventive measure upon diagnosis of highly metastatic hematogenous cancers such as those originating in breast, prostate, and lung.

FIGURE 7.1: ES/TRAIL LIPOSOMES ADHESIVELY INTERACT WITH AND KILL CANCER CELLS UNDER UNIFORM SHEAR FLOW. (A) Synthesis of ES, TRAIL, and ES/TRAIL unilamellar liposomes using a thin film hydration method. Briefly, lipids in chloroform were dried overnight to form a thin lipid film. Lipids were then hydrated and subjected to freeze-thaw cycles to form multilamellar liposomes, which were extruded through membranes to form unilamellar liposomes. ES, TRAIL, or a combination of ES and TRAIL were then conjugated to Ni-NTA on the liposome surface. To assess the ability of ES/TRAIL liposomes to target and kill cancer cells under flow, ES/TRAIL liposomes were added to a suspension of COLO 205 cancer cells and exposed to shear flow in a cone-and-plate viscometer at a shear rate of 188 s^{-1} for 2 h. Cells were then removed, washed, placed into culture for 24 h, and assessed for cell viability. (B) COLO 205 morphology after treatment with ES (top) and ES/TRAIL (bottom) liposomes under shear flow. Scale bar = 20 μm. (C-G) Representative propidium iodide/Annexin-V flow cytometry plots of unsheared cancer cells (C) and cells sheared with naked (D), TRAIL-bound (E), ES-bound (F), and ES/TRAIL-bound liposomes (G) under shear flow. Cells were classified into four categories based on dye uptake: viable cells (negative for Annexin-V and propidium iodide (PI)), early apoptotic cells (positive for Annexin-V only), late apoptotic cells (positive for Annexin-V and PI) and necrotic cells (positive for PI only). (H) Percent of viable cells after treatment for each group. n = 3 for all samples. Bars represent the mean ± SD in each treatment group. ***P <0.0001 (one-way ANOVA with Tukey post test).

FIGURE 7.1: ES/TRAIL LIPOSOMES ADHESIVELY INTERACT WITH AND KILL CANCER CELLS UNDER UNIFORM SHEAR FLOW.

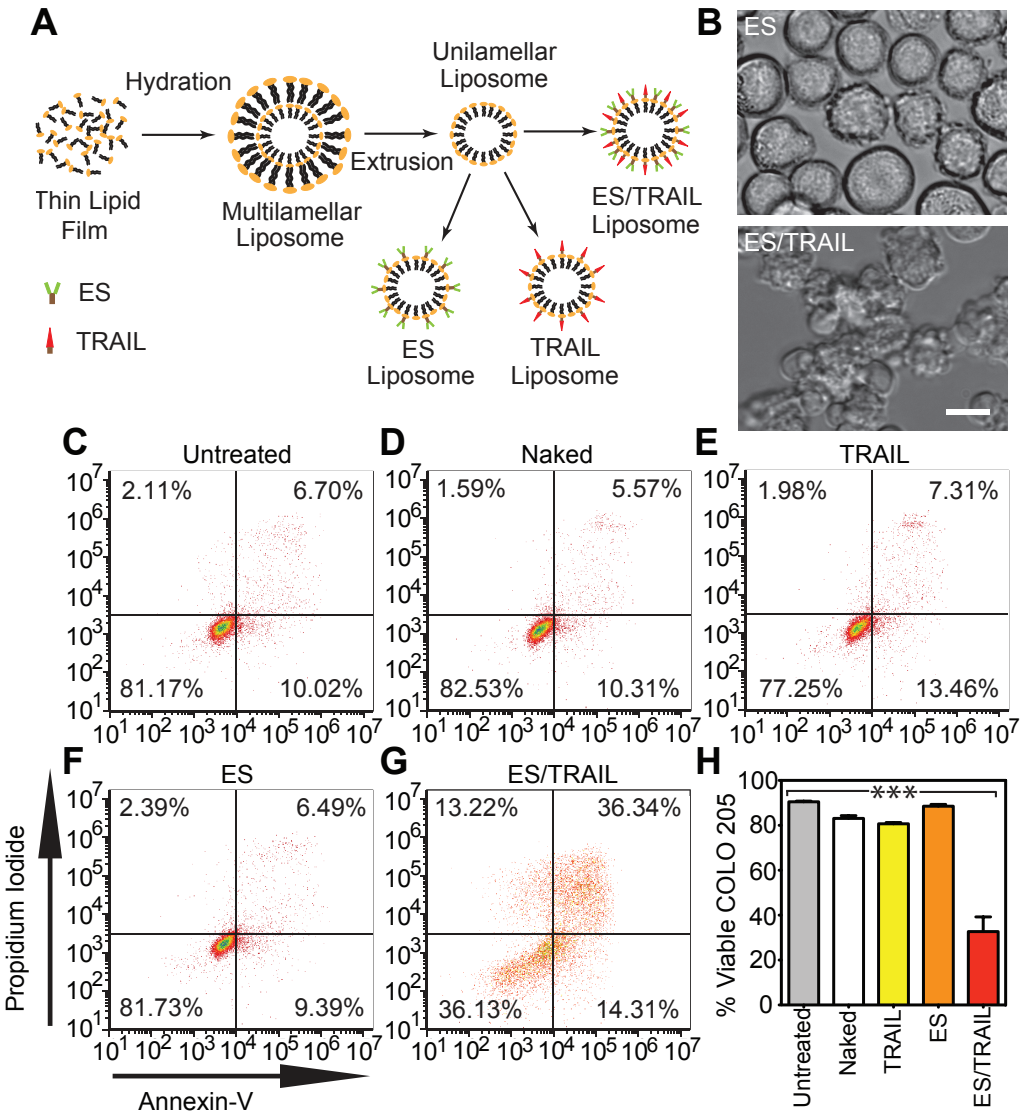

FIGURE 7.2: INCORPORATION OF NI-NTA CONJUGATED LIPIDS ON LIPOSOMES MAXIMIZES PROTEIN CONJUGATION TO THE LIPOSOME SURFACE. To determine how much Ni-NTA conjugated lipid is required to bind TRAIL and ES to the liposome surface, COLO 205 cells were incubated with supernatant left after liposome preparation and assayed for cell viability. Increased cell death is indicative of more unbound TRAIL protein in solution. (A-D) Annexin-V apoptosis assay of COLO 205 cell viability after incubation with supernatant of liposomes conjugated to 0% (A), 1% (B), 5% (C), and 10% Ni-NTA (D) post-ultracentrifugation, with varying amounts of Ni-NTA conjugated to the liposome surface. Cells were classified into four categories based on dye uptake: viable cells (negative for Annexin-V and propidium iodide (PI)), early apoptotic cells (positive for Annexin-V only), late apoptotic cells (positive for Annexin-V and PI) and necrotic cells (positive for PI only). (E) COLO 205 cell viability after treatment with unbound TRAIL and ES in liposome supernatant. n = 3 for all samples. Bars represent the mean ± SD in each treatment group. (F) Representative micrographs of untreated COLO 205 cells (top) and those treated with the supernatant of liposomes conjugated to 0% (middle) and 10% Ni-NTA (bottom). 10% Ni-NTA conjugated lipid on the liposome leads to nearly complete incorporation onto the liposome surface. Scale bar = 50 μm.

FIGURE 7.2: INCORPORATION OF NI-NTA CONJUGATED LIPIDS ON LIPOSOMES MAXIMIZES PROTEIN CONJUGATION TO THE LIPOSOME SURFACE.

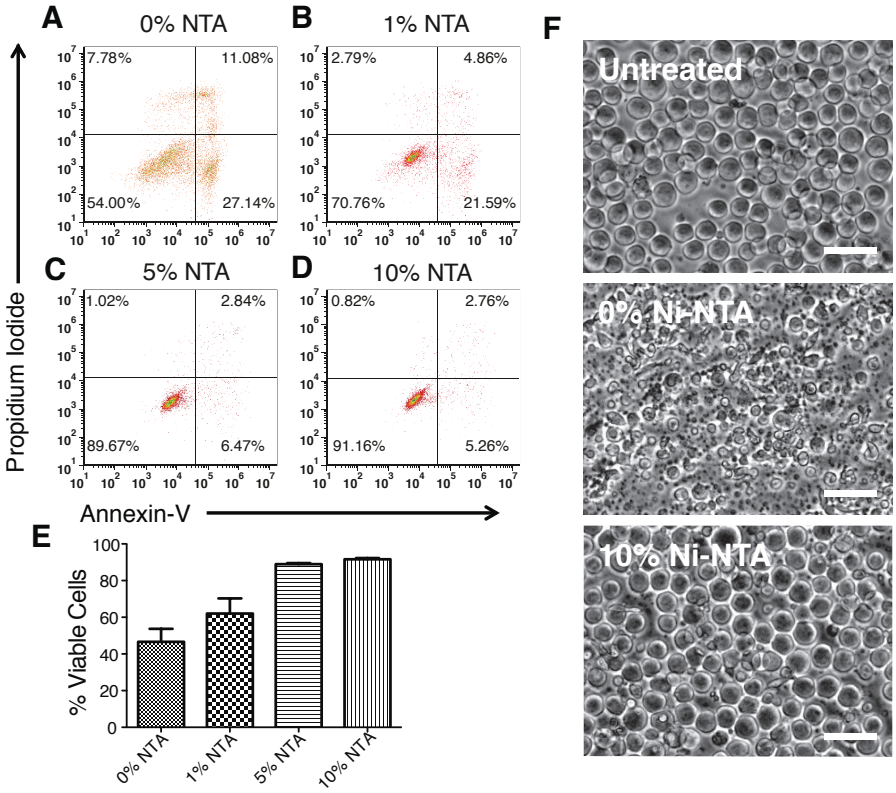

TABLE 7.1: WEIGHT RATIOS OF LIPOSOME FORMULATIONS. With increasing amounts of Ni-NTA conjugated lipid, the corresponding amount of Egg PC lipid was decreased.

DOGS NTA-Ni	Egg PC	Egg SM	Chol/Bdp-Chol*
0% NTA	60	30	10
1% NTA	59	30	10
5% NTA	55	30	10
10% NTA	50	30	10

FIGURE 7.3: ES/TRAIL LIPOSOMES ARE SOMEWHAT EFFECTIVE IN TARGETING AND KILLING COLO 205 CELLS UNDER STATIC CONDITIONS. (A-D) Annexin-V apoptosis plots of COLO 205 cells treated with ES/TRAIL liposomes consisting of 0% (A), 1% (B), 5% (C), and 10% Ni-NTA (D) for 24 h. (E) Representative micrographs showing COLO 205 cells after 24 h incubation with liposomes. Scale bar = 50 μm. (F) COLO 205 cell viability following incubation with liposomes with varying amounts of Ni-NTA on the liposome surface. n = 3 for all samples. Bars represent the mean ± SEM in each treatment group.

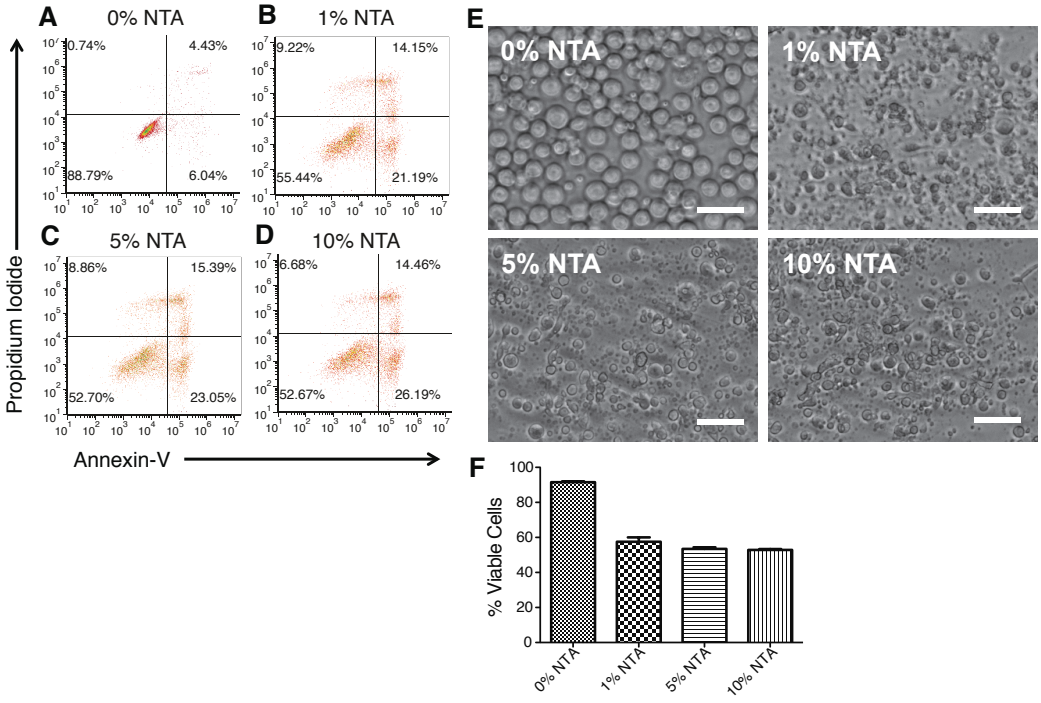

FIGURE 7.4: ES/TRAIL LIPOSOMES ADHESIVELY INTERACT WITH CANCER CELLS. (A) Flow cytometry plots of cancer cells positive for fluorescently tagged ES/TRAIL liposomes (green). Grey population represents fluorescence of COLO 205 cells in the absence of fluorescent ES/TRAIL liposomes. (B) Percent of COLO 205 cells adhered to liposomes following shear flow at a shear rate of $188s^{-1}$. n = 3 for all samples. Bars represent the mean ± SEM in each treatment group. (C,D) Representative fluorescent (left) and brightfield overlay (right) micrographs of COLO 205 cells adhered to fluorescently tagged liposomes following shear flow. Scale bar = 20 µm.

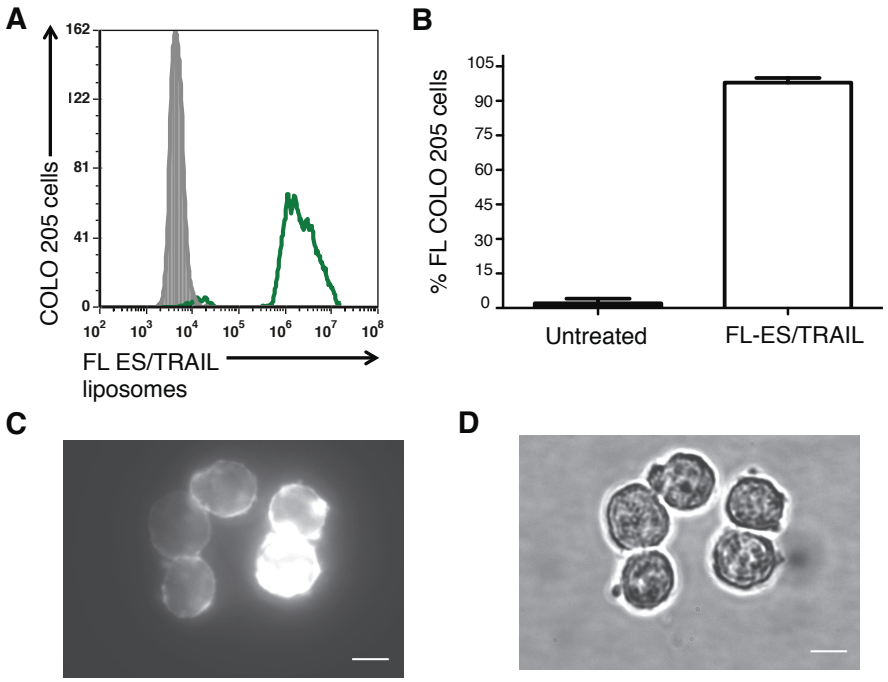

FIGURE 7.5: ES/TRAIL LIPOSOMES ADHERE TO MULTIPLE LEUKOCYTE SUBPOPULATIONS AFTER EXPOSURE TO SHEAR FLOW IN WHOLE BLOOD. (A) Confocal images of ES/TRAIL liposomes (green) bound to human leukocytes (blue = cell nuclei) after exposure to shear flow in whole blood in a cone-and-plate viscometer at 188 s^{-1} for 30 min. Leukocytes have nuclear morphology characteristic of monocytes (left), lymphocytes (middle), and neutrophils (right). Scale bar = 5 μm. (B-G) To assess which leukocyte subpopulations ES/TRAIL liposomes adhesively interact with, fluorescent ES/TRAIL liposomes were added to human blood and exposed to shear flow in a cone-and-plate viscometer at a shear rate of 188 s^{-1} for 30 min. Leukocytes were isolated from blood using a Polymorphs density gradient, and labeled with CD3, CD14, CD16, CD19, and CD56, which is typically expressed on T-lymphocytes, monocytes, neutrophils, B-lymphocytes, and natural killer cells, respectively. Expression of fluorescent ES/TRAIL (FL ES/TRAIL) liposomes on the surface of leukocytes that are CD3+ (B), CD14+ (C), CD16+ (D), CD19+ (E), and CD56+ (F), determined using flow cytometry. Expression of CD3, CD14, CD16, CD19, and CD56 on the leukocyte surface was determined using isotype controls. No label: unsheared cells that were not treated with fluorescent ES/TRAIL liposomes. ES block: cells treated with fluorescent ES/TRAIL liposomes that were pretreated with an ES functional blocking antibody. Post-mix: cells labeled with fluorescent ES/TRAIL liposomes immediately after mixing liposomes in whole blood. (G) Percent of CD3+, CD14+, CD16+, CD19+, and CD56+ leukocytes adhered to ES/TRAIL liposomes. n = 3 for all samples. Bars represent the mean ± SD in each treatment group. ***P <0.0001 (one-way ANOVA with Tukey post test).

FIGURE 7.5: ES/TRAIL LIPOSOMES ADHERE TO MULTIPLE LEUKOCYTE SUBPOPULATIONS AFTER EXPOSURE TO SHEAR FLOW IN WHOLE BLOOD.

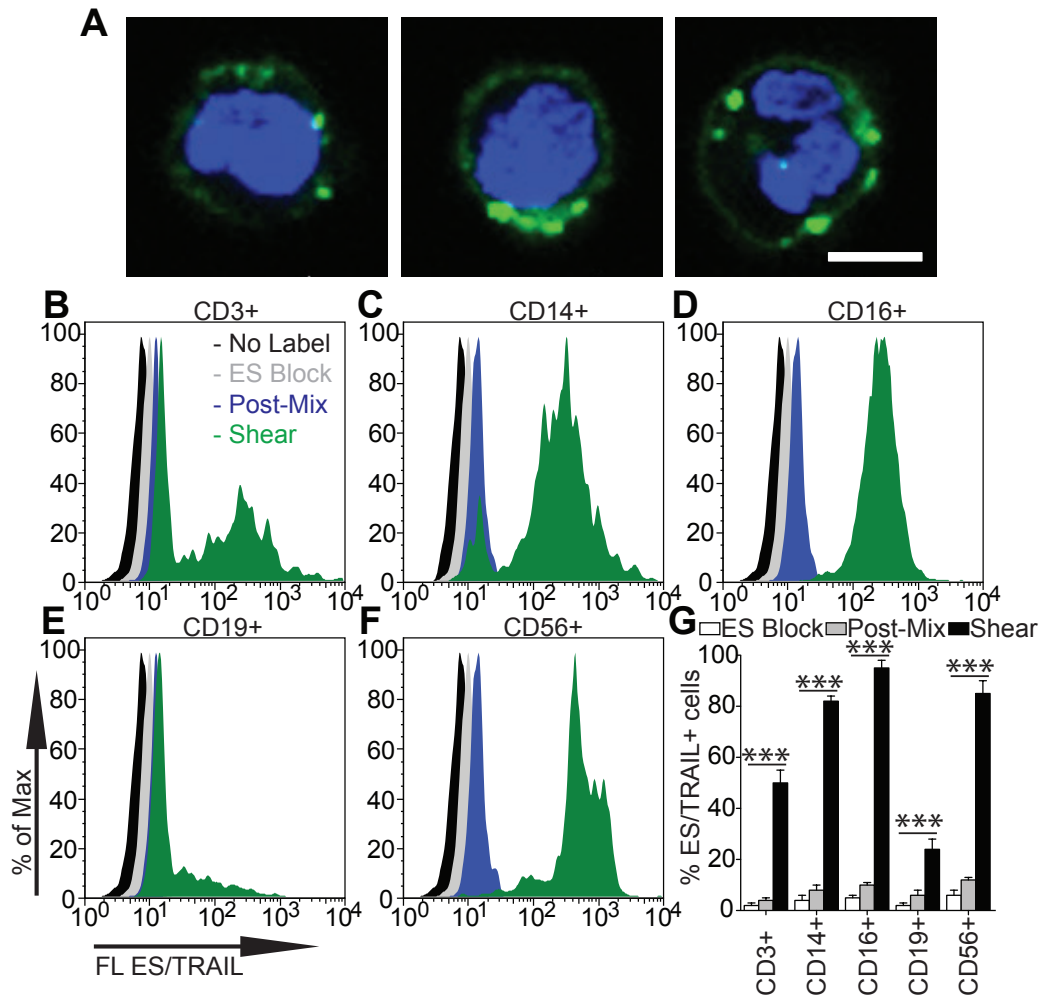

FIGURE 7.6: LEUKOCYTE FUNCTIONALIZATION WITH ES/TRAIL DOES NOT INDUCE SIGNIFICANT LEUKOCYTE DEATH. (A-C) Representative propidium iodide/Annexin-V flow cytometry plots of untreated mononuclear cells (A) and those treated with ES (B) and ES/TRAIL (C) liposomes under static conditions for 24 h. (D) Viability of mononuclear cells following incubation with liposomes for 24 h. n = 3 for all samples. Bars represent the mean ± SEM in each treatment group. NS: not significant (one-way ANOVA with Tukey post test). (E-G) Representative propidium iodide/Annexin-V flow cytometry plots of untreated mononuclear cells (E) and those treated with ES (F) and ES/TRAIL (G) liposomes under shear flow (shear rate: 188 s^{-1}) for 2 h. (H) Viability of MNCs treated with liposomes under shear flow for 2 h. n = 3 for all samples. Bars represent the mean ± SD in each treatment group. NS: not significant (one-way ANOVA with Tukey post test).

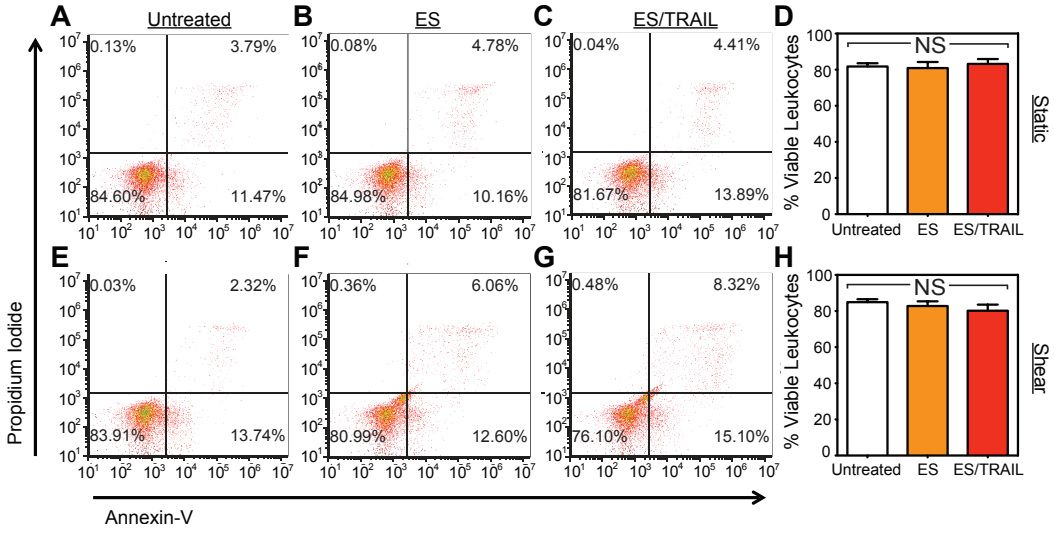

FIGURE 7.7: LEUKOCYTE FUNCTIONALIZATION WITH ES/TRAIL DOES NOT INDUCE SIGNIFICANT ENDOTHELIAL CELL DEATH. (A) Representative images of HUVECs immobilized on coverslips immediately after treatment in human blood, with various drug treatments, under shear flow (shear rate: 188 s^{-1}) for 4 h at 37°C. Scale bar = 100 μm. (B-D) Representative propidium iodide/Annexin-V flow cytometry plots of untreated HUVECs (B) and those treated with ES/TRAIL (C; TRAIL concentration: 0.3 μg/mL) or soluble TRAIL (D; TRAIL concentration: 0.3 μg/mL) in human blood under shear flow for 4 h at 37°C. (E) As a positive control, HUVECs were treated with a high dosage of TRAIL (15 μg/mL) in human blood under shear flow for 4 h at 37°C. HUVECs were classified into four categories based on dye uptake: viable cells (negative for Annexin-V and propidium iodide (PI)), early apoptotic cells (positive for Annexin-V only), late apoptotic cells (positive for Annexin-V and PI) and necrotic cells (positive for PI only). (F) Percent viability of HUVECs after various drug treatments in human blood under shear flow for 4 h at 37°C. n = 3 for all samples. Bars represent the mean ± SD in each treatment group. $^{**}P < 0.001$. NS: not significant (one-way ANOVA with Tukey post test).

FIGURE 7.7: LEUKOCYTE FUNCTIONALIZATION WITH ES/TRAIL DOES NOT INDUCE SIGNIFICANT ENDOTHELIAL CELL DEATH.

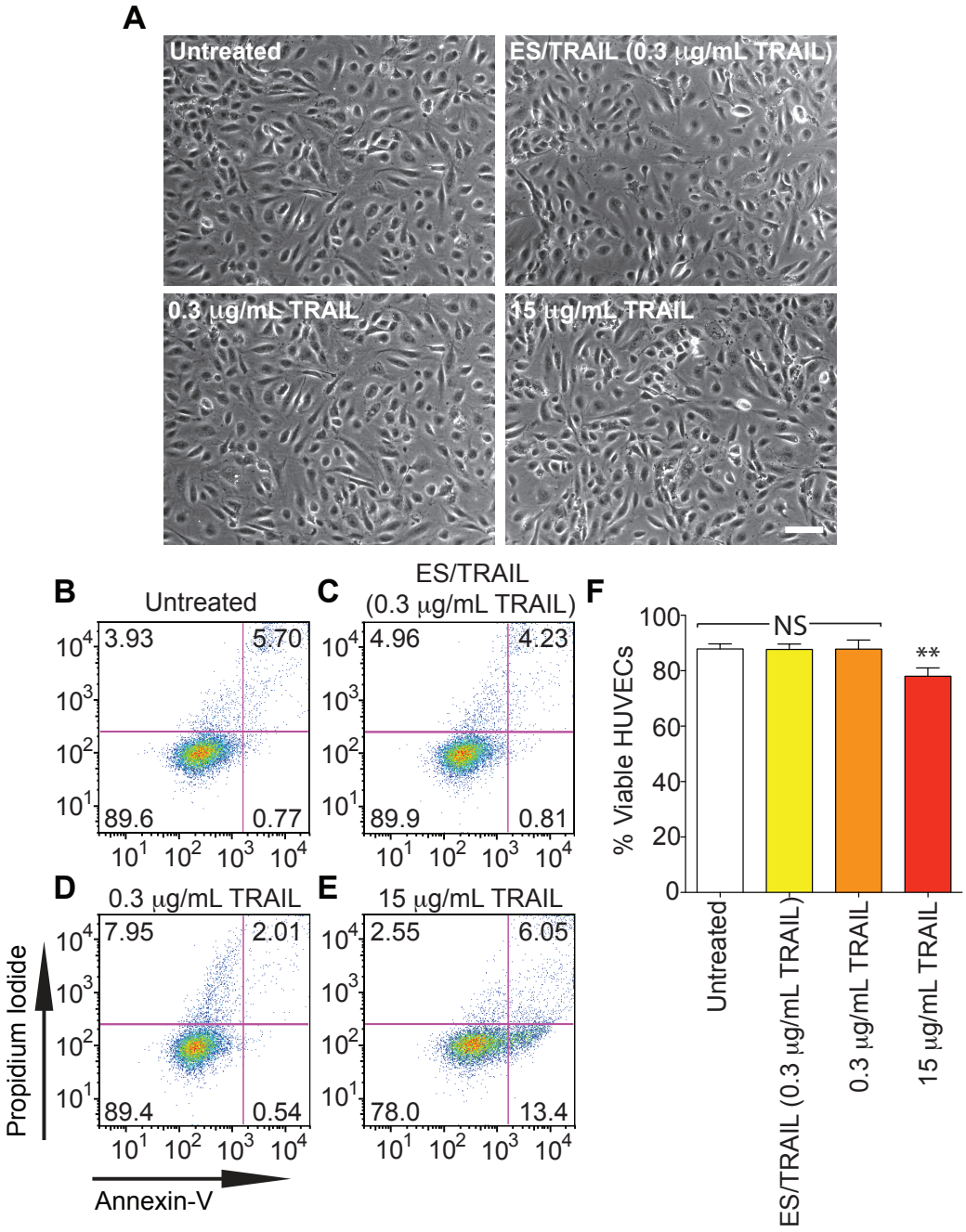

FIGURE 7.8: ES/TRAIL LIPOSOME THERAPEUTIC EFFECTS ARE ENHANCED IN HUMAN BLOOD UNDER FLOW *IN VITRO*. (A) Flow cytometry of COLO 205 cancer cells after treatment with ES/TRAIL or ES liposomes in blood under shear flow in a cone-and-plate viscometer at 188 s^{-1} for 2 h. Unsheared: viable untreated cancer cell control. (B) Representative flow cytometry histogram showing the number of viable cancer cells collected. (C) Representative micrographs of COLO 205 cells (white) in blood when treated with ES/TRAIL (left) and ES only (right) liposomes in blood under shear flow. Scale bar = 50 μm. (D) Number of viable COLO 205 and PC-3 cells per volume of blood after treatment with ES/TRAIL or ES liposomes in blood under shear flow. n = 3 for all samples. Bars represent the mean ± SD in each treatment group. $^{**}P$ <0.001, $^{***}P$ <0.0001 (unpaired t-test). (E) Comparison of fraction of COLO 205 and PC-3 cells that remained viable after treatment with ES/TRAIL liposomes in buffer versus blood. n = 3 for all samples. Bars represent the mean ± SD in each treatment group. $^{***}P$ <0.0001 (unpaired t-test). (F) Fraction of COLO 205 and PC-3 cells that remained viable after treatment with ES/TRAIL liposomes in blood with varying percentages of normal hematocrit. Hematocrit was varied while other blood components remained constant, based on a normal hematocrit of 45%. Plasma indicates removal of all blood cells. n = 3 for all samples. Bars represent the mean ± SD in each treatment group. $^{*}P$ <0.05 (one-way ANOVA with Tukey post test).

FIGURE 7.8: ES/TRAIL LIPOSOME THERAPEUTIC EFFECTS ARE ENHANCED IN HUMAN BLOOD UNDER FLOW *IN VITRO*.

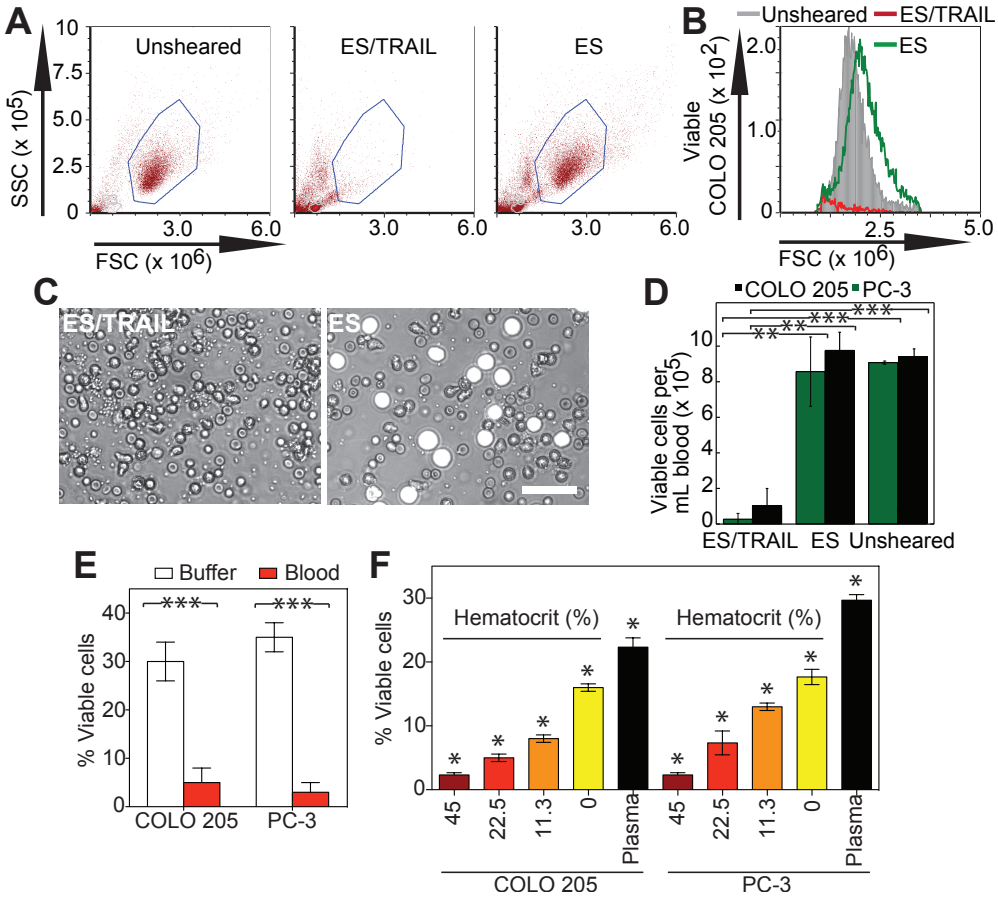

FIGURE 7.9: ES/TRAIL LIPOSOMES FUNCTIONALIZE LEUKOCYTES UNDER SHEAR FLOW *IN VITRO* TO TARGET AND KILL CANCER CELLS. (A) Flow cytometry plots of COLO 205 cells in untreated samples (left) and when treated in human blood with ES (middle) or ES/TRAIL (right) functionalized leukocytes (but no unbound liposomes) under shear flow. (B,C) Number of viable COLO 205 (B) and PC-3 (C) cells per volume of blood after treatment with leukocytes functionalized with ES/TRAIL or ES liposomes, but with no unbound liposomes, in human blood (Washed), or after treatment with ES or ES/TRAIL liposomes in blood (Unwashed). $n = 3$ for all samples. Bars represent the mean ± SD in each treatment group. $^{**}P < 0.001$, $^{***}P < 0.0001$ (unpaired t-test). (D,E) Schematic of the two-step mechanism involving decoration of leukocytes with liposomes (D), which then contact circulating cancer cells and activate the death receptor (E).

FIGURE 7.9: ES/TRAIL LIPOSOMES FUNCTIONALIZE LEUKOCYTES UNDER SHEAR FLOW *IN VITRO* TO TARGET AND KILL CANCER CELLS.

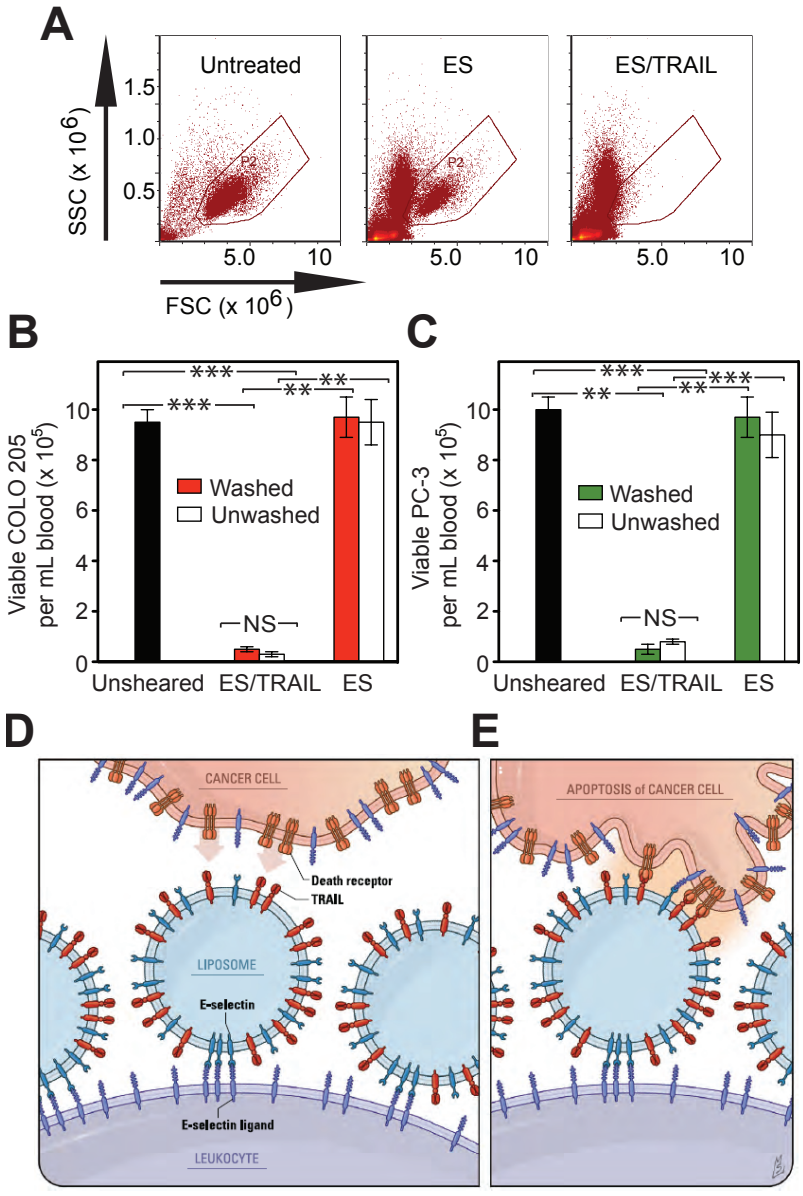

FIGURE 7.10: LOW TOXICITY OF BLOOD PLASMA AFTER TREATMENT WITH ES/TRAIL LIPOSOMES. (A) Viability of COLO 205 cells after treatment with plasma from normal healthy blood for 24 h. (B) Viability of COLO 205 cells after treatment with plasma extracted from blood that had been sheared with ES/TRAIL liposomes for 30 min. Cells were incubated with plasma and any remaining unbound ES/TRAIL liposomes and/or liposome fragments in the plasma for 24 h, and analyzed for cell viability.

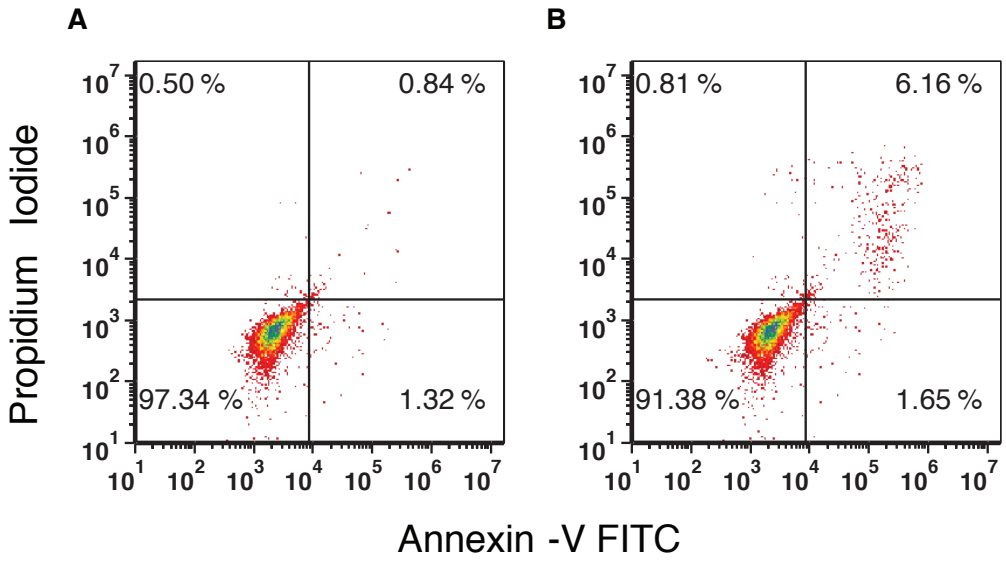

FIGURE 7.11: ES/TRAIL FUNCTIONALIZED LEUKOCYTES TARGET AND KILL CANCER CELLS IN THE CIRCULATION OF MICE *IN VIVO*. (A) Schematic of *in vivo* mouse experiment. (B) Flow cytometry of untreated COLO 205 cancer cells (left) and those recovered from cardiac puncture from mice treated with ES (middle) and ES/TRAIL liposomes (right). (C) Number of viable cancer cells recovered per volume of mouse blood for mice treated with ES/TRAIL liposomes, soluble TRAIL (sTRAIL), ES liposomes, and buffer injections. $n = 3$ for all samples. Bars represent the mean ± SD in each treatment group. $^{*}P < 0.01$, $^{**}P < 0.001$, $^{***}P < 0.0001$ (one-way ANOVA with Tukey post test). (D) Representative micrographs of COLO 205 cells removed from circulation in mice treated with ES/TRAIL liposomes (top left), sTRAIL (top right), ES liposomes (bottom left), and buffer (bottom right) injections. Scale bar = 20 μm. (E) Leukocytes functionalized with fluorescent ES/TRAIL liposomes (green) upon removal from mouse circulation 2.5 h after injection. Scale bar = 50 μm.

FIGURE 7.11: ES/TRAIL FUNCTIONALIZED LEUKOCYTES TARGET AND KILL CANCER CELLS IN THE CIRCULATION OF MICE *IN VIVO*.

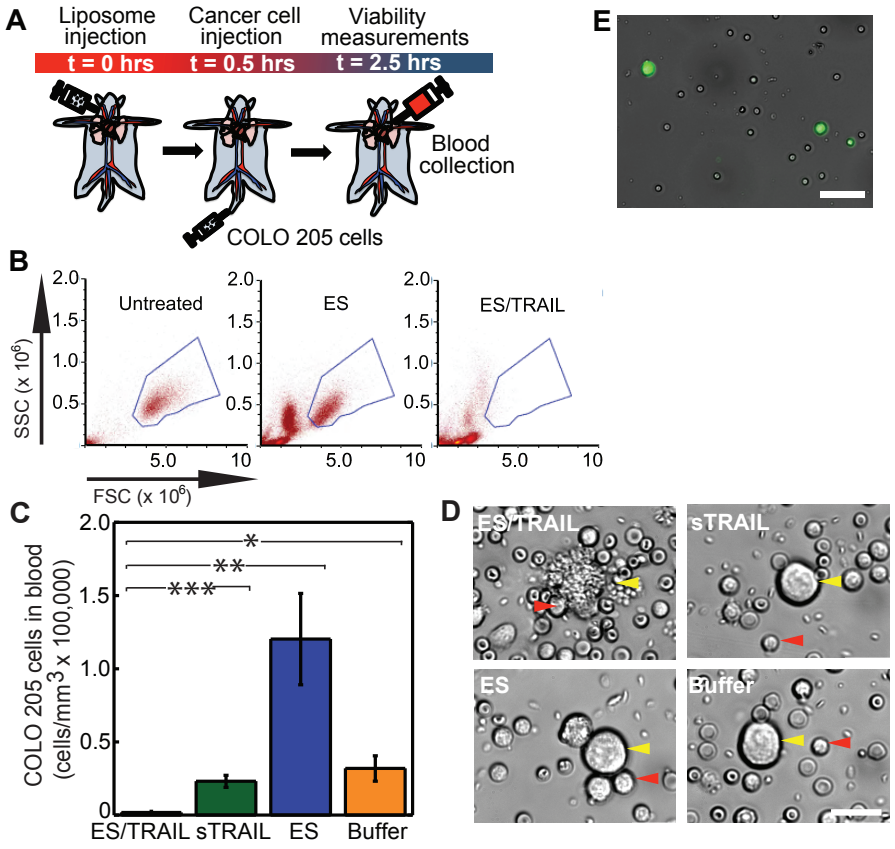

FIGURE 7.12: DECREASED NUMBER AND INCREASED APOPTOSIS IN COLO 205 CELLS LODGED IN MOUSE LUNG AFTER TREATMENT WITH ES/TRAIL LIPOSOMES. (A) Schematic of mouse lung and example two-photon excited fluorescence (2PEF) image stack from mouse lung where Hoechst-labeled COLO 205 cells (green) are arrested in lung tissue (visible by autofluorescence, yellow). Scale bar = 80 μm. (B) 2PEF images of Hoescht-labeled COLO 205 cells (green) with Alexa Flour 568 labeled Annexin V apoptosis probe (red) for each experimental group. Red arrows point to apoptotic COLO 205 cells (red and green colocalized), blue arrows indicate non-apoptotic COLO 205 cells (green only). White circles indicate regions of autofluorescence from lung tissue. Scale bar = 30 μm. (C) Density of COLO 205 cells lodged in the lung for each experimental group. (D) Percentage of lodged COLO 205 cells positive for Annexin-V probe for each experimental group. Individual data points represent data from one image stack, with points shown in the same color representing image stacks from the same animal. Superimposed box plots bound the 25th to 75th percentage of all data points and the whiskers extend 1.5 times the interquartile range beyond the boxes. The horizontal lines within the boxplot represent the median. n = 3 animals for each experimental group. *P <0.01, **P <0.0001 (one-way ANOVA with Tukey post test).

FIGURE 7.12: DECREASED NUMBER AND INCREASED APOPTOSIS IN COLO 205 CELLS LODGED IN MOUSE LUNG AFTER TREATMENT WITH ES/TRAIL LIPOSOMES.

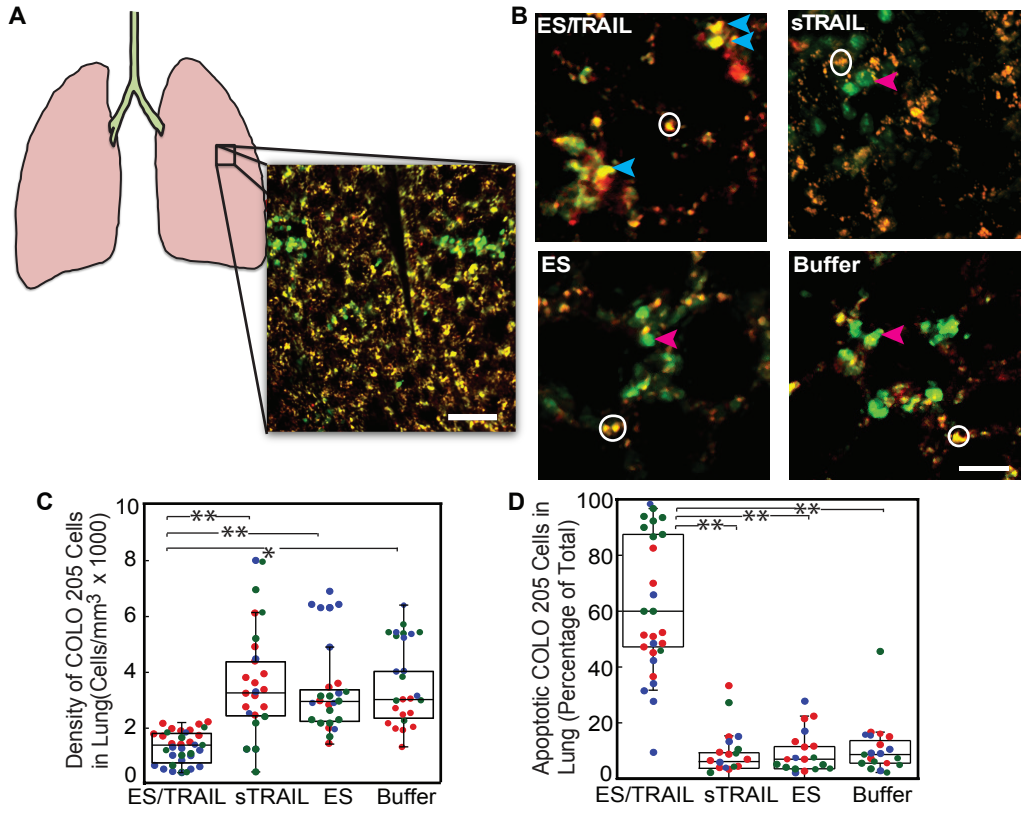

CHAPTER 8: AN NSF GK-12 EXPERIENCE. FABRICATION OF JELL-O MILLI-FLUIDIC CHIPS FOR INQUIRY-BASED EDUCATION OF HEMODYNAMICS AND BLOOD CELL ADHESION

8.1 INTRODUCTION AND SCIENCE CONTENT FOR TEACHERS

The forces generated by blood flow in small blood vessels known as post-capillary venules play a crucial role in the adhesion of a variety of types of circulating cells to the blood vessel wall. The adhesion of blood cells to the blood vessel walls (known as the endothelium) play a critical role in how the human body responds to infection (known as inflammation), and also the process which causes bleeding to stop (known as hemostasis). While blood cell adhesion is important physiologically, it can also promote the progression of various human diseases, including arthritis, thrombosis, and cancer.

One class of white blood cells, known as neutrophils, can adhere to blood vessel walls under inflammatory conditions, and can act as "first-responders" in fighting off infection. Under normal conditions, neutrophils can freely circulate throughout the bloodstream. However, in the case of inflammation, neutrophils can adhere to the blood vessel wall via receptor-ligand interactions (Figure 1.6B). During inflammation, endothelial cells will express adhesion receptors on their surface, one of which is E-selectin. Neutrophils possess ligands for E-selectin, which allow them to form bonds with the endothelial cells that make up the blood vessel wall. The bonds that neutrophils initially form with the blood vessel have rapid, force-dependent binding kinetics. These bonds are short lived however, as neutrophils eventually detach from these bonds, while forming new selectin-mediated bonds with E-selectin receptors further downstream. This process is known as cell rolling adhesion. Rolling adhesion of neutrophils can continue on the endothelial cell wall until they come into

contact with intercellular adhesion molecule-1 (ICAM-1), which allows the neutrophil to become firmly adhered to the cell wall via adhesion molecules known as integrins. Once firmly adhered, neutrophils can "squeeze" through the vessel wall, and migrate to the site of infection to engulf and kill bacteria.

Conversely, a similar process is also used in the spread of cancer throughout the body, known as metastasis. Metastasis, the spread of cancer cells from a primary tumor to a secondary site, is the cause of over 90% of cancer related deaths. When cancer cells remain within the primary tumor, the tumor is typically treatable via surgery. However, tumor cells can migrate from the primary tumor into the bloodstream in a process called intravasation, and circulate through the bloodstream as circulating tumor cells (CTCs). Once in the bloodstream, CTCs can adhere to blood vessels in different organs of the body, in a manner very similar to white blood cells (Figure 1.6B). CTCs can also express selectin ligands, which allow CTCs to roll and subsequently adhere to the blood vessel wall. From there, tumor cells can migrate to different parts of the body to form secondary tumors. This process leads to a poor patient prognosis, as new tumors (known as micrometastases) are very small and hard to detect in time to develop effective treatments for the patient.

Advances in microfluidics have allowed for the development of devices that can recreate the complex microenvironment of the bloodstream. In particular, our lab has recently developed microscale flow devices that mimic postcapillary venules to study the basic mechanisms of cancer metastasis [391] and inflammation [390,425]. Such devices have also been adapted to kill cancer cells in the bloodstream [82], and isolate circulating tumor cells from patient blood [336]. As the clinical benefits of

microfluidics are becoming apparent, it is essential to educate young students on basic fluidic principles and their potential impact on human disease diagnosis and treatment. A simple fabrication technique was demonstrated using Jell-O to teach high school students the essential components of blood flow, and its subsequent effects on cell adhesion in inflammation and cancer.

8.2 MATERIALS AND METHODS

Model milli-fluidic devices were fabricated using a soft lithography technique consisting of foam plates, coffee stirrers, single- and double-sided tape, and Jell-O. Briefly, coffee stirrers were cut, connected, and arranged in various formations and adhered to foam plates using double-sided tape. Single-sided tape was placed on top of the coffee stirrers to create a smooth surface. A Jell-O liquid was prepared as per manufacturer's instructions, poured onto molds, and left to cure inside a refrigerator for 2 days. Jell-O chips were then peeled from molds and placed onto aluminum plates. Inlets and outlets were created within the chips, and liquid was perfused through the device using disposable transfer pipets. For model blood cell adhesion experiments, glass slides were incubated with a solution of 2:8 (0.02 wt%) poly-l-lysine (Sigma-Aldrich) for 10 mins prior to placing chips onto glass slides. As a model of cell adhesion, a 1:10 dilution in distilled water of the original negatively charged, 90 μm polymeric microspheres solution (Polysciences, Cat # 07315) was perfused through the device, and were allowed to adhere to the positively charged poly-l-lysine functionalized surface.

8.3 CLASSROOM PROCEDURE

Day 1

Students will begin the fabrication their own Jell-O devices in what will be a two-day process (Figure 8.1, Figure 8.2). Initially, students will have to use a foam plate and coffee stirrers to create their own model of a microfluidic network. To make the "negative mold", students can cut, connect, and shape coffee stirrers, which they can then adhere to the foam plate using double-sided tape. To smooth the top surface of the stirrer, students can use single-sided tape on the top surfaces of the adhered stirrers (Figure 8.1). Students can be encouraged to make sure that all stirrer junctions are smooth, to facilitate fluid flow in later portions of the experiment. The negative mold can then be sprayed with cooking oil, to allow the Jell-O mold to be easily removed from the negative mold.

Once the negative mold is complete, students can then mix together Jell-O powder and gelatin together in hot water, as directed in the Jell-O manufacturer's instructions (NOTE: Jell-O mixture should be mixed with half the amount of liquid recommended by the manufacturer, in order to make a stable Jell-O mold). Students should be careful to pour the hot Jell-O mixture over the mold, to ensure that there are minimal air bubbles, while also ensuring that the coffee stirrers remain adhered to the foam plate. Teachers can then place the Jell-O devices in a refrigerator overnight to allow the molds to form (NOTE: for optional day 3 activity, extra Jell-O molds should be made and incubated overnight).

Day 2

By day 2, the Jell-O mold should be formed, and students can carefully remove the mold from the plate. Students can do this by gently using their fingers or by maneuvering a coffee stirrer under the edge of the mold and peeling it off. The mold should be placed channel side down, on a smooth aluminum surface (plate or foil). Jell-O mold should be pressed down gently to ensure a good seal.

Students can then carefully punch inlet and outlet holes at either end of the channels using a straw. Using syringes and/or transfer pipets, students can perfuse colored water through the device, and record how much fluid is drawn into the syringe in Table 8.1. The syringe can then be placed perpendicular to the flow of the chip, and students can begin to push the fluid into the chip at a constant rate, and start the timer as soon as they start pushing. Students should also time how long it takes to completely empty the syringe. Record this time in table 1. To record the velocity of the fluid, students should measure how long it takes the fluid to travel a given distance within their device, and record the measurement (in meters per second (m/s)) in figure 1. Students can calculate the Reynolds Number of chip by using the following equation $Re = udp/v$, where u is the velocity in m/s, d is the diameter of the tube (in this case, we will estimate using the width of the channel, since it is rectangular), p is the density of the fluid, and v is the viscosity of the fluid.

Record this data in Table 8.1. Students can then compare their numbers to corresponding flow conditions in Table 8.2 (NOTE: for optional day 3 activity, equal

numbers of glass slides should be incubated with either 2:8 (0.02 wt%) poly-l-lysine solution or distilled water overnight in a refrigerator).

Day 3 (Optional):

NOTE: For this activity, teachers should use extra molds made in day 1 to adhere onto glass slides incubated in poly-l-lysine solution or distilled water after day 2.

In this optional activity, students can develop an understanding of the basic mechanisms of cell adhesion in the bloodstream by developing an assay that is free of potentially harmful biological materials. Teachers will distribute Jell-O devices that have been incubated with poly-l-lysine solution. Students can rinse their devices of excess NaL solution with distilled water, and place their devices on an inverted light microscope. Students can then draw a 1:10 dilution of polymer microspheres into a transfer pipet and perfuse the microspheres through the device. After a period of 10 minutes, students can then rinse the device of unbound microspheres with distilled water. Using the light microscope, students can count the number of remaining microspheres adhered within the Jell-O device (on the glass slide preferably, where NaL solution has been incubated). Students should write down the number of spheres adhered into Table 8.3.

Teachers will then give students Jell-O devices that have been incubated with water. Students can rinse their devices with distilled water, and place their devices on an inverted light microscope. Students can then draw the same solution of polymer

microspheres into a transfer pipet and perfuse the microspheres through the device. After a rinse of the device with distilled water, students can count the number of microspheres adhered within the Jell-O device via a light microscope. Students should write down the number of spheres adhered into Table 8.3. Students can then be introduced to the idea of the negatively charged spheres binding to the positively charged glass surface (due to incubation with poly-l-lysine solution). Meanwhile, little to no microsphere binding will be seen in the device coated with water, as the negatively charged microspheres will not be attracted to the glass surface in the absence of the negatively charged surfactant. Microsphere adhesion can be used as a model of actual cell adhesion in microfluidic devices, where cells can bind via receptor:ligand interactions.

8.4 ASSESSMENT

A rubric (Table 8.4) can be used to assess students during each part of the activity. The term “expectations” here refers to the content, process and attitudinal goals for this activity. Evidence for understanding may be in the form of oral as well as written communication, both with the teacher as well as observed communication with other students. Specifics are listed in Table 8.4.

iClickers can also be used to administer a pre and post-assessment of students’ understand of the laboratory. Below are examples of questions that can be asked before and after the laboratory:

1. What does a high Reynolds number usually indicate?

A. Laminar flow

B. Turbulent flow

C. Intermediate flow

D. Cladistic flow

2. What benefits can a microfluidic chip provide?

A. Quick diagnosis

B. They are very easy to produce

C. They can model several different animals at one time

D. The chips can provide quick drug delivery when implanted

3. What enables white blood cells to exhibit different types of movement?

A. The cells have different DNA

B. The cells can change the way their mitochondria function

C. The cells can express different surface proteins

D. The cells have multiple cell membranes

4. What is viscosity?

A. How thin a liquid is

B. How much a fluid resists flow

C. The average Reynolds number of a fluid

D. The median flow rate of a fluid

5. Which is NOT a function of immune cells?

A. To engulf invading cells

B. To identify invading cells

C. They migrate to sites of injury

D. They secrete hormones to identify pathogens

6. Why is the shape of a protein so important?

A. Proteins need a specific shape to fit through the capillary wall

B. Proteins that are improperly shaped will never be degraded

C. The shape of a protein is directly related to its function

D. Each protein must be slightly different to avoid autolysis

7. Why must white blood cells be activated in the bloodstream?

A. They must be activated in order to leave the bloodstream

B. If they are not activated, they will never circulate in the blood.

C. The cells must only be activated to destroy bacteria

D. The cells will not duplicate if they are not activated first.

8. How do some white blood cells find a site of infection?

A. They always migrate toward blood

B. Many bacteria have shapes that are similar to white blood cells

C. The cells can migrate toward chemical signals

D. The cells polarize and use their flagella to sense inflammation

9. How can various parts of the blood be separated in the lab?

A. Using electrophoresis

B. By centrifugation

C. By adding white blood cells to capture other blood components

D. Using a small pipette to separate the layers

10. Which of the choices can influence how white blood cells are activated?

A. The shape of the blood vessel

B. The DNA of the white blood cells

C. The application of shear stress on the cells

D. The location of the cell in the body

Finally, students can be asked the following essay questions to assess their understand of the laboratory:

QUESTION 1: Compare your Reynolds Number with that of a few other students. Were they the same or different? Can you find a pattern?

QUESTION 2: Describe a use for a microfluidic device where it might be beneficial to have laminar flow.

QUESTION 3: Describe a use for a microfluidic device where it might be beneficial to have turbulent flow.

QUESTION 4: There are several uses for microfluidic devices. One such use is a "lab on a chip." What this means is that instead of using a large volume of a sample (such as blood), doctors might be able to use just a few drops and perform their tests on a very small scale. Explain at least two benefits and two detriments of such a system in the space below.

QUESTION 5: Microfluidic devices might also be used for personalizing medicines. For example, cells could be collected from various organs in a patient's body, placed in a microfluidic device, and then blood with a particular medicine could be profused through the device. What benefits might this have for the patient?

8.5 RESULTS AND DISCUSSION

High school students successfully fabricated model milli-fluidic devices consisting of varying fluidic networks (Figure 8.1). Comparisons of Jell-O chip versus polydimethylsiloxane (PDMS) microfluidic chip fabrication in biomedical research were highlighted throughout the fabrication process. The concept of pressure-driven flow was demonstrated using Jell-O chips in the absence of an outlet, as fluid could not flow due to air present in the channel, which could not escape due to the absence of an outlet. High school students calculated flow rate by measuring the flow of a set volume of fluid through the device over time (Figure 8.3). The concept of laminar flow was demonstrated to students via perfusion of both a light and a dark-colored fluid through a Y-shaped Jell-O chip, as fluids perfused through channels

simultaneously did not mix. Jell-O chips were also used to demonstrate a model of cell adhesion, as poly-l-lysine coated devices successfully induced polymeric microsphere adhesion.

8.6 CONCLUSION

I have shown that simple, inexpensive Jell-O microfluidic devices can successfully demonstrate the basic principles of blood flow in a hands-on high school laboratory setting. The fabrication and use of devices can benefit students by introducing them to current biomedical technologies and applications, and encourage the pursuit of engineering and science degrees at the university level.

FIGURE 8.1: SCHEMATIC TO FABRICATE JELL-O CHIPS USING SOFT LITHOGRAPHY. (A) Top view of a negative mold consisting of coffee stirrers and a foam plate. (B) Side view of coffee stirrers adhered to foam plate using tape. (C) Liquid Jell-O is poured onto the mold. (D) Chip is solidified over using refrigeration and then peeled from plate. (E) Chip is adhered to aluminum plate or foil for use.

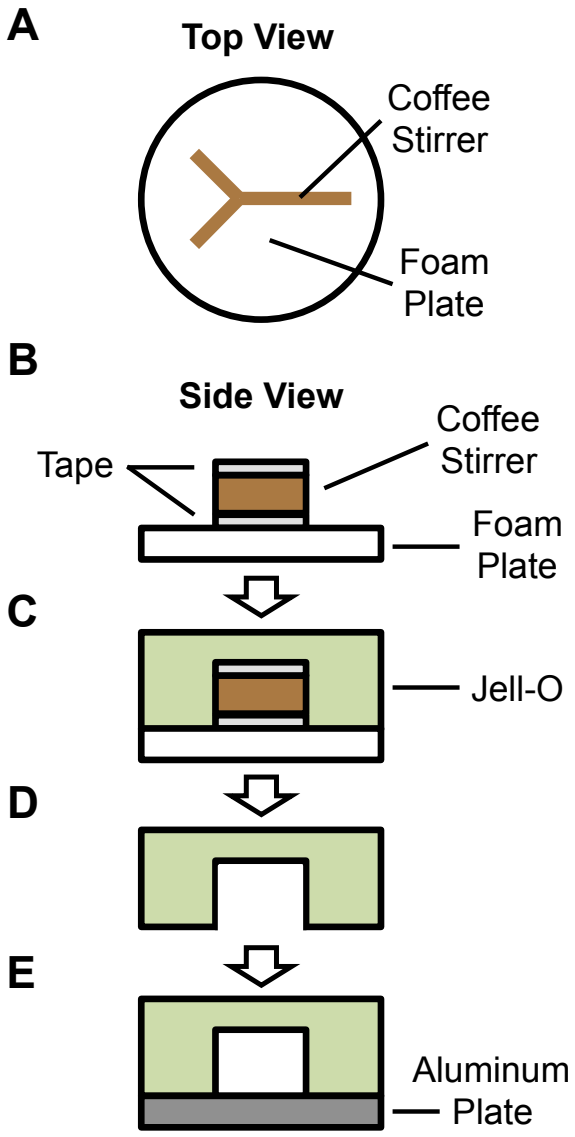

FIGURE 8.2: MATERIALS NEEDED FOR OUTREACH ACTIVITY

TABLE 8.1: DATA FOR CALCULATION OF REYNOLDS NUMBER.

Amount of fluid in syringe/ Time to empty syringe	
Velocity of fluid	
Reynolds Number	
Laminar, transitional or turbulent flow?	

TABLE 8.2: REYNOLDS NUMBERS THAT INDICATE VARIOUS FLOW CONDITIONS.

Condition	Reynolds Number
Laminar	Less than 2300
Transitional	2300-4000
Turbulent	More than 4000

TABLE 8.3: NUMBER OF MICROSPHERES ADHERED TO JELL-O DEVICES.

Number of spheres adhered, device 1	
Number of sphered adhered, device 2	

TABLE 8.4: RUBRIC TO ASSESS STUDENTS DURING OUTREACH ACTIVITY.

	Engage	Explore	Explain	Expand/Synthesis
1				
2				
3				
4				

1= exceeds expectations

2= meets expectations consistently

3= meets expectations occasionally

4= not meeting expectations

FIGURE 8.3: PERFUSION OF FLUID THROUGH A JELL-O MILLI-FLUIDIC CHIP.

CHAPTER 9: CONCLUSIONS AND FUTURE WORK

9.1 INTRODUCTION

Collectively, I have demonstrated the fluid shear stress plays a critical role in the mechanotransduction and therapeutic targeting of cells in the circulation. Fluid shear stress exposure can both sensitize and desensitize leukocyte activation in the bloodstream, in the presence of various chemoattractants, and thus affect the inflammatory response. Cancer cells exposed to fluid stress can be sensitized to the apoptosis-inducing ligand TRAIL, but not traditional chemotherapeutics such as doxorubicin, suggesting that perhaps TRAIL is well suited for systemic delivery to circulating tumor cells. Utilizing this newly discovered knowledge of TRAIL mechanotransduction, novel selectin-based therapeutic approaches were developed to specifically target and kill circulating circulating cells via TRAIL-mediated apoptosis. Specifically, E-selectin functionalized liposomes were developed to target cancer cells in the circulation. Demonstrating the feasibility of such an approach, immobilized E-selectin functionalized liposomes rapidly adhered to flowing cancer cells, due to the rapid, force-dependent binding kinetics of selectins, to deliver therapeutic cargo and induce cancer cell death *in vitro.* In combination with immobilized halloysite nanotubes, this liposome-based approach was successful at repelling leukocytes, which also possess ligands for E-selectin while delivering therapeutics to cancer cells. A combination of both E-selectin and TRAIL were then both functionalized to the surface of liposomes to target and kill cancer cells in the circulation *in vivo*. This novel therapeutic approach was found to be highly ineffective in human blood *in vitro* and in the peripheral circulation of mice *in vivo*.

9.2 FLUID SHEAR STRESS DIFFERENTIALLY ALTERS NEUTROPHIL ACTIVATION IN THE PRESENCE OF CHEMOATTRACTANTS

The results from Chapter 2 suggest that fluid shear stress has a significant effect on the activation of circulating neutrophils in the presence of the chemoattractant fMLP. Neutrophils acquired a fluid shear stress-induced resistance to activation via FPR, the receptor for fMLP. The resistance was shown to be dependent on shear stress magnitude, as the resistance response increased with increasing shear stress. The mechanical response was also shown to be dependent on shear stress duration, as neutrophils increased their resistance with increased shear stress exposure time. A decrease in FPR surface expression was observed under fluid shear stress, and high-resolution confocal microscopy revealed that FPR was internalized within the cells. While other studies on mechanotransduction in neutrophils have mostly focused on morphological changes, the present study demonstrated that fluid shear stress has a significant effect on the earliest stages of neutrophil activation, specifically fMLP-induced L-selectin shedding and $\alpha_M\beta_2$ integrin activation.

Conversely, results from Chapter 3 showed that human neutrophil pre-exposure to fluid shear stress can increase, rather than decrease, neutrophil activation in the presence of different inflammatory mediator platelet-activating factor (PAF). Fluid shear stress exposure increased PAF-induced neutrophil activation in terms of L-selectin shedding, $\alpha_M\beta_2$ integrin activation, and morphological changes. Neutrophil activation via PAF was found to correlate with fluid shear stress exposure, as neutrophil activation increased in a shear stress magnitude- and time-dependent

manner. These results indicate that fluid shear stress exposure increases neutrophil activation to PAF, and, taken together with previous observations, differentially controls how neutrophils respond to chemoattractants. fMLP is a peptide chemoattractant released by certain bacteria and mitochondria at a site of tissue infection and/or injury, and activates neutrophils by interacting with the formyl peptide receptor on the neutrophil surface [316]. In humans, fMLP is present only at very low concentrations in the bloodstream, compared to sites of tissue infection and/or injury. Sustained activation to fMLP stimuli in the bloodstream could hinder the neutrophil response to infection by promoting pseudopod projection, increasing neutrophil transit time in blood, and enhancing neutrophil retention in the microvasculature [317,318]. Thus, if neutrophils pre-exposed to hemodynamic shear forces in the bloodstream increased fMLP-induced activation, neutrophils would be fully activated in the bloodstream and less efficient at transmigrating into localized tissues. Additionally, activation of neutrophils via fMLP also induces production of reactive oxygen species (ROS) [319], and thus shear-induced resistance to fMLP can reduce ROS-induced damage to healthy blood vessels. By developing a resistance to fMLP-induced activation when exposed to shear in the bloodstream, neutrophils avoid unnecessary activation in the bloodstream, facilitating extravasation and subsequent migration in tissues. In contrast, PAF-induced activation of neutrophils in the bloodstream is physiologically important.

Taken together, these results indicate that the complete signaling pathways of these receptors deserve further study, along with the molecules that mediate GPCR internalization. Other receptors that have shown high constitutive activity should be

investigated to understand their contributions to the mechanosensing response of cells within the vascular microenvironment.

9.3 FLUID SHEAR STRESS ENHANCES TRAIL-MEDIATED APOPTOSIS OF CIRCULATING CANCER CELLS

The results from Chapter 4 indicate that hemodynamic shear forces have a significant effect on receptor-mediated apoptosis of cancer cells in the presence of TRAIL. Fluid shear stress was found to sensitize both colon and prostate cancer cell lines to TRAIL-mediated apoptosis. Cancer cells were not sensitized to TRAIL-mediated necrosis upon exposure to fluid shear stress. TRAIL sensitization was shown to be shear stress dose-dependent, as sensitization was found to increase with increasing fluid shear stress. TRAIL sensitization was also fluid shear stress time-dependent, as sensitization to apoptosis was enhanced with increasing fluid shear stress exposure time. The response was TRAIL-specific, as shear stress did not sensitize cancer cells to doxorubicin treatment over varying shear stress magnitudes and exposure times. Caspase inhibition assays revealed the sensitization response to be caspase-dependent. These results shed new light on the cancer cell response to soluble apoptotic agents within the circulation. The effects of fluid shear stress on mechanosensing death receptors on the cancer cell surface, along with their signaling pathways, can reveal new strategies for treating circulating cancer cells and reducing the likelihood of metastasis. Taken as is, the results from this study provide evidence that TRAIL is well suited for systemic deliver to therapeutically target circulating

tumor cells, compared to traditional therapeutics such as doxorubicin, which do not enact their therapeutic effect via receptors on the cancer cell surface.

9.4 E-SELECTIN FUNCTIONALIZED LIPOSOMES TO TARGET CANCER CELLS AND DELIVER THERAPEUTIC CARGO UNDER FLOW

In Chapter 5, I demonstrated the efficacy of targeting, capturing, and killing model CTCs using immobilized E-selectin functionalized liposomal doxorubicin within a biomimetic microtube flow device. Due to its rapid, force-dependent binding kinetics, E-selectin functionalized liposomal doxorubicin was shown to enhance cancer cell killing in both static conditions and conditions mimicking the microcirculation. Cone-and-plate shear experiments demonstrated the effectiveness of target-specific nanoparticles in solution, which can aid in the development of drugs intended for systemic delivery. Taken together, these results demonstrate that E-selectin is an effective targeting agent for cancer cell under flow conditions typically observed in the microcirculation.

Since it is challenging to deliver E-selectin functionalized nanoparticles while avoiding adhesion to healthy blood cells, as many possess ligands that adhesively interact with selectins, I expanded on this nanoparticle platform in Chapter 6 to create a nanostructured surface to capture flowing cancer cells while preventing human neutrophil adhesion. Microtube surfaces with immobilized halloysite nanotubes (HNTs) and E-selectin functionalized liposomal doxorubicin (ES-PEG L-DXR) significantly increased the number of breast adenocarcinoma MCF7 cells captured

from flow, yet also significantly reduced the number of captured neutrophils. Neutrophils firmly adhered and projected pseudopods on surfaces coated only with liposomes, while neutrophils adhered to HNT-liposome surfaces maintained a round morphology. Perfusion of both MCF7 cells and neutrophils resulted in primarily cancer cell adhesion to the HNT-liposome surface, and induced significant cancer cell death. This work demonstrates that nanostructured surfaces consisting of HNTs and ES-PEG L-DXR can increase CTC recruitment for chemotherapeutic delivery, while also preventing healthy cell adhesion and uptake of therapeutic intended for CTCs. One advantage of this device for capturing and killing of CTCs is that by immobilizing liposomes onto the microtube surface, the potential distribution of targeted L-DXR into circulation is reduced and a lower dose of the drug is necessary. The proposed device, which can be implemented as a vascular stent or arteriovenous shunt, can potentially be utilized for reducing the probability of metastasis, and suggests new strategies for enhancing targeted delivery of chemotherapeutics to CTCs.

9.5 TRAIL-COATED LEUKOCYTES TARGET AND KILL CANCER CELLS IN FLOWING HUMAN BLOOD IN VITRO AND IN THE PERIPHERAL CIRCULATION OF MICE IN VIVO

In Chapter 7, I utilized liposomes functionalized with a combination of E-selectin and TRAIL to rapidly target and kill CTCs in the circulation *in vivo*. CTCs are essentially surrounded by white blood cells in the circulation, as deformable red blood cells tend to flow towards the center of the blood vessel while white blood cells and

CTCs are pushed towards the vessel wall during a process known as margination [162]. With this in mind, I developed a reverse approach, utilizing the surface of the body's white blood cells to create "Unnatural Killer Cells" (UnKs) to target and deliver a cell death signal to CTCs in blood [209].

Since both white blood cells and CTCs adhere to ES in blood, I developed nanoscale liposomes conjugated with ES, to mediate interactions between both cell types, and tumor necrosis factor-related apoptosis-inducing ligand (TRAIL), a therapeutic that induces cell death in numerous cancer cell types while exerting minimal toxic effects on normal cells [236]. *In vitro*, liposomes functionalized with ES and TRAIL (ES/TRAIL) were generally effective at targeting cancer cells and inducing apoptosis under both static conditions and flow conditions mimicking the circulatory system. Additionally, ES/TRAIL liposomes were found to adhere to a range of white blood cells isolated from human blood under flow conditions *in vitro*, demonstrating that UnKs could target CTCs in a complex fluid such as blood. The results were surprising and unexpected, however, as human blood *enhanced* the therapeutic effect of ES/TRAIL, with minimal live cancer cells remaining in human blood after exposure to flow conditions for as little as two hours *in vitro*.

The presence of whole blood enhanced the therapeutic effect of ES/TRAIL in two ways: (i) the presence of red blood cells, and (ii) the formation of UnKs after treatment with ES/TRAIL liposomes under flow. By simply increasing the number of red blood cells from low levels to normal hematocrit levels found in blood, the therapeutic effect of ES/TRAIL exerted on cancer cells significantly increased. Perhaps most interesting, however, was utilizing UnKs alone to target cancer cells

under blood flow conditions. By adhering ES/TRAIL liposomes to the surface of white blood cells and removing unbound ES/TRAIL liposomes from blood, the maximal therapeutic effect was still achieved, demonstrating UnKs as the essential component for killing circulating cancer cells.

UnKs have numerous benefits for targeting CTCs in the circulation *in vivo*. From a biophysical perspective, the collisions between CTCs and white blood cells can act to flatten the matrix of biological molecules that make up the CTC glycocalyx [237], allowing for exposure of TRAIL death receptors that would not be possible to target using nanoparticles alone. Additionally, while TRAIL alone is not effective means to target CTCs due to its short half life *in vivo* [416], the formation of UnKs in the circulation acts to increase TRAIL circulation time, effectively avoiding renal clearance mechanisms to enhance the therapeutic effects on CTCs *in vivo*.

Initial *in vivo* experiments to target CTCs in the circulation have proven to be similarly promising. ES/TRAIL liposomes were injected into the peripheral circulation of mice for 30 min, allowing for UnKs to form in blood. As a straightforward and widely-used model of lung metastasis *in vivo* [240], fluorescently labeled cancer cells were injected via tail vein and allowed to circulate for 2 hours, after which the mice were sacrificed and cancer cells were recovered from blood via cardiac puncture. Interestingly, mice with UnKs showed >98% less cancer cells in blood than control mice that only displayed ES on the white blood cell surface. Injection with the soluble TRAIL alone was ineffective, due to its short half-life in the circulation. In this model of lung metastasis, it is known that cancer cells also lodge within the blood vessels of the lung. Thus, we utilized multiphoton microscopy to assess the number and viability

of cancer cells lodged within the lung. Interestingly, fewer cancer cells were found in mice with UnKs, indicating that most cancer cells underwent apoptosis and dissociated by the time of imaging. Of the cancer cells remaining in UnK mice, the majority of the cells stained positive for the apoptosis marker Annexin-V, while a minimal number of cells in control mice were apoptotic. Thus, the formation of UnKs in mice suggests that cancer cells within the circulation can be targeted and killed, before they are able to form new micrometastases.

The use of UnKs to target and kill bloodborne cancer cells has to potential to be translated into the clinic, as Amgen/Genentech's recombinant human TRAIL/Apo2L (also known as PRO1762), has undergone Phase 1, 1a, 2, and 3 clinical trials over the past decade, with minimal adverse effects reported [248]. Given that this new therapeutic approach is focused on the vascular microenvironment, we also validated that cells that comprise the circulation such as leukocytes and endothelial cells remain unharmed by this approach [209]. In fact, most normal cells in the body are protected from TRAIL-induced cell death through intracellular proteins such as the class of inhibitors of apoptosis proteins (IAPs) [236]. For CTCs that exhibit reduced sensitivity to the effects of TRAIL, the approach may also be combined in regimens with other low cytotoxic agents, such as aspirin or the turmeric spice compound curcumin [85,426], to synergistically kill CTCs.

9.6 FUTURE WORK

If introduced at the appropriate time points, unnatural killer cells may serve as a means to target and kill CTCs before they are able to form new metastases. Such an approach could constrain cancerous cells within the primary tumor, which is typically treatable via surgery, radiation, and/or chemotherapy. To address the translatability of unnatural killer cells into future clinical trials, future work focused on the prevention of metastases in longer term animal models will be needed. I have initiated this work by developing a spontaneous metastasis model to assess the therapeutic efficacy of unnatural killer cells. My initial work in Chapter 7 demonstrated that unnatural killer cells kill circulating cancer cells *in vivo*. However, a spontaneous metastasis model is more physiologically relevant, due the fact the CTCs can disseminate from the primary tumor and form metastases spontaneously. The ultimate goal of this future work would be to reduce the formation of secondary tumors, and potentially exert a therapeutic effect on the primary tumor.

Spontaneous Metastasis Model of Prostate Cancer

I have developed a spontaneous metastasis model by injecting luciferase-expressing metastatic DU145 prostate cancer cell orthotopically into mice. Utilizing bioluminescent imaging, luciferase-expressing DU145 cells can be detected in the primary tumor over time, and can also be used to determine the onset and location of anatomically distant metastases (Figure 9.1). The presence of CTCs can also be

detected with this model as blood can from mice via submandibular bleeds, or via cardiac puncture, for CTC isolation. I have demonstrated that CTCs can isolated from this model 6 weeks post-orthotopic injection (Figure 9.2). Additionally, I have shown that anatomically distant metastases do form within the lungs of this orthotopic mouse model over time, as shown by detection of metastases in lung via BLI (Figure 9.1) and also by the presence of white metastatic nodules on mouse lung (Figure 9.3). Taken together, a combination of CTCs detected in blood combined with the presence of metastases in anatomically distant organs suggest that metastases can form following the entry of CTCs within the circulation.

Using this model, future work will focus on introducing unnatural killer cells upon first detection of CTCs in blood, before the formation of metastases, in order to prevent the formation of secondary tumors. I have shown that the enhanced apoptotic effect of cancer cells in the presence of unnatural killer cells also holds true for DU145 metastatic prostate cancer cells. While DU145 cells remain viable after exposure to human blood under flow conditions, negligible viable cancer cells remain after treatment with unnatural killer cells in human blood under flow conditions (Figure 9.4), which is consistent with the results from Chapter 7, where negligible COLO 205 and PC-3 cancer cells remained after treatment in human blood under flow conditions.

An appropriate therapeutic time point will be determined by detecting the presence of CTCs and metastases in the model over time. After orthotopic injection, mice will be sacrificed every week, ranging from a 1-12 week time period post-orthotopic injection. At every week time point, each mouse will be assessed for (1) the presence of CTCs in blood, and (2) the presence of micrometastases in lymph nodes,

lungs, liver, bone and brain, using BLI imaging. After identifying the first week at which CTCs and micrometastases are detected in mice, the initial therapeutic treatments will begin 2 weeks before initial detection of CTCs. For example, if CTCs are first detected in mice 5 weeks post-orthotopic injection, then first therapeutic treatments of ES/TRAIL liposomes will begin 3 week post-orthotopic injection in new mice. ES/TRAIL liposomes will be injected daily over a 3-5 week time period, via tail vein and retro-orbital injections. To determine efficacy, the presence of CTCs, the number of metastases, the size of primary and secondary tumors, and overall survival of treated, orthotopically injected mice will be compared to untreated, orthotopically injected control mice.

Combination Therapies

Future work will utilize unnatural killer cells in combination with compounds that demonstrate minimal side effects *in vivo*, to expand this approach to cancers which show differential sensitivity to TRAIL. Results from Chapter 4 will also play a crucial role in this future work. Due to the fact that fluid shear stress has been shown to enhance cancer cell apoptosis in the presence of TRAIL, it is possible that this phenomenon can also be applied to a variety of apoptosis-inducing ligands that can trigger cancer cell death. While TRAIL has been shown to be effect at inducing apoptosis in a variety of cancer cells, the use of other apoptosis-inducing ligands can expand our current approaches to therapeutically target even cancer cell types. One can envision using E-selectin functionalized liposomes with a variety to apoptosis-

inducing ligands, to create various forms of unnatural killer cells within the circulation. I feel that the current approach, however, represents an important initial step in utilizing white blood cells within the bloodstream to eliminate CTCs *in vivo*.

Unnatural Killer Cell-Mediated Therapies Targeting Primary Tumors

Due to the fact that surgical resection of primary tumors leads to immediate dissemination of CTCs in blood, which can lodge within anatomically distant organs and form micrometastases, it is important to also expand the unnatural killer cells approach to also target primary tumors. Given that subpopulations of leukocytes have the innate ability to infiltrate solid tumors, it is possible that unnatural killer cells can be utilized to infiltrate solid tumors, and deliver ligands such as TRAIL to induce cancer cell apoptosis. This would fill an immediate need, as currently drugs that are administered systemically will rarely reach the target tumor site, due to a lack of a functional vasculature. Unnatural killer cells present an entirely new approach to reach these sites, as leukocytes can use their innate ability to migrate along chemoattractant gradients to reach the primary tumor site.

Shear Stress-Based Control of Leukocyte Infiltration to Primary Tumors

While this innate ability of leukocytes suggests that unnatural killer cells can infiltrate the primary tumor, determining the number of leukocytes that invade the tumor, along with determining the number of unnatural killer cells needed to induce

reduction of primary tumors remains a challenge. Thus, a greater understand of leukocyte activation in the presence of shear forces will eventually be needed to harness the ability of unnatural killer cells to target primary tumors. Results from Chapter 2 and 3 have shown promise that this can potentially be accomplished. I have shown in these chapters that fluid shear forces can exert great control over how leukocytes activate under inflammatory conditions, which are also present in the case cancer. By further studying how these forces control leukocyte activation at the receptor level, we can potentially control the activation of leukocytes under the inflammatory conditions of cancer. One can envision altering the forces exerted on leukocytes in blood, in order to control the number of leukocytes that become activated and eventually disseminate to tumor sites.

FIGURE 9.1: BIOLUMINESCENT IMAGING (BLI) OF A SPONTANEOUS METASTASIS MODEL OF PROSTATE CANCER. Luciferase-expressing DU145 metastatic prostate cancer cells were injected orthotopically into mice. The formation of primary and secondary tumors was detected over a time span of 12 weeks.

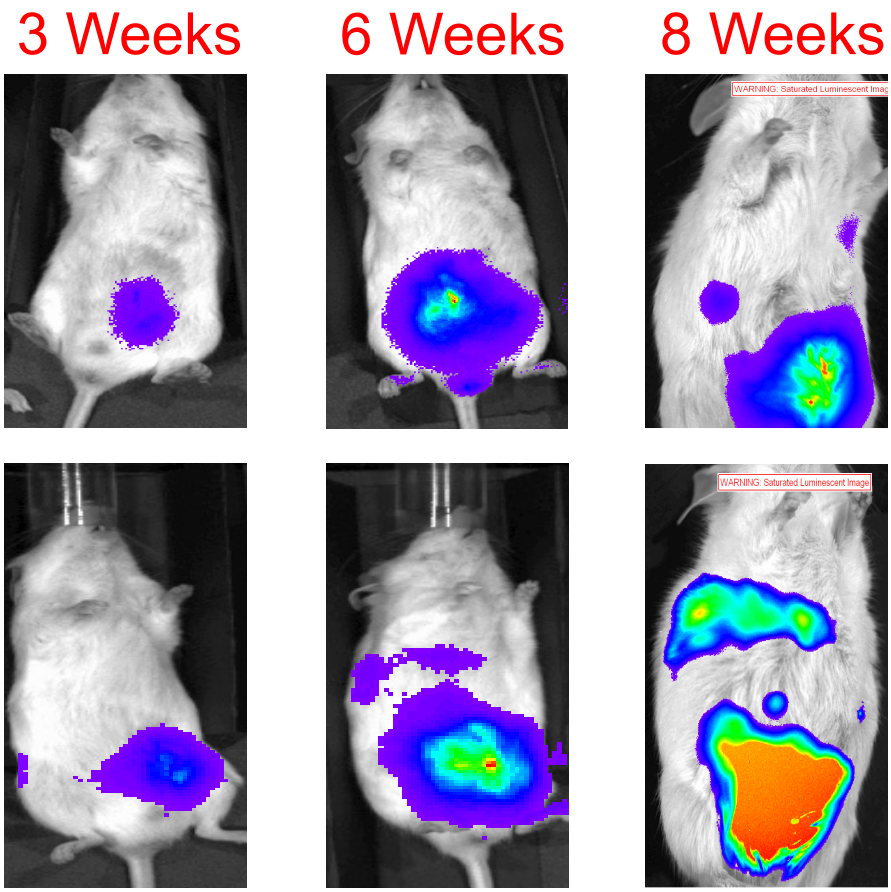

FIGURE 9.2: CIRCULATING TUMOR CELLS (CTC) ISOLATED FROM A SPONTANEOUS METASTASIS MOUSE MODEL OF PROSTATE CANCER. CTCs were isolated 6 weeks after orthotopic injection of DU145 prostate cancer cells into mice. Controls denote mice that were not injected orthotopically. Red cells denote luciferase-expressing DU145 cells. Blue denotes cell nuclei.

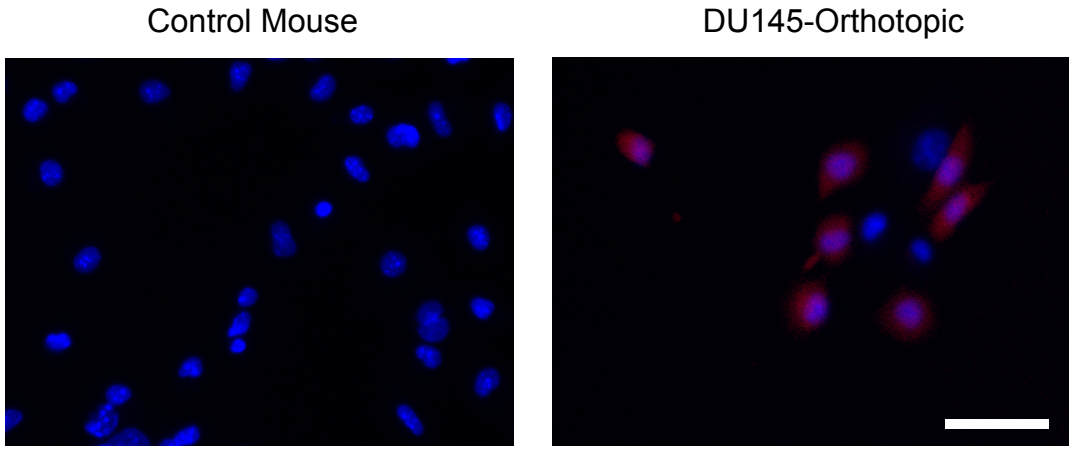

FIGURE 9.3: FORMATION OF METASTASES IN MOUSE LUNG IN A SPONTANEOUS METASTASIS MODEL OF PROSTATE CANCER. Mouse lungs were excised and assessed for the presence of metastases (indicated by white nodules) 9 weeks after orthotopic injection of DU145 prostate cancer cells. Control denotes mouse lungs from healthy mice.

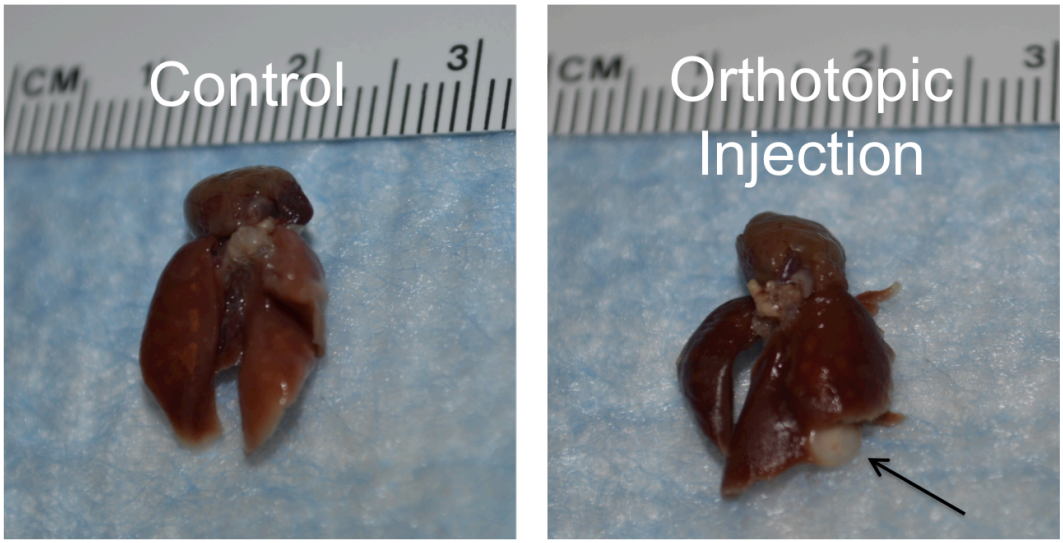

FIGURE 9.4: UNNATURAL KILLER CELLS INDUCE DU145 CANCER CELL DEATH IN HUMAN BLOOD UNDER FLOW *IN VITRO*. DU145 prostate cancer cells were labeled with a fluorescent viability dye and exposed to ES/TRAIL liposomes in human blood under flow conditions in a cone-and-plate viscometer for 3 h. Viable cancer cells were gated and detected for fluorescence using flow cytometry.

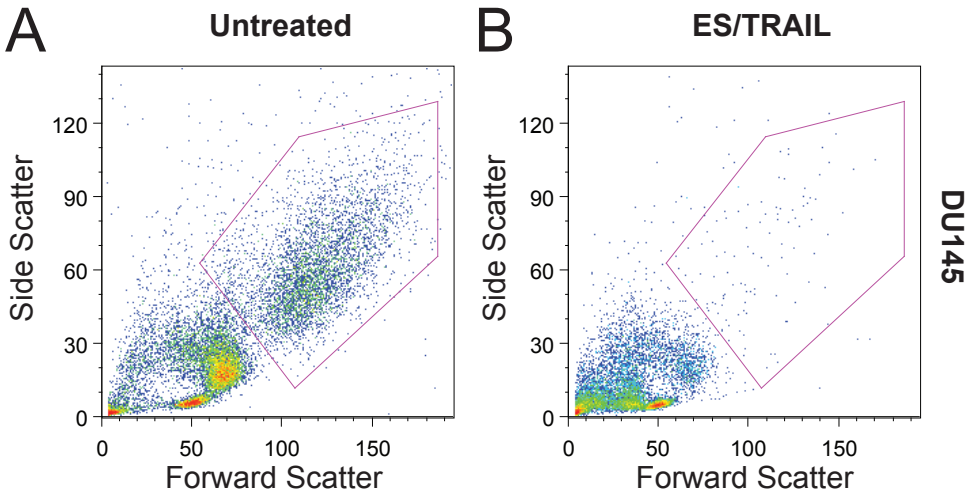

APPENDIX I: THE ROLE OF CELL GLYCOCALYX IN VASCULAR TRANSPORT OF CIRCULATING TUMOR CELLS

*This section is adapted from the following publication: M.J. Mitchell and M.R. King. *American Journal of Physiology – Cell Physiology.* 306(2): C89-C97, 2014.

I.1 INTRODUCTION

Metastasis contributes to approximately 90% of cancer-related deaths [1,427], yet many aspects of metastasis remain poorly understood. Cancer cells originating from the primary tumor undergo a sequence of steps to metastasize via the bloodstream to anatomically distant organs, including detachment from the primary tumor, invasion into surrounding tissues, and intravasation into the vascular circulation as circulating tumor cells (CTCs) [51,223]. CTCs can then be transported through the vascular system to the postcapillary venules of distant tissues, undergo adhesive interactions with the microvessel wall, exit the bloodstream in a process known as extravasation, survive in distant tissues, and proliferate to form secondary tumors [365]. While primary tumors are generally treatable via radiation, chemotherapy, and/or surgical removal, the systemic nature of metastasis makes the disease difficult to treat [335]. A better understanding of the vascular transport of CTCs can reveal key checkpoints for the intervention and treatment of metastasis.

Receptor-ligand interactions play a key role in both the adhesion and therapeutic treatment of CTCs in the bloodstream. To adhere to the microvasculature in distant tissues, sialylated carbohydrate ligands expressed on CTCs can bind to selectin receptors on the surface of inflamed endothelial cells [52,365]. This adhesion mechanism has been used in recent biomimetic approaches to target CTCs via immobilized E-selectin receptors under physiological flow conditions [84,85,335]. Such techniques can allow flowing cancer cells to interact with apoptosis-inducing ligands [84,85], which can bind with receptors on the cancer cell surface to trigger

programmed cell death. The ability of CTCs to undergo such receptor-ligand interactions can be dictated by a physical barrier on the surface of cells known as the glycocalyx.

The glycocalyx is a sugar-rich coating that is found on the surface of both endothelial cells and tumor cells. The endothelial cell glycocalyx serves as a vascular permeability barrier, a mechanotransducer of hemodynamic shear forces to endothelial cells, and a regulator of adhesive interactions between circulating cells and the endothelium [428]. Tumor cells can overexpress certain building blocks of the glycocalyx, and which can facilitate tumor progression by enhancing angiogenesis, tumor growth, and invasion [429]. Given that the size of this layer can approach 0.5 μm in thickness while receptors are mostly less than 100 nm in size, the glycocalyx can act to control receptor interactions with their respective ligands [428,430]. Thus, the thickness of the glycocalyx can affect CTC adhesion to the endothelium, along with therapeutic ligand delivery to the surface of CTCs.

Herein, I discuss a range of potential effects on the vascular transport of CTCs due to the glycocalyx. First, the structure and composition of the glycocalyx, found on both endothelial cells and tumor cells, is reviewed. The factors that contribute to endothelial cell glycocalyx remodeling and disruption are then described, along with their subsequent effects on the adhesion of circulating cells. I conclude with novel therapeutic strategies for CTCs, the glycocalyx as a barrier for CTC drug delivery, and approaches to disrupt the glycocalyx for efficient therapeutic treatment of CTCs.

I.2 ENDOTHELIAL CELL GLYCOCALYX STRUCTURE

The structure of the endothelial cell (EC) glycocalyx is discussed here briefly, as this has been discussed in detail by others [428,430-432]. The glycocalyx is a thin, gel-like layer of glycoproteins on the apical surface of vascular endothelial cells, with an estimated thickness ranging from 150-500 nm [428] (Figure I.1A). Glycocalyx measurements are based on *in vivo* experimental observations by Vink & Duling [433] using intravital microscopy, electron microscopy (EM) studies by van den Berg et al. [434], and others [435-437]. The glycocalyx on the surface of postcapillary venules has been measured using capillary tube hematocrit, or the instantaneous volume fraction of postcapillary venules filled with red blood cells [438-440]. Reductions in the perfused capillary volume are indicative of the glycocalyx extending from the EC surface [433,441]. EM images by Squire et al. [442] showed that the EC glycocalyx brush structure has a characteristic spacing of 20 nm in all directions (Figure 1A). Computational models [443,444] and experimental observations [445,446] have shown that such spacing can act as a "molecular sieve" for plasma proteins, and thus create differences in plasma protein concentration between tissue and the luminal surface of the endothelium.

The glycocalyx on the EC surface primarily consists of glycosaminoglycans (GAGs), linear heteropolysaccharides that possess characteristic disaccharide unit repeats [447]. GAGs that comprise the EC glycocalyx include heparan sulfate, hyaluronan, and chondroitin sulfate [448]. Sulfated GAGs, specifically heparan sulfate and chondroitin sulfate, are linked to EC membrane-bound proteoglycans, which link

the glycocalyx to the actin cytoskeleton [442]. Proteoglycans are proteins that have specific sites to covalently link sulfated GAGs, and consist of transmembrane syndecans, membrane-bound glypicans, and matrix-localized perlecans [449]. Hyaluronan does not possess sulfated groups and is not covalently linked to proteoglycans; its interaction with the glycocalyx is mediated by cell surface receptors such as CD44, as well as by chondroitin sulfate chains [450]. Other important glycoproteins on the cell surface include adhesion receptors, such as integrins, immunoglobulins, and selectins [166]. Under normal physiological conditions, various bloodborne proteins will also incorporate into the EC glycocalyx [451].

I.3 TUMOR CELL GLYCOCALYX STRUCTURE

The tumor cell glycocalyx, much like that of ECs, consists of a variety of proteoglycans and glycosaminoglycans, in addition to fibrous proteins, such as collagen, which comprise the surrounding extracellular matrix [452]. The synthesis of hyaluronan in tumor cells, however, is frequently impaired during malignant transformation and can result in the excess production of hyaluronan [453-456] (Figure I.1B). In nontransformed cells, hyaluronan incorporates into the surrounding cell matrix by forming aggregates with hyaluronan-binding molecules, and can regulate cell adhesion, motility, growth, and differentiation. Hyaluronan synthase genes (HAS1, HAS2, and HAS3) encode key enzymes in hyaluronan synthesis, which can regulate the ability to form hyaluronan matrices and determine hyaluronan molecular size [457]. In tumor cells, however, expression of HAS genes is often

increased, resulting in excess hyaluronan production. Experiments forcing expression of HAS2 and HAS3 resulted in a drastic increase of hyaluronan production and subsequent tumorigenicity of mesothelioma, melanoma, and fibrosarcoma [458-460]. Additionally, transfection of HAS1 into mouse mammary carcinoma mutants rescued hyaluronan matrix production and metastatic potential [461]. Expression of hyaluronan cell surface receptor CD44 has also been shown to be increased in tumor cells [462,463] (Figure 1B). CD44+ cancer cells from head and neck squamous cell carcinoma can possess properties of cancer stem cells, including cancer stem cell renewal and differentiation [464]. CD44 variant isoforms are highly expressed in carcinomas of epithelial origin, and relate to tumor progression and metastatic potential of some cancers [465-467]. In addition to these components, tumor cells have a variety of cell and matrix adhesion molecules embedded in the glycocalyx, including integrins and selectin ligands [12,48].

To date, the circulating tumor cell (CTC) glycocalyx has not been well characterized. Paszek et al. recently developed scanning angle interference microscopy to measure variations in glycocalyx thicknesses of single epithelial cells on the nanometer scale [468]. This technique could be utilized to characterize the glycocalyx of CTCs. While typically associated with disease progression and poor prognosis, a significant number CTCs in blood are typically apoptotic [366,469]. This is in part due to anoikis, a form of programmed cell death that occurs due to the loss of cell-cell and/or cell-matrix adherence in CTCs [43]. This raises the intriguing possibility that viable CTCs that contribute to metastasis, which are typically characterized by the epithelial-mesenchymal transition (EMT) [470-472], can also retain their glycocalyx

and other matrix components. The glycocalyx coating could allow CTCs to evade anoikis or other forms of cell death due to harsh shear stress exposure in the circulation. In particular, clusters of CTCs known as circulating tumor microemboli (CTM) can retain their viability in part due to retention of glycocalyx, surrounding matrix components, and cell-cell adherence, in addition to processes such as EMT [471,473,474].

I.4 EC GLYCOCALYX EFFECTS ON CTC ADHESION

It is believed that CTCs can leave the bloodstream during hematogenous metastasis in a manner similar to leukocyte extravasation during the inflammatory response. In this process, cells initially tether and roll on the activated endothelium, followed by firm adhesion and subsequent transmigration through the blood vessel wall into inflamed tissue [15,52]. The initial tethering and rolling of leukocytes to ECs is mediated by E-, L-, and P-selectins binding to ligands on both the microvilli of leukocytes or the surface of ECs [91,278,475,476], with firm adhesion mediated by ICAM-1 and β_2 integrins on the EC and leukocyte surfaces, respectively [175,176]. E-selectin on the EC surface has also been shown to facilitate cancer metastasis in vivo [183,184]. Additionally, E-selectin can induce the rolling and tethering of cancer cells originating from breast [54,180], colon [180,182], and prostate [53,179] under flow.

The EC glycocalyx can control the spacing between E-selectin receptors on the EC surface and selectin ligands on CTCs, however its effects on CTC adhesion to the blood vessel wall has received less attention to date. Cell adhesion molecules on the

EC surface, such as ICAM-1 and selectins, can range in length from 20-40 nm [166,170]. However, the thickness of the glycocalyx can be several hundreds of nanometers, and thus affects receptor-mediated cell adhesion under physiological flow [428,477] (Figure I.2A). For example, Robert et al. utilized both computational and experimental models to measure the effect of the glycocalyx layer on the adhesion of functionalized microbeads to immobilized ICAM-1 under flow [478]. Using hyaluronan as a model glycocalyx, the frequency of adhesion to ICAM-1 under flow increased with decreasing concentrations of hyaluronan, along with an increase in the force between the bead and the substrate, and a decrease in the bead distance from the surface [478]. Multiple studies using leukocytes have shown that decreases in glycocalyx thickness directly correlate with increased cell adhesion [423,479,480].

Inflammation, exposure to extracellular proteases, and changes in hemodynamic shear stress can alter glycocalyx molecular composition and thickness (Figure I.2B), suggesting that such factors may promote or inhibit CTC-EC adhesion.

Glycocalyx remodeling during inflammation

The EC glycocalyx can be dramatically remodeled during inflammation, a process which is also critical to the progression of cancer metastasis [52,481]. *In vivo*, Henry and Duling found that exposure to proinflammatory cytokine tumor necrosis factor-α (TNF-α) can disrupt and increase the entry of macromolecules into the EC glycocalyx [482]. Mulivor and Lipowsky showed that superperfusion of the chemoattractant formyl-methionyl-leucyl-phenylalanine (fMLP) into rats induced

significant shedding of GAGs from the EC surface [483]. Treatment of postcapillary venules with either fMLP or heparinase increased exposure and availability of ICAM-1 on the EC surface [484], as measured by the perfusion and adhesion of fluorescent microbeads coated with antibodies specific for ICAM-1. In an *in vivo* model of septic shock, administration of bacterial endotoxins induced a significant increase in circulating glycocalyx degradation products such as heparan sulfate [485]. Pro-inflammatory low-density lipoproteins (LDL) have been shown to degrade the EC glycocalyx in postcapillary venules, as measured by increased capillary hematocrit [486]. There is also evidence that major cardiopulmonary bypass surgery can cause shedding of heparan sulfate and syndecan-1 from the EC glycocalyx of patients [487]. Given the increased thickness of the glycocalyx under normal physiological conditions, it is likely that inflammatory conditions promote CTC adhesion to the endothelium by both shedding and disruption of the EC glycocalyx, which increases the availability of EC cell adhesion molecules to CTCs.

Matrix metalloproteinase (MMP) effects on glycocalyx shedding

Extracellular proteases, such as matrix metalloproteinases (MMPs), can induce glycocalyx shedding and promote cell adhesion in the microvasculature (Figure I.2B). MMPs are a family of zinc-dependent enzymes that can regulate the turnover of the glycocalyx and other ECMs during processes including inflammation, wound healing, and tumor progression [52,488-490]. *In vivo*, arterial ECs show increased expression of MMPs in areas of atherosclerotic plaques and lesions [491,492]. MMPs have also

been found by Gronski et al. and Endo et al. to directly cleave chondroitin sulfate and proteoglycan syndecan-1, respectively [493,494].

Endothelial cells have the ability to store, activate, and release MMPs into the surrounding glycocalyx. Utilizing matrix metalloproteinase (MMPs) inhibitors, Fitzgerald et al. found that multiple cell signaling pathways can converge and activate MMPs, after PMA treatment, to cleave syndecans from the cell surface [495]. Taraboletti et al. found that human umbilical vein endothelial cells shed microvesicles from the plasma membrane, which contain active and pro-enzyme forms of MMP-2 and MMP-9 [496]. Yu et al. found evidence that both MMP-2 and MMP-9 can bind to heparan sulfate in the glycocalyx [497]. ECs were also found to utilize microvesicles to release tissue inhibitors of metalloproteinases (TIMPs), endogenous inhibitors which can regulate MMP activity [496]. Thus, shedding of the glycocalyx can in part be regulated by MMPs derived from the endothelium. Given that nearly all tumor cells overexpress MMPs [498], including MMP-2 and MMP-9 as mentioned previously, CTCs may also contribute to MMP-induced glycocalyx shedding.

Glycocalyx response to fluid shear stress

The EC glycocalyx is exposed to hemodynamic shear stresses ranging from 4.0-30.0 dyn/cm^2 and 0.5-4.0 dyn/cm^2 in the arterial and venous circulation, respectively [46]. Shear rates can range from approximately 900 s^{-1} in arteries to 160 s^{-1} in veins [159]. Exposure to such forces can affect the biosynthesis of EC glycocalyx components, activate EC-derived proteases, and disrupt glycocalyx structure and

molecular components [499]. *In vivo* studies by Mulivor and Lipowsky showed that induction of ischemia for 60 min led to an increase in glycocalyx thickness on the surface of the post-capillary venules [483], which then decreased upon reperfusion of the venules. Grimm et al. showed that exposure to low shear stress (1.0 dyn/cm^2) inhibited GAG synthesis in cultured ECs, while Arisaka et al. showed that greater shear stresses (>15.0 dyn/cm^2) stimulated the synthesis of GAGs in ECs [499]. Zeng et al. found that specific components of the EC glycocalyx, such as heparan sulfate, can cluster at endothelial cell junctions through the mobility of glypican-1 in lipid rafts [500]. Other components, such as chondroitin sulfate and syndecan, remained immobilized on the EC glycocalyx [500]. Koo et al. measured the components of the glycocalyx after human EC exposure to shear stress waveforms characteristic of atherosclerosis-resistant and atherosclerosis-susceptible regions of the arteries [501]. Glycocalyx components increased in expression and were distributed evenly on the EC surface after exposure to atherosclerosis-resistant waveforms, but was irregularly distributed and decreased in expression upon exposure to atherosclerosis-susceptible waveforms [501].

In the tumor microenvironment, blood vessels are characterized as disorganized, tortuous, leaky, and dilated [502]. While normal vessels typically branch via bifurcations with even branch diameters, the tumor vasculature can exhibit trifurcations and uneven branch diameters [502], all of which can dramatically alter the local shear stress environment. Proliferating tumor cells can also exert solid stresses on the surrounding vasculature, causing blood and lymphatic vessels to collapse and inducing heterogeneous blood flows and subsequent shear stresses

[23,503]. Given that fluid shear stress can affect glycocalyx thickness and composition, it is likely that alterations are also seen in the cancer microenvironment. Such shear-induced effects on the EC glycocalyx have not been previously characterized, and could provide new insight into the vascular transport of CTCs.

Glycocalyx effects on leukocyte adhesion

Like CTCs, leukocytes express selectin ligands that facilitate their adhesion to the endothelium. Given that selectins on the EC surface do not extend as far from the EC surface as the glycocalyx, it is likely that inflammatory conditions, MMP exposure, and fluid shear forces can remodel the glycocalyx to promote the adhesion of circulating cells. A theoretical model was developed by Zhao et al. to examine how fluid shear forces can amplify the penetration forces of leukocyte microvilli into the EC glycocalyx [422]. Leukocyte microvilli range from 0.3 to 0.7 μm in length, which can place leukocytes within a reactive distance of selectins of the EC surface [504]. The model predicts that physiological shear forces can amplify the gravitational contact forces of leukocytes by almost two orders of magnitude to 100 pN, which can allow leukocyte microvilli to penetrate the EC glycocalyx [422].

In vivo, TNF-α is found to disrupt the glycocalyx of postcapillary venules, decrease leukocyte rolling velocity, and increase the number of adherent leukocytes [482]. Treatment with the P-selectin antagonist fucoidan both reduced the number of adherent leukocytes and increased the average leukocyte rolling velocity, demonstrating that TNF-α-induced glycocalyx disruption enhances selectin-mediated

leukocyte adhesion [482]. Superperfusion of the rat mesentery with fMLP increased glycocalyx shedding in a process mediated by EC G-protein signaling [483], increasing exposure of EC adhesion receptors and subsequent leukocyte adhesion [484]. Treatment of mouse cremaster venules with the enzyme heparitinase degraded heparan sulfate from the EC glycocalyx, and increased the number of leukocytes adhered to the venules [505]. Doxycycline, a member of the tetracycline antibiotics, is a broad spectrum MMP inhibitor that was recently shown to both promote and inhibit leukocyte adhesion [506,507]. Superperfusion of rat mesentery with doxycycline alone increased baseline levels of leukocyte adhesion by reducing sheddase activity and subsequent cleavage of adhesion molecules [506]. However, treatment with fMLP followed by doxycycline significantly reduced leukocyte adhesion compared to treatment with fMLP alone, indicating the doxycycline treatment can also inhibit fMLP-induced glycocalyx shedding and reduce the availability of EC adhesion molecules [506].

Under normal physiological conditions, the thick EC glycocalyx can serve as a physical barrier that prevents the adhesion of immune cells and CTCs (Figure I.2A). This barrier can be compromised by a variety of factors, including pro-inflammatory molecules, MMPs, and fluid shear stress. Given that many CTCs present selectin ligands similar to leukocytes, it is expected that glycocalyx shedding and disruption may exert similar effects on the adhesion of CTCs (Figure I.2B). However, CTCs can differ greatly from leukocytes in terms of size, morphology, selectin ligand expression, deformability, and membrane composition [48,508-514]. Additionally, CTCs can possess glycocalyx components such as chondroitin sulfate GAGs, which

serve as major P-selectin ligands on metastatic breast cancer cells [515].Thus, the effects of glycocalyx thickness and composition on CTC adhesion and subsequent formation of distant metastases is not fully elucidated and deserves further study.

I.5 GLYCOCALYX EFFECTS ON THERAPEUTIC TREATMENT OF CTCs

CTC-targeted therapies

Therapeutic treatment of CTCs in blood can potentially hinder the vascular transport of CTCs to anatomically distant organs, and prevent the onset of metastasis. Recently, novel approaches to both target and treat CTCs within the bloodstream have been developed [516]. E-selectin is currently being explored to target therapeutics to CTCs under blood flow conditions, due to the rapid, force-dependent binding kinetics between E-selectin and selectin ligands on CTCs [335] (Figure I.3). Our group recently developed an approach to deliver doxorubicin-containing E-selectin conjugated nanoparticles to flowing tumor cells [82,83]. Doxorubicin is an adriamyacin anthracycline antibiotic that is utilized as a chemotherapeutic agent, which can induce tumor cell death by DNA-intercalation, inhibition of topoisomerase-II, and formation of free radicals [88,89,368]. Under physiological shear stresses, tumor cells rapidly bound to E-selectin conjugated nanoparticles, as confocal microscopy revealed fluorescent nanoparticles decorating the tumor cell surface [82]. Doxorubicin-loaded nanoparticles were subsequently internalized by tumor cells, and induced significant cell death.

The use of tumor necrosis factor (TNF)-related apoptosis-inducing ligand (TRAIL) to induce apoptosis in circulating cancer cells has recently been investigated. TRAIL binds to trimeric death receptors DR4 and DR5 on the surface of a variety of tumor cells, and subsequently signals for apoptosis [84]. TRAIL is an ideal therapeutic for CTCs because it does not exert toxic effects on most normal cells, with the exception of hepatocytes [87,424]. Thus upon delivery to the bloodstream, TRAIL would likely have negligible effects on circulating cells such as erythrocytes and leukocytes. Utilizing immobilized E-selectin and TRAIL, Rana et al. created novel surfaces to both capture and deliver apoptotic signals to flowing cancer cells [84,85]. Cancer cells exhibited rolling adhesion on E-selectin, and subsequently interacted with immobilized TRAIL on the surface to induce apoptosis [84]. Combination therapy of aspirin pretreatment followed by perfusion over E-selectin/TRAIL surfaces sensitized tumor cells to TRAIL-induced apoptosis, significantly increasing the number of apoptotic tumor cells compared to cells exposed to E-selectin/TRAIL surfaces alone [85]. Mitchell et al. assessed the effects of physiological shear stress exposure on TRAIL-induced apoptosis of tumor cells. Fluid shear stress exposure of 2.0 dyn/cm^2 nearly doubled the amount of apoptotic cancer cells in the presence of TRAIL, compared to TRAIL-treated cells exposed to static conditions [86]. Interestingly, the response was found to be TRAIL-specific, as shear forces did not sensitize cancer cells to doxorubicin-induced apoptosis [86].

Glycocalyx as a therapeutic barrier

Increased expression of hyaluronan on the tumor cell glycocalyx can hinder the delivery of therapeutics. High expression levels of hyaluronan can create a hydrated connective tissue matrix, which can attach to the tumor cell surface via CD44 to form a protective coating around the cell [517]. This coating may limit therapeutic efficacy by providing a cover over drug binding sites on cancer cells (Figure I.4), along with attenuating the diffusion of drug molecules to the cell surface. Brekken et al. found that increased production of hyaluronan increased interstitial fluid pressure in solid tumors, which can limit the delivery of therapeutics via the circulation by collapsing nearby blood vessels [23,503] and eliminating pressure difference-driven transport of therapeutics toward the tumor interior [518]. To quantify glycocalyx effects on the diffusion of drugs to tumor cells, Eikenes et al. measured the diffusion of fluorescein isothiocyanate (FITC)-conjugated dextran macromolecules through the glycocalyx using fluorescence recovery after photobleaching (FRAP) based on two-photon scanning laser excitation [519]. The diffusion coefficient of 150-kDa FITC dextran molecules decreased in tumor spheroids, and even more so in human osteosarcoma xenografts, in part due to the presence of hyaluronan [519]. The delivery of drugs such as docetaxel and liposomal doxorubicin to PC-3 tumors was reduced, due to the accumulation of hyaluronan [520]. Pályi-Krekk et al. investigated the role of hyaluronan and CD44 in trastuzumab resistance [521,522]. Trastuzumab is a recombinant humanized anti-ErbB2 antibody used in the treatment of breast cancer, however the mechanisms of resistance are poorly understood [521]. CD44 was found

to be overexpressed in the trastuzumab-resistant cell line JIMT-1, and flow cytometry fluorescence resonance energy transfer (FRET) measurements showed that CD44 interacts with ErbB2 [521]. In mouse JIMT-1 xenografts, CD44 enhanced trastuzumab internalization while hyaluronan blocked the availability of ErbB2 to bind to trastuzumab, implicating the CD44-hyaluronan complex in the attenuation of receptor-mediated therapy of tumor cells [521].

Tumor cell glycocalyx-targeted treatments

The use of glycocalyx-degrading enzymes, such as hyaluronidases, have been explored as agents to degrade the glycocalyx coating and subsequently increase therapeutic diffusion and uptake to tumor cells. Early work by Brekken et al. investigated the effects on hyaluronidase on interstitial fluid pressure in solid tumors [518]. Intratumoral injections of bovine testicular hyaluronidase reduced interstitial fluid pressure of solid tumors up to 40%, 60 min post-injection [518]. Hyaluronidase treatment increased the diffusion of FITC-conjugated dextran macromolecules in human osteosarcomas grown as tumor spheroids and in tumor tissue *in vivo*, as measured using FRAP [519]. In terms of therapeutic delivery, hyaluronidase-treated orthotopic tumors increased the uptake and distribution of liposomal doxorubicin [523]. Thompson et al. utilized recombinant human hyaluronan-degrading enzyme rHuPH20 to deplete HA from the tumor cell surface, but found that its short serum half-life (< 3 min) made *in vivo* use impractical [520]. However, PEGlyation of rHuPH20 (PEGPH20) increased the serum half-life to over 10 h, depleted hyaluronan,

decreased interstitial fluid pressure by 84%, and decompressed tumor blood vessels [520]. PEGPH20 treatment increased the activity of both liposomal doxorubicin and docetaxel in PC-3 tumors.

Given its physiological role and its presence throughout the human body, systemic administration of hyaluronidase could have unwanted side effects. Enzymatic degradation via hyaluronidase can induce inflammation and pain in joints, and its pH sensitivity and short half life in serum makes it difficult to efficiently administer [524]. To combat this, Yang et al. recently developed oligosaccharides of hyaluronan (oHA)-lipid-paclitaxel nanoparticles to breach the glycocalyx barrier for therapeutic delivery [525]. oHA is broken down from hyaluronan by hyaluronidase, possesses binding sites for CD44, and can act as an antagonist of CD44 interactions [526,527]. Additionally, due to its small size, oHA nanoparticles are able to breach through the glycocalyx barrier to access CD44 receptors. Upon treatment with oHA, the glycocalyx of MDA-MB-231 and BT-249 breast cancer cells was disrupted via oHA interactions with CD44, and subsequent detachment of hyaluronan from the cell surface [525]. Compared to treatment with lipid-paclitaxel nanoparticles alone, which induced apoptosis in approximately 30% of both breast cancer cell lines, the addition of oHA to nanoparticles extended apoptosis to over 90% of cells [525]. The efficacy of the approach was also confirmed *in vivo* using a mouse xenograft model [525].

Surprisingly, little is known about CTC glycocalyx thickness and composition, and subsequent glycocalyx-mediated CTC resistance to therapeutics. While CTCs in blood are frequently apoptotic [469], it is possible that those that metastasize to anatomically distant organs have distinct survival advantages through retention of

their glycocalyx. The glycocalyx can allow CTCs to evade anoikis, while also providing a barrier for therapeutics to bind to cell surface receptors [43]. In particular, CTC therapeutic strategies involving E-selectin targeting and TRAIL-induced apoptosis can be affected by the presence of a CTC glycocalyx layer by blocking interactions with E-selectin ligands and death receptors on CTCs. Glycocalyx-degrading enzymes can thus increase the availability of CTC ligands for therapeutic purposes. In contrast, if CTCs that remain viable do not possess a glycocalyx layer, then targeting mechanisms utilizing E-selectin can provide an efficient method to localize therapeutic ligands to the CTC surface under physiological flow conditions. Future work should focus on direct glycocalyx measurements on CTCs, tumor cell-specific glycocalyx-degrading enzymes to increase the availability of drug binding sites, and subsequent therapeutic treatment of CTCs.

I.6 CONCLUSION

The transport of CTCs via the bloodstream can be altered due to the presence of the glycocalyx expressed on ECs and CTCs. On surface of ECs, the glycocalyx can act a barrier to prevent interactions between adhesion receptors on ECs and ligands on the CTC surface. Inflammation, MMPs, and changes in fluid shear stress can act to disrupt, remodel, and induce shedding of the glycocalyx. These factors can increase the availability of adhesion receptors on the EC surface, which in turn may promote CTC adhesion to the endothelium. Similar adhesive interactions can be utilized to target therapeutics to CTCs, such as apoptosis-inducing ligands, to potentially reduce

the spread of metastasis. However, overexpression of hyaluronan leads to the formation of thicker glycocalyx coating around tumor cells, providing a "shield" against therapeutic ligand delivery to the cell surface. Recent advances that aim to disrupt glycocalyx adhesion to the tumor cell surface provide a means to more effectively deliver therapeutic agents to CTCs. A better understanding of the factors that disrupt the EC glycocalyx to promote tumor cell adhesion, along with strategies to breach CTC therapeutic barriers, will lead to greater control and potential intervention of CTC vascular transport.

FIGURE I.1: SCHEMATICS OF THE ENDOTHELIAL CELL AND TUMOR CELL GLYCOCALYX. Schematics of the endothelial cell (**A**) and tumor cell (**B**) glycocalyx (not drawn to scale). (**A**) Endothelial cell glycocalyx can extend 150-500 nm from the endothelial cell surface, with a typical spacing of 20 nm between glycocalyx components (adapted from Weinbaum et al. [528]). (**B**) Tumor cell glycocalyx consists of similar components, but is characterized by greater hyaluronan content, which is tethered to the tumor cell membrane by CD44.

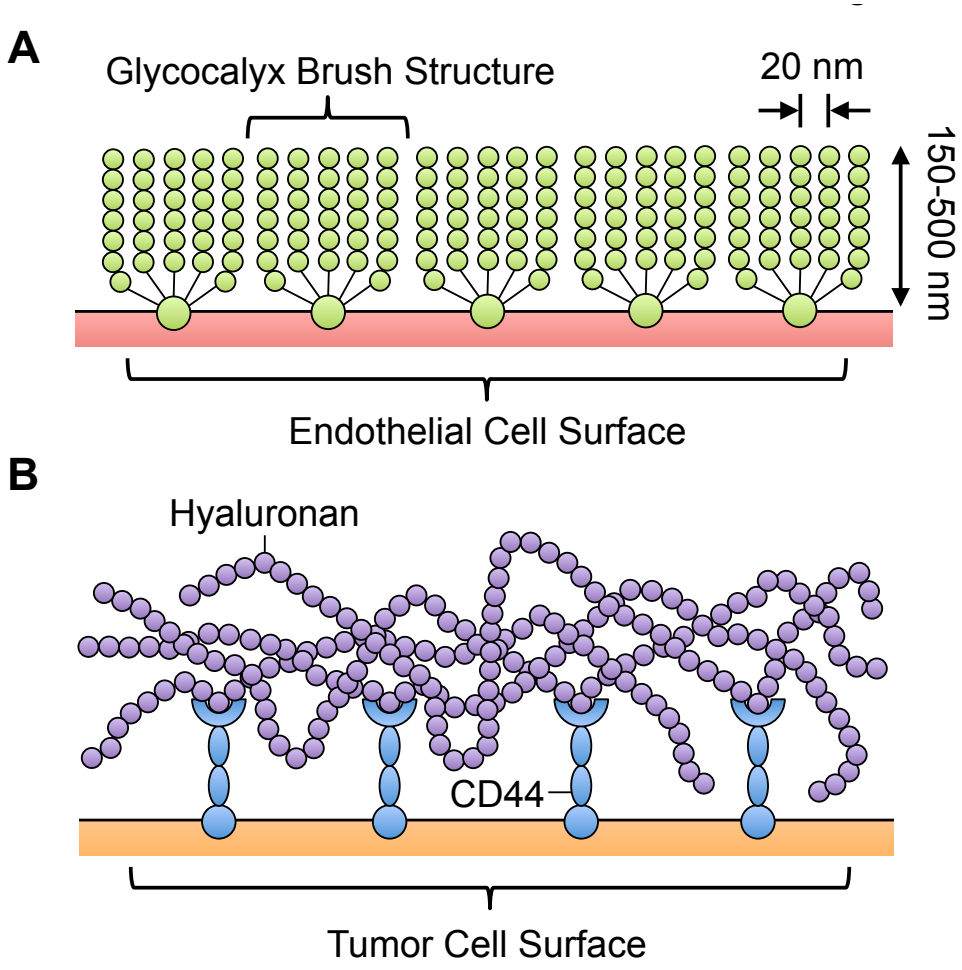

FIGURE I.2: GLYCOCALYX EFFECTS ON CIRCULATING TUMOR CELL (CTC) ADHESION IN THE MICROVASCULATURE. Glycocalyx effects on circulating tumor cell (CTC) adhesion in the microvasculature. (**A**) Under normal physiological conditions, the endothelial cell glycocalyx thickness is greater than the length of most adhesion receptors, and acts as a barrier to cell adhesion. (**B**) Alterations in shear stress, inflammatory conditions, and matrix metalloproteinase (MMP) exposure can cause shedding and/or remodeling of the glycocalyx, increasing the number of available receptors to bind to adhesion ligands on CTCs.

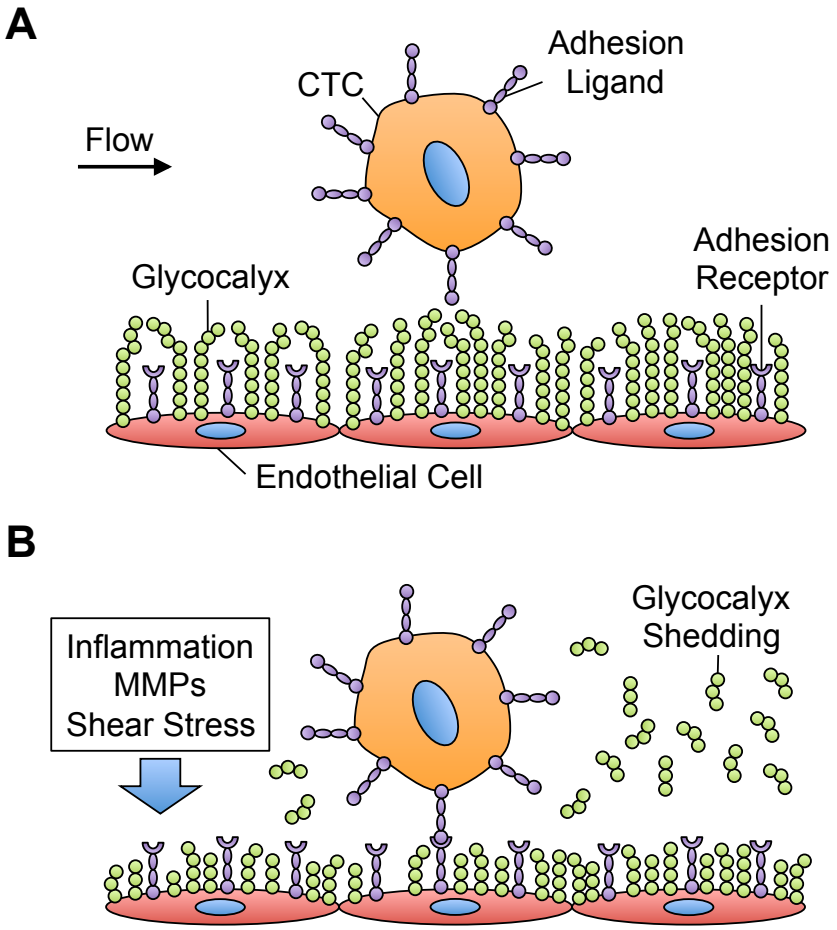

FIGURE I.3: E-SELECTIN MEDIATED DELIVERY OF THERAPEUTICS TO CIRCULATING TUMOR CELLS (CTCS) IN THE BLOODSTREAM. Under physiological flow conditions, E-selectin conjugated nanoparticles can rapidly bind to E-selectin ligands on the CTC surface. This adhesive interaction can be utilized to deliver a variety of therapeutic ligands or small molecules to CTCs, which can then induce CTC apoptosis.

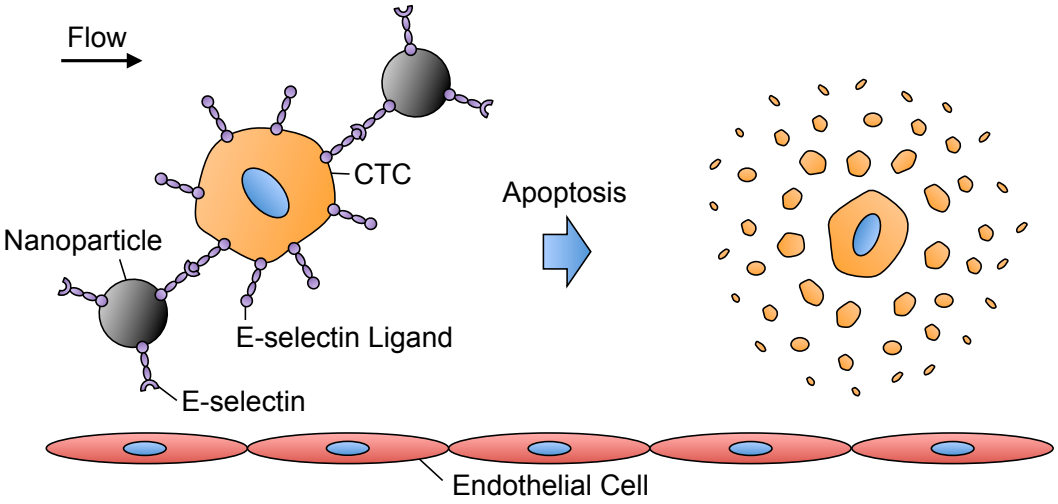

FIGURE I.4: GLYCOCALYX AS A BARRIER TO THERAPEUTIC DELIVERY. Overexpression of glycocalyx components, such as hyaluronan, can create a molecular barrier to "shield" therapeutic-binding receptors from interaction with therapeutic ligands.

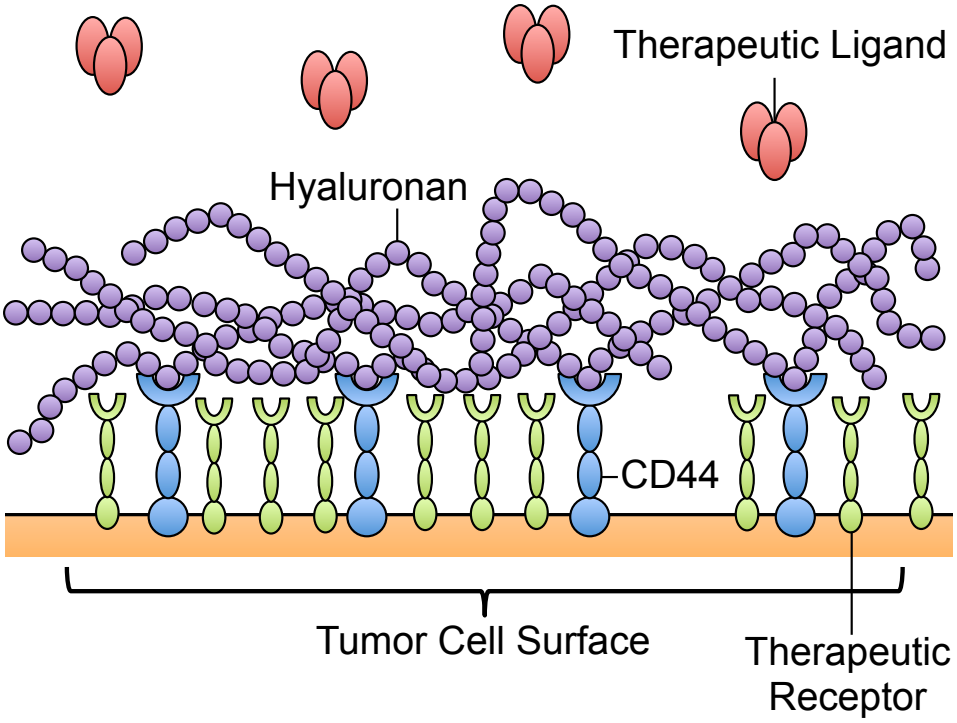

APPENDIX II: MILLISECOND PULSES OF FLUID SHEAR STRESS SUPPRESS CHEMOATTRACTANT-INDUCED NEUTROPHIL ACTIVATION

II.1 INTRODUCTION

Fluid shear stress (FSS) is a ubiquitous component of the microenvironment for leukocytes, as they carry out the physiological processes of initial adhesion to the endothelium, the formation of pseudopods, and migration into tissues [176]. Our lab has recently shown that leukocytes exposed to low venular fluid shear stresses (0.1-4.0 dyn/cm^2) develop a resistance to chemoattractant-induced activation [91]. However, leukocytes can transiently encounter FSS values >1000 dyn/cm^2 in the heart, near the walls of large blood vessels, and at vessel bifurcations. Herein, we evaluated the effect of millisecond FSS pulses on the neutrophil response to chemoattractants.

II.2 MATERIALS AND METHODS

Neutrophils isolated from peripheral human blood following informed consent were exposed to 1-10 millsecond FSS pulses via perfusion through microscale conduits using a high-pressure syringe pump, followed by exposure to the chemoattractant formyl-methionyl-leucyl-phenylalanine (fMLP, 10 nM) or tumor necrosis factor alpha (TNF-alpha, 20 nM). Expression and spatial distribution of L-selectin, activated $\alpha_M\beta_2$ integrins, and formyl peptide receptors (FPR) were analyzed using flow cytometry and confocal microscopy. Neutrophil morphology and the appearance of pseudopods were imaged using brightfield and phase contrast microscopy, with images used to measure neutrophil shape factor using an edge detection function.

II.3 RESULTS AND DISCUSSION

In the absence of fMLP stimulation (Figure II.1), neutrophils exhibited minimal activation when exposed to either static conditions or 5 millisecond FSS pulses (wall shear stress (WSS) = 5920 dynes/cm^2, exposure time = 1.08 ms). Neutrophil samples exposed to static conditions followed by 10 nM fMLP stimulation resulted in a 36% loss of L-selectin and 34% $\alpha_M\beta_2$ integrin activation (Figure II.1). However, neutrophil exposure to 5 millisecond FSS pulses followed by stimulation with 10 nM fMLP reduced L-selectin loss to 16%, and $\alpha_M\beta_2$ integrin activation to 9% (Figure II.1). No significant difference in L-selectin shedding and $\alpha_M\beta_2$ integrin activation was found between sheared and nonsheared neutrophils, whereas a significant reduction in fMLP-induced L-selectin shedding and $\alpha_M\beta_2$ integrin activation was found in neutrophils exposed to FSS pulses (Figure II.2). Neutrophil resistance to fMLP-induced activation was FSS pulse-dependent, as 5 pulses of FSS were required to induce neutrophil resistance to activation (Figure II.3).

To compare the effects of increasing shear stress exposure time versus increasing shear stress magnitude, the integral of shear stress magnitude over exposure time was kept constant, while either shear exposure time or shear stress magnitude was increased (Figure II.4). With a decrease in shear stress magnitude (5920 to 2960 dyn/cm^2) and increase in shear exposure time (1.08 to 2.16 ms), fMLP-induced neutrophil activation decreased, as indicated by decreased L-selectin shedding from 22% to 12%, and decreased $\alpha_M\beta_2$ integrin activation from 23% to 11% (Figure II.4). Further decreases in shear stress magnitude and increases in shear stress exposure time

decreased fMLP-induced neutrophil activation (Figure II.5), demonstrating that increasing shear stress exposure time has a greater effect on neutrophil resistance to fMLP-induced activation than increasing shear stress magnitude.

To assess the effect of fluid shear stress on non-G protein coupled receptors, neutrophils were exposed to millisecond shear stress pulses followed by incubation with 20 nM TNF-alpha, which binds to membrane bound receptors TNFR1 and TNFR2. Millisecond fluid shear stress pulses did not have a significant effect on TNF-alpha induced neutrophil activation, as compared to static controls (Figure II.6).

To determine the effect of millisecond fluid shear stress on fMLP-induced neutrophil morphological changes, neutrophils were fixed and imaged using brightfield microscopy. Based on contrast, neutrophils were thresholded (Figure II.7), and shape factor was calculated as detailed in Chapter 2. Preliminary results indicate that millisecond pulses of fluid shear suppress fMLP-induced morphological changes, as indicated by increased shape factor values for neutrophils pre-exposed to FSS followed by fMLP treatment (Figure II.8) compared to static samples exposed to fMLP. These results suggest that millisecond pulses of high FSS can decrease fMLP-induced neutrophil morphological changes.

II.4. CONCLUSION

We have shown that brief exposure to millisecond pulses of FSS can induce a mechanosensitive response in human neutrophils. Exposure to high FSS pulses reduce neutrophil activation in the presence of bacterial peptides, and likely serve as a

physiological regulator of neutrophil activation and invasion into tissues. Insight into the molecular basis of the neutrophil response can reveal important drug targets for inflammation and hemostasis.

FIGURE II.1: REPRESENTATIVE FLOW CYTOMETRY PLOTS OF FMLP-INDUCED NEUTROPHIL ACTIVATION AFTER EXPOSURE TO MILLISECOND FLUID SHEAR STRESS PULSES. Neutrophils exposed to static conditions or 5 submillisecond pulses of FSS (WSS= 5920 dyn/cm^2, pulse time = 1.08 ms) followed by 10 nM fMLP treatment. As indicators of activation, neutrophils were labeled for L-selectin expression and $\alpha_M\beta_2$ activation and analyzed using flow cytometry.

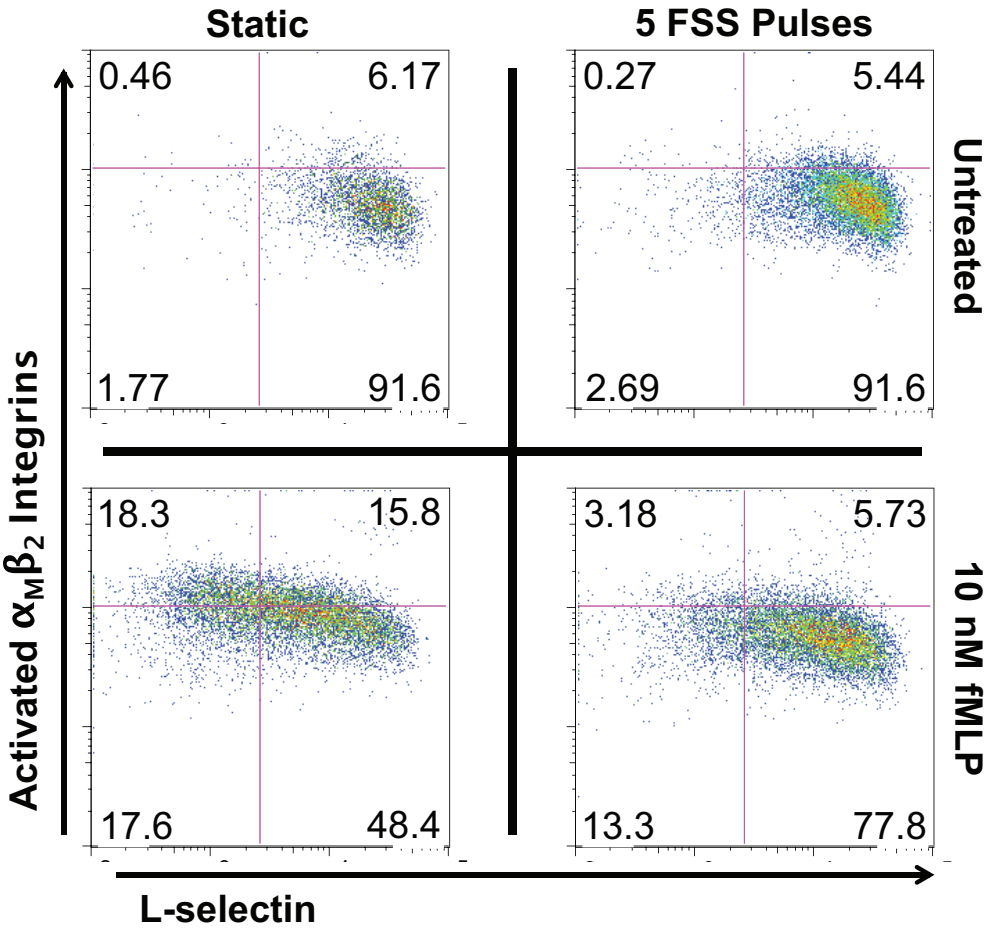

FIGURE II.2: MILLISECOND PULSES OF FLUID SHEAR STRESS SUPPRESS FMLP-INDUCED NEUTROPHIL ACTIVATION. Neutrophil L-selectin shedding and $\alpha_M\beta_2$ activation from n = 4 donors, when exposed to FSS (WSS= 5920 dyn/cm^2, pulse time = 1.08 ms) and/or 10 nM fMLP.

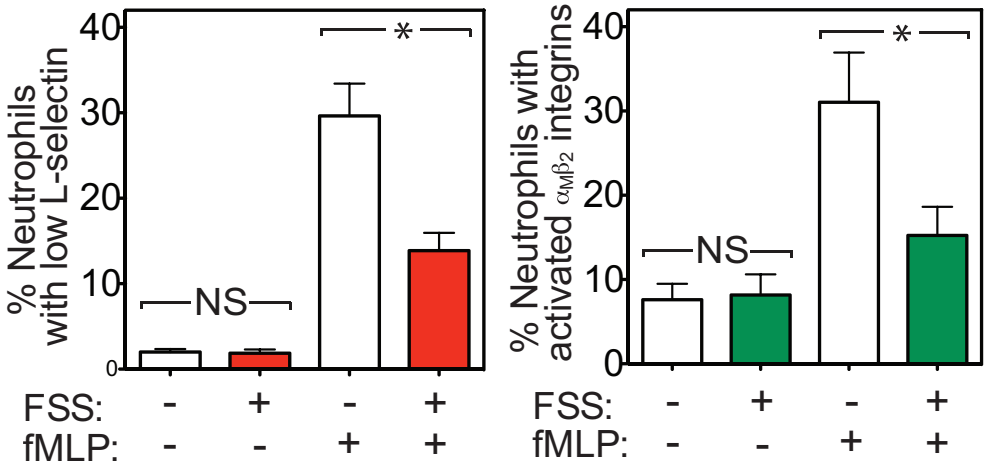

FIGURE II.3: SUPPRESSION OF FMLP-INDUCED NEUTROPHIL ACTIVATION IS FLUID SHEAR STRESS PULSE-DEPENDENT. Neutrophil fMLP-induced (10 nM fMLP) L-selectin shedding and $\alpha_M\beta_2$ activation after exposure to 1-10 millisecond FSS pulses (WSS= 5920 dyn/cm^2, pulse time = 1.08 ms).

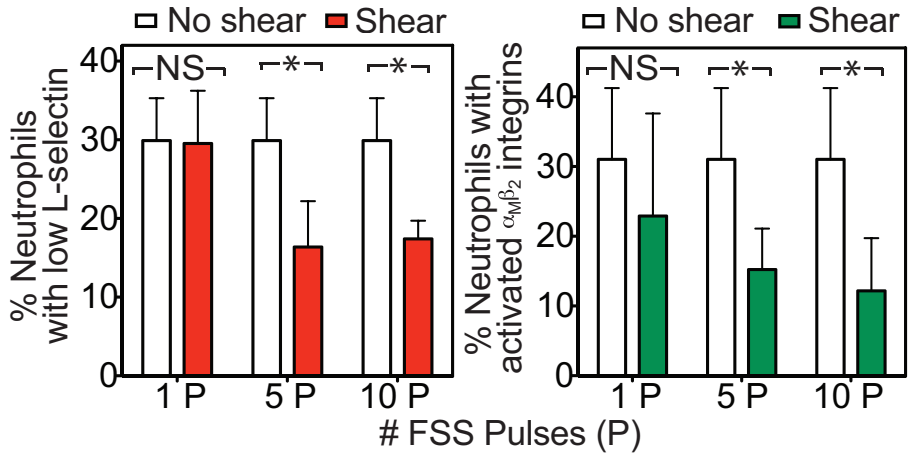

FIGURE II.4: DEPENDENCE OF SHEAR STRESS MAGNITUDE AND SHEAR STRESS EXPOSURE TIME ON FMLP-INDUCED NEUTROPHIL ACTIVATION. Neutrophil fMLP-induced (10 nM fMLP) L-selectin shedding and $\alpha_M\beta_2$ activation after exposure to FSS pulses of decreasing shear stress magnitude and increasing shear exposure time.

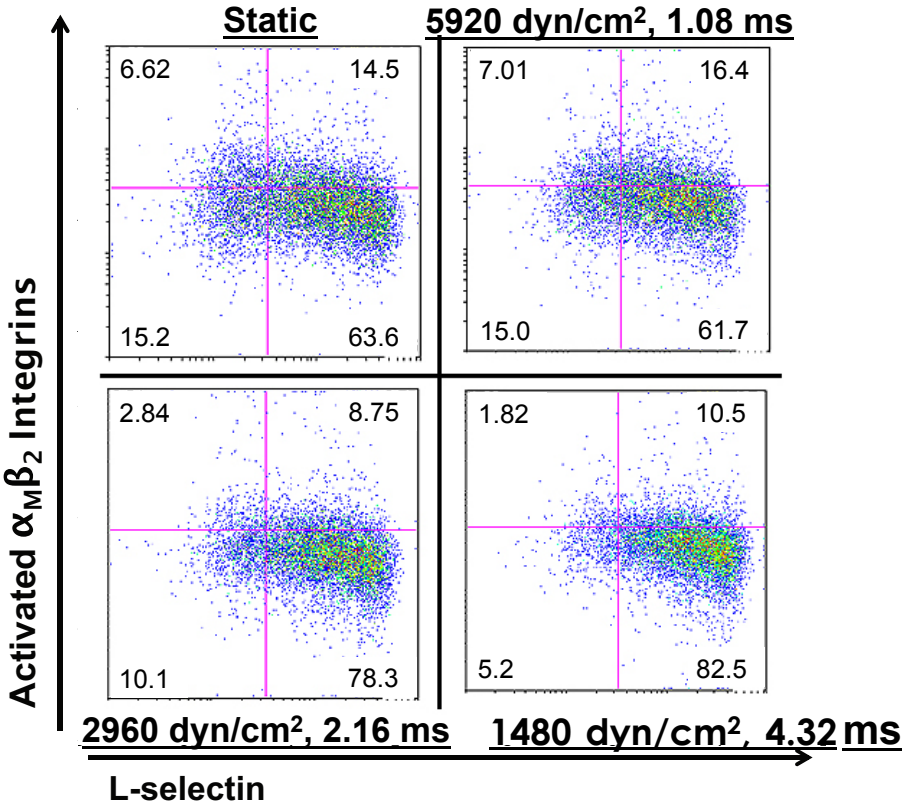

FIGURE II.5: SHEAR STRESS EXPOSURE TIME HAS A LARGER EFFECT ON NEUTROPHIL ACTIVATION SUPPRESSION THAN SHEAR STRESS MAGNITUDE. Neutrophil fMLP-induced L-selectin shedding and $\alpha_M\beta_2$ activation after exposure to FSS pulses of decreasing shear stress magnitude and increasing shear exposure time for n = 2 donors.

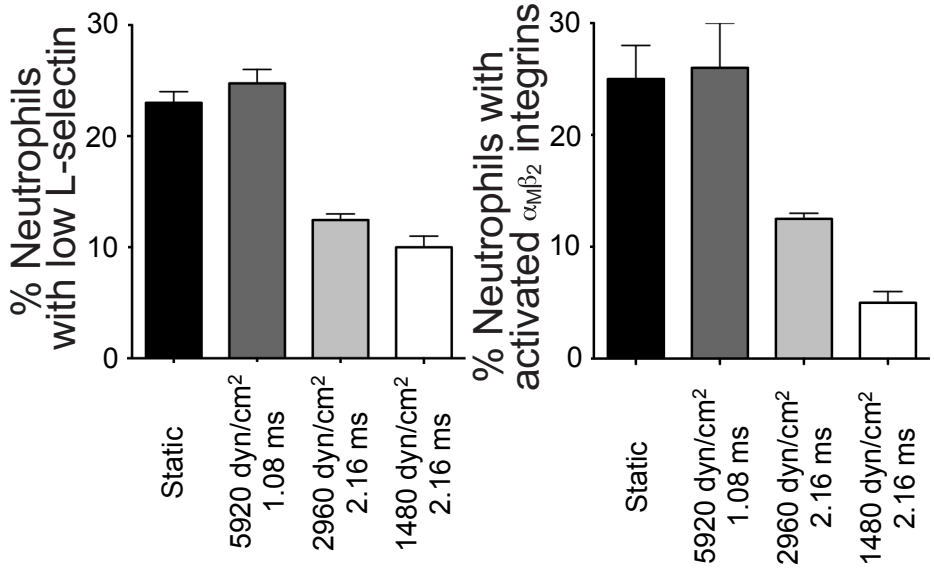

FIGURE II.6: EFFECT OF MILLISECOND FLUID SHEAR STRESS PULSE PRE-EXPOSURE ON TNF-ALPHA INDUCED NEUTROPHIL ACTIVATION. Neutrophils exposed to static conditions or 5 submillisecond pulses of FSS (WSS= 6400 dyn/cm^2, pulse time = 0.89 ms) followed by 20 nM TNF-alpha treatment (treated samples). As indicators of activation, neutrophils were labeled for L-selectin expression and $\alpha_M\beta_2$ activation and analyzed using flow cytometry.

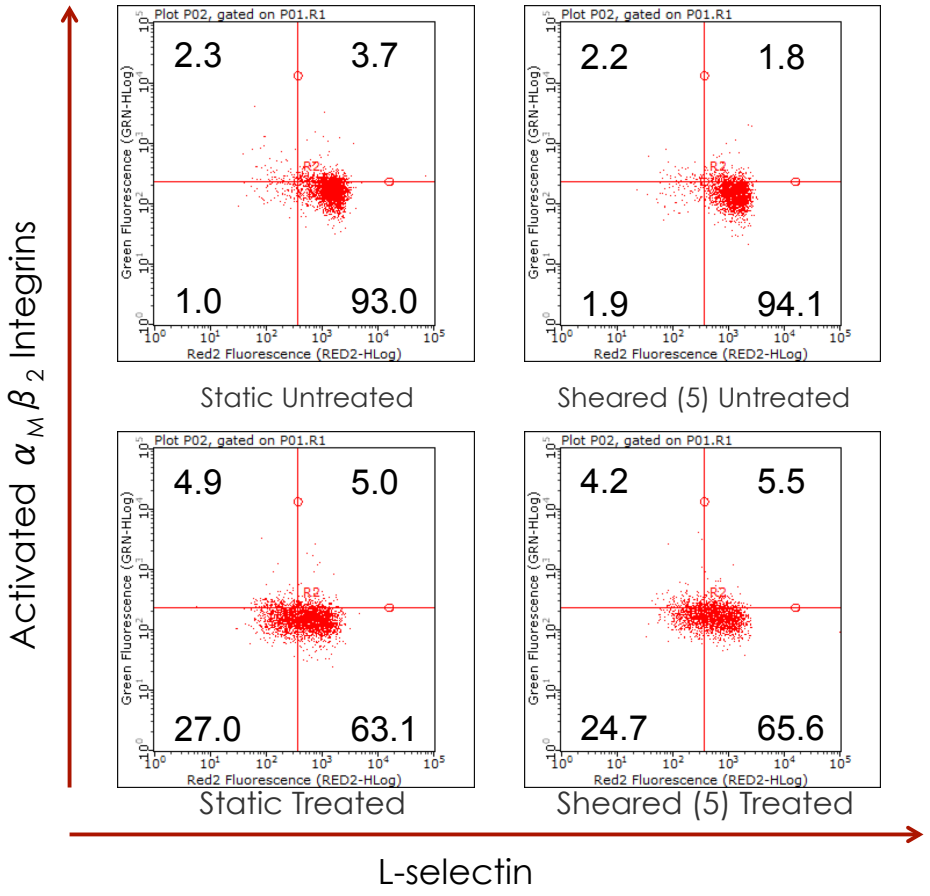

FIGURE II.7: REPRESENTATIVE NEUTROPHIL THRESHOLDING FOR SHAPE FACTOR CALCULATIONS. Neutrophils exposed to untreated static conditions or 10 nM fMLP were imaged using brightfield microscopy. Neutrophils were thresholded based on contrast, and utilized for shape factor calculations.

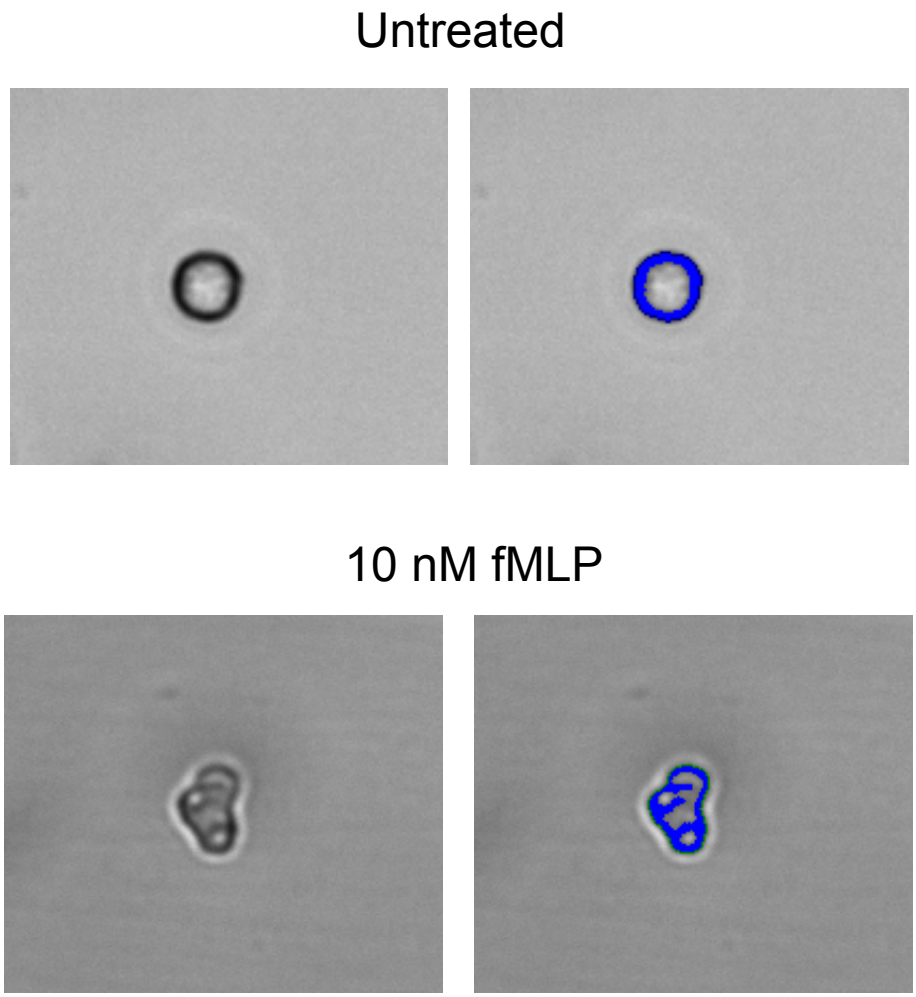

FIGURE II.8: SHAPE FACTOR CALCULATIONS OF NEUTROPHILS AFTER MILLISECOND SHEAR STRESS PULSE EXPOSURE AND FMLP TREATMENT. Neutrophils exposed to static conditions or 5 submillisecond pulses of FSS (WSS= 6400 dyn/cm^2, pulse time = 0.89 ms) followed by 10 nM fMLP treatment. Shape factors were calculated based on thresholded neutrophils.

Treatment	Shape Factor
Static, Untreated	0.895973
Static, Treated	0.812171
Sheared, Untreated	0.883005
Sheared, Treated	0.860058

APPENDIX III: LAMIN A/C DEFICIENCY REDUCES TUMOR CELL RESISTANCE TO FLUID SHEAR STRESS

III.1 INTRODUCTION

Metastasis is the cause approximately 90% cancer-related deaths [1,333]. Metastasis can involve the presence of circulating tumor cells (CTCs) in the bloodstream, which are believed to undergo an adhesion cascade similar to leukocytes. This process consists of a discrete sequence of steps involving tethering, rolling, and firm adhesion between CTCs and the inflamed endothelium [51,52]. Cancer cells from the primary tumor detach, invade the surrounding tissue, and intravasate into the bloodstream as CTCs [1,51,365,366]. Following intravasation, CTCs interact with the vasculature by selectin-mediated rolling and cell arrest, can extravasate into the tissue of anatomically distant organs and proliferate to form a secondary tumor [1,51,52]. Although only a small fraction of CTCs survive within the circulation [334,367], the development of metastases remains as the primary cause of cancer-related mortality.

Fluid shear stress is one of the key factors can affect the viability of cancer cells in the bloodstream. Cancer cells are exposed to fluid shear stresses in the bloodstream ranging from 1.0-4.0 dyn/cm^2 in the venous circulation and 4.0-30.0 dyn/cm^2 in arterial circulation [46]. Such shear stresses can affect cancer cell viability and thus the chances of metastasis. For example, B16 melanoma cell exposure to fluid shear stress in a cone-and-plate viscometer at shear rates greater than 300 s^{-1} induced a significant loss of cell viability [47].

Recently, a microfluidic protocol was developed to assess the cancer cell response to fluid shear stress [92]. In the protocol, dilute cancer cell suspensions were drawn up into a syringe, which is then loaded into an automatic syringe pump. Cancer cell

suspensions were exposed to brief, millisecond pulses of high fluid shear stress as they were expelled from the syringe pump, and subsequently analyzed for cell viability using bioluminescent imaging. The maximum fluid shear stress that cancer cells were briefly exposed to in this experiment reached 6400 dyn/cm^2. CTCs are momentarily exposed to shear stresses as high as 3000 dyn/cm^2 at vessel bifurcations, in the heart, and near the walls of large blood vessels [93,94]. Notably, it was found that malignant epithelial cells were more resistant to fluid shear stress than their non-malignant counterparts. However, the cellular structural components that contribute to this resistance remain poorly understood. Herein, were assessed the contribution of lamin A/C nuclear structural proteins to cancer cell resistance to fluid shear stress.

III.2 MATERIALS AND METHODS

Neutrophils isolated from peripheral human blood (following informed consent), metastatic breast cancer MDA-MB-231, and mammary breast MCF10A cell lines were labeled with a fluorescent BCECF viability dye and exposed to 1-10 millsecond FSS pulses (WSS: 5920 dyn/cm^2, Pulse time = 1.08 ms) via perfusion through microscale conduits using a high-pressure syringe pump (Figure III.1A). siRNA knockdown was utilized to create lamin A/C deficient MDA-MB-231 cancer cells from both heterogeneous and clonal populations for FSS pulse studies. To mimic physiological exposure to high FSS, cells were exposed to a pulse of high FSS once over a 90 s time period. Cells were placed into culture overnight for ~ 24 h, and the number of viable cells expressing BCECF was quantified via flow cytometry.

To characterize the mode of cell death, non-labeled cells were exposed to 10 pulses of high fluid shear stress (WSS: 5920 dyn/cm^2), placed back into culture for 90 min, and assessed for apoptosis and necrosis using a dual-labeling annexin-V/propidium iodide (PI) assay. Cell populations were gated based on viable cell controls. Lower left-hand quadrant (Annexin-V negative, PI negative) denotes viable cells. Upper left-hand quadrant (Annexin-V negative, PI positive) denotes necrotic cells. Lower right-hand quadrant (Annexin-V positive, PI negative) denotes early-apoptotic cells. Upper right-hand quadrant (Annexin-V positive, PI positive) denotes late-apoptotic cells.

III.3 RESULTS AND DISCUSSION

We initially compared the viability of primary leukocytes, malignant breast MDA-MB-231, and non-malignant MCF10A cell lines after exposure to pulses of high FSS (Figure III.1). Under static conditions, all cell types remained generally viable (Figure III.1B). However, malignant MDA-MB-231 cell viability was significantly higher than the viability of non-malignant MCF10A cells after exposure to pulses of high fluid shear stress (Figure III.1B). The response is fluid shear stress pulse-dependent, as MDA-MB-231 cells remained significantly more viable than MCF10A cells, which significantly decreased in viability with increased number of high FSS pulses (Figure III.1C). Leukocytes, which are typically exposed to high FSS in the circulation, remained generally viable throughout all experiments.

To assess the mode of cell death, MDA-MB-231 and MCF10A cells were assessed for apoptosis and necrosis using an Annexin-V assay. After FSS exposure, an increase in both apoptosis and necrosis was observed in both MDA-MB-231 and MCF10A cells (Figure III.2), compared to static controls. A significant increase in both apoptosis and necrosis was observed for non-malignant MCF10A cells exposed to pulses of high FSS, compared to malignant MDA-MB-231 cells exposed to high FSS (Figure III.3). Taken together, these results suggest that while cancer cell viability is decreased upon high FSS exposure, malignant epithelial cells are relatively more resistant to high FSS than their non-malignant epithelial counterparts.

To assess the role of lamin A/C nuclear structural proteins on cancer cell resistance to FSS, lamin A/C deficient MDA-MB-231 cancer cell lines (both clonal and heterogeneous populations) were developed via siRNA knockdown. All cell lines, including scambled controls, remained generally viable under static conditions, compared to parental cell line samples (Figure III.4). Upon exposure to pulses of high FSS, a significant decrease in cell viability was observed in lamin A/C deficient MDA-MB-231 cancer cell lines, both from clonal and heterogeneous populations, compared to scrambled and parental controls exposed to pulses of high FSS. The response is FSS pulse-dependent, as the viability of lamin A/C deficient MDA-MB-231 cancer cell lines from clonal and heterogeneous populations significantly decreased with increasing number of FSS pulses, compared to scrambled and parental controls (Figure III.5).

To assess the mode of cell death, lamin A/C deficient MDA-MB-231 cells were assessed for apoptosis and necrosis using an Annexin-V assay. FSS exposure

was found to induce both apoptosis and necrosis in lamin A/C deficient MDA-MB-231 cancer cells (Figure III.6). Interestingly, exposure to pulses of high FSS only induced a significant increase in apoptosis in lamin A/C deficient MDA-MB-231 cells, compared to scrambled and parental cell controls (Figure III.7). After exposure to pulses of high FSS, no significant differences in cell necrosis were observed between lamin A/C deficient MDA-MB-231 cells and controls (Figure III.7). Taken together, these results suggest lamin A/C deficiency can reduce tumor cell resistance to FSS, through an increase in cell apoptosis.

III.4 CONCLUSIONS

I have shown that high pulses of FSS can affect cancer cell viability, compared to normal blood cells that typically reside in the circulation. However, malignant epithelial cells were shown to be relatively resistant to pulses of high FSS compared to non-malignant epithelial cells. Cancer cell resistance to FSS is pulse-dependent, as cancer cell viability remained significantly higher than non-malignant epithelial cells with increased number of FSS pulses. Utilizing cancer cells deficient of the lamin A/C nuclear structural protein, it was shown that cancer cell viability significantly decreased upon exposure to FSS, due to an increase in cellular apoptosis. Thus, lamin A/C could play a key role in CTCs survival in the bloodstream, and subsequent formation of secondary tumors.

FIGURE III.1: TUMOR CELLS RESIST FLUID SHEAR STRESS-INDUCED CELL DEATH COMPARED TO NON-MALIGNANT EPITHELIAL CELLS. **(A)** Schematic of microscale conduit used to expose cells in suspension to millisecond pulses of high fluid shear stress. WSS: wall shear stress. L: length of microscale conduit. R: radius of microscale conduit. **(B)** Percentage of viable leukocytes, tumor cells (MDA-MB-231), and non-malignant epithelial cells (MCF10A) after exposure to static conditions (static) or 10 millisecond pulses of fluid shear stress (shear). All cell types were labeled with a cell viability dye (BCECF), exposed to fluid shear stress, and immediately placed back into culture for ~ 24 h. Viability determined via flow cytometry by number of cells expressing BCECF. WSS = 5920 dyn/cm^2. (**C**) Dose response of cells to fluid shear stress. Cell types were exposed to 0-10 pulses of fluid shear stress. $^{*}P < 0.05$. $^{**}P < 0.01$. NS: not significant. Data are mean ± SEM of three independent measurements.

FIGURE III.1: TUMOR CELLS RESIST FLUID SHEAR STRESS-INDUCED CELL DEATH COMPARED TO NON-MALIGNANT EPITHELIAL CELLS.

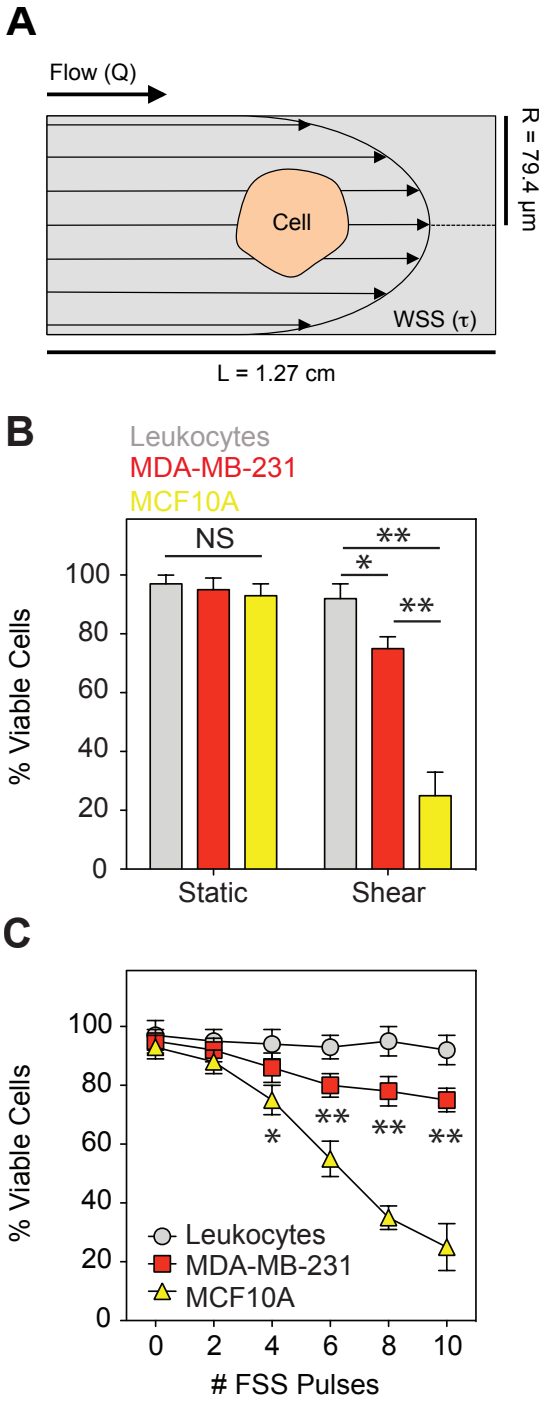

FIGURE III.2: EXPOSURE TO FSS INDUCES BOTH APOPTOTIC AND NECROTIC CELL DEATH IN MDA-MB-231 AND MCF10A CELLS. Cells were exposed to 10 pulses of high fluid shear stress (WSS: 5920 dyn/cm^2), placed back into culture for 90 min, and assessed for apoptosis and necrosis using an annexin-V/propidium iodide (PI) assay. (**A-D**) Annexin-V/propidium iodide (PI) flow cytometry plots of MDA-MB-231 (**A,C**) and MCF10A (**B,D**) cells exposed to static conditions (**A,B**) and millisecond pulses of fluid shear stress (**C,D)**. Lower left-hand quadrant (Annexin-V negative, PI negative) denotes viable cells. Upper left-hand quadrant (Annexin-V negative, PI positive) denotes necrotic cells. Lower right-hand quadrant (Annexin-V positive, PI negative) denotes early-apoptotic cells. Upper right-hand quadrant (Annexin-V positive, PI positive) denotes late-apoptotic cells.

FIGURE III.2: EXPOSURE TO FSS INDUCES BOTH APOPTOTIC AND NECROTIC CELL DEATH IN MDA-MB-231 AND MCF10A CELLS.

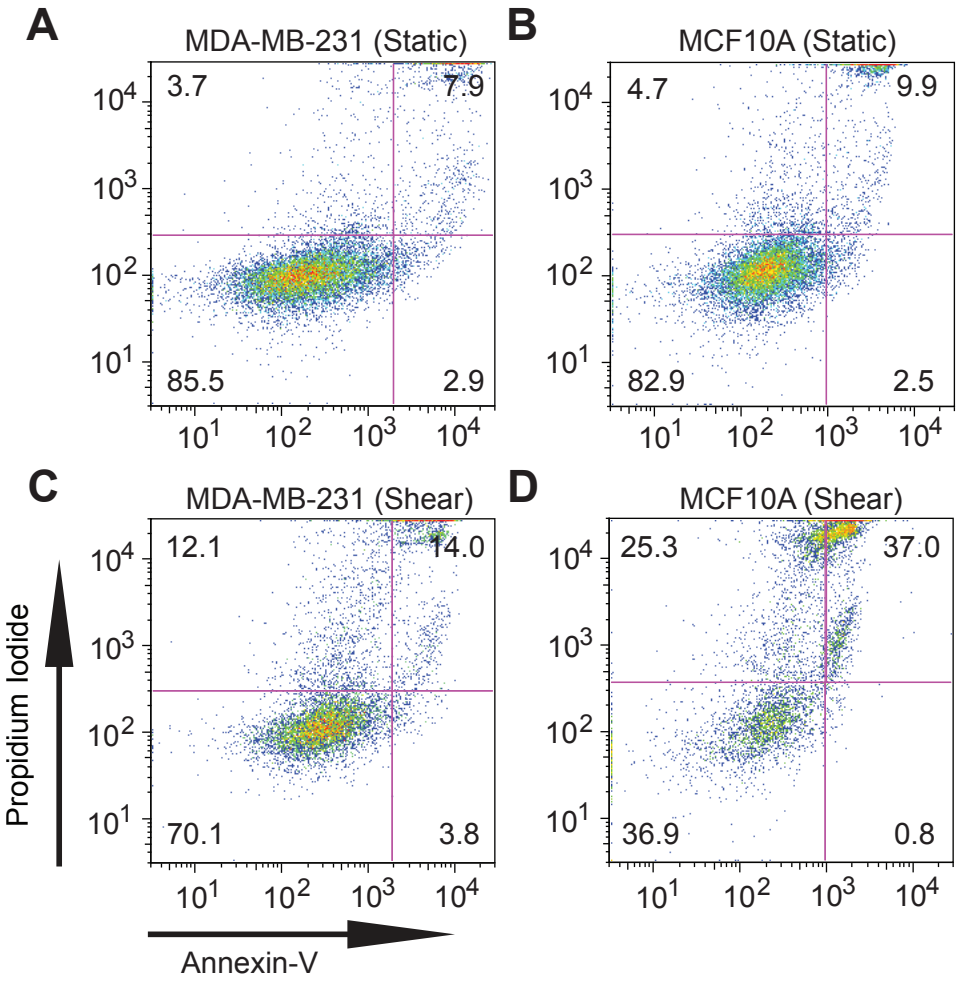

FIGURE III.3: DECREASED APOPTOSIS AND NECROSIS IN MALIGNANT MDA-MB-231 CELLS COMPARED TO NON-MALIGNANT MCF10A CELLS. Cells were exposed to 10 pulses of high fluid shear stress (WSS: 5920 dyn/cm^2), placed back into culture for 90 min, and assessed for apoptosis and necrosis using an annexin-V/propidium iodide (PI) assay. (**A**) Percentage of viable MDA-MB-231 and MCF10A cells after exposure to static conditions (static) or 10 pulses of high fluid shear stress (shear). (**B**) Percentage of apoptotic MDA-MB-231 and MCF10A cells after exposure to static conditions (static) or 10 pulses of high fluid shear stress (shear). (**C**) Percentage of necrotic MDA-MB-231 and MCF10A cells after exposure to static conditions (static) or 10 pulses of high fluid shear stress (shear). $^{*}P < 0.05$. NS: not significant. Data are mean ± SEM of three independent measurements.

FIGURE III.3: DECREASED APOPTOSIS AND NECROSIS IN MALIGNANT MDA-MB-231 CELLS COMPARED TO NON-MALIGNANT MCF10A CELLS.

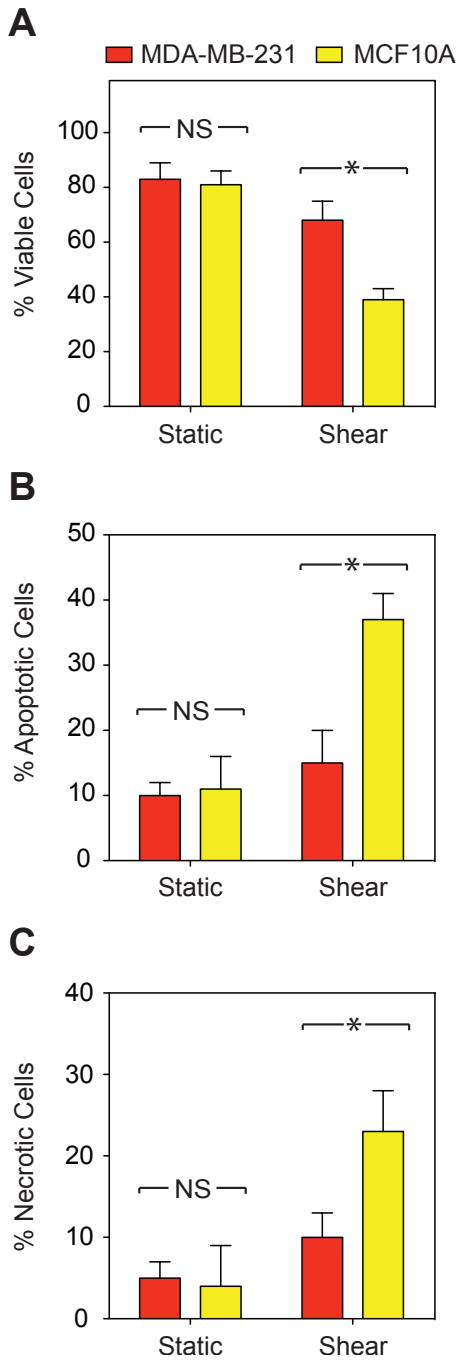

FIGURE III.4: LAMIN A/C DEFICIENCY REDUCES TUMOR CELL RESISTANCE TO FLUID SHEAR STRESS. Percentage of viable parental, clonal (scrambled and lamin A/C siRNA knockdown), and heterogeneous (scrambled and lamin A/C siRNA knockdown) populations of MDA-MB-231 cells after exposure to static conditions or 10 millisecond pulses of fluid shear stress. All cell types were labeled with a cell viability dye (BCECF), exposed to fluid shear stress, and immediately placed back into culture for ~ 24 h. Viability determined via flow cytometry by number of cells expressing BCECF. WSS = 5920 dyn/cm^2.

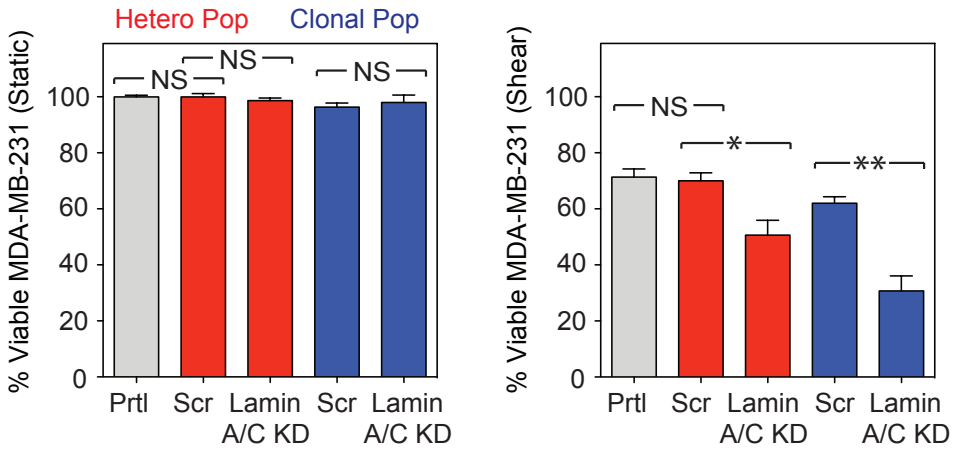

FIGURE III.5: FLUID SHEAR STRESS-INDUCED CELL DEATH IN LAMIN A/C-DEFICIENT MDA-MB-231 TUMOR CELLS IS FLUID SHEAR STRESS DOSE-DEPENDENT. Cell types were fluorescently tagged with a viability dye (BCECF) and exposed to 0-10 millisecond pulses of fluid shear stress (WSS = 5920 dyn/cm^2). Cells were placed back into culture for ~24 h and assessed for viability using flow cytometry. (**A**) Dose response of parental and heterogenous (scrambled and lamin A/C siRNA knockdown) populations of MDA-MB-231 cells to fluid shear stress. (**B**) Dose response of parental and clonal (scrambled and lamin A/C siRNA knockdown) populations of MDA-MB-231 cells to fluid shear stress. $^{*}P < 0.05$. $^{**}P < 0.01$. NS: not significant. Data are mean ± SEM of three independent measurements.

FIGURE III.5: FLUID SHEAR STRESS-INDUCED CELL DEATH IN LAMIN A/C-DEFICIENT MDA-MB-231 TUMOR CELLS IS FLUID SHEAR STRESS DOSE-DEPENDENT.

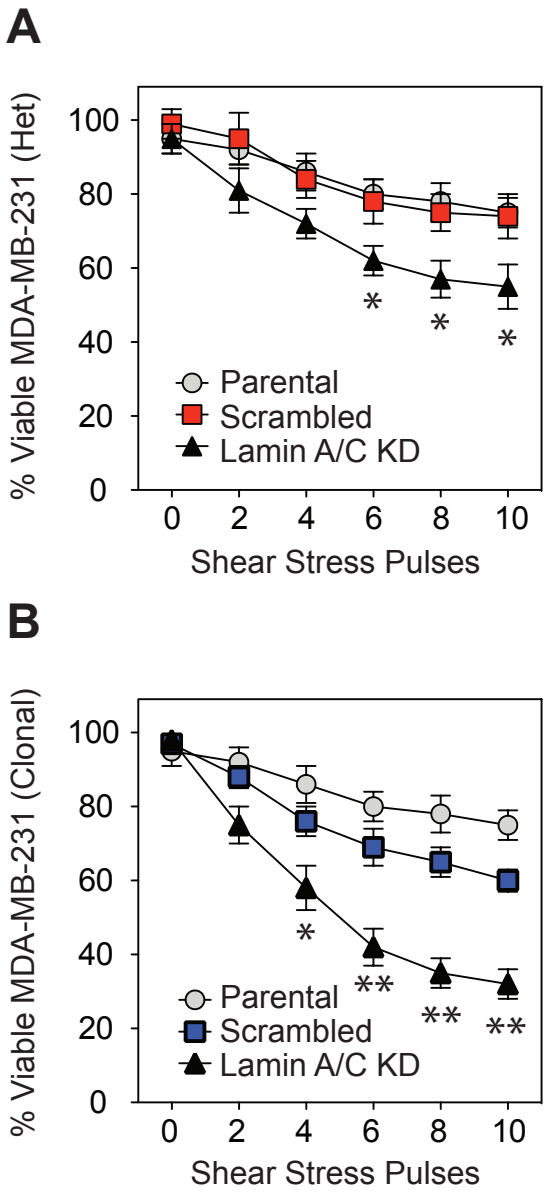

FIGURE III.6: EXPOSURE TO FSS INDUCES BOTH APOPTOTIC AND NECROTIC CELL DEATH IN LAMIN A/C-DEFICIENT MDA-MB-231 CELLS. Cells were exposed to 10 pulses of high fluid shear stress (WSS: 5920 dyn/cm^2), placed back into culture for 90 min, and assessed for apoptosis and necrosis using an annexin-V/propidium iodide (PI) assay. (**A-D**) Annexin-V/propidium iodide (PI) flow cytometry plots of scrambled (**A,C**) and lamin A/C-deficient (**B,D**) MDA-MB-231 cells derived a clonal population, exposed to static conditions (**A,B**) and millisecond pulses of fluid shear stress (**C,D)**. Lower left-hand quadrant (Annexin-V negative, PI negative) denotes viable cells. Upper left-hand quadrant (Annexin-V negative, PI positive) denotes necrotic cells. Lower right-hand quadrant (Annexin-V positive, PI negative) denotes early-apoptotic cells. Upper right-hand quadrant (Annexin-V positive, PI positive) denotes late-apoptotic cells.

FIGURE III.6: EXPOSURE TO FSS INDUCES BOTH APOPTOTIC AND NECROTIC CELL DEATH IN LAMIN A/C-DEFICIENT MDA-MB-231 CELLS.

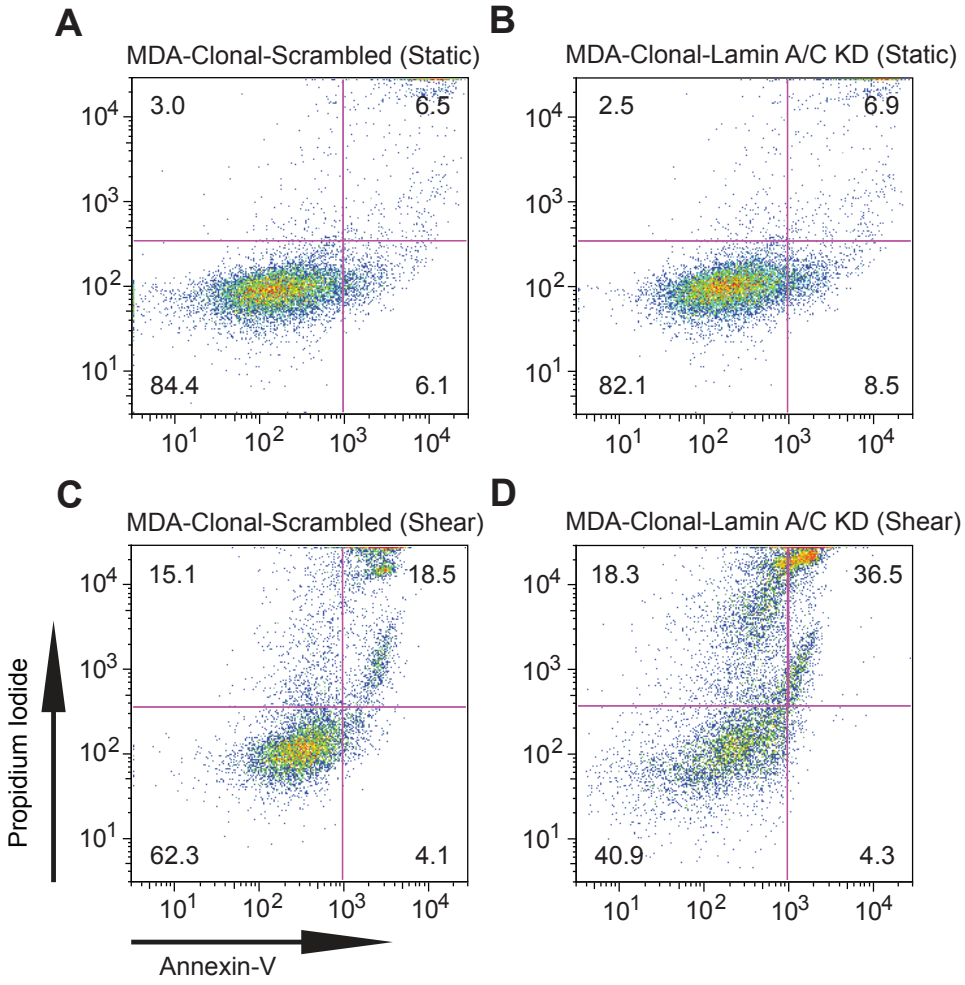

FIGURE III.7: INCREASED APOPTOSIS AND NECROSIS IN LAMIN A/C-DEFICIENT MDA-MB-231 TUMOR CELLS. Cells were exposed to 10 pulses of high fluid shear stress (WSS: 5920 dyn/cm^2), placed back into culture for 90 min, and assessed for apoptosis and necrosis using an annexin-V/propidium iodide (PI) assay. (**A,B**) Percentage of viable MDA-MB-231 cells after exposure to static conditions (**A**) or 10 pulses of high fluid shear stress (**B**). (**C,D**) Percentage of apoptotic MDA-MB-231 cells after exposure to static conditions (**C**) or 10 pulses of high fluid shear stress (**D**). (**E,F**) Percentage of necrotic MDA-MB-231 cells after exposure to static conditions (**E**) or 10 pulses of high fluid shear stress (**F**). Prtl: parental MDA-MB-231 cell population. Scr: scrambled MDA-MB-231 cell population. $^{*}P < 0.05$. NS: not significant. Data are mean ± SEM of three independent measurements.

FIGURE III.7: INCREASED APOPTOSIS AND NECROSIS IN LAMIN A/C-DEFICIENT MDA-MB-231 TUMOR CELLS.

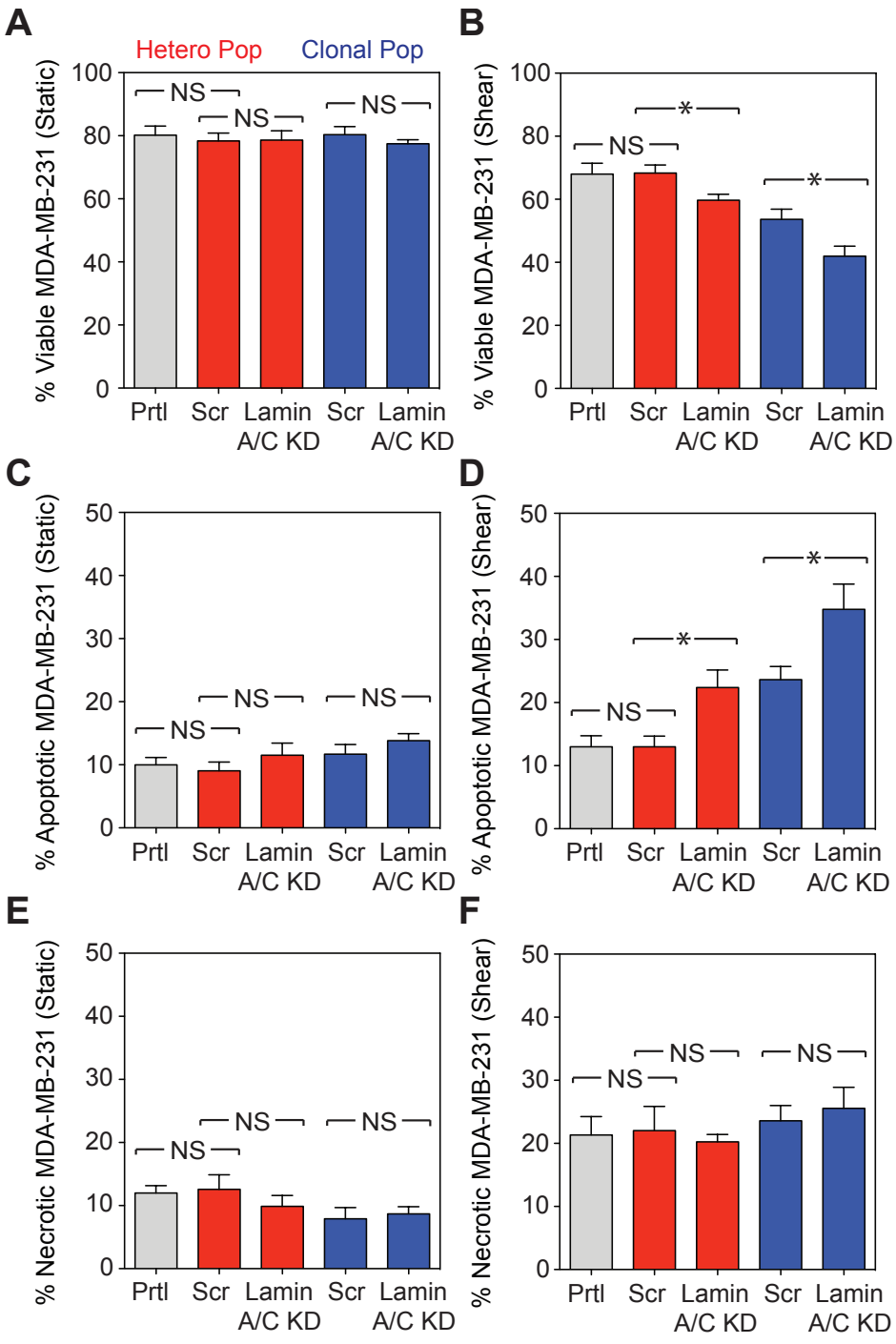

REFERENCES

[1] C.L. Chaffer, R.A. Weinberg, A Perspective on Cancer Cell Metastasis, Science. 331 (2011) 1559–1564.

[2] A.F. Chambers, A.C. Groom, I.C. MacDonald, Dissemination and growth of cancer cells in metastatic sites, Nat Rev Cancer. (2002).

[3] P.S. Steeg, Tumor metastasis: mechanistic insights and clinical challenges, Nature Medicine. 12 (2006) 895–904. doi:10.1038/nm1469.

[4] C.C. DuFort, M.J. Paszek, V.M. Weaver, Balancing forces: architectural control of mechanotransduction, Nat Rev Mol Cell Biol. 12 (2011) 308–319. doi:10.1038/nrm3112.

[5] D.T. Butcher, T. Alliston, V.M. Weaver, A tense situation: forcing tumour progression, Nat Rev Cancer. 9 (2009) 108–122. doi:10.1038/nrc2544.

[6] D. Wirtz, K. Konstantopoulos, P.C. Searson, The physics of cancer: the role of physical interactions and mechanical forces in metastasis, Nat Rev Cancer. 11 (2011) 512–522. doi:10.1038/nrc3080.

[7] Y. Tseng, J.S.H. Lee, T.P. Kole, I. Jiang, D. Wirtz, Micro-organization and visco-elasticity of the interphase nucleus revealed by particle nanotracking, Journal of Cell Science. 117 (2004) 2159–2167. doi:10.1242/jcs.01073.

[8] A.D. Hughes, M.R. King, Nanobiotechnology for the capture and manipulation of circulating tumor cells, WIREs Nanomed Nanobiotechnol. 4 (2011) 291–309. doi:10.1002/wnan.168.

[9] F. Moazzam, F. DeLano, B. Zweifach, G. Schmid-Schonbein, The leukocyte

response to fluid stress, Proc Natl Acad Sci USA. 94 (1997) 5338–5343.

[10] M. Civelek, K. Ainslie, J.S. Garanich, J.M. Tarbell, Smooth muscle cells contract in response to fluid flow via a Ca2+-independent signaling mechanism, J. Appl. Physiol. 93 (2002) 1907–1917.

[11] Y.-S.J. Li, J.H. Haga, S. Chien, Molecular basis of the effects of shear stress on vascular endothelial cells, J Biomech. 38 (2005) 1949–1971. doi:10.1016/j.jbiomech.2004.09.030.

[12] M.A. Swartz, A.W. Lund, Lymphatic and interstitial flow in the tumour microenvironment: linking mechanobiology with immunity, Nat Rev Cancer. 12 (2012) 210–219. doi:10.1038/nrc3186.

[13] F. Michor, J. Liphardt, M. Ferrari, J. Widom, What does physics have to do with cancer? Nat Rev Cancer. 11 (2011) 657–670. doi:doi:10.1038/nrc3092.

[14] A.C. Shieh, M.A. Swartz, Regulation of tumor invasion by interstitial fluid flow, Phys Biol. 8 (2011) 015012. doi:10.1088/1478-3975/8/1/015012.

[15] L.S.L. Cheung, P.S. Raman, E.M. Balzer, D. Wirtz, K. Konstantopoulos, Biophysics of selectin-ligand interactions in inflammation and cancer, Phys Biol. 8 (2011) 015013. doi:10.1088/1478-3975/8/1/015013.

[16] G.W. Schmid-Schonbein, Microlymphatics and lymph flow, Physiol. Rev. (1990).

[17] M.A. Swartz, M.E. Fleury, Interstitial flow and its effects in soft tissues, Annu Rev Biomed Eng. 9 (2007) 229–256. doi:10.1146/annurev.bioeng.9.060906.151850.

[18] H. Dafni, T. Israely, Z.M. Bhujwalla, L.E. Benjamin, M. Neeman,

Overexpression of Vascular Endothelial Growth Factor 165 Drives Peritumor Interstitial Convection and Induces Lymphatic Drain, Cancer Research. 62 (2002) 6731–6739.

[19] S.R. Chary, R.K. Jain, Direct measurement of interstitial convection and diffusion of albumin in normal and neoplastic tissues by fluorescence photobleaching, Proc Natl Acad Sci USA. 86 (1989) 5385–5389.

[20] J.A. Pedersen, F. Boschetti, M.A. Swartz, Effects of extracellular fiber architecture on cell membrane shear stress in a 3D fibrous matrix, J Biomech. 40 (2007) 1484–1492. doi:10.1016/j.jbiomech.2006.06.023.

[21] J.M. Tarbell, Z.D. Shi, Effect of the glycocalyx layer on transmission of interstitial flow shear stress to embedded cells, Biomech Model Mechanobiol. (2012). doi:10.1007/s10237-012-0385-8.

[22] M.I. Harrell, B.M. Iritani, A. Ruddell, Tumor-Induced Sentinel Lymph Node Lymphangiogenesis and Increased Lymph Flow Precede Melanoma Metastasis, The American Journal of Pathology. 170 (2007) 774–786. doi:10.2353/ajpath.2007.060761.

[23] Y. Boucher, R.K. Jain, Microvascular pressure is the principal driving force for interstitial hypertension in solid tumors: implications for vascular collapse, Cancer Research. 52 (1992) 5110–5114.

[24] Y. Boucher, M. Leunig, R.K. Jain, Tumor Angiogenesis and Interstitial Hypertension, Cancer Research. (1996).

[25] Y. Boucher, L.T. Baxter, R.K. Jain, Interstitial pressure gradients in tissue-isolated and subcutaneous tumors: implications for therapy, Cancer

Research. 50 (1990) 4478–4484.

[26] P.A. Netti, L.T. Baxter, Y. Boucher, R. Skalak, R.K. Jain, Time-dependent behavior of interstitial fluid pressure in solid tumors: implications for drug delivery, Cancer Research. 55 (1995) 5451–5458.

[27] S.J. Lunt, A. Fyles, R.P. Hill, M. Milosevic, Interstitial fluid pressure in tumors: therapeutic barrier and biomarker of angiogenesis, Future Oncol. 4 (2008) 793–802. doi:10.2217/14796694.4.6.793.

[28] D.O. Miteva, J.M. Rutkowski, J.B. Dixon, W. Kilarski, J.D. Shields, M.A. Swartz, Transmural flow modulates cell and fluid transport functions of lymphatic endothelium, Circ. Res. 106 (2010) 920–931. doi:10.1161/CIRCRESAHA.109.207274.

[29] J.D. Shields, M.S. Emmett, D.B.A. Dunn, K.D. Joory, L.M. Sage, H. Rigby, et al., Chemokine-mediated migration of melanoma cells towards lymphatics – a mechanism contributing to metastasis, Oncogene. 26 (2006) 2997–3005. doi:10.1038/sj.onc.1210114.

[30] L.A. Johnson, S. Clasper, A.P. Holt, P.F. Lalor, D. Baban, D.G. Jackson, An inflammation-induced mechanism for leukocyte transmigration across lymphatic vessel endothelium, The Journal of Experimental Medicine. 203 (2006) 2763–2777. doi:10.1084/jem.20051759.

[31] C.P. Ng, M.A. Swartz, Mechanisms of interstitial flow-induced remodeling of fibroblast-collagen cultures, Ann Biomed Eng. 34 (2006) 446–454. doi:10.1007/s10439-005-9067-3.

[32] C.P. Ng, B. Hinz, M.A. Swartz, Interstitial fluid flow induces myofibroblast

differentiation and collagen alignment in vitro, Journal of Cell Science. 118 (2005) 4731–4739. doi:10.1242/jcs.02605.

[33] P.-J. Wipff, D.B. Rifkin, J.-J. Meister, B. Hinz, Myofibroblast contraction activates latent TGF-beta1 from the extracellular matrix, The Journal of Cell Biology. 179 (2007) 1311–1323. doi:10.1083/jcb.200704042.

[34] J. Ahamed, N. Burg, K. Yoshinaga, C.A. Janczak, D.B. Rifkin, B.S. Coller, In vitro and in vivo evidence for shear-induced activation of latent transforming growth factor-β1, Blood. 112 (2008) 3650–3660. doi:10.1182/blood-2008-04-151753.

[35] O. De Wever, W. Westbroek, A. Verloes, N. Bloemen, M. Bracke, C. Gespach, et al., Critical role of N-cadherin in myofibroblast invasion and migration in vitro stimulated by colon-cancer-cell-derived TGF-β or wounding, Journal of Cell Science. 117 (2004) 4691–4703.

[36] O. De Wever, Tenascin-C and SF/HGF produced by myofibroblasts in vitro provide convergent proinvasive signals to human colon cancer cells through RhoA and Rac, The FASEB Journal. (2004). doi:10.1096/fj.03-1110fje.

[37] A. Orimo, R.A. Weinberg, Stromal Fibroblasts in Cancer: A Novel Tumor-Promoting Cell Type, Cell Cycle. 5 (2006) 1597–1601. doi:10.4161/cc.5.15.3112.

[38] B. Hinz, G. Gabbiani, C. Chaponnier, The NH2-terminal peptide of alpha-smooth muscle actin inhibits force generation by the myofibroblast in vitro and in vivo, The Journal of Cell Biology. 157 (2002) 657–663. doi:10.1083/jcb.200201049.

[39] A.C. Shieh, H.A. Rozansky, B. Hinz, M.A. Swartz, Tumor cell invasion is promoted by interstitial flow-induced matrix priming by stromal fibroblasts, Cancer Research. 71 (2011) 790–800. doi:10.1158/0008-5472.CAN-10-1513.

[40] M. Bockhorn, R.K. Jain, L.L. Munn, Active versus passive mechanisms in metastasis: do cancer cells crawl into vessels, or are they pushed? Lancet Oncol. 8 (2007) 444–448. doi:10.1016/S1470-2045(07)70140-7.

[41] S. Khuon, L. Liang, R.W. Dettman, P. Sporn, Myosin light chain kinase mediates transcellular intravasation of breast cancer cells through the underlying endothelial cells: a three-dimensional FRET study, Journal of Cell Science. 123 (2010) 431–440.

[42] S. Maheswaran, D.A. Haber, Circulating tumor cells: a window into cancer biology and metastasis, Current Opinion in Genetics & Development. 20 (2010) 96–99. doi:10.1016/j.gde.2009.12.002.

[43] M. Yu, S. Stott, M. Toner, S. Maheswaran, D.A. Haber, Circulating tumor cells: approaches to isolation and characterization, The Journal of Cell Biology. 192 (2011) 373–382.

[44] L.J. Gay, B. Felding-Habermann, Contribution of platelets to tumour metastasis, Nat Rev Cancer. 11 (2011) 123–134.

[45] O. McCarty, S. Mousa, P. Bray, K. Konstantopoulos, Immobilized platelets support human colon carcinoma cell tethering, rolling, and firm adhesion under dynamic flow conditions, Blood. 96 (2000) 1789–1797.

[46] V.T. Turitto, Blood viscosity, mass transport, and thrombogenesis, Prog

Hemost Thromb. 6 (1982) 139–177.

[47] D.E. Brooks, The biorheology of tumor cells, Biorheology. 21 (1984) 85–91.

[48] S. Gout, P. Tremblay, J. Huot, Selectins and selectin ligands in extravasation of cancer cells and organ selectivity of metastasis, Clinical & Experimental Metastasis. 25 (2008) 335–344.

[49] S. Köhler, S. Ullrich, U. Richter, U. Schumacher, E-/P-selectins and colon carcinoma metastasis: first in vivo evidence for their crucial role in a clinically relevant model of spontaneous metastasis formation in the lung, British Journal of Cancer. 102 (2010) 602–609. doi:10.1038/sj.bjc.6605492.

[50] H. Läubli, L. Borsig, Selectins promote tumor metastasis, Seminars in Cancer Biology. 20 (2010) 169–177.

[51] A.F. Chambers, I.C. MacDonald, E.E. Schmidt, S. Koop, V.L. Morris, R. Khokha, et al., Steps in tumor metastasis: new concepts from intravital microscopy, Cancer and Metastasis Reviews. 14 (1995) 279–301.

[52] L.M. Coussens, Z. Werb, Inflammation and cancer, Nature. 420 (2002) 860–867. doi:10.1038/nature01322.

[53] S.R. Barthel, G.K. Wiese, J. Cho, M.J. Opperman, D.L. Hays, J. Siddiqui, et al., Alpha 1,3 fucosyltransferases are master regulators of prostate cancer cell trafficking, Proc Natl Acad Sci USA. 106 (2009) 19491–19496.

[54] R. Giavazzi, M. Foppolo, R. Dossi, A. Remuzzi, Rolling and adhesion of human tumor cells on vascular endothelium under physiological flow conditions, Journal of Clinical Investigation. 92 (1993) 3038–3044.

[55] M. Fischer, U.K. Franzeck, I. Herrig, U. Costanzo, S. Wen, M. Schiesser, et al., Flow velocity of single lymphatic capillaries in human skin, American Journal of Physiology - Cell Physiology. 270 (1996) H358–H363.

[56] V.A. Resto, M.M. Burdick, N.M. Dagia, L-selectin-mediated Lymphocyte-Cancer Cell Interactions under Low Fluid Shear Conditions, Journal of Biological cHemistry. 283 (2008) 15816–15824.

[57] H.C. Brinkman, A calculation of the viscous force exerted by a flowing fluid on a dense swarm of particles, Appl. Sci. Res. 1 (1949) 27–34. doi:10.1007/BF02120313.

[58] El Rasheid Zakaria, J. Lofthouse, M.F. Flessner, In vivo hydraulic conductivity of muscle: effects of hydrostatic pressure, Am J Physiol Heart Circ Physiol. 273 (1997) H2774–H2782.

[59] J.L. Bert, R.K. Reed, Flow conductivity of rat dermis is determined by hydration, Biorheology. 32 (1995) 17–27.

[60] J.R. Levick, Flow through interstitium and other fibrous matrices, Q J Exp Physiol. 72 (1987) 409–437.

[61] S. McGuire, D. Zaharoff, F. Yuan, Nonlinear dependence of hydraulic conductivity on tissue deformation during intratumoral infusion, Ann Biomed Eng. 34 (2006) 1173–1181. doi:10.1007/s10439-006-9136-2.

[62] P.A. Netti, D.A. Berk, M.A. Swartz, A.J. Grodzinsky, R.K. Jain, Role of extracellular matrix assembly in interstitial transport in solid tumors, Cancer Research. 60 (2000) 2497–2503.

[63] C.P. Ng, M.A. Swartz, Fibroblast alignment under interstitial fluid flow

using a novel 3-D tissue culture model, American Journal of Physiology - Cell Physiology. 284 (2003) H1771–7. doi:10.1152/ajpheart.01008.2002.

[64] S.L. Diamond, Engineering design of optimal strategies for blood clot dissolution, Annu Rev Biomed Eng. 1 (1999) 427–462. doi:10.1146/annurev.bioeng.1.1.427.

[65] M.K. Kwan, W.M. Lai, V.C. Mow, Fundamentals of fluid transport through cartilage in compression, Ann Biomed Eng. 12 (1984) 537–558.

[66] A.J. Grodzinsky, M.E. Levenston, M. Jin, E.H. Frank, Cartilage tissue remodeling in response to mechanical forces, Annu Rev Biomed Eng. 2 (2000) 691–713. doi:10.1146/annurev.bioeng.2.1.691.

[67] C. Hellmich, F.-J. Ulm, Drained and Undrained Poroelastic Properties of Healthy and Pathological Bone: A Poro-Micromechanical Investigation, Transp Porous Med. 58 (2005) 243–268. doi:10.1007/s11242-004-6298-y.

[68] D.M. Wang, J.M. Tarbell, Modeling interstitial flow in an artery wall allows estimation of wall shear stress on smooth muscle cells, J Biomech Eng. 117 (1995) 358–363.

[69] M.A. Swartz, A. Kaipainen, P.A. Netti, C. Brekken, Y. Boucher, A.J. Grodzinsky, et al., Mechanics of interstitial-lymphatic fluid transport: theoretical foundation and experimental validation, J Biomech. 32 (1999) 1297–1307.

[70] D.A. Hammer, D.A. Lauffenburger, A dynamical model for receptor-mediated cell adhesion to surfaces, Biophysical Journal. 52 (1987) 475–487. doi:10.1016/S0006-3495(87)83236-8.

[71] D.A. Hammer, S.M. Apte, Simulation of cell rolling and adhesion on surfaces in shear flow: general results and analysis of selectin-mediated neutrophil adhesion, Biophysical Journal. (1992).

[72] G.I. Bell, M. Dembo, P. Bongrand, Cell adhesion. Competition between nonspecific repulsion and specific bonding, Biophysical Journal. 45 (1984) 1051–1064. doi:10.1016/S0006-3495(84)84252-6.

[73] G.I. Bell, Models for the specific adhesion of cells to cells, Science. (1978).

[74] M.R. King, R. Sumagin, C.E. Green, S.I. Simon, Rolling dynamics of a neutrophil with redistributed L-selectin, Math Biosci. 194 (2005) 71–79. doi:10.1016/j.mbs.2004.12.008.

[75] K.C. Chang, D.F. Tees, D.A. Hammer, The state diagram for cell adhesion under flow: leukocyte rolling and firm adhesion, Proc Natl Acad Sci USA. 97 (2000) 11262–11267. doi:10.1073/pnas.200240897.

[76] K.E. Caputo, D.A. Hammer, Effect of microvillus deformability on leukocyte adhesion explored using adhesive dynamics simulations, Biophysical Journal. 89 (2005) 187–200. doi:10.1529/biophysj.104.054171.

[77] M.R. King, D.A. Hammer, Multiparticle adhesive dynamics: Hydrodynamic recruitment of rolling leukocytes, Proc Natl Acad Sci USA. 98 (2001) 14919–14924. doi:10.1073/pnas.261272498.

[78] M.R. King, D.A. Hammer, Multiparticle Adhesive Dynamics. Interactions between Stably Rolling Cells, Biophysical Journal. 81 (2001) 799–813. doi:10.1016/S0006-3495(01)75742-6.

[79] M.J. Smith, E.L. Berg, M.B. Lawrence, A direct comparison of selectin-

mediated transient, adhesive events using high temporal resolution, Biophysical Journal. 77 (1999) 3371–3383. doi:10.1016/S0006-3495(99)77169-9.

[80] V.S. Shirure, N.M. Reynolds, M.M. Burdick, Mac-2 Binding Protein Is a Novel E-Selectin Ligand Expressed by Breast Cancer Cells, PLoS ONE. 7 (2012) e44529. doi:10.1371/journal.pone.0044529.

[81] S.N. Thomas, F. Zhu, R.L. Schnaar, C.S. Alves, K. Konstantopoulos, Carcinoembryonic Antigen and CD44 Variant Isoforms Cooperate to Mediate Colon Carcinoma Cell Adhesion to E- and L-selectin in Shear Flow, J Biol Chem. 283 (2008) 15647–15655.

[82] M.J. Mitchell, C.S. Chen, V. Ponmudi, A.D. Hughes, M.R. King, E-selectin liposomal and nanotube-targeted delivery of doxorubicin to circulating tumor cells, Journal of Controlled Release. 160 (2012) 609–617. doi:10.1016/j.jconrel.2012.02.018.

[83] M.J. Mitchell, C.A. Castellanos, M.R. King, Nanostructured Surfaces to Target and Kill Circulating Tumor Cells While Repelling Leukocytes, Journal of Nanomaterials. 2012 (2012) 1–10.

[84] K. Rana, J.L. Liesveld, M.R. King, Delivery of apoptotic signal to rolling cancer cells: A novel biomimetic technique using immobilized TRAIL and E-selectin, Biotechnol. Bioeng. 102 (2009) 1692–1702. doi:10.1002/bit.22204.

[85] K. Rana, C.A. Reinhart-King, M.R. King, Inducing Apoptosis in Rolling Cancer Cells: A Combined Therapy with Aspirin and Immobilized TRAIL

and E-Selectin, Molecular Pharmaceutics. 9 (2012) 2219–2227. doi:10.1021/mp300073j.

[86] M.J. Mitchell, M.R. King, Fluid shear stress sensitizes cancer cells to receptor-mediated apoptosis via trimeric death receptors, New Journal of Physics. 15 (2013) 015008. doi:10.1088/1367-2630/15/1/015008.

[87] A. Ashkenazi, Targeting death and decoy receptors of the tumour-necrosis factor superfamily, Nat Rev Cancer. 2 (2002) 420–430. doi:10.1038/nrc821.

[88] R.C. Young, R.F. Ozols, C.E. Myers, The Anthracycline Antineoplastic Drugs, New England Journal of Medicine. 305 (1981) 139–153.

[89] N. Osheroff, A.H. Corbett, M.J. Robinson, Mechanism of action of topoisomerase II-targeted antineoplastic drugs, Advances in Pharmacology. 29 (1994) 105–126.

[90] A. Makino, E. Prossnitz, M. Bunemann, J. Wang, W. Yao, G. Schmid-Schonbein, G protein-coupled receptors serve as mechanosensors for fluid shear stress in neutrophils, American Journal of Physiology - Cell Physiology. 290 (2006) C1633–C1639.

[91] M.J. Mitchell, M.R. King, Shear-Induced Resistance to Neutrophil Activation via the Formyl Peptide Receptor, Biophysical Journal. 102 (2012) 1804–1814. doi:10.1016/j.bpj.2012.03.053.

[92] J.M. Barnes, J.T. Nauseef, M.D. Henry, Resistance to Fluid Shear Stress Is a Conserved Biophysical Property of Malignant Cells, PLoS ONE. 7 (2012) e50973. doi:10.1371/journal.pone.0050973.t002.

[93] A.M. Malek, S.L. Alper, S. Izumo, Hemodynamic Shear Stress and Its Role

in Atherosclerosis, Jama. 282 (1999) 2035–2042. doi:10.1001/jama.282.21.2035.

[94] J. Strony, A. Beaudoin, D. Brands, B. Adelman, Analysis of shear stress and hemodynamic factors in a model of coronary artery stenosis and thrombosis, Am J Physiol Heart Circ Physiol. 265 (1993) H1787–1796.

[95] M. Terasaki, K. Miyake, P.L. McNeil, Large plasma membrane disruptions are rapidly resealed by Ca2+-dependent vesicle-vesicle fusion events, The Journal of Cell Biology. 139 (1997) 63–74.

[96] J.D. Shields, M.E. Fleury, C. Yong, A.A. Tomei, G.J. Randolph, M.A. Swartz, Autologous chemotaxis as a mechanism of tumor cell homing to lymphatics via interstitial flow and autocrine CCR7 signaling, Cancer Cell. 11 (2007) 526–538. doi:10.1016/j.ccr.2007.04.020.

[97] H. Qazi, Z.D. Shi, J.M. Tarbell, Fluid Shear Stress Regulates the Invasive Potential of Glioma Cells via Modulation of Migratory Activity and Matrix Metalloproteinase Expression, PLoS ONE. 6 (2011) e20348.

[98] Z.D. Shi, J.M. Tarbell, Fluid flow mechanotransduction in vascular smooth muscle cells and fibroblasts, Ann Biomed Eng. 39 (2011) 1608–1619. doi:10.1007/s10439-011-0309-2.

[99] J.S. Garanich, R.A. Mathura, Z.D. Shi, J.M. Tarbell, Effects of fluid shear stress on adventitial fibroblast migration: implications for flow-mediated mechanisms of arterialization and intimal hyperplasia, American Journal of Physiology - Cell Physiology. 292 (2007) H3128–35. doi:10.1152/ajpheart.00578.2006.

[100] H. Yokota, M.B. Goldring, H.B. Sun, CITED2-mediated regulation of MMP-1 and MMP-13 in human chondrocytes under flow shear, J. Biol. Chem. 278 (2003) 47275–47280. doi:10.1074/jbc.M304652200.

[101] V.J. Fincham, The catalytic activity of Src is dispensable for translocation to focal adhesions but controls the turnover of these structures during cell motility, The EMBO Journal. 17 (1998) 81–92. doi:10.1093/emboj/17.1.81.

[102] D.J. Sieg, D. Ilić, K.C. Jones, C.H. Damsky, T. Hunter, D.D. Schlaepfer, Pyk2 and Src-family protein-tyrosine kinases compensate for the loss of FAK in fibronectin-stimulated signaling events but Pyk2 does not fully function to enhance FAK- cell migration, The EMBO Journal. 17 (1998) 5933–5947. doi:10.1093/emboj/17.20.5933.

[103] W.J. Polacheck, J.L. Charest, R.D. Kamm, Interstitial flow influences direction of tumor cell migration through competing mechanisms, Proc Natl Acad Sci USA. (2011).

[104] C.-H. Heldin, K. Rubin, K. Pietras, A. Ostman, High interstitial fluid pressure - an obstacle in cancer therapy, Nat Rev Cancer. 4 (2004) 806–813. doi:10.1038/nrc1456.

[105] S. Li, M. Kim, Y.L. Hu, S. Jalali, D.D. Schlaepfer, T. Hunter, et al., Fluid shear stress activation of focal adhesion kinase. Linking to mitogen-activated protein kinases, J. Biol. Chem. 272 (1997) 30455–30462.

[106] S. Jalali, Y.S. Li, M. Sotoudeh, S. Yuan, S. Li, S. Chien, et al., Shear stress activates p60src-Ras-MAPK signaling pathways in vascular endothelial cells, Arteriosclerosis, Thrombosis, and Vascular Biology. 18 (1998) 227–

234.

[107] Y. Yao, A. Rabodzey, C.F. Dewey, Glycocalyx modulates the motility and proliferative response of vascular endothelium to fluid shear stress, American Journal of Physiology - Cell Physiology. 293 (2007) H1023–30. doi:10.1152/ajpheart.00162.2007.

[108] Z.D. Shi, H. Wang, J.M. Tarbell, Heparan sulfate proteoglycans mediate interstitial flow mechanotransduction regulating MMP-13 expression and cell motility via FAK-ERK in 3D collagen, PLoS ONE. 6 (2011) e15956. doi:10.1371/journal.pone.0015956.

[109] H. Krähling, S. Mally, J.A. Eble, J. Noël, A. Schwab, C. Stock, The glycocalyx maintains a cell surface pH nanoenvironment crucial for integrin-mediated migration of human melanoma cells, Pflugers Arch. 458 (2009) 1069–1083. doi:10.1007/s00424-009-0694-7.

[110] T.W. Secomb, R. Hsu, A.R. Pries, Effect of the endothelial surface layer on transmission of fluid shear stress to endothelial cells, Biorheology. 38 (2001) 143–150.

[111] E.F. Krasik, K.L. Yee, D.A. Hammer, Adhesive dynamics simulation of neutrophil arrest with deterministic activation, Biophysical Journal. 91 (2006) 1145–1155. doi:10.1529/biophysj.105.070706.

[112] E.F. Krasik, K.E. Caputo, D.A. Hammer, Adhesive Dynamics Simulation of Neutrophil Arrest with Stochastic Activation, Biophysical Journal. 95 (2008) 1716–1728. doi:10.1529/biophysj.107.119677.

[113] K.E. Caputo, D.A. Hammer, Adhesive Dynamics Simulation of G-Protein-

Mediated Chemokine-Activated Neutrophil Adhesion, Biophysical Journal. 96 (2009) 2989–3004. doi:10.1016/j.bpj.2008.12.3930.

[114] M.T. Beste, D. Lee, M.R. King, G.A. Koretzky, D.A. Hammer, An integrated stochastic model of "inside-out" integrin activation and selective T-lymphocyte recruitment, Langmuir. 28 (2012) 2225–2237. doi:10.1021/la203803e.

[115] M.J. Paszek, D. Boettiger, V.M. Weaver, D.A. Hammer, Integrin clustering is driven by mechanical resistance from the glycocalyx and the substrate, PLoS Comp Biol. 5 (2009) e1000604. doi:10.1371/journal.pcbi.1000604.

[116] R.O. Hynes, Integrins: Bidirectional, Allosteric Signaling Machines, Cell. (2002).

[117] C.K. Miranti, J.S. Brugge, Sensing the environment: a historical perspective on integrin signal transduction, Nat. Cell Biol. 4 (2002) E83–90. doi:10.1038/ncb0402-e83.

[118] A.L. Berrier, K.M. Yamada, Cell–matrix adhesion, J. Cell. Physiol. 213 (2007) 565–573.

[119] M. Ostoja-Starzewski, P.Y. Sheng, K. Alzebdeh, Spring network models in elasticity and fracture of composites and polycrystals, Computational Materials Science. 7 (1996) 82–93.

[120] C. Cluzel, F. Saltel, J. Lussi, F. Paulhe, B.A. Imhof, B. Wehrle-Haller, The mechanisms and dynamics of αvβ3 integrin clustering in living cells, The Journal of Cell Biology. (2005).

[121] A. Schroeder, D.A. Heller, M.M. Winslow, J.E. Dahlman, G.W. Pratt, R.

Langer, et al., Treating metastatic cancer with nanotechnology, Nat Rev Cancer. 12 (2011) 39–50. doi:10.1038/nrc3180.

[122] T. Safra, F. Muggia, S. Jeffers, D.D. Tsao-Wei, S. Groshen, O. Lyass, et al., Pegylated liposomal doxorubicin (doxil): Reduced clinical cardiotoxicity in patients reaching or exceeding cumulative doses of 500 mg/m2, Annals of Oncology. 11 (2000) 1029–1033.

[123] G. Christofori, New signals from the invasive front, Nature. 441 (2006) 444–450. doi:10.1038/nature04872.

[124] J.M. Brown, The Hypoxic Cell, Cancer Research. 59 (1999) 5863–5870.

[125] I. Mellman, G. Coukos, G. Dranoff, Cancer immunotherapy comes of age, Nature. 480 (2011) 480–489.

[126] A.Z. Wang, R. Langer, O.C. Farokhzad, Nanoparticle Delivery of Cancer Drugs, Annu. Rev. Med. 63 (2012) 185–198.

[127] D. Peer, J.M. Karp, S. Hong, O.C. Farokhzad, R. Margalit, R. Langer, Nanocarriers as an emerging platform for cancer therapy, Nature Nanotechnology. 2 (2007) 751–760. doi:10.1038/nnano.2007.387.

[128] S.H. Kim, J.H. Jeong, K.W. Chun, T.G. Park, Target-specific cellular uptake of PLGA nanoparticles coated with poly(L-lysine)-poly(ethylene glycol)-folate conjugate, Langmuir. 21 (2005) 8852–8857. doi:10.1021/la0502084.

[129] O.C. Farokhzad, S. Jon, A. Khademhosseini, T.-N.T. Tran, D.A. Lavan, R. Langer, Nanoparticle-aptamer bioconjugates: a new approach for targeting prostate cancer cells, Cancer Research. 64 (2004) 7668–7672. doi:10.1158/0008-5472.CAN-04-2550.

[130] L. Zhang, F.X. Gu, J.M. Chan, A.Z. Wang, Nanoparticles in Medicine: Therapeutic Applications and Developments, Clinical Pharmacology & Therapeutics. 83 (2008) 761–769.

[131] F. Alexis, E. Pridgen, L.K. Molnar, O.C. Farokhzad, Factors affecting the clearance and biodistribution of polymeric nanoparticles, Molecular Pharmaceutics. 5 (2008) 505–515. doi:10.1021/mp800051m.

[132] F. Gu, L. Zhang, B.A. Teply, N. Mann, A. Wang, A.F. Radovic-Moreno, et al., Precise engineering of targeted nanoparticles by using self-assembled biointegrated block copolymers, Proc Natl Acad Sci USA. 105 (2008) 2586–2591. doi:10.1073/pnas.0711714105.

[133] L. Brannon-Peppas, J.O. Blanchette, Nanoparticle and targeted systems for cancer therapy, Advanced Drug Delivery Reviews. 64 (2012) 206–212. doi:10.1016/j.addr.2012.09.033.

[134] I. Bala, S. Hariharan, M.N.V.R. Kumar, PLGA nanoparticles in drug delivery: the state of the art, Crit Rev Ther Drug Carrier Syst. 21 (2004) 387–422.

[135] P. Calvo, C. Remuñan-López, J.L. Vila-Jato, M.J. Alonso, Chitosan and chitosan/ethylene oxide-propylene oxide block copolymer nanoparticles as novel carriers for proteins and vaccines, Pharm. Res. 14 (1997) 1431–1436.

[136] J.S. Hrkach, M.T. Peracchia, A. Bomb, N. Lotan, R. Langer, Nanotechnology for biomaterials engineering: structural characterization of amphiphilic polymeric nanoparticles by 1H NMR spectroscopy, Biomaterials. 18 (1997) 27–30. doi:10.1016/S0142-9612(96)00077-4.

[137] A.D. Bangham, Liposomes: the Babraham connection, Chemistry and Physics of Lipids. 64 (1993) 275–285. doi:10.1016/0009-3084(93)90071-A.

[138] V.P. Torchilin, Recent advances with liposomes as pharmaceutical carriers, Nat Rev Drug Discov. 4 (2005) 145–160. doi:10.1038/nrd1632.

[139] Y. Barenholz, Doxil® — The first FDA-approved nano-drug: Lessons learned, Journal of Controlled Release. 160 (2012) 117–134.

[140] R.C.F. Leonard, S. Williams, A. Tulpule, A.M. Levine, S. Oliveros, Improving the therapeutic index of anthracycline chemotherapy: Focus on liposomal doxorubicin (Myocet™), The Breast. 18 (2009) 218–224. doi:10.1016/j.breast.2009.05.004.

[141] S. Lal, S.E. Clare, N.J. Halas, Nanoshell-enabled photothermal cancer therapy: impending clinical impact, Acc. Chem. Res. 41 (2008) 1842–1851. doi:10.1021/ar800150g.

[142] M.-R. Choi, K.J. Stanton-Maxey, J.K. Stanley, C.S. Levin, R. Bardhan, D. Akin, et al., A Cellular Trojan Horse for Delivery of Therapeutic Nanoparticles into Tumors, Nano Lett. 7 (2007) 3759–3765. doi:10.1021/nl072209h.

[143] J.-H. Park, G. von Maltzahn, M.J. Xu, V. Fogal, V.R. Kotamraju, E. Ruoslahti, et al., Cooperative nanomaterial system to sensitize, target, and treat tumors, Proc Natl Acad Sci USA. 107 (2010) 981–986. doi:10.1073/pnas.0909565107.

[144] C. Minelli, S.B. Lowe, M.M. Stevens, Engineering nanocomposite materials for cancer therapy, Small. 6 (2010) 2336–2357.

doi:10.1002/smll.201000523.

[145] S.K. Libutti, G.F. Paciotti, A.A. Byrnes, H.R. Alexander, W.E. Gannon, M. Walker, et al., Phase I and pharmacokinetic studies of CYT-6091, a novel PEGylated colloidal gold-rhTNF nanomedicine, Clin. Cancer Res. 16 (2010) 6139–6149. doi:10.1158/1078-0432.CCR-10-0978.

[146] N. Lewinski, V. Colvin, R. Drezek, Cytotoxicity of Nanoparticles, Small. 4 (2008) 26–49.

[147] W. Yang, P. Thordarson, J.J. Gooding, S.P. Ringer, F. Braet, Carbon nanotubes for biological and biomedical applications, Nanotechnology. 18 (2007) 412001. doi:10.1088/0957-4484/18/41/412001.

[148] P. Chakravarty, R. Marches, N.S. Zimmerman, A.D.-E. Swafford, P. Bajaj, I.H. Musselman, et al., Thermal ablation of tumor cells with antibody-functionalized single-walled carbon nanotubes, Proc Natl Acad Sci USA. 105 (2008) 8697–8702. doi:10.1073/pnas.0803557105.

[149] K. Welsher, Z. Liu, D. Daranciang, H. Dai, Selective probing and imaging of cells with single walled carbon nanotubes as near-infrared fluorescent molecules, Nano Lett. 8 (2008) 586–590. doi:10.1021/nl072949q.

[150] Z. Liu, K. Chen, C. Davis, S. Sherlock, Q. Cao, X. Chen, et al., Drug Delivery with Carbon Nanotubes for In vivo Cancer Treatment, Cancer Research. 68 (2008) 6652–6660.

[151] H. Dumortier, S. Lacotte, G. Pastorin, R. Marega, W. Wu, D. Bonifazi, et al., Functionalized carbon nanotubes are non-cytotoxic and preserve the functionality of primary immune cells, Nano Lett. 6 (2006) 1522–1528.

doi:10.1021/nl061160x.

[152] D. Cui, F. Tian, C.S. Ozkan, M. Wang, H. Gao, Effect of single wall carbon nanotubes on human HEK293 cells, Toxicol. Lett. 155 (2005) 73–85. doi:10.1016/j.toxlet.2004.08.015.

[153] C.-W. Lam, J.T. James, R. McCluskey, R.L. Hunter, Pulmonary toxicity of single-wall carbon nanotubes in mice 7 and 90 days after intratracheal instillation, Toxicol. Sci. 77 (2004) 126–134. doi:10.1093/toxsci/kfg243.

[154] J.C. Yang, L. Haworth, R.M. Sherry, P. Hwu, D.J. Schwartzentruber, S.L. Topalian, et al., A randomized trial of bevacizumab, an anti-vascular endothelial growth factor antibody, for metastatic renal cancer, N. Engl. J. Med. 349 (2003) 427–434. doi:10.1056/NEJMoa021491.

[155] S.X. Yang, Bevacizumab and breast cancer: current therapeutic progress and future perspectives, Expert Rev Anticancer Ther. 9 (2009) 1715–1725. doi:10.1586/era.09.153.

[156] H. de Lavallade, J.F. Apperley, J.S. Khorashad, D. Milojkovic, A.G. Reid, M. Bua, et al., Imatinib for Newly Diagnosed Patients With Chronic Myeloid Leukemia: Incidence of Sustained Responses in an Intention-to-Treat Analysis, Journal of Clinical Oncology. 26 (2008) 3358–3363. doi:10.1200/JCO.2007.15.8154.

[157] Y.-J. Bang, E. Van Cutsem, A. Feyereislova, H.C. Chung, L. Shen, A. Sawaki, et al., Trastuzumab in combination with chemotherapy versus chemotherapy alone for treatment of HER2-positive advanced gastric or gastro-oesophageal junction cancer (ToGA): a phase 3, open-label,

randomised controlled trial, The Lancet. 376 (2010) 687–697. doi:10.1016/S0140-6736(10)61121-X.

[158] J. Baselga, E.A. Perez, T. Pienkowski, R. Bell, Adjuvant Trastuzumab: A Milestone in the Treatment of HER-2-Positive Early Breast Cancer, The Oncologist. 11 (2006) 4–12.

[159] M.J. Mitchell, M.R. King, Computational and experimental models of cancer cell response to fluid shear stress, Frontiers in Oncology. 3 (2013) 1–11. doi:10.3389/fonc.2013.00044/abstract.

[160] G.W. Schmid-Schönbein, S. Usami, R. Skalak, S. Chien, The interaction of leukocytes and erythrocytes in capillary and postcapillary vessels, Microvasc. Res. 19 (1980) 45–70. doi:10.1016/0026-2862(80)90083-7.

[161] K. Ley, Molecular mechanisms of leukocyte recruitment in the inflammatory process, Cardiovascular Research. 32 (1996) 733–742.

[162] H.L. Goldsmith, S. Spain, Margination of leukocytes in blood flow through small tubes, Microvasc. Res. 27 (1984) 204–222.

[163] J.C. Firrell, H.H. Lipowsky, Leukocyte margination and deformation in mesenteric venules of rat, Am J Physiol Heart Circ Physiol. 256 (1989) H1667–74.

[164] U. Nobis, A.R. Pries, G.R. Cokelet, P. Gaehtgens, Radial distribution of white cells during blood flow in small tubes, Microvasc. Res. 29 (1985) 295–304.

[165] E.C. Butcher, Leukocyte-endothelial cell recognition: Three (or more) steps to specificity and diversity, Cell. 67 (1991) 1033–1036. doi:10.1016/0092-

8674(91)90279-8.

[166] T.A. Springer, Adhesion receptors of the immune system, Nature. 346 (1990) 425–434.

[167] P. Sundd, M. Pospieszalska, L. Cheung, K. Konstatopoulos, K. Ley, Biomechanics of leukocyte rolling, Biorheology. 48 (2011) 1–35.

[168] P. Sundd, M.K. Pospieszalska, K. Ley, Neutrophil rolling at high shear: flattening, catch bond behavior, tethers and slings, Mol. Immunol. 55 (2013) 59–69. doi:10.1016/j.molimm.2012.10.025.

[169] E. Finger, K. Puri, R. Alón, M. Lawrence, U. von Andrian, T. Springer, Adhesion through L-selectin requires a threshold hydrodynamic shear, Nature. 379 (1996) 266–268.

[170] T.M. Cao, M.J. Mitchell, J. Liesveld, M.R. King, Stem Cell Enrichment with Selectin Receptors: Mimicking the pH Environment of Trauma, Sensors. 13 (2013) 12516–12526.

[171] G.S. Kansas, Selectins and their ligands: current concepts and controversies, Blood. 88 (1996) 3259–3287.

[172] M.J. Mitchell, K.S. Lin, M.R. King, Fluid Shear Stress Increases Neutrophil Activation via Platelet-Activating Factor, Biophysical Journal. 106 (2014) 2243–2253. doi:10.1016/j.bpj.2014.04.001.

[173] Z.M. Ding, J.E. Babensee, S.I. Simon, H. Lu, J.L. Perrard, D.C. Bullard, et al., Relative contribution of LFA-1 and Mac-1 to neutrophil adhesion and migration, J. Immunol. 163 (1999) 5029–5038.

[174] M.S. Diamond, ICAM-1 (CD54): a counter-receptor for Mac-1

(CD11b/CD18), The Journal of Cell Biology. 111 (1990) 3129–3139. doi:10.1083/jcb.111.6.3129.

[175] B. Hughes, J. Hollers, E. Crockett-Torabi, C.W. Smith, Recruitment of CD11b/CD18 to the neutrophil surface and adherence-dependent cell locomotion, Journal of Clinical Investigation. 90 (1992) 1687–1696.

[176] T.A. Springer, Traffic signals for lymphocyte recirculation and leukocyte emigration: The multistep paradigm, Cell. 76 (1994) 301–314. doi:10.1016/0092-8674(94)90337-9.

[177] T.M. van Ginhoven, J.W. van den Berg, W.A. Dik, J.N.M. Ijzermans, R.W.F. de Bruin, Preoperative dietary restriction reduces hepatic tumor load by reduced E-selectin-mediated adhesion in mice, J Surg Oncol. 102 (2010) 348–353. doi:10.1002/jso.21649.

[178] B. McDonald, J. Spicer, B. Giannais, L. Fallavollita, P. Brodt, L. Ferri, Systemic inflammation increases cancer cell adhesion to hepatic sinusoids by neutrophil mediated mechanisms, International Journal of Cancer. 125 (2009) 1298–1305.

[179] C.J. Dimitroff, M. Lechpammer, D. Long-Woodward, J. Kutok, Rolling of Human Bone-Metastatic Prostate Tumor Cells on Human Bone Marrow Endothelium under Shear Flow Is Mediated by E-Selectin, Cancer Research. 64 (2004) 5261–5269. doi:10.1158/0008-5472.CAN-04-0691.

[180] A. Tözeren, H.K. Kleinman, D.S. Grant, D. Morales, A. Mercurio, S. Byers, E-selectin-mediated dynamic interactions of breast-and colon-cancer cells with endothelial-cell monolayers, Int. J. Cancer. 60 (1995) 426–431.

[181] J.H. Myung, K.A. Gajjar, R.M. Pearson, C.A. Launiere, D.T. Eddington, S. Hong, Direct measurements on CD24-mediated rolling of human breast cancer MCF-7 cells on E-selectin, Analytical Chemistry. 83 (2011) 1078–1083. doi:10.1021/ac102901e.

[182] M.M. Burdick, J.T. Chu, S. Godar, R. Sackstein, HCELL Is the Major E- and L-selectin Ligand Expressed on LS174T Colon Carcinoma Cells, Journal of Biological cHemistry. 281 (2006) 13899–13905. doi:10.1074/jbc.M513617200.

[183] P. Brodt, L. Fallavollita, R.S. Bresalier, S. Meterissian, C.R. Norton, B.A. Wolitzky, Liver endothelial E-selectin mediates carcinoma cell adhesion and promotes liver metastasis, Int. J. Cancer. 71 (1997) 612–619.

[184] L. Biancone, M. Araki, K. Araki, P. Vassalli, I. Stamenkovic, Redirection of tumor metastasis by expression of E-selectin in vivo, The Journal of Experimental Medicine. 183 (1996) 581–587.

[185] J.J. Rahn, J.W. Chow, G.J. Horne, B.K. Mah, J.T. Emerman, P. Hoffman, et al., MUC1 mediates transendothelial migration in vitro by ligating endothelial cell ICAM-1, Clinical & Experimental Metastasis. 22 (2005) 475–483. doi:10.1007/s10585-005-3098-x.

[186] D. Raman, T. Sobolik-Delmaire, A. Richmond, Chemokines in health and disease, Exp. Cell Res. 317 (2011) 575–589.

[187] F.R. Balkwill, The chemokine system and cancer, J. Pathol. 226 (2011) 148–157. doi:10.1002/path.3029.

[188] T. Kishimoto, M. Jutila, E. Butcher, Identification of a human peripheral

lymph node homing receptor: a rapidly down-regulated adhesion molecule, Proc Natl Acad Sci USA. 87 (1990) 2244–2248.

[189] T. Kishimoto, M. Jutila, E. Berg, E. Butcher, Neutrophil Mac-1 and MEL-14 adhesion proteins inversely regulated by chemotactic factors, Science. 245 (1989) 1238–1241. doi:10.1126/science.2551036.

[190] A.J. Ridley, M.A. Schwartz, K. Burridge, R. Firtel, M.H. Ginsberg, G. Borisy, et al., Cell Migration: Integrating Signals from Front to Back, Science. 302 (2003) 1704–1709.

[191] R.P. McEver, K.L. Moore, R.D. Cummings, Leukocyte trafficking mediated by selectin-carbohydrate interactions, J. Biol. Chem. 270 (1995) 11025–11028.

[192] D. Vestweber, J.E. Blanks, Mechanisms That Regulate the Function of the Selectins and Their Ligands, Physiol. Rev. 79 (1999) 181–213.

[193] P. Friedl, S. Alexander, Cancer Invasion and the Microenvironment: Plasticity and Reciprocity, Cell. 147 (2011) 992–1009. doi:10.1016/j.cell.2011.11.016.

[194] S. Bajpai, M.J. Mitchell, M.R. King, C.A. Reinhart-King, A microfluidic device to select for cells based on chemotactic phenotype, Technology. 02 (2014) 101–105. doi:10.1142/S2339547814200015.

[195] G. Lazennec, A. Richmond, Chemokines and chemokine receptors: new insights into cancer-related inflammation, Trends in Molecular Medicine. 16 (2010) 133–144.

[196] V.S. Salsman, K.K.H. Chow, D.R. Shaffer, H. Kadikoy, X.-N. Li, C.

Gerken, et al., Crosstalk between medulloblastoma cells and endothelium triggers a strong chemotactic signal recruiting T lymphocytes to the tumor microenvironment, PLoS ONE. 6 (2011) e20267. doi:10.1371/journal.pone.0020267.

[197] N. Martinet, G. Beck, V. Bernard, F. Plenat, P. Vaillant, F. Schooneman, et al., Mechanism for the recruitment of macrophages to cancer site. In vivo concentration gradient of monocyte chemotactic activity, Cancer. 70 (1992) 854–860.

[198] A. Mantovani, Cancer: Inflaming metastasis, Nature. 457 (2009) 36–37. doi:10.1038/457036b.

[199] A. Mantovani, P. Allavena, A. Sica, F. Balkwill, Cancer-related inflammation, Nature. 454 (2008) 436–444.

[200] A.J. Swiston, J.B. Gilbert, D.J. Irvine, R.E. Cohen, M.F. Rubner, Freely suspended cellular “backpacks” lead to cell aggregate self-assembly, Biomacromolecules. 11 (2010) 1826–1832. doi:10.1021/bm100305h.

[201] A.J. Swiston, C. Cheng, S.H. Um, D.J. Irvine, R.E. Cohen, M.F. Rubner, Surface Functionalization of Living Cells with Multilayer Patches, Nano Lett. 8 (2008) 4446–4453. doi:10.1021/nl802404h.

[202] F.C. Vasconcellos, A.J. Swiston, M.M. Beppu, R.E. Cohen, M.F. Rubner, Bioactive Polyelectrolyte Multilayers: Hyaluronic Acid Mediated B Lymphocyte Adhesion, Biomacromolecules. 11 (2010) 2407–2414. doi:10.1021/bm100570r.

[203] N. Doshi, A.J. Swiston, J.B. Gilbert, M.L. Alcaraz, R.E. Cohen, M.F.

Rubner, et al., Cell-based drug delivery devices using phagocytosis-resistant backpacks, Advanced Materials. 23 (2011) H105–9. doi:10.1002/adma.201004074.

[204] H.C. Loughrey, L.S. Choi, P.R. Cullis, M.B. Bally, Optimized procedures for the coupling of proteins to liposomes, Journal of Immunological Methods. 132 (1990) 25–35. doi:10.1016/0022-1759(90)90394-B.

[205] L. Nobs, F. Buchegger, R. Gurny, E. Allémann, Current methods for attaching targeting ligands to liposomes and nanoparticles, J Pharm Sci. 93 (2004) 1980–1992. doi:10.1002/jps.20098.

[206] N. Donoghue, P.T. Yam, X.M. Jiang, P.J. Hogg, Presence of closely spaced protein thiols on the surface of mammalian cells, Protein Sci. 9 (2000) 2436–2445. doi:10.1110/ps.9.12.2436.

[207] D.A. Lawrence, R. Song, P. Weber, Surface thiols of human lymphocytes and their changes after in vitro and in vivo activation, Journal of Leukocyte Biology. 60 (1996) 611–618.

[208] M.T. Stephan, J.J. Moon, S.H. Um, A. Bershteyn, D.J. Irvine, Therapeutic cell engineering with surface-conjugated synthetic nanoparticles, Nature Medicine. 16 (2010) 1035–1041. doi:10.1038/nm.2198.

[209] M.J. Mitchell, E. Wayne, K. Rana, C.B. Schaffer, M.R. King, TRAIL-coated leukocytes that kill cancer cells in the circulation, Proc Natl Acad Sci USA. 111 (2014) 930–935. doi:10.1073/pnas.1316312111.

[210] J.A. Badwey, M.L. Karnovsky, Active oxygen species and the functions of phagocytic leukocytes, Annu. Rev. Biochem. 49 (1980) 695–726.

doi:10.1146/annurev.bi.49.070180.003403.

[211] D.C. Dale, L. Boxer, W.C. Liles, The phagocytes: neutrophils and monocytes, Blood. 112 (2008) 935–945. doi:10.1182/blood-2007-12-077917.

[212] J. Choi, H.Y. Kim, E.J. Ju, J. Jung, J. Park, H.K. Chung, et al., Use of macrophages to deliver therapeutic and imaging contrast agents to tumors, Biomaterials. 33 (2012) 4195–4203.

[213] M.-R. Choi, R. Bardhan, K.J. Stanton-Maxey, S. Badve, H. Nakshatri, K.M. Stantz, et al., Delivery of nanoparticles to brain metastases of breast cancer using a cellular Trojan horse, Cancer Nano. 3 (2012) 47–54. doi:10.1007/s12645-012-0029-9.

[214] A.M. Brynskikh, Y. Zhao, R.L. Mosley, S. Li, M.D. Boska, N.L. Klyachko, et al., Macrophage delivery of therapeutic nanozymes in a murine model of Parkinson's disease, Nanomedicine (Lond). 5 (2010) 379–396. doi:10.2217/nnm.10.7.

[215] E.V. Batrakova, S. Li, A.D. Reynolds, R.L. Mosley, T.K. Bronich, A.V. Kabanov, et al., A Macrophage−Nanozyme Delivery System for Parkinson's Disease, Bioconjug. Chem. 18 (2007) 1498–1506. doi:10.1021/bc700184b.

[216] L.R. Hirsch, R.J. Stafford, J.A. Bankson, S.R. Sershen, B. Rivera, R.E. Price, et al., Nanoshell-mediated near-infrared thermal therapy of tumors under magnetic resonance guidance, Proc Natl Acad Sci USA. 100 (2003) 13549–13554. doi:10.1073/pnas.2232479100.

[217] C.L. Graff, G.M. Pollack, Drug Transport at the Blood-Brain Barrier and the

Choroid Plexus, Curr Drug Metab. 5 (2004) 95–108. doi:10.2174/1389200043489126.

[218] W.M. Pardridge, The blood-brain barrier: Bottleneck in brain drug development, Neurotherapeutics. 2 (2005) 3–14. doi:10.1602/neurorx.2.1.3.

[219] G. Schackert, R.D. Simmons, T.M. Buzbee, D.A. Hume, I.J. Fidler, Macrophage Infiltration Into Experimental Brain Metastases: Occurrence Through an Intact Blood-Brain Barrier, Journal of the National Cancer Institute. 80 (1988) 1027–1034.

[220] Robert A Morantz, Gary W Wood, Marsha Foster, Martina Clark, Katherine Gollahon, Macrophages in experimental and human brain tumors, Journal of Neurosurgery. 50 (1979) 305–311.

[221] B.R. Smith, E. Ghosn, H. Rallapalli, J.A. Prescher, T. Larson, L.A. Herzenberg, et al., Selective uptake of single-walled carbon nanotubes by circulating monocytes for enhanced tumour delivery, Nature Nanotechnology. 9 (2014) 481–487.

[222] M.T. Stephan, S.B. Stephan, P. Bak, J. Chen, D.J. Irvine, Synapse-directed delivery of immunomodulators using T-cell-conjugated nanoparticles, Biomaterials. 33 (2012) 5776–5787. doi:10.1016/j.biomaterials.2012.04.029.

[223] S.Y. Wong, R.O. Hynes, Lymphatic or Hematogenous Dissemination: How Does a Metastatic Tumor Cell Decide? Cell Cycle. 5 (2006) 812–817. doi:10.4161/cc.5.8.2646.

[224] H. Wikman, R. Vessella, K. Pantel, Cancer micrometastasis and tumour

dormancy, Apmis. 116 (2008) 754–770. doi:10.1111/j.1600-0463.2008.01033.x.

[225] L. Zamai, C. Ponti, P. Mirandola, G. Gobbi, S. Papa, L. Galeotti, et al., NK Cells and Cancer, The Journal of Immunology. 178 (2007) 4011–4016. doi:10.4049/jimmunol.178.7.4011.

[226] B. Nieswandt, M. Hafner, B. Echtenacher, D.N. Männel, Lysis of Tumor Cells by Natural Killer Cells in Mice Is Impeded by Platelets, Cancer Research. 59 (1999) 1295–1300.

[227] M. Bajénoff, B. Breart, A.Y.C. Huang, H. Qi, J. Cazareth, V.M. Braud, et al., Natural killer cell behavior in lymph nodes revealed by static and real-time imaging, Journal of Experimental Medicine. 203 (2006) 619–631. doi:10.1084/jem.20051474.

[228] G.P. Dunn, A.T. Bruce, H. Ikeda, L.J. Old, R.D. Schreiber, Cancer immunoediting: from immunosurveillance to tumor escape, Nat. Immunol. 3 (2002) 991–998.

[229] A.D. Hartkopf, M. Banys, N. Krawczyk, A. Staebler, S. Becker, J. Hoffman, et al., Bone marrow versus sentinel lymph node involvement in breast cancer: a comparison of early hematogenous and early lymphatic tumor spread, Breast Cancer Res Treat. 131 (2012) 501–508.

[230] B. Gerber, A. Krause, H. Müller, D. Richter, T. Reimer, J. Makovitzky, et al., Simultaneous Immunohistochemical Detection of Tumor Cells in Lymph Nodes and Bone Marrow Aspirates in Breast Cancer and Its Correlation With Other Prognostic Factors, Journal of Clinical Oncology. 19 (2001)

960–971.

[231] B. Kubuschok, B. Passlick, J.R. Izbicki, O. Thetter, K. Pantel, Disseminated Tumor Cells in Lymph Nodes as a Determinant for Survival in Surgically Resected Non–Small-Cell Lung Cancer, Journal of Clinical Oncology. 17 (1999) 19–24.

[232] A. Ashkenazi, P. Holland, S.G. Eckhardt, Ligand-Based Targeting of Apoptosis in Cancer: The Potential of Recombinant Human Apoptosis Ligand 2/Tumor Necrosis Factor-Related Apoptosis-Inducing Ligand (rhApo2L/TRAIL), Journal of Clinical Oncology. 26 (2008) 3621–3630. doi:10.1200/JCO.2007.15.7198.

[233] H. Walczak, R.E. Miller, K. Ariail, B. Gliniak, T.S. Griffith, M. Kubin, et al., Tumoricidal activity of tumor necrosis factor−related apoptosis−inducing ligand in vivo, Nature Medicine. 5 (1999) 157–163. doi:10.1038/5517.

[234] S. Lopez-Verges, J.M. Milush, S. Pandey, V.A. York, J. Arakawa-Hoyt, H. Pircher, et al., CD57 defines a functionally distinct population of mature NK cells in the human CD56dimCD16+ NK-cell subset, Blood. 116 (2010) 3865–3874. doi:10.1182/blood-2010-04-282301.

[235] Q. Wing-Han Yuen, Y.P. Zheng, Y.P. Huang, J.F. He, M. Ying, In-vitro Strain and Modulus Measurements in Porcine Cervical Lymph Nodes, The Open Biomedical Engineering Journal. 5 (2011) 39–46.

[236] X.D. Zhang, T. Nguyen, W.D. Thomas, J.E. Sanders, P. Hersey, Mechanisms of resistance of normal cells to TRAIL induced apoptosis vary

between different cell types, FEBS Lett. 482 (2000) 193–199. doi:10.1016/S0014-5793(00)02042-1.

[237] M.J. Mitchell, M.R. King, Theme: Physical Biology in Cancer. 3. The role of cell glycocalyx in vascular transport of circulating tumor cells, AJP: Cell Physiology. 306 (2014) C89–C97. doi:10.1152/ajpcell.00285.2013.

[238] W.J. Allard, J. Matera, M.C. Miller, M. Repollet, M.C. Connelly, C. Rao, et al., Tumor Cells Circulate in the Peripheral Blood of All Major Carcinomas but not in Healthy Subjects or Patients With Nonmalignant Diseases, Clinical Cancer Research. 10 (2004) 6897–6904.

[239] L. Yan, Q. Cai, Y. Xu, The Ubiquitin-CXCR4 Axis Plays an Important Role in Acute Lung Infection-Enhanced Lung Tumor Metastasis, Clin. Cancer Res. 19 (2013) 4706–4716. doi:10.1158/1078-0432.CCR-13-0011.

[240] P. Tucci, M. Agostini, F. Grespi, E.K. Markert, A. Terrinoni, K.H. Vousden, et al., Loss of p63 and its microRNA-205 target results in enhanced cell migration and metastasis in prostate cancer, Proc Natl Acad Sci USA. 109 (2012) 15312–15317. doi:10.1073/pnas.1110977109.

[241] C.-Y. Chang, S.-C. Lin, W.-H. Su, C.-M. Ho, Y.-S. Jou, Somatic LMCD1 mutations promoted cell migration and tumor metastasis in hepatocellular carcinoma, Oncogene. 31 (2012) 2640–2652. doi:10.1038/onc.2011.440.

[242] S. Kim, H. Takahashi, W.-W. Lin, P. Descargues, S. Grivennikov, Y. Kim, et al., Carcinoma-produced factors activate myeloid cells through TLR2 to stimulate metastasis, Nature. 457 (2009) 102–106. doi:10.1038/nature07623.

[243] I.J. Fidler, Biological Behavior of Malignant Melanoma Cells Correlated to

Their Survival in Vivo, Cancer Research. 35 (1975) 218–224.

[244] I.J. Fidler, Inhibition of Pulmonary Metastasis by Intravenous Injection of Specifically Activated Macrophages, Cancer Research. 34 (1974) 1074–1078.

[245] I.J. Fidler, G.L. Nicolson, Organ Selectivity for Implantation Survival and Growth of B16 Melanoma Variant Tumor Lines, Journal of the National Cancer Institute. 57 (1976) 1199–1202.

[246] M.J. Mitchell, M.R. King, Unnatural killer cells to preventbloodborne metastasis: inspiration frombiology and engineering, Expert Rev Anticancer Ther. 14 (2014) 641–644. doi:10.1586/14737140.2014.916619.

[247] V. Subbiah, R.E. Brown, J. Buryanek, J. Trent, A. Ashkenazi, R. Herbst, et al., Targeting the apoptotic pathway in chondrosarcoma using recombinant human Apo2L/TRAIL (dulanermin), a dual proapoptotic receptor (DR4/DR5) agonist, Molecular Cancer Therapeutics. 11 (2012) 2541–2546. doi:10.1158/1535-7163.MCT-12-0358.

[248] R.S. Herbst, S.G. Eckhardt, R. Kurzrock, S. Ebbinghaus, P.J. O'Dwyer, M.S. Gordon, et al., Phase I Dose-Escalation Study of Recombinant Human Apo2L/TRAIL, a Dual Proapoptotic Receptor Agonist, in Patients With Advanced Cancer, Journal of Clinical Oncology. 17 (2010) 2839–2846.

[249] S.K. Bhatia, M.R. King, D.A. Hammer, The state diagram for cell adhesion mediated by two receptors, Biophysical Journal. 84 (2003) 2671–2690. doi:10.1016/S0006-3495(03)75073-5.

[250] S. Chandrasekaran, M.J. McGuire, M.R. King, Sweeping lymph node

micrometastases off their feet: an engineered model to evaluate natural killer cell mediated therapeutic intervention of circulating tumor cells that disseminate to the lymph nodes, Lab Chip. 14 (2014) 118–127. doi:10.1039/C3LC50584G.

[251] R.P. McEver, Selectins: lectins that initiate cell adhesion under flow, Current Opinion in Cell Biology. 14 (2002) 581–586. doi:10.1016/S0955-0674(02)00367-8.

[252] U. von Andrian, J. Chambers, E. Berg, S. Michie, D. Brown, D. Karolak, et al., L-selectin mediates neutrophil rolling in inflamed venules through sialyl LewisX-dependent and -independent recognition pathways, Blood. 82 (1993) 182–191.

[253] T.F. Tedder, D.A. Steeber, P. Pizcueta, L-selectin-deficient mice have impaired leukocyte recruitment into inflammatory sites, The Journal of Experimental Medicine. 181 (1995) 2259–2264.

[254] D.A. Steeber, N.E. Green, S. Sato, T.F. Tedder, Humoral Immune Response in L-Selectin-Deficient Mice, The Journal of Immunology. 157 (1996) 4899–4907.

[255] A. Palecanda, B. Walcheck, D.K. Bishop, M.A. Jutila, Rapid activation-independent shedding of leukocyte L-selectin induced by cross-linking of the surface antigen, Eur. J. Immunol. 22 (1992) 1279–1286.

[256] G.S. Elemer, T.S. Edgington, Monoclonal Antibody to an Activation Neoepitope of Alpha-M Beta-2 Inhibits Multiple Alpha-M Beta-2 Functions, J. Immunol. 152 (1994) 5836–5844.

[257] M. Diamond, J. Garcia-Aguilar, The I domain is a major recognition site on the leukocyte integrin Mac-1 (CD11b/CD18) for four distinct adhesion ligands, The Journal of Cell Biology. (1993).

[258] H. Fan, Ectodomain shedding of TGF-alpha and other transmembrane proteins is induced by receptor tyrosine kinase activation and MAP kinase signaling cascades, The EMBO Journal. 18 (1999) 6962–6972. doi:10.1093/emboj/18.24.6962.

[259] M. Jutila, L. Rott, E. Berg, E. Butcher, Function and regulation of the neutrophil MEL-14 antigen in vivo: comparison with LFA-1 and MAC-1, The Journal of Immunology. 143 (1989) 3318–3324.

[260] K. Wenzel-Seifert, High Constitutive Activity of the Human Formyl Peptide Receptor, J Biol Chem. 273 (1998) 24181–24189. doi:10.1074/jbc.273.37.24181.

[261] K. Wenzel-Seifert, J. Arthur, H. Liu, Quantitative Analysis of Formyl Peptide Receptor Coupling to Giα1, Giα2, and Giα3, J. Biol. Chem. 274 (1999) 33259–33266.

[262] A. Makino, M. Glogauer, G.M. Bokoch, S. Chien, G.W. Schmid-Schönbein, Control of neutrophil pseudopods by fluid shear: role of Rho family GTPases, American Journal of Physiology - Cell Physiology. 288 (2005) C863–71. doi:10.1152/ajpcell.00358.2004.

[263] T. Dewitz, T. Hung, R. Martin, L. McIntire, Mechanical trauma in leukocytes, The Journal of Laboratory and Clinical Medicine. 90 (1977) 728–736.

[264] S. Fukuda, G. Schmid-Schonbein, Centrifugation attenuates the fluid shear response of circulating leukocytes, Journal of Leukocyte Biology. 72 (2002) 133–139.

[265] S. Fukuda, H. Mitsuoka, Leukocyte fluid shear response in the presence of glucocorticoid, Journal of Leukocyte Biology. 75 (2004) 664–670.

[266] M. Coughlin, G. Schmid-Schonbein, Pseudopod Projection and Cell Spreading of Passive Leukocytes in Response to Fluid Shear Stress, Biophysical Journal. 87 (2004) 2035–2042.

[267] S. Fukuda, T. Yasu, D. Predescu, G. Schmid-Schonbein, Mechanisms for Regulation of Fluid Shear Stress Response in Circulating Leukocytes, Circ. Res. 86 (2000) e13–e18.

[268] J. Middleton, S. Neil, J. Wintle, I. Clark-Lewis, H. Moore, C. Lam, et al., Transcytosis and Surface Presentation of IL-8 by Venular Endothelial Cells, Cell. 91 (1997) 385–395.

[269] A. Rot, Neutrophil attractant/activation protein-1 (interleukin-8) inducesin vitro neutrophil migration by haptotactic mechanism, Eur. J. Immunol. 23 (1993) 303–306. doi:10.1002/eji.1830230150.

[270] Y. Tanaka, D. Adams, S. Shaw, Proteoglycans on endothelial cells present adhesion-inducing cytokines to leukocytes, Immunology Today. 14 (1993) 111–115.

[271] D. Hall, I. Beresford, C. Browning, H. Giles, Signalling by CXC-chemokine receptors 1 and 2 expressed in CHO cells: a comparison of calcium mobilization, inhibition of adenylyl cyclase and stimulation of GTPgS

binding induced by IL-8 and GROa, British Journal of Pharmacology. 126 (1999) 810–818.

[272] M. Burger, J. Burger, R. Hoch, Z. Oades, H. Takamori, I. Schraufstatter, Point Mutation Causing Constitutive Signaling of CXCR2 Leads to Transforming Activity Similar to Kaposi's Sarcoma Herpesvirus-G Protein-Coupled Receptor, The Journal of Immunology. 163 (1999) 2017–2022.

[273] G. Chen, J. Way, S. Armour, C. Watson, K. Queen, C. Jayawickreme, et al., Use of Constitutive G Protein-Coupled Receptor Activity for Drug Discovery, Molecular Pharmacology. 57 (2000) 125–134.

[274] M.B. Kim, I.H. Sarelius, Distributions of Wall Shear Stress in Venular Convergences of Mouse Cremaster Muscle, Microcirculation. 10 (2003) 167–178. doi:10.1038/sj.mn.7800182.

[275] D. Zhelev, A. Alteraifi, Controlled Pseudopod Extension of Human Neutrophils Stimulated with Different Chemoattractants, Biophysical Journal. 87 (2004) 688–695.

[276] A. Makino, H. Shin, Y. Komai, S. Fukuda, M. Coughlin, M. Sugihara-Seki, et al., Mechanotransduction in leukocyte activation: A review, Biorheology. 44 (2007) 221–249.

[277] S. Fukuda, G.W. Schmid-Schönbein, Regulation of CD18 expression on neutrophils in response to fluid shear stress, Proc Natl Acad Sci USA. 100 (2003) 13152–13157.

[278] D. Lee, J.B. Schultz, P.A. Knauf, M.R. King, Mechanical Shedding of L-selectin from the Neutrophil Surface during Rolling on Sialyl Lewis x under

Flow, J. Biol. Chem. 282 (2007) 4812–4820. doi:10.1074/jbc.M609994200.

[279] S.S. Su, G.W. Schmid-Schönbein, Internalization of Formyl Peptide Receptor in Leukocytes Subject to Fluid Stresses, Cel. Mol. Bioeng. 3 (2010) 20–29. doi:10.1007/s12195-010-0111-5.

[280] G.W. Schmid-Schonbein, Y.Y. Shih, S. Chien, Morphometry of human leukocytes, Blood. 56 (1980) 866–875.

[281] J. Pillay, I. den Braber, N. Vrisekoop, L.M. Kwast, R.J. de Boer, J.A.M. Borghans, et al., In vivo labeling with 2H2O reveals a human neutrophil lifespan of 5.4 days, Blood. 116 (2010) 625–627. doi:10.1182/blood-2010-01-259028.

[282] A.Y. Chen, F.A. DeLano, S.R. Valdez, J.N. Ha, H.Y. Shin, G.W. Schmid-Schonbein, Receptor cleavage reduces the fluid shear response in neutrophils of the spontaneously hypertensive rat, AJP: Cell Physiology. 299 (2010) C1441–C1449. doi:10.1152/ajpcell.00157.2010.

[283] H. Ali, R. Richardson, B. Haribabu, R. Snyderman, Chemoattractant Receptor Cross-desensitization, Journal of Biological cHemistry. 274 (1999) 6027–6030.

[284] R. Lefkowitz, G Protein-coupled Receptors III: New Roles for Receptor Kinases and β-Arrestins in Receptor Signaling and Desensitization, Journal of Biological cHemistry. 273 (1998) 18677–18680.

[285] J. Didsbury, R. Uhring, E. Tomhave, C. Gerard, N. Gerard, R. Snyderman, Receptor class desensitization of leukocyte chemoattractant receptors, in: Proc Natl Acad Sci USA, 1991: pp. 11564–11568.

[286] R. Richardson, H. Ali, E. Tomhave, B. Haribabu, R. Snyderman, Cross-desensitization of Chemoattractant Receptors Occurs at Multiple Levels, Journal of Biological cHemistry. 270 (1995) 27829–27833. doi:10.1074/jbc.270.46.27829.

[287] R. Richardson, B. Haribabu, R. Snyderman, Cross-desensitization Among Receptors for Platelet Activating Factor and Peptide Chemoattractants: Evidence for Independent Regulatory Pathways, Journal of Biological cHemistry. 271 (1996) 28717–28724. doi:10.1074/jbc.271.45.28717.

[288] E.A. Sprague, B.L. Steinbach, R.M. Nerem, C.J. Schwartz, Influence of a laminar steady-state fluid-imposed wall shear stress on the binding, internalization, and degradation of low-density lipoproteins by cultured arterial endothelium, Circulation. 76 (1987) 648–656.

[289] S. Funamoto, R. Meili, S. Lee, L. Parry, R. Firtel, Spatial and Temporal Regulation of 3-Phosphoinositides by PI 3-Kinase and PTEN Mediates Chemotaxis, Cell. 109 (2002) 611–623.

[290] B. Heit, L. Liu, P. Colarusso, K. Puri, P. Kubes, PI3K accelerates, but is not required for, neutrophil chemotaxis to fMLP, Journal of Cell Science. 121 (2008) 205–214.

[291] S. Merlot, R. Firtel, Leading the way: directional sensing through phosphatidylinositol 3-kinase and other signaling pathways, Journal of Cell Science. 116 (2003) 3471–3476.

[292] A. Sasaki, C. Chun, K. Takeda, R. Firtel, Localized Ras signaling at the leading edge regulates PI3K, cell polarity, and directional cell movement,

The Journal of Cell Biology. 167 (2004) 505–518.

[293] L.A. Sklar, D.A. Finney, Z.G. Oades, A.J. Jesaitis, R.G. Painter, C.G. Cochrane, The dynamics of ligand-receptor interactions. Real-time analyses of association, dissociation, and internalization of an N-formyl peptide and its receptors on the human neutrophil, J Biol Chem. 259 (1984) 5661–5669.

[294] C. Koo, R.J. Lefkowitz, R. Snyderman, The oligopeptide chemotactic factor receptor on human polymorphonuclear leukocyte membranes exists in two affinity states, Biochem. Biophys. Res. Commun. 106 (1982) 442–449.

[295] S.H. Zigmond, S.J. Sullivan, D.A. Lauffenburger, Kinetic Analysis of Chemotactic Peptide Receptor Modulation, The Journal of Cell Biology. 92 (1982) 34–43.

[296] M.P. Bevilacqua, R.M. Nelson, G. Mannori, O. Cecconi, Endothelial-Leukocyte Adhesion Molecules in Human Disease, Annu. Rev. Med. 45 (1994) 361–378. doi:10.1146/annurev.med.45.1.361.

[297] S. Schmidt, M. Moser, M. Sperandio, The molecular basis of leukocyte recruitment and its deficiencies, Mol. Immunol. 55 (2013) 49–58. doi:10.1016/j.molimm.2012.11.006.

[298] C.J. Ball, A.J. Reiffel, S. Chintalapani, M. Kim, J.A. Spector, M.R. King, Hydrogen Sulfide Reduces Neutrophil Recruitment in Hind-Limb Ischemia-Reperfusion Injury in an L-Selectin and ADAM-17–Dependent Manner, Plastic and Reconstructive Surgery. 131 (2013) 487–497. doi:10.1097/PRS.0b013e31827c6e9c.

[299] S.I. Simon, C.E. Green, Molecular mechanics and dynamics of leukocyte

recruitment during inflammation, Annu Rev Biomed Eng. 7 (2005) 151–185. doi:10.1146/annurev.bioeng.7.060804.100423.

[300] W. Deng, S. Srinivasan, X. Zheng, J.A. Putkey, R. Li, Interaction of Calmodulin with l-Selectin at the Membrane Interface: Implication on the Regulation of L-Selectin Shedding, Journal of Molecular Biology. 411 (2011) 220–233. doi:10.1016/j.jmb.2011.05.041.

[301] G.A. Zimmerman, T.M. McIntyre, M. Mehra, S.M. Prescott, Endothelial cell-associated platelet-activating factor: a novel mechanism for signaling intercellular adhesion, The Journal of Cell Biology. 110 (1990) 529–540.

[302] S.M. Prescott, G.A. Zimmerman, D.M. Stafforini, T.M. McIntyre, Platelet-activating factor and related lipid mediators, Annu. Rev. Biochem. 69 (2000) 419–445.

[303] P. Anton, J. O'Connell, D. O'Connell, L. Whitaker, G.C. O'Sullivan, J.K. Collins, et al., Mucosal subepithelial binding sites for the bacterial chemotactic peptide, formyl-methionyl-leucyl-phenylalanine (FMLP), Gut. 42 (1998) 374–379.

[304] W.A. Marasco, S.H. Phan, H. Krutzsch, H.J. Showell, D.E. Feltner, R. Nairn, et al., Purification and identification of formyl-methionyl-leucyl-phenylalanine as the major peptide neutrophil chemotactic factor produced by Escherichia coli, J. Biol. Chem. 259 (1984) 5430–5439.

[305] F. Mariano, B. Bussolati, M. Migliori, S. Russo, G. Triolo, G. Camussi, Platelet-activating factor synthesis by neutrophils, monocytes, and endothelial cells is modulated by nitric oxide production, Shock. 19 (2003)

339–344.

[306] S.M. Prescott, G.A. Zimmerman, T.M. McIntyre, Platelet-activating factor, J Biol Chem. 265 (1990) 17381–17384.

[307] E.J. Carolan, T.B. Casale, Degree of platelet activating factor-induced neutrophil migration is dependent upon the molecular species, J. Immunol. 145 (1990) 2561–2565.

[308] W. Zhou, M.A. Javors, M.S. Olson, Impaired surface expression of PAF receptors on human neutrophils is dependent upon cell activation, Archives of Biochemistry and Biophysics. 308 (1994) 439–445.

[309] G.A. Zimmerman, T.M. McIntyre, S.M. Prescott, Adhesion and signaling in vascular cell-cell interactions, Journal of Clinical Investigation. 98 (1996) 1699–1702. doi:10.1172/JCI118967.

[310] J.A. Nick, N.J. Avdi, S.K. Young, C. Knall, P. Gerwins, G.L. Johnson, et al., Common and Distinct Intracellular Signaling Pathways in Human Neutrophils Utilized by Platelet Activating Factor and FMLP, Journal of Clinical Investigation. 99 (1997) 1–12.

[311] C. Berends, B. Dijkhuizen, J.G. de Monchy, A.E. Dubois, J. Gerritsen, H.F. Kauffman, Inhibition of PAF-induced expression of CD11b and shedding of L-selectin on human neutrophils and eosinophils by the type IV selective PDE inhibitor, rolipram, Eur. Respir. J. 10 (1997) 1000–1007.

[312] S.S. Segal, Regulation of Blood Flow in the Microcirculation, Microcirculation. 12 (2005) 33–45. doi:10.1080/10739680590895028.

[313] J.E. Smolen, T.K. Petersen, C. Koch, S.J. O'Keefe, W.A. Hanlon, S. Seo, et

al., L-selectin signaling of neutrophil adhesion and degranulation involves p38 mitogen-activated protein kinase, J. Biol. Chem. 275 (2000) 15876–15884. doi:10.1074/jbc.M906232199.

[314] A.-P.J. Huovila, A.J. Turner, M. Pelto-Huikko, I. Kärkkäinen, R.M. Ortiz, Shedding light on ADAM metalloproteinases, Trends Biochem. Sci. 30 (2005) 413–422. doi:10.1016/j.tibs.2005.05.006.

[315] P. Marschel, G.W. Schmid-Schönbein, Control of Fluid Shear Response in Circulating Leukocytes by Integrins, Ann Biomed Eng. 30 (n.d.) 333–343. doi:10.1114/1.1475342.

[316] J. Pugin, How tissue injury alarms the immune system and causes a systemic inflammatory response syndrome, Annals of Intensive Care. 2 (2012) 27. doi:10.1186/2110-5820-2-27.

[317] M.J. Eppihimer, H.H. Lipowsky, Effects of leukocyte-capillary plugging on the resistance to flow in the microvasculature of cremaster muscle for normal and activated leukocytes, Microvasc. Res. 51 (1996) 187–201. doi:10.1006/mvre.1996.0020.

[318] G.S. Worthen, B. Schwab, E.L. Elson, G.P. Downey, Mechanics of stimulated neutrophils: cell stiffening induces retention in capillaries, Science. 245 (1989) 183–186.

[319] H. Zhang, C. Sun, M. Glogauer, G.M. Bokoch, Human Neutrophils Coordinate Chemotaxis by Differential Activation of Rac1 and Rac2, The Journal of Immunology. 183 (2009) 2718–2728. doi:10.4049/jimmunol.0900849.

[320] G.A. Zimmerman, T.M. McIntyre, S.M. Prescott, D.M. Stafforini, The platelet-activating factor signaling system and its regulators in syndromes of inflammation and thrombosis, Crit Care Med. 30 (2002) S294–S301.

[321] J. Herter, A. Zarbock, Integrin Regulation during Leukocyte Recruitment, The Journal of Immunology. 190 (2013) 4451–4457. doi:10.4049/jimmunol.1203179.

[322] J. Merlijn van den Berg, F.P.J. Mul, E. Schippers, J.J. Weening, D. Roos, T.W. Kuijpers, B_1 integrin activation on human neutrophils promotes B_2 integrin-mediated adhesion to fibronectin, Eur. J. Immunol. 31 (2013) 276–284.

[323] J.F. DiPersio, P. Billing, R. Williams, J. Gasson, Human Granulocyte-Macrophage Colony-Stimulating Factor and Other Cytokines Prime Human Neutrophils for Enhanced Arachidonic Acid Release and Leukotriene B_4 Synthesis, The Journal of Immunology. 140 (2001) 4315–4322.

[324] S.D. Shukla, Platelet-activating receptor and signal transduction mechanisms, The FASEB Journal. 6 (1992) 2296–2301.

[325] W. Chao, M.S. Olson, Platelet-activating factor: receptors and signal transduction, Biochem. J. 292 (1993) 617–629.

[326] J.L. Parent, C. Le Gouill, A.J. de Brum-Fernandes, M. Rola-Plezscyznski, J. Stankova, Mutations of Two Adjacent Amino Acids Generate Inactive and Constitutively Active Forms of the Human Platelet-activating Factor Receptor, Journal of Biological cHemistry. 271 (1996) 7949–7955. doi:10.1074/jbc.271.14.7949.

[327] N. Ohshima, S. Ishii, T. Izumi, T. Shimizu, Receptor-dependent metabolism of platelet-activating factor in murine macrophages, J. Biol. Chem. 277 (2002) 9722–9727. doi:10.1074/jbc.M112406200.

[328] D.J. Dupré, Z. Chen, C. Le Gouill, C. Thériault, J.-L. Parent, M. Rola-Pleszczynski, et al., Trafficking, ubiquitination, and down-regulation of the human platelet-activating factor receptor, J. Biol. Chem. 278 (2003) 48228–48235. doi:10.1074/jbc.M304082200.

[329] D.J. Killock, A. Ivetić, The cytoplasmic domains of TNFα-converting enzyme (TACE/ADAM17) and L-selectin are regulated differently by p38 MAPK and PKC to promote ectodomain shedding, Biochem. J. 428 (2010) 293–304. doi:10.1074/jbc.275.19.14608.

[330] T.A. Imaizumi, D.M. Stafforini, Y. Yamada, T.M. McIntyre, S.M. Prescott, G.A. Zimmerman, Platelet-activating factor: a mediator for clinicians, Journal of Internal Medicine. 238 (1995) 5–20.

[331] P. Vadas, M. Gold, B. Perelman, G.M. Liss, G. Lack, T. Blyth, et al., Platelet-Activating Factor, PAF Acetylhydrolase, and Severe Anaphylaxis, New England Journal of Medicine. 358 (2007) 28–35.

[332] D.E. Lorant, K.D. Patel, T.M. McIntyre, R.P. McEver, S.M. Prescott, G.A. Zimmerman, Coexpression of GMP-140 and PAF by Endothelium Stimulated by Histamine or Thrombin: A Juxtacrine System for Adhesion and Activation of Neutrophils, The Journal of Cell Biology. 115 (1991) 223–234.

[333] P. Mehlen, A. Puisieux, Metastasis: a question of life or death, Nat Rev

Cancer. 6 (2006) 449–458. doi:10.1038/nrc1886.

[334] I.C. MacDonald, A.C. Groom, A.F. Chambers, Cancer spread and micrometastasis development: Quantitative approaches for in vivo models, Bioessays. 24 (2002) 885–893. doi:10.1002/bies.10156.

[335] J. Li, M.R. King, Adhesion receptors as therapeutic targets for circulating tumor cells, Frontiers in Oncology. 2 (2012) 1–9. doi:10.3389/fonc.2012.00079/abstract.

[336] A.D. Hughes, J. Mattison, L.T. Western, J.D. Powderly, B.T. Greene, M.R. King, Microtube Device for Selectin-Mediated Capture of Viable Circulating Tumor Cells from Blood, Clinical Chemistry. 58 (2012) 846–853. doi:10.1373/clinchem.2011.176669.

[337] B.T. Greene, A.D. Hughes, M.R. King, Circulating Tumor Cells: The Substrate of Personalized Medicine? Frontiers in Oncology. 2 (2012) 1–6. doi:10.3389/fonc.2012.00069.

[338] R.M. Pitti, S.A. Marsters, S. Ruppert, C.J. Donahue, A. Moore, A. Ashkenazi, Induction of Apoptosis by Apo-2 Ligand, a New Member of the Tumor Necrosis Factor Cytokine Family, Journal of Biological cHemistry. 271 (1996) 12687–12690.

[339] M. Plasilova, J. Zivny, J. Jelinek, R. Neuwirtova, J. Cermak, E. Necas, et al., TRAIL (Apo2L) suppresses growth of primary human leukemia and myelodysplasia progenitors, Leukemia. 16 (2002) 67–73.

[340] M.J. Smyth, Y. Hayakawa, K. Takeda, H. Yagita, New aspects of natural killer cell surveillance and therapy of cancer, Nat Rev Cancer. 2 (2002)

850–861.

[341] E. Cretney, K. Takeda, H. Yagita, M. Glaccum, J.J. Peschon, M.J. Smyth, Increased Susceptibility to Tumor Initiation and Metastasis in TNF-Related Apoptosis-Inducing Ligand-Deficient Mice, The Journal of Immunology. 168 (2002) 1356–1361.

[342] K. Takeda, Y. Hayakawa, M.J. Smyth, N. Kayagaki, N. Yamaguchi, S. Kakuta, et al., Involvement of tumor necrosis factor-related apoptosis-inducing ligand in surveillance of tumor metastasis by liver natural killer cells, Nature Medicine. 7 (2001) 94–100.

[343] M.J. Smyth, E. Cretney, K. Takeda, R.H. Wiltrout, L.M. Sedger, N. Kayagaki, et al., Tumor Necrosis Factor–Related Apoptosis-Inducing Ligand (Trail) Contributes to Interferon γ–Dependent Natural Killer Cell Protection from Tumor Metastasis, The Journal of Experimental Medicine. 193 (2001) 661–670.

[344] I.J. Fidler, S. Yano, R.D. Zhang, T. Fujimaki, C.D. Bucana, The seed and soil hypothesis: vascularisation and brain metastases, Lancet Oncol. 3 (2002) 53–57.

[345] M.M. Burdick, J.M. McCaffery, Y.S. Kim, B.S. Bochner, K. Konstantopoulos, Colon carcinoma cell glycolipids, integrins, and other glycoproteins mediate adhesion to HUVECs under flow, American Journal of Physiology - Cell Physiology. 284 (2003) C977–87. doi:10.1152/ajpcell.00423.2002.

[346] J.P. Herbeuval, C. Lambert, O. Sabido, M. Cottier, P. Fournel, M. Dy, et al.,

Macrophages From Cancer Patients: Analysis of TRAIL, TRAIL Receptors, and Colon Tumor Cell Apoptosis, Journal of the National Cancer Institute. 95 (2003) 611–621.

[347] N.A. Thornberry, Y.L. Lazebnik, Caspases: Enemies Within, Science. 281 (1998) 1312–1316. doi:10.1126/science.281.5381.1312.

[348] K.M. Kim, J.J. Song, J.Y. An, Y.T. Kwon, Y.J. Lee, Pretreatment of Acetylsalicylic Acid Promotes Tumor Necrosis Factor-related Apoptosis-inducing Ligand-induced Apoptosis by Down-regulating BCL-2 Gene Expression, Journal of Biological cHemistry. 280 (2005) 41047–41056. doi:10.1074/jbc.M503713200.

[349] S. Fulda, K.M. Debatin, 5-Aza-2′-deoxycytidine and IFN-γ cooperate to sensitize for TRAIL-induced apoptosis by upregulating caspase-8, Oncogene. 25 (2006) 5125–5133. doi:10.1038/sj.onc.1209518.

[350] S. Fulda, W. Wick, M. Weller, K.M. Debatin, Smac agonists sensitize for Apo2L/TRAIL- or anticancer drug-induced apoptosis and induce regression of malignant glioma in vivo, Nature Medicine. 8 (2002) 808–815.

[351] T.J. Kemp, J.S. Kim, S.A. Crist, T.S. Griffith, Induction of necrotic tumor cell death by TRAIL/Apo-2L, Apoptosis. 8 (2003) 587–599. doi:10.1023/A:1026286108366.

[352] N. Holler, R. Zaru, O. Micheau, M. Thome, A. Attinger, S. Valitutti, et al., Fas triggers an alternative, caspase-8-independent cell death pathway using the kinase RIP as effector molecule, Nat. Immunol. 1 (2000) 489–495. doi:10.1038/82732.

[353] O. Meurette, A. Rebillard, L. Huc, G. Le Moigne, D. Merino, O. Micheau, et al., TRAIL induces receptor-interacting protein 1-dependent and caspase-dependent necrosis-like cell death under acidic extracellular conditions, Cancer Research. 67 (2007) 218–226. doi:10.1158/0008-5472.CAN-06-1610.

[354] O. Meurette, L. Huc, A. Rebillard, G. Le Moigne, D. Lagadic-Gossmann, M.-T. Dimanche-Boitrel, TRAIL (TNF-related apoptosis-inducing ligand) induces necrosis-like cell death in tumor cells at acidic extracellular pH, Ann. N. Y. Acad. Sci. 1056 (2005) 379–387. doi:10.1196/annals.1352.018.

[355] J.M. Rutkowski, M.A. Swartz, A driving force for change: interstitial flow as a morphoregulator, Trends Cell Biol. 17 (2007) 44–50. doi:10.1016/j.tcb.2006.11.007.

[356] A. Arlt, J. Vorndamm, M. Breitenbroich, U.R. Fölsch, H. Kalthoff, W.E. Schmidt, et al., Inhibition of NF-κB sensitizes human pancreatic carcinoma cells to apoptosis induced by etoposide (VP16) or doxorubicin, Oncogene. 20 (2001) 859–868. doi:10.1038/sj.onc.1204168.

[357] S. Li, Y. Zhou, R. Wang, H. Zhang, Y. Dong, C. Ip, Selenium sensitizes MCF-7 breast cancer cells to doxorubicin-induced apoptosis through modulation of phospho-Akt and its downstream substrates, Molecular Cancer Therapeutics. 6 (2007) 1031–1038. doi:10.1158/1535-7163.MCT-06-0643.

[358] H.K. Koblish, S. Zhao, C.F. Franks, R.R. Donatelli, R.M. Tominovich, L.V. LaFrance, et al., Benzodiazepinedione inhibitors of the Hdm2:p53 complex

suppress human tumor cell proliferation in vitro and sensitize tumors to doxorubicin in vivo, Molecular Cancer Therapeutics. 5 (2006) 160–169. doi:10.1158/1535-7163.MCT-05-0199.

[359] A. Ashkenazi, R.C. Pai, S. Fong, S. Leung, D.A. Lawrence, S.A. Marsters, et al., Safety and antitumor activity of recombinant soluble Apo2 ligand, J. Clin. Invest. 104 (1999) 155–162. doi:10.1172/JCI6926.

[360] S.A. Quast, A. Berger, N. Buttstädt, K. Friebel, R. Schönherr, J. Eberle, General Sensitization of Melanoma Cells for TRAIL-Induced Apoptosis by the Potassium Channel Inhibitor TRAM-34 Depends on Release of SMAC, PLoS ONE. 7 (2012) e39290. doi:10.1371/journal.pone.0039290.

[361] E. Norberg, S. Orrenius, B. Zhivotovsky, Mitochondrial regulation of cell death: processing of apoptosis-inducing factor (AIF), Biochem. Biophys. Res. Commun. 396 (2010) 95–100. doi:10.1016/j.bbrc.2010.02.163.

[362] V. Stagni, M. Mingardi, S. Santini, D. Giaccari, D. Barilà, ATM kinase activity modulates cFLIP protein levels: potential interplay between DNA damage signalling and TRAIL-induced apoptosis, Carcinogenesis. 31 (2010) 1956–1963. doi:10.1093/carcin/bgq193.

[363] S.V. Garimella, A. Rocca, S. Lipkowitz, WEE1 Inhibition Sensitizes Basal Breast Cancer Cells to TRAIL-Induced Apoptosis, Molecular Cancer Research. 10 (2012) 75–85.

[364] A. Suliman, A. Lam, R. Datta, R.K. Srivastava, Intracellular mechanisms of TRAIL: apoptosis through mitochondrial-dependent and -independent pathways, Oncogene. 20 (2001) 2122–2133.

[365] I. Fidler, The pathogenesis of cancer metastasis: the “seed and soil” hypothesis revisited, Nat Rev Cancer. 3 (2003) 1–6.

[366] P. Paterlini-Brechot, N.L. Benali, Circulating tumor cells (CTC) detection: clinical impact and future directions, Cancer Letters. 253 (2007) 180–204. doi:10.1016/j.canlet.2006.12.014.

[367] A. Chambers, G. Naumov, S. Vantyghem, Tuck, AB, Molecular biology of breast metastasis: Clinical implications of experimental studies on metastatic inefficiency, Breast Cancer Research. 2 (2000) 400–407.

[368] J. Bouma, J.H. Beijnen, A. Bult, W.J.M. Underberg, Anthracycline antitumour agents, Pharmaceutisch Weekblad Scientific Edition. 8 (1986) 109–133. doi:10.1007/BF02086146.

[369] L. Reddy, Drug delivery to tumours: recent strategies, Journal of Pharmacy and Pharmacology. 57 (2005) 1231–1242.

[370] A. Fritze, F. Hens, R. Kimpfler, R. Schubert, R. Peschka-Suss, Remote loading of doxorubicin into liposomes driven by a transmembrane phosphate gradient, Biochimica Et Biophysica Acta. 1758 (2006) 1633–1640. doi:10.1016/j.bbamem.2006.05.028.

[371] M. Saad, O.B. Garbuzenko, E. Ber, P. Chandna, J.J. Khandare, V.P. Pozharov, et al., Receptor targeted polymers, dendrimers, liposomes: Which nanocarrier is the most efficient for tumor-specific treatment and imaging? Journal of Controlled Release. 130 (2008) 107–114. doi:10.1016/j.jconrel.2008.05.024.

[372] E. Herman, A. Rahman, V. Ferrans, J. Vick, P. Schein, Prevention of

Chronic Doxorubicin Cardiotoxicity in Beagles by Liposomal Encapsulation, Cancer Research. 43 (1983) 5427–5432.

[373] R. Krishna, N. McIntosh, K. Riggs, Doxorubicin Encapsulated in Sterically Stabilized Liposomes Exhibits Renal and Biliary Clearance Properties That Are Independent of Valspodar (PSC 833) under Conditions That Significantly Inhibit Nonencapsulated Drug Excretion, Clinical Cancer Research. 5 (1999) 2939–2947.

[374] A.A. Gabizon, Pegylated Liposomal Doxorubicin: Metamorphosis of an Old Drug into a New Form of Chemotherapy, Cancer Investigation. 19 (2001) 424–436.

[375] W. Saltzman, Drug delivery: engineering principles for drug therapy, New York: Oxford University Press, 2001.

[376] A. Soundararajan, A. Bao, W. Phillips, R. Perez III, B. Goins, [186Re]Liposomal doxorubicin (Doxil): in vitro stability, pharmacokinetics, imaging and biodistribution in a head and neck squamous cell carcinoma xenograft model, Nuclear Medicine and Biology. 36 (2009) 515–524.

[377] D.D. Lasic, Doxorubicin in sterically stabilized liposomes, Nature. 380 (1996) 561–562. doi:10.1038/380561a0.

[378] M. Silvander, Steric stabilization of liposomes - a review, Progress in Colloid Polymer Science. 120 (2002) 35–40.

[379] A. Gabzion, H. Shmeeda, Y. Barenholz, Pharmacokinetics of Pegylated Liposomal Doxorubicin: Review of Animal and Human Studies, Clinical Pharmacokinetics. 42 (2003) 419–436.

[380] C. Carrion, M. De Madariaga, J. Domingo, In vitro cytotoxic study of immunoliposomal doxorubicin targeted to human CD34+ leukemic cells, Life Sciences. 75 (2004) 313–328.

[381] H.D. Han, A. Lee, T. Hwang, C.K. Song, H. Seong, J. Hyun, et al., Enhanced circulation time and antitumor activity of doxorubicin by comblike polymer-incorporated liposomes, Journal of Controlled Release. 120 (2007) 161–168. doi:10.1016/j.jconrel.2007.03.020.

[382] B. Ceh, M. Winterhalter, P. Frederik, J. Vallner, D. Lasic, Stealth® liposomes: from theory to product, Advanced Drug Delivery Reviews. 24 (1997) 165–177.

[383] J. Kitayama, N. Tsuno, E. Sunami, T. Osada, T. Muto, H. Nagawa, E-selectin can mediate the arrest type of adhesion of colon cancer cells under physiological shear flow, European Journal of Cancer. 36 (2000) 121–127.

[384] T. Krause, G.A. Turner, Are selectins involved in metastasis? Clinical & Experimental Metastasis. 17 (1999) 183–192. doi:10.1023/A:1006626500852.

[385] A.D. Hughes, M.R. King, Use of Naturally Occurring Halloysite Nanotubes for Enhanced Capture of Flowing Cells, Langmuir. 26 (2010) 12155–12164. doi:10.1021/la101179y.

[386] S. Amselem, R. Cohen, S. Druckmann, A. Gabizon, D. Goren, R.M. Abra, et al., Preparation and Characterization of Liposomal Doxorubicin for Human Use, Journal of Liposome Research. 2 (1992) 93–123.

[387] G. Haran, R. Cohen, L. Bar, Y. Barenholz, Transmembrane ammonium

sulfate gradients in liposomes produce efficient and stable entrapment of amphipathic weak bases, Biochimica Et Biophysica Acta. 1151 (1993) 201–215.

[388] Z. Huang, M. King, An immobilized nanoparticle-based platform for efficient gene knockdown of targeted cells in the circulation, Gene Therapy. 16 (2009) 1271–1282.

[389] J. Wojciechowski, S. Narasipura, N. Charles, D. Mickelsen, K. Rana, M. Blair, et al., Capture and enrichment of CD34-positive haematopoietic stem and progenitor cells from blood circulation using P-selectin in an implantable device, British Journal of Hematology. 140 (2008) 673–681.

[390] C. Ball, M. King, Role of c-Abl in L-selectin shedding from the neutrophil surface, Blood Cells, Molecules, and Diseases. 46 (2011) 246–251.

[391] X. Yin, K. Rana, V. Ponmudi, M. King, Knockdown of fucosyltransferase III disrupts the adhesion of circulating cancer cells to E-selectin without affecting hematopoietic cell adhesion, Carbohydrate Research. 345 (2010) 2334–2342.

[392] F. Orr, H. Wang, R. Lafrenie, S. Scherbarth, D. Nance, Interactions between cancer cells and the endothelium in metastasis, J. Pathol. 190 (2000) 310–329.

[393] Y. Kim, L. Borsig, H. Han, N. Varki, A. Varki, Distinct Selectin Ligands on Colon Carcinoma Mucins Can Mediate Pathological Interactions among Platelets, Leukocytes, and Endothelium, The American Journal of Pathology. 155 (1999) 461.

[394] B. Ceh, D. Lasic, A rigorous theory of remote loading of drugs into liposomes, Langmuir. 11 (1995) 3356–3368.

[395] C. Chemin, J. Péan, C. Bourgaux, G. Pabst, P. Wuthrich, P. Couvreur, et al., Supramolecular organization of S12363-liposomes prepared with two different remote loading processes, Biochimica Et Biophysica Acta. 1788 (2009) 926–935.

[396] E. Forssen, M. Willis, Ligand-targeted liposomes, Advanced Drug Delivery Reviews. 29 (1998) 249–271.

[397] R. Nallamothu, G. Wood, C. Pattillo, R. Scott, M. Kiani, B. Moore, et al., A tumor vasculature targeted liposome delivery system for combretastatin A4: design, characterization, and in vitro evaluation, AAPS PharmSciTech. 7 (2006) E1–E10.

[398] R. Kannagi, M. Izawa, T. Koike, K. Miyazaki, N. Kimura, Carbohydrate-mediated cell adhesion in cancer metastasis and angiogenesis, Cancer Science. 95 (2004) 377–384.

[399] J. Magnani, The discovery, biology, and drug development of sialyl Lea and sialyl Lex, Archives of Biochemistry and Biophysics. 426 (2004) 122–131.

[400] J. Ogawa, H. Inoue, S. Koide, Expression of α-1,3-Fucosyltransferase Type IV and VII Genes Is Related to Poor Prognosis in Lung Cancer, Cancer Research. 56 (1996) 325–329.

[401] W. Tsuruta, H. Tsurushima, T. Yamamoto, K. Suzuki, N. Yamazaki, A. Matsumura, Application of liposomes incorporating doxorubicin with sialyl Lewis X to prevent stenosis after rat carotid artery injury, Biomaterials. 30

(2009) 118–125.

[402] A.N. Lukyanov, T.A. Elbayoumi, A.R. Chakilam, V.P. Torchilin, Tumor-targeted liposomes: doxorubicin-loaded long-circulating liposomes modified with anti-cancer antibody, Journal of Controlled Release. 100 (2004) 135–144. doi:10.1016/j.jconrel.2004.08.007.

[403] C.G. Begley, A.F. Lopez, N.A. Nicola, D.J. Warren, M.A. Vadas, C.J. Sanderson, et al., Purified colony-stimulating factors enhance the survival of human neutrophils and eosinophils in vitro: a rapid and sensitive microassay for colony-stimulating factors, Blood. 68 (1986) 162–166.

[404] S. Riethdorf, H. Wikman, K. Pantel, Review: Biological relevance of disseminated tumor cells in cancer patients, International Journal of Cancer. 123 (2008) 1991–2006. doi:10.1002/ijc.23825.

[405] P. Gassmann, M.L. Kang, S.T. Mees, J. Haier, In vivo tumor cell adhesion in the pulmonary microvasculature is exclusively mediated by tumor cell--endothelial cell interaction, BMC Cancer. 10 (2010) 177. doi:10.1186/1471-2407-10-177.

[406] Y.S. Chang, E. di Tomaso, D.M. McDonald, R. Jones, R.K. Jain, L.L. Munn, Mosaic blood vessels in tumors: frequency of cancer cells in contact with flowing blood, Proc Natl Acad Sci USA. 97 (2000) 14608–14613. doi:10.1073/pnas.97.26.14608.

[407] T.P. Butler, P.M. Gullino, Quantitation of cell shedding into efferent blood of mammary adenocarcinoma, Cancer Research. 35 (1975) 512–516.

[408] C. Huang, J.T. Mason, Geometric packing constraints in egg

phosphatidylcholine vesicles, Proc. Natl. Acad. Sci. U.S.a. 75 (1978) 308–310.

[409] T.A. Doherty, N. Khorram, J.E. Chang, H.-K. Kim, P. Rosenthal, M. Croft, et al., STAT6 regulates natural helper cell proliferation during lung inflammation initiated by Alternaria, Am. J. Physiol. Lung Cell Mol. Physiol. 303 (2012) L577–88. doi:10.1152/ajplung.00174.2012.

[410] P. Malý, A. Thall, B. Petryniak, C.E. Rogers, P.L. Smith, R.M. Marks, et al., The alpha(1,3)fucosyltransferase Fuc-TVII controls leukocyte trafficking through an essential role in L-, E-, and P-selectin ligand biosynthesis, Cell. 86 (1996) 643–653.

[411] E.M. Janssen, N.M. Droin, E.E. Lemmens, M.J. Pinkoski, S.J. Bensinger, B.D. Ehst, et al., CD4+ T-cell help controls CD8+ T-cell memory via TRAIL-mediated activation-induced cell death, Nature. 434 (2005) 88–93. doi:10.1038/nature03337.

[412] H.L. Goldsmith, The microrheology of red blood cell suspensions, J. Gen. Physiol. 52 (1968) 5–28.

[413] H.L. Goldsmith, D.N. Bell, S. Braovac, A. Steinberg, F. McIntosh, Physical and chemical effects of red cells in the shear-induced aggregation of human platelets, Biophysical Journal. 69 (1995) 1584–1595. doi:10.1016/S0006-3495(95)80031-7.

[414] N. Kato, Y. Yuzawa, T. Kosugi, A. Hobo, W. Sato, Y. Miwa, et al., The E-Selectin Ligand Basigin/CD147 Is Responsible for Neutrophil Recruitment in Renal Ischemia/Reperfusion, Journal of the American Society of

Nephrology. 20 (2009) 1565–1576. doi:10.1681/ASN.2008090957.

[415] I.J. Fidler, G.L. Nicolson, Fate of Recirculating B16 Melanoma Metastatic Variant Cells in Parabiotic Syngeneic Recipients: Brief Communication, Journal of the National Cancer Institute. 58 (1977) 1867–1872.

[416] H. Xiang, C.B. Nguyen, S.K. Kelley, N. Dybdal, E. Escandon, Tissue distribution, stability, and pharmacokinetics of Apo2 ligand/tumor necrosis factor-related apoptosis-inducing ligand in human colon carcinoma COLO205 tumor-bearing nude mice, Drug Metabolism and Disposition. 32 (2004) 1230–1238. doi:10.1124/dmd.104.000323.

[417] K. Takeda, E. Cretney, Y. Hayakawa, T. Ota, H. Akiba, K. Ogasawara, et al., TRAIL identifies immature natural killer cells in newborn mice and adult mouse liver, Blood. 105 (2005) 2082–2089. doi:10.1182/blood-2004-08-3262.

[418] I. Waldhauer, A. Steinle, NK cells and cancer immunosurveillance, Oncogene. 27 (2008) 5932–5943. doi:10.1038/onc.2008.267.

[419] M.Y. Kim, T. Oskarsson, S. Acharyya, D.X. Nguyen, X.H.F. Zhang, L. Norton, et al., Tumor self-seeding by circulating cancer cells, Cell. 139 (2009) 1315–1326. doi:10.1016/j.cell.2009.11.025.

[420] M. Bernal, A. Concha, P. Sáenz-López, A.I. Rodriguez, T. Cabrera, F. Garrido, et al., Leukocyte infiltrate in gastrointestinal adenocarcinomas is strongly associated with tumor microsatellite instability but not with tumor immunogenicity, Cancer Immunol Immunother. 60 (2011) 869–882.

[421] H. Shankaran, S. Neelamegham, Hydrodynamic forces applied on

intercellular bonds, soluble molecules, and cell-surface receptors, Biophysical Journal. 86 (2004) 576–588. doi:10.1016/S0006-3495(04)74136-3.

[422] Y. Zhao, S. Chien, S. Weinbaum, Dynamic contact forces on leukocyte microvilli and their penetration of the endothelial glycocalyx, Biophysical Journal. 80 (2001) 1124–1140. doi:10.1016/S0006-3495(01)76090-0.

[423] S. Sabri, M. Soler, C. Foa, A. Pierres, A. Benoliel, P. Bongrand, Glycocalyx modulation is a physiological means of regulating cell adhesion, Journal of Cell Science. 113 (2000) 1589–1600.

[424] M. Jo, T.H. Kim, D.W. Seol, J.E. Esplen, K. Dorko, T.R. Billiar, et al., Apoptosis induced in normal human hepatocytes by tumor necrosis factor-related apoptosis-inducing ligand, Nature Medicine. 6 (2000) 564–567. doi:10.1038/75045.

[425] T.M. Cao, T. Takatani, M.R. King, Effect of extracellular pH on selectin adhesion: theory and experiment, Biophysical Journal. 104 (2013) 292–299. doi:10.1016/j.bpj.2012.12.005.

[426] D. Deeb, H. Jiang, X. Gao, M.S. Hafner, H. Wong, G. Divine, et al., Curcumin sensitizes prostate cancer cells to tumor necrosis factor-related apoptosis-inducing ligand/Apo2L by inhibiting nuclear factor-kappaB through suppression of IkappaBalpha phosphorylation, Molecular Cancer Therapeutics. 3 (2004) 803–812.

[427] B. Weigelt, J.L. Peterse, L.J. van't Veer, Breast cancer metastasis: markers and models, Nat Rev Cancer. 5 (2005) 591–602. doi:10.1038/nrc1670.

[428] S. Weinbaum, J.M. Tarbell, E.R. Damiano, The structure and function of the endothelial glycocalyx layer, Annu Rev Biomed Eng. 9 (2007) 121–167. doi:10.1146/annurev.bioeng.9.060906.151959.

[429] B.P. Toole, T.N. Wight, M.I. Tammi, Hyaluronan-cell interactions in cancer and vascular disease, J. Biol. Chem. 277 (2002) 4593–4596. doi:10.1074/jbc.R100039200.

[430] H.H. Lipowsky, The endothelial glycocalyx as a barrier to leukocyte adhesion and its mediation by extracellular proteases, Ann Biomed Eng. 40 (2012) 840–848. doi:10.1007/s10439-011-0427-x.

[431] A.R. Pries, T.W. Secomb, P. Gaehtgens, The endothelial surface layer, Pflugers Arch. 440 (2000) 653–666. doi:10.1007/s004240000307.

[432] S. Reitsma, D.W. Slaaf, H. Vink, M.A.M.J. Zandvoort, M.G.A. oude Egbrink, The endothelial glycocalyx: composition, functions, and visualization, Pflugers Arch. 454 (2007) 345–359. doi:10.1007/s00424-007-0212-8.

[433] H. Vink, B.R. Duling, Identification of distinct luminal domains for macromolecules, erythrocytes, and leukocytes within mammalian capillaries, Circ. Res. 79 (1996) 581–589.

[434] B.M. van den Berg, H. Vink, J.A.E. Spaan, The endothelial glycocalyx protects against myocardial edema, Circ. Res. 92 (2003) 592–594. doi:10.1161/01.RES.0000065917.53950.75.

[435] J. Rostgaard, K. Qvortrup, Electron Microscopic Demonstrations of Filamentous Molecular Sieve Plugs in Capillary Fenestrae, Microvasc. Res.

53 (1997) 1–13.

[436] E.R. Damiano, D.S. Long, F.H. El-Khatib, On the motion of a sphere in a Stokes flow parallel to a Brinkman half-space, Journal of Fluid Mechanics. 500 (2004) 75–101.

[437] E.R. Damiano, D.S. Long, M.L. Smith, Estimation of viscosity profiles using velocimetry data from parallel flows of linearly viscous fluids: application to microvascular haemodynamics, Journal of Fluid Mechanics. 512 (2004) 1–19.

[438] M.W. Keller, D.N. Damon, B.R. Duling, Determination of capillary tube hematocrit during arteriolar microperfusion, Am. J. Physiol. 266 (1994) H2229–38.

[439] B. Klitzman, B.R. Duling, Microvascular hematocrit and red cell flow in resting and contracting striated muscle, Am J Physiol Heart Circ Physiol. 237 (1979) H481–90.

[440] I.H. Sarelius, B.R. Duling, Direct measurement of microvessel hematocrit, red cell flux, velocity, and transit time, Am J Physiol Heart Circ Physiol. 243 (1982) H1018–26.

[441] C. Desjardins, B.R. Duling, Heparinase treatment suggests a role for the endothelial cell glycocalyx in regulation of capillary hematocrit, Am. J. Physiol. 258 (1990) H647–54.

[442] J.M. Squire, M. Chew, G. Nneji, C. Neal, J. Barry, C. Michel, Quasi-periodic substructure in the microvessel endothelial glycocalyx: a possible explanation for molecular filtering? J. Struct. Biol. 136 (2001) 239–255.

doi:10.1006/jsbi.2002.4441.

[443] C.C. Michel, Starling: the formulation of his hypothesis of microvascular fluid exchange and its significance after 100 years, Exp. Physiol. 82 (1997) 1–30.

[444] X. Hu, S. Weinbaum, A New View of Starling's Hypothesis at the Microstructural Level, Microvasc. Res. 58 (1999) 281–304.

[445] Z. Pang, J.M. Tarbell, In vitro Study of Starling's Hypothesis in a Cultured Monolayer of Bovine Aortic Endothelial Cells, J Vasc Res. 40 (2003) 351–358. doi:10.1159/000072699.

[446] R.H. Adamson, J.F. Lenz, X. Zhang, G.N. Adamson, S. Weinbaum, F.E. Curry, Oncotic pressures opposing filtration across non-fenestrated rat microvessels, The Journal of Physiology. 557 (2004) 889–907. doi:10.1113/jphysiol.2003.058255.

[447] R.L. Jackson, S.J. Busch, A.D. Cardin, Glycosaminoglycans: molecular properties, protein interactions, and role in physiological processes, Physiol. Rev. 71 (1991) 481–539.

[448] A. Oohira, T.N. Wight, P. Bornstein, Sulfated proteoglycans synthesized by vascular endothelial cells in culture, J. Biol. Chem. 258 (1983) 2014–2021.

[449] R.D. Rosenberg, N.W. Shworak, J. Liu, J.J. Schwartz, L. Zhang, Heparan sulfate proteoglycans of the cardiovascular system. Specific structures emerge but how is synthesis regulated? Journal of Clinical Investigation. 99 (1997) 2062–2070. doi:10.1172/JCI119377.

[450] C.B. Henry, B.R. Duling, Permeation of the luminal capillary glycocalyx is

determined by hyaluronan, Am J Physiol Heart Circ Physiol. 277 (1999) H508–14.

[451] V.H. Huxley, F.E. Curry, Differential actions of albumin and plasma on capillary solute permeability, Am. J. Physiol. 260 (1991) H1645–54.

[452] R.K. Sironen, M. Tammi, R. Tammi, P.K. Auvinen, M. Anttila, V.-M. Kosma, Hyaluronan in human malignancies, Exp. Cell Res. 317 (2011) 383–391. doi:10.1016/j.yexcr.2010.11.017.

[453] N. Itano, K. Kimata, Altered hyaluronan biosynthesis in cancer progression, Seminars in Cancer Biology. 18 (2008) 268–274. doi:10.1016/j.semcancer.2008.03.006.

[454] D. Hamerman, G.J. Todaro, H. Green, The production of hyaluronate by spontaneously established cell lines and viral transformed lines of fibroblastic origin, Biochimica Et Biophysica Acta (BBA) - Mucoproteins and Mucopolysaccharides. 101 (1965) 343–351. doi:10.1016/0926-6534(65)90013-8.

[455] J.J. Hopwood, A. Dorfman, Glycosaminoglycan synthesis by cultured human skin fibroblasts after transformation with simian virus 40, Journal of Biological cHemistry. 252 (1977) 4777–4785.

[456] J.G. Leonard, A.H. Hale, D.E. Roll, H.E. Conrad, M.J. Weber, Turnover of Cellular Carbohydrates in Normal and Rous Sarcoma Virus-transformed Cells, Cancer Research. 38 (1978) 185–188.

[457] N. Itano, T. Sawai, M. Yoshida, P. Lenas, Y. Yamada, M. Imagawa, et al., Three isoforms of mammalian hyaluronan synthases have distinct enzymatic

properties, J. Biol. Chem. 274 (1999) 25085–25092.

[458] N. Liu, F. Gao, Z. Han, X. Xu, C.B. Underhill, L. Zhang, Hyaluronan Synthase 3 Overexpression Promotes the Growth of TSU Prostate Cancer Cells, Cancer Research. 61 (2001) 5207–5214.

[459] Y. Li, P. Heldin, Hyaluronan production increases the malignant properties of mesothelioma cells, British Journal of Cancer. 85 (2001) 600–607. doi:10.1054/bjoc.2001.1922.

[460] R. Kosaki, K. Watanabe, Y. Yamaguchi, Overproduction of Hyaluronan by Expression of the Hyaluronan Synthase Has2 Enhances Anchorage-independent Growth and Tumorigenicity, Cancer Research. 59 (1999) 1141–1145.

[461] N. Itano, T. Sawai, O. Miyaishi, K. Kimata, Relationship between hyaluronan production and metastatic potential of mouse mammary carcinoma cells, Cancer Research. 59 (1999) 2499–2504.

[462] P. Klingbeil, R. Natrajan, G. Everitt, R. Vatcheva, C. Marchio, J. Palacios, et al., CD44 is overexpressed in basal-like breast cancers but is not a driver of 11p13 amplification, Breast Cancer Res Treat. 120 (2010) 95–109.

[463] M. Götte, G.W. Yip, Heparanase, hyaluronan, and CD44 in cancers: a breast carcinoma perspective, Cancer Research. 66 (2006) 10233–10237. doi:10.1158/0008-5472.CAN-06-1464.

[464] M.E. Prince, R. Sivanandan, A. Kaczorowski, G.T. Wolf, M.J. Kaplan, P. Dalerba, et al., Identification of a subpopulation of cells with cancer stem cell properties in head and neck squamous cell carcinoma, Proc. Natl. Acad.

Sci. U.S.a. 104 (2007) 973–978. doi:10.1073/pnas.0610117104.

[465] O. Nagano, S. Okazaki, H. Saya, Redox regulation in stem-like cancer cells by CD44 variant isoforms, Oncogene. (2013). doi:10.1038/onc.2012.638.

[466] S. Seiter, R. Arch, S. Reber, D. Komitowski, M. Hofmann, H. Ponta, et al., Prevention of tumor metastasis formation by anti-variant CD44, The Journal of Experimental Medicine. 177 (1993) 443–455.

[467] U. Günthert, M. Hofmann, W. Rudy, S. Reber, M. Zöller, I. Haussmann, et al., A new variant of glycoprotein CD44 confers metastatic potential to rat carcinoma cells, Cell. 65 (1991) 13–24.

[468] M.J. Paszek, C.C. DuFort, M.G. Rubashkin, M.W. Davidson, K.S. Thorn, J.T. Liphardt, et al., Scanning angle interference microscopy reveals cell dynamics at the nanoscale, Nat Meth. 9 (2012) 825–827. doi:10.1038/nmeth.2077.

[469] G. Méhes, A. Witt, E. Kubista, P.F. Ambros, Circulating breast cancer cells are frequently apoptotic, The American Journal of Pathology. 159 (2001) 17–20. doi:10.1016/S0002-9440(10)61667-7.

[470] M. Yu, A. Bardia, B.S. Wittner, S.L. Stott, M.E. Smas, D.T. Ting, et al., Circulating Breast Tumor Cells Exhibit Dynamic Changes in Epithelial and Mesenchymal Composition, Science. 339 (2013) 580–584. doi:10.1126/science.1228522.

[471] R. Kalluri, R. Weinberg, The basics of epithelial-mesenchymal transition, The Journal of Clinical Investigation. 119 (2009) 1420. doi:10.1172/JCI39104.

[472] J.P. Thiery, Epithelial–mesenchymal transitions in tumour progression, Nat Rev Cancer. 2 (2002) 442–454. doi:10.1038/nrc822.

[473] D.G. Duda, A.M.M.J. Duyverman, M. Kohno, M. Snuderl, E.J.A. Steller, D. Fukumura, et al., Malignant cells facilitate lung metastasis by bringing their own soil, Proc. Natl. Acad. Sci. U.S.a. 107 (2010) 21677–21682.

[474] J.-M. Hou, M.G. Krebs, L. Lancashire, R. Sloane, A. Backen, R.K. Swain, et al., Clinical significance and molecular characteristics of circulating tumor cells and circulating tumor microemboli in patients with small-cell lung cancer, Journal of Clinical Oncology. 30 (2012) 525–532. doi:10.1200/JCO.2010.33.3716.

[475] M.B. Lawrence, T.A. Springer, Leukocytes roll on a selectin at physiologic flow rates: distinction from and prerequisite for adhesion through integrins, Cell. 65 (1991) 859–873.

[476] M.B. Lawrence, T.A. Springer, Neutrophils roll on E-selectin, The Journal of Immunology. 151 (1993) 6339–6346.

[477] J. Vitte, A.M. Benoliel, A. Pierres, P. Bongrand, Regulation of cell adhesion, Clinical Hemorheology and Microcirculation. 33 (2005) 167–188.

[478] P. Robert, A. Nicolas, S. Aranda-Espinoza, P. Bongrand, L. Limozin, Minimal encounter time and separation determine ligand-receptor binding in cell adhesion, Biophysical Journal. 100 (2011) 2642–2651. doi:10.1016/j.bpj.2011.04.011.

[479] M. Soler, S. Desplat-Jego, B. Vacher, L. Ponsonnet, M. Fraterno, P. Bongrand, et al., Adhesion-related glycocalyx study: quantitative approach

with imaging-spectrum in the energy filtering transmission electron microscope (EFTEM), FEBS Lett. 429 (1998) 89–94.

[480] M. Soler, C. Merant, C. Servant, M. Fraterno, C. Allasia, J.C. Lissitzky, et al., Leukosialin (CD43) behavior during adhesion of human monocytic THP-1 cells to red blood cells, Journal of Leukocyte Biology. 61 (1997) 609–618.

[481] S.I. Grivennikov, F.R. Greten, M. Karin, Immunity, Inflammation, and Cancer, Cell. 140 (2010) 883–899. doi:10.1016/j.cell.2010.01.025.

[482] C.B.S. Henry, B.R. Duling, TNF-α increases entry of macromolecules into luminal endothelial cell glycocalyx, American Journal of Physiology - Cell Physiology. 279 (2000) H2815–H2823.

[483] A.W. Mulivor, H.H. Lipowsky, Inflammation- and ischemia-induced shedding of venular glycocalyx, American Journal of Physiology - Cell Physiology. 286 (2004) H1672–80. doi:10.1152/ajpheart.00832.2003.

[484] A.W. Mulivor, H.H. Lipowsky, Role of glycocalyx in leukocyte-endothelial cell adhesion, American Journal of Physiology - Cell Physiology. 283 (2002) H1282–91. doi:10.1152/ajpheart.00117.2002.

[485] K.F. Hofmann-Kiefer, G.I. Kemming, D. Chappell, M. Flondor, H. Kisch-Wedel, A. Hauser, et al., Serum heparan sulfate levels are elevated in endotoxemia, European Journal of Medical Research. 14 (2009) 526–531. doi:10.1186/2047-783X-14-12-526.

[486] A.A. Constantinescu, H. Vink, J.A.E. Spaan, Elevated capillary tube hematocrit reflects degradation of endothelial cell glycocalyx by oxidized

LDL, American Journal of Physiology - Cell Physiology. 280 (2001) H1051–H1057.

[487] M. Rehm, D. Bruegger, F. Christ, P. Conzen, M. Thiel, M. Jacob, et al., Shedding of the endothelial glycocalyx in patients undergoing major vascular surgery with global and regional ischemia, Circulation. 116 (2007) 1896–1906. doi:10.1161/CIRCULATIONAHA.106.684852.

[488] N. Mitsiades, W. Yu, V. Poulaki, M. Tsokos, I. Stamenkovic, Matrix Metalloproteinase-7-mediated Cleavage of Fas Ligand Protects Tumor Cells from Chemotherapeutic Drug Cytotoxicity, Cancer Research. 61 (2001) 577–581.

[489] M. Madlener, W.C. Parks, S. Werner, Matrix metalloproteinases (MMPs) and their physiological inhibitors (TIMPs) are differentially expressed during excisional skin wound repair, Exp. Cell Res. 242 (1998) 201–210. doi:10.1006/excr.1998.4049.

[490] P. Martin, Wound Healing--Aiming for Perfect Skin Regeneration, Science. 276 (1997) 75–81.

[491] Z.S. Galis, G.K. Sukhova, M.W. Lark, P. Libby, Increased expression of matrix metalloproteinases and matrix degrading activity in vulnerable regions of human atherosclerotic plaques, Journal of Clinical Investigation. 94 (1994) 2493–2503.

[492] Z. Li, L. Li, R. Zielke, L. Cheng, R. Xiao, M.T. Crow, et al., Increased expression of 72-kd type IV collagenase (MMP-2) in human aortic atherosclerotic lesions, The American Journal of Pathology. 148 (1996) 121.

[493] T.J. Gronski, R.L. Martin, D.K. Kobayashi, B.C. Walsh, M.C. Holman, M. Huber, et al., Hydrolysis of a broad spectrum of extracellular matrix proteins by human macrophage elastase, J. Biol. Chem. 272 (1997) 12189–12194.

[494] K. Endo, T. Takino, H. Miyamori, H. Kinsen, T. Yoshizaki, M. Furukawa, et al., Cleavage of syndecan-1 by membrane type matrix metalloproteinase-1 stimulates cell migration, J. Biol. Chem. 278 (2003) 40764–40770. doi:10.1074/jbc.M306736200.

[495] M.L. Fitzgerald, Z. Wang, P.W. Park, G. Murphy, M. Bernfield, Shedding of syndecan-1 and -4 ectodomains is regulated by multiple signaling pathways and mediated by a TIMP-3-sensitive metalloproteinase, The Journal of Cell Biology. 148 (2000) 811–824.

[496] G. Taraboletti, S. D'Ascenzo, P. Borsotti, R. Giavazzi, A. Pavan, V. Dolo, Shedding of the matrix metalloproteinases MMP-2, MMP-9, and MT1-MMP as membrane vesicle-associated components by endothelial cells, The American Journal of Pathology. 160 (2002) 673–680. doi:10.1016/S0002-9440(10)64887-0.

[497] W.H. Yu, J.F. Woessner, Heparan sulfate proteoglycans as extracellular docking molecules for matrilysin (matrix metalloproteinase 7), J. Biol. Chem. 275 (2000) 4183–4191.

[498] L.M. Coussens, B. Fingleton, L.M. Matrisian, Matrix metalloproteinase inhibitors and cancer: trials and tribulations, Science. 295 (2002) 2387–2392. doi:10.1126/science.1067100.

[499] T. Arisaka, M. Mitsumata, M. Kawasumi, T. Tohjima, S. Hirose, Y.

Yoshida, Effects of shear stress on glycosaminoglycan synthesis in vascular endothelial cells, Ann. N. Y. Acad. Sci. 748 (1995) 543–554.

[500] Y. Zeng, M. Waters, A. Andrews, P. Honarmandi, E. Ebong, V. Rizzo, et al., Fluid Shear Stress induces the Clustering of Heparan Sulfate via Mobility of Glypican-1 in Lipid Rafts, AJP: Heart and Circulatory Physiology. (2013). doi:10.1152/ajpheart.00764.2012.

[501] A. Koo, C.F. Dewey, G. Garcia-Cardena, Hemodynamic shear stress characteristic of atherosclerosis-resistant regions promotes glycocalyx formation in cultured endothelial cells, AJP: Cell Physiology. 304 (2013) C137–C146. doi:10.1152/ajpcell.00187.2012.

[502] R.K. Jain, Determinants of tumor blood flow: a review, Cancer Research. 48 (1988) 2641–2658.

[503] D. Fukumura, R.K. Jain, Tumor microenvironment abnormalities: causes, consequences, and strategies to normalize, J. Cell. Biochem. 101 (2007) 937–949. doi:10.1002/jcb.21187.

[504] R.E. Bruehl, T.A. Springer, D.F. Bainton, Quantitation of L-selectin distribution on human leukocyte microvilli by immunogold labeling and electron microscopy, J. Histochem. Cytochem. 44 (1996) 835–844.

[505] A.A. Constantinescu, H. Vink, J. Spaan, Endothelial Cell Glycocalyx Modulates Immobilization of Leukocytes at the Endothelial Surface, Arteriosclerosis, Thrombosis, and Vascular Biology. 23 (2003) 1541–1547. doi:10.1161/01.ATV.0000085630.24353.3D.

[506] H.H. Lipowsky, R. Sah, A. Lescanic, Relative roles of doxycycline and

cation chelation in endothelial glycan shedding and adhesion of leukocytes, AJP: Heart and Circulatory Physiology. 300 (2011) H415–H422. doi:10.1152/ajpheart.00923.2010.

[507] H.H. Lipowsky, A. Lescanic, The effect of doxycycline on shedding of the glycocalyx due to reactive oxygen species, Microvasc. Res. (2013). doi:10.1016/j.mvr.2013.07.004.

[508] C.A. Reis, H. Osorio, L. Silva, C. Gomes, L. David, Alterations in glycosylation as biomarkers for cancer detection, Journal of Clinical Pathology. 63 (2010) 322–329. doi:10.1136/jcp.2009.071035.

[509] J. Guck, S. Schinkinger, B. Lincoln, F. Wottawah, S. Ebert, M. Romeyke, et al., Optical deformability as an inherent cell marker for testing malignant transformation and metastatic competence, Biophysical Journal. 88 (2005) 3689–3698. doi:10.1529/biophysj.104.045476.

[510] J.S. Kuo, Y. Zhao, P.G. Schiro, L. Ng, D.S.W. Lim, J.P. Shelby, et al., Deformability considerations in filtration of biological cells, Lab Chip. 10 (2010) 837–842. doi:10.1039/b922301k.

[511] S.J. Tan, L. Yobas, G.Y.H. Lee, C.N. Ong, C.T. Lim, Microdevice for the isolation and enumeration of cancer cells from blood, Biomed Microdevices. 11 (2009) 883–892. doi:10.1007/s10544-009-9305-9.

[512] S. Zheng, H. Lin, J.-Q. Liu, M. Balic, R. Datar, R.J. Cote, et al., Membrane microfilter device for selective capture, electrolysis and genomic analysis of human circulating tumor cells, Journal of Chromatography A. 1162 (2007) 154–161. doi:10.1016/j.chroma.2007.05.064.

[513] G. Vona, A. Sabile, M. Louha, V. Sitruk, S. Romana, K. Schütze, et al., Isolation by size of epithelial tumor cells : a new method for the immunomorphological and molecular characterization of circulating tumor cells, The American Journal of Pathology. 156 (2000) 57–63. doi:10.1016/S0002-9440(10)64706-2.

[514] S. Matsumoto, Y. Imaeda, S. Umemoto, K. Kobayashi, H. Suzuki, T. Okamoto, Cimetidine increases survival of colorectal cancer patients with high levels of sialyl Lewis-X and sialyl Lewis-A epitope expression on tumour cells, British Journal of Cancer. 86 (2002) 161–167. doi:10.1038/sj.bjc.6600048.

[515] B. Monzavi-Karbassi, J.S. Stanley, L. Hennings, F. Jousheghany, C. Artaud, S. Shaaf, et al., Chondroitin sulfate glycosaminoglycans as major P-selectin ligands on metastatic breast cancer cell lines, Int. J. Cancer. 120 (2007) 1179–1191. doi:10.1002/ijc.22424.

[516] M.R. King, Rolling in the deep: therapeutic targeting of circulating tumor cells, Frontiers in Oncology. 2 (2012). doi:10.3389/fonc.2012.00184.

[517] K. Rilla, R. Tiihonen, A. Kultti, M. Tammi, R. Tammi, Pericellular hyaluronan coat visualized in live cells with a fluorescent probe is scaffolded by plasma membrane protrusions, J. Histochem. Cytochem. 56 (2008) 901–910. doi:10.1369/jhc.2008.951665.

[518] C. Brekken, C. de Lange Davies, Hyaluronidase reduces the interstitial fluid pressure in solid tumours in a non-linear concentration-dependent manner, Cancer Letters. 131 (1998) 65–70.

[519] L. Eikenes, I. Tufto, E.A. Schnell, A. Bjorkoy, C. de L. Davies, Effect of Collagenase and Hyaluronidase on Free and Anomalous Diffusion in Multicellular Spheroids and Xenografts, Anticancer Research. 30 (2010) 359–368.

[520] C.B. Thompson, H.M. Shepard, P.M. O'Connor, S. Kadhim, P. Jiang, R.J. Osgood, et al., Enzymatic depletion of tumor hyaluronan induces antitumor responses in preclinical animal models, Molecular Cancer Therapeutics. 9 (2010) 3052–3064. doi:10.1158/1535-7163.MCT-10-0470.

[521] Z. Pályi-Krekk, M. Barok, J. Isola, M. Tammi, J. Szöllosi, P. Nagy, Hyaluronan-induced masking of ErbB2 and CD44-enhanced trastuzumab internalisation in trastuzumab resistant breast cancer, Eur. J. Cancer. 43 (2007) 2423–2433. doi:10.1016/j.ejca.2007.08.018.

[522] Z. Pályi-Krekk, M. Barok, T. Kovács, H. Saya, O. Nagano, J. Szöllosi, et al., EGFR and ErbB2 are functionally coupled to CD44 and regulate shedding, internalization and motogenic effect of CD44, Cancer Letters. 263 (2008) 231–242. doi:10.1016/j.canlet.2008.01.014.

[523] A. Erikson, I. Tufto, A.B. Bjønnum, Ø.S. Bruland, C. de L. Davies, The impact of enzymatic degradation on the uptake of differently sized therapeutic molecules, Anticancer Research. 28 (2008) 3557–3566.

[524] C.J. Whatcott, H. Han, R.G. Posner, G. Hostetter, D.D. Von Hoff, Targeting the Tumor Microenvironment in Cancer: Why Hyaluronidase Deserves a Second Look, Cancer Discovery. 1 (2011) 291–296.

[525] C. Yang, Y. Liu, Y. He, Y. Du, W. Wang, X. Shi, et al., The use of HA

oligosaccharide-loaded nanoparticles to breach the endogenous hyaluronan glycocalyx for breast cancer therapy, Biomaterials. 34 (2013) 6829–6838. doi:10.1016/j.biomaterials.2013.05.036.

[526] B.P. Toole, M.G. Slomiany, Hyaluronan: a constitutive regulator of chemoresistance and malignancy in cancer cells, Seminars in Cancer Biology. 18 (2008) 244–250. doi:10.1016/j.semcancer.2008.03.009.

[527] C. Yang, M. Cao, H. Liu, Y. He, J. Xu, Y. Du, et al., The high and low molecular weight forms of hyaluronan have distinct effects on CD44 clustering, Journal of Biological cHemistry. 287 (2012) 43094–43107. doi:10.1074/jbc.M112.349209.

[528] S. Weinbaum, X. Zhang, Y. Han, H. Vink, S.C. Cowin, Mechanotransduction and flow across the endothelial glycocalyx, Proc. Natl. Acad. Sci. U.S.a. 100 (2003) 7988–7995. doi:10.1073/pnas.1332808100.